Jacobus (Koos) Frederick van Staden WEBSITE-PCE-38-2022-ENG

Exploratory Research Project (PCE-38)-2021-2023

New Improved Reliable Platforms with Modern Nano-Technology for On-site Real-Time Detection in Automated Data-Intensive Process MONitor and Control Systems

Contract Nr. PCE 38/2021: Noi platforme fiabile cu nano-tehnologie modernă pentru detectie on-site, în timp real în procesul de monitorizare automata de date intensive si sisteme de control

(Acronim: PORAPMONS)

PN-III-P4-ID-PCE-2020-0059

PL's Project Leader (PL): Prof. Univ. Dr. CS1 Jacobus (Koos) Frederick van Staden

PL's Project Laboratory: PATLAB, Bucharest of INCDEMC, Timisoara

Host Institution for the project: National Institute of Research and Development for Electrochemistry and Condensed Matter (INCDEMC), Timisoara

Project duration in months: 36 months (2021-2023)

Project budget: 1 198 032.00 LEI

Project Summary

The purpose of the proposal is to explore and push our analytical reliable platform technology to a novel higher

scientific dimension of small smart real-time in-line surface to transducer dynamic engineered system devices. The measurements will be done on-site using real samples from beverage/food and fresh water production, environment, and micro-plastics leaching. Various architectures and advanced new modern micro/nano-technologies will be designed. The final end-product will be complete integrated small smart interactive intelligent advanced process portable real-time multi-detection/sensing platform devices. The complete portable system will be linked to very small smart novel compact chip-based systems on site with profound impact of data-collection and transmittance via wireless communications. PORAPMONS will further add value to small data-intensive process engineering systems beyond the current state-of-art with the incentive of a new fast real-time communication to data base adaptive resource management information systems. This will be done for water/food/agricultural/medical industries in Europe (Worldwide) for risk analysis and for interpretative inter-operative technical solutions. This will form a forefront for the enhancement of investment and settlement of local industrial ventures inside Romania for upliftment of the standards of living in the country.

Team Members

Name	Role in the project
Jacobus Frederick van Staden, DSc, Prof., CSI	Director of Project
Raluca-Ioana van Staden, PhD, Prof., CSI	Principal Researcher
Ionela-Raluca Stancu	Postdoc Researcher
Ramona Georgescu State	Postdoc Researcher
Catalina Negut	Postdoc Researcher
Ruxandra Maria Ilie-Mihai	Postdoc Researcher
Bianca Maria Tuchiu	Doctorand
Damaris Cristina Gheorghe	Doctorand
Irina-Alina Chera-Anghel	Doctorand
Roxana Andreea Niculae	Doctorand
Carmen Pandurescu	Researcher

Issues.

The current massive dumping of waste material, raw polluted material and waste water (including plastic material) containing a large number of hazard toxic substances create a enormous concern in Romania (Worldwide) for the production of safe, secure and suitable food, beverages, juices, drinking water and even pharmaceutical products and medicines. To remove these toxic substances (e.g. pollutants, pesticides, mycotoxins, toxic metals, Endocrine Disruptive Chemicals (EDC's) from resources needs sufficient suitable modern micro/nano-technology and methodology for qualitative and quantitative data to leave only the suitable proper levels of substances needed for sustainable and healthy human life (e.g. vitamins, minerals, antioxidants) in the food-chain, clean water, and agricultural and pharmaceutical productions. Furthermore consumption of these toxic-contaminated commodities is related to several acute fast developing chronic diseases, can cause cancerous tumors and other disorders and can be very hazardous to humans. It is currently very difficult to solve this problem completely in raw materials and even production of safe and secure commodities due to the large unknown (numbers, levels, types) of substances involved. Comprehensive data retrieval from different scientific data bases shows that although various research projects in this regard have been completed and are in-progress with a number of procedures, measurements and methods available to try and solve these problems completely and to improve production of various commodities, they are not completely suitable, reliable, safely and with high security. This is still mainly due to slow time-consumed measurement procedures and production of final results including manual sampling and transport to laboratories. Furthermore, currently no global attention was given towards the development of new innovative improved automated real-time/on-line on-site detection, accumulation with data-intensive process, monitor and control systems engineering, and chemical engineering using reliable, suitable and sustainable platforms with modern high micro/nano-technology to ensure a sufficiently good safe, secure product quality.

Objectives

Therefore the purpose of this current second PN-III-P4-ID-PCE-2020-0059 project is to explore and push our current reliable and sustainable platform technology to a novel far higher intense

scientific dimension of small smart real-time inline surface to transducer system devices in dynamic real beverage/food production, freshwater production, packaging, environmental pollution and micro-plastic leaching for safety and life security. We intend to improve our current reliable and sustainable platform systems from basic research design, structuring, optimization, evaluation and validation with new various possible architectures and advanced new modern micro/nano-technologies to real-time on-site detection devices as final small compact handheld detection sensor platform devices link to very compact chip-based cyber systems as Automated Data-Intensive Process Monitoring and Control Systems on-line.

The project has the following key strategic objectives (some of them are already in an advance stage)

O1: To track, explore and target the most toxic and dangerous substances from waste material and additives in food and also healthy components (vitamins, antioxidants metals) in food;

O2: To setup appropriate portable platform process systems specifications for proper management with strategic planning;

O3: Identification, Selection, Design, Development, Evaluation of Modified/Screen-Printed Electrochemical/Optical Platform sensors/probes/devices;

O4: To evaluate and validate Single Modified/Screen-Printed Electrochemical/Optical Platform sensors/probes/devices and integrate them into Integrated Detection Platforms for sustainable monitoring and control with innovative decision-making tools;

O5: To implement and open new insight micro-technological horizons with complete integrated smart interactive intelligent advanced process portable real-time multi-detection/sensing platform devices linked to very small smart novel compact chip-based systems on site for real-time communication from the complete integrated on-site (in-line) Automated Data-Intensive Process Monitoring, Control and Management System.

Methodology

The scientific work and technological development are structured distributed into SEVEN (7) core workpackages (WP's) and *intermediate Milestones (MS)* with each WP divided into tasks (activities-A) and deliverables-D:-

WP1: Selection of Specific Toxic Substances and Healthy components (vitamins, antioxidants metals) (M1-M8); O1.

Tasks (Activities) A1.1 To select the most prominent problematic specific toxic substances (e.g. pollutants, pesticides, mycotoxins, toxic metals, Endocrine Disruptive Chemicals (EDC's) from waste material, raw polluted material and waste water (including plastic material) and preservatives, additives and emerging pollutants from food-chains;

A1.2 To select the most prominent healthy components (vitamins, antioxidants, metals etc.) from the food-chain, clean water, and agricultural and pharmaceutical productions.

D1- Report Data retrieval of selections. (M8).

Milestones(MS1). Selection of Specific Toxic Substances and Healthy components (vitamins, antioxidants metals) (M8).

WP2: Appropriate portable platform process systems specifications for proper management. (M1-M12); O2.

A2.1 Setup of appropriate process systems specifications with strategic planning for research studies needed to implement reliable and sustainable small compact handheld portable platform devices for proper management.

A2.2 Preliminary investigation of dynamic surface to transducer portable devices coupled to a selection of proper modified/screen-printed platform detection probes. D2- Report Data retrieval, specifications, innovative portable platform detection probes (M12).

***Milestones(MS1). Appropriate portable platform process systems specifications for proper management (M12)*.**

WP3: Development, Evaluation of Modified/Screen-Printed Electrochemical/Optical Platform sensors/probes/devices. (M7-M26); O3.

A3.1 Identification and selection of proper suitable modified/screen-printed material, and design of suitable sensor membrane/surface, sensor transducer, signal transport, amplification, processing for electrochemical/optical sensor platform.

A3.2 Construction and integration of different parts of the sensor platform into a suitable nano-structured sensing platform probe.

A3.3 In-depth investigation and characterization of the functionality of the physical and chemical parameters of the sensing platform probe.

A3.4 Optimization with constant in-depth evaluation of the sensing platform in terms of concentration range, selectivity, response characteristics and detection limit for each of the selected target analytes/substance.

A3.5 Evaluation of the platform sensing devices on standard solutions of target analytes on laboratory scale.

A3.6 Evaluation of interference matrices.

Milestones(M3)Performance of different electrochemical sensor/probes/devices.

D3.1-D3.6. Various reports on the outcome of the different tasks M26.

WP4: Single Modified/Screen-Printed Electrochemical/Optical Platform sensors/probes/devices and Integrated Detection Platforms for sustainable monitoring and control with innovative decision-making tools (M12-M36).; 04.

A4.1 Evaluate and validate the optimum reliable and suitable electrochemical/optical platform sensors/probes/devices in WP3 to

single type detection platforms on real samples for selected emerging pollutants and healthy components (vitamins, antioxidants, metals etc.).

A4.2 Integrate the single type detection platforms into multi-functional fast-responding, reliable, smart, intelligent interactive sensor detection device arrays for sustainable monitoring and control with innovative decision-making tools into integrated sensor-detection platform systems with significant feasibility for use at on-site areas.

Milestones(M4)Performance of different Single Modified/Screen-Printed Electrochemical/Optical Platform sensors/probes/devices and Integrated Detection Platforms **D4.1-D4.2. Various reports on the outcome of the different tasks M36**

WP5: Small Rapid Smart Real-time Interactive Portable Process Platform Sensing Devices for Automated Data-Intensive Process Monitoring, Control and Management Systems (M12-M36).

A5.1 To implement cutting edge dynamic applications with small smart real-time interactive in-vivo inline surface to transducer system portable process sensing devices on-site to give a feasible, reliable and sustainable secure system.

A5.2 To open new insight micro-technological horizons with complete integrated smart interactive intelligent advanced process portable real-time multi-detection/sensing platform devices linked to very small smart novel compact chip-based systems on site with profound impact on applications of data-collection and transmittance via wireless communications.

A5.3 Real-time communication from the complete integrated on-site (in-line) Interactive Portable Process Platform Sensing Device via the Automated Data-Intensive Process Monitoring, Control and Management System will be continuously supplied to data base adaptive water/food/agricultural/medical resource management information systems in Europe (-and Worldwide-) for risk analysis and for interpretative inter-operative technical solutions and services with a Real-time Quality Data Management System.

Milestones(M5) Performance of the Smart Real-time Interactive Portable Process Sensing Devices

D5.1- D5.3. Final report M36.

<u>WP6: Project Management.(M1-M36)</u>

A6.1 Continuous progress evaluation and assessment of the project.

A6.2 Continuous proper coordination and project management. The Project Director (PD-KVS), with support from responsible team members will be responsible for the respective activities in WP6.

<u>WP7: Dissemination.(M1-M36)</u>

A7.1 Dissemination with a website, flyers and of results through patents, published papers in ISI peer-reviewed journals, presentations at workshops, conferences, seminars

A7.2 Integration of knowledge with training/education of students/young researchers. The Project Director (PD) with all team members will be involved in WP7.

Dissemination

Published works:

1. **Review. Recent Trends on the Electrochemical Sensors Used for the Determination of Tartrazine and Sunset Yellow FCF from Food and Beverage Products**
   Ramona Georgescu State, Jacobus (Koos) Frederick van Staden and Raluca-Ioana Stefan-van Staden
   Journal of the Electrochemical Society 169 (2022) 017509; https://doi.org/10.1149/1945-7111/ac4a4c

2. **Mini Review- recent developments in electrochemical detection of atrazine**
   Ionela Raluca Comnea-Stancu, Jacobus (Koos) Frederick van Staden and Raluca-Ioana Stefan-van Staden
   Analytical Letters 2022; https://doi.org/10.1080/00032719.2022.2107659

3. **Rapid and sensitive electrochemical determination of tartrazine in commercial food samples using IL/AuTiO2/GO composite modified carbon paste electrode**
   Ramona Georgescu State, Jacobus (Koos) Frederick van Staden, Razvan State, and Florica Papa
   Food Chemistry 385 (2022) 132616; https://doi.org/10.1016/j.foodchem.2022.132616

4. **Mini-Review: Electrochemical Sensors Used for the Determination of Water- and Fat-Soluble Vitamins**
Damaris-Cristina Gheorghe, Raluca-Ioana Stefan-van Staden and Jacobus (Koos) Frederick van Staden
Critical Reviews in Analytical Chemistry. Published Online: 26 Feb 2022 https://doi.org/10.1080/10408347.2022.2045557

5. **Review - Progress in electroanalysis of p53, CEA and CA19-9.**
Ruxandra-Maria Ilie-Mihai, Raluca-Ioana Stefan-van Staden, and Jacobus (Koos) Frederick van Staden
Journal of the Electrochemical Society 169 (3) (2022) 037158.

6. **Recent electrochemical methods proposed for the detection of hepatitis C virus. A minireview**
Ruxandra-Maria Ilie-Mihai, Raluca-Ioana Stefan-van Staden, Jacobus (Koos) Frederick van Staden, Hassan Y. Aboul-Enein
Revista de Chimie 2022, 73 (2), 1-16, https://doi.org/10.37358/RC.22.2.8515

7. **Minireview: Current Trends, and Future Challenges for the determination of Patulin in Food Products.**
Catalina Cioates Negut, Raluca-Ioana Stefan-van Staden and Jacobus Frederick van Staden
Analytical Letters 2022.; https://doi.org/10.1080/00032719.2022.2083146

8. **Recent Trends in Ibuprofen and Ketoprofen Electrochemical Quantification – A Review**
Bianca-Maria Țuchiu, Raluca-Ioana Stefan-van Staden, Marius Bădulescu and Jacobus Frederick van Staden
Critical Reviews in Analytical Chemistry 2022 DOI: 10.1080/10408347.2022.2050348 .

9. **Disposable stochastic sensors for fast analysis of ibuprofen, ketoprofen, and flurbiprofen in their topical pharmaceutical formulations**
Bianca-Maria Țuchiu, Raluca-Ioana Stefan-van Staden, Marius Bădulescu and Jacobus Frederick van Staden
Journal of Pharmaceutical and Biomedical Analysis 215 (2022) 114758; https://doi.org/10.1016/j.jpba.2022.114758

10. **Nanographene-based electrochemical sensors for ultrasensitive determination of sorbic acid from food.**
Raluca-Ioana Stefan-van Staden, Andreea-Roxana Niculae, Jacobus Frederick van Staden, Ramona State, Paula Sfirloaga
Analytical and Bioanalytical Chemistry. 414, (2022) 6813–6824.

11. **N-methylfulleropyrrolidine based multimode sensor for determination of butoconazole nitrate**
Bianca-Maria Țuchiu, Raluca-Ioana Stefan-van Staden and Jacobus (Koos) Frederick van Staden
ACS Omega, 7(46) (2022) 42537-42544. https://doi.org/10.1021/acsomega.2c05904

12. **Mini-Review−Electrochemical sensors used for the determination of some antifungal azoles**
Bianca-Maria Țuchiu, Raluca-Ioana Stefan-van Staden and Jacobus (Koos) Frederick van Staden.
ECS Sensors Plus 1 (2022) 030601; https://doi.org/10.1149/2754-2726/ac88e3

13. **Sulfur-doped graphene based electrochemical sensors for fast and sensitive determination of (R)-(+)-Limonene from beverages**
Andreea-Roxana Niculae, Raluca-Ioana Stefan-van Staden, Jacobus Frederick van Staden, and Ramona Georgescu State
Sensors 22(15), (2022) 5851; https://doi.org/10.3390/s22155851.

14. **Carbon Nanopowder Based Stochastic Sensor for Ultrasensitive assay of CA 15-3, CEA and HER2 in whole blood.**
Raluca-Ioana Stefan-van Staden, Oana-Raluca Musat, Damaris-Cristina Gheorghe, Ruxandra-Maria Ilie-Mihai and Jacobus (Koos) Frederick van Staden.
Nanomaterials 12 (2022) 3111. https://doi.org/10.3390/nano12183111

15. **Sodium Metabisulfite in Food and Biological Samples: A Rapid and Ultra-Sensitive Electrochemical Detection Method**
Ruxandra-Maria Ilie-Mihai, Bianca Cristina Ion and Jacobus (Koos) Frederick van Staden
Micromachines 13(10) (2022) 1707; https://doi.org/10.3390/mi13101707

16. **Sodium Metabisulfite in Food and Biological Samples: A Rapid and Ultra-Sensitive Electrochemical Detection Method**
Ruxandra-Maria Ilie-Mihai, Bianca Cristina Ion and Jacobus (Koos) Frederick van Staden
Micromachines 13(10) (2022) 1707; https://doi.org/10.3390/mi13101707

17. **Ultrasensitive assay of HER-1, HER-2, and heregulin-α in whole blood**
Raluca-Ioana Stefan-van Staden, Oana-Raluca Musat, Damaris Cristina Gheorghe, Catalina Cioates Negut, Paula Sfirloaga
Talanta Open 6 (2022) 2022; https://doi.org/10.1016/j.talo.2022.100151

18. **Stochastic Sensors for the Enantioselective Determination of Serine in Blood for the Early Diagnosis of Breast Cancer**
Oana Raluca Musat, Raluca-Ioana Stefan-van Staden
Analytical Letters, 55(13) (2022) 2124-2131; https://doi.org/10.1080/00032719.2022.2047999

Conferences

Carbon Nanopowder Based Stochastic Sensor for Ultrasensitive assay of CA 15-3, CEA and HER2 in whole blood
Oana-Raluca Musat, Raluca-Ioana Stefan-van Staden, Damaris-Cristina Gheorghe, Ruxandra-Maria Ilie-Mihai, and Jacobus (Koos) Frederick van Staden
The International Symposium "PRIOrities of CHEMistry for a sustainable development" PRIOCHEM XVIII-th Edition October 26-28, 2022, Bucharest, Romania

Reports:

2021:- Stage 1-Selection of specific toxic substances and of healthy components and configuring of the appropriate specifications of the process systems of the portable platform for appropriate manage

Review- recent developments in electrochemical detection of atrazine

Abstract

This review aims to discuss all the recent developments in terms of electroanalytical detection of the pesticide atrazine from the past five years. Atrazine it is a common triazine herbicide that it is very persistent in the environment due to its water solubility and slow degradation. Some of the effects of the atrazine exposure can be: immnue suppression, carcinogenity, hormone disruptions and reproductive anomalies.

1. Introduction

Pesticides are being widely used in the agricultural sector to have a better control on food production and to limit the existence of some pests (like insects, herbs, fungi, etc). Even if they are being used for the favorable effects on the food management, their continous usage and exposure can also bring undesirable effects on human health like carcinogenity, infertility, neurological, imunological and respiratory diseases. They can be classified by their use (figure 1) or by their chemical structure/composition. The World Health Organization (WHO) classified them as carcinogenic, neurotoxic and teratogenic [1].

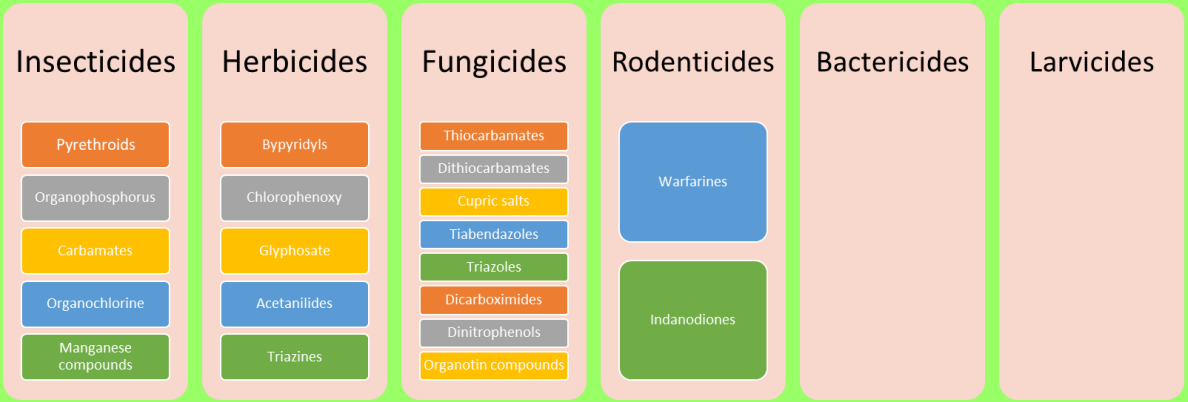

Fig. 1. Classification of pesticides based on the use of the pest they kill

Atrazine is a synthetic herbicide that was licensed for the first time in the year of 1958 in Switzerland and afterwards was registered in 1959 in the United States for commercial use, succeeding to a global utilization[2]. Its usage had proven to be polemical for the reason that on

the strength of its persistence and mobility, atrazine had been found in places like: soil, plantations, reservoirs used for public water supply, groundwater, streams, lakes, rivers, seas, and even glaciers in remote areas[3]. The European Union banned atrazine use completely in 2004[4], however its presence it was still noticed along the coast waters in Europe, especially in the Aegean Sea, that relates and exchanges water with the Marmara Sea and the Black Sea which are natural border with countries where atrazine is still applied [5].

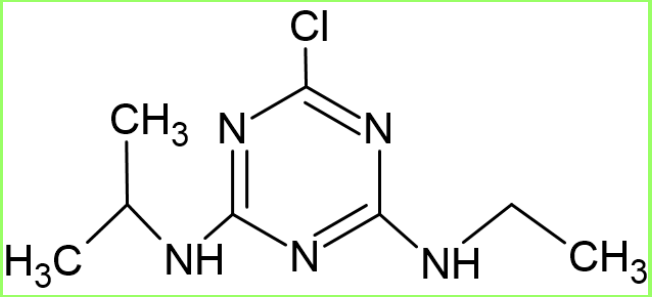

Fig.2. Chemical structure of atrazine

Before it was completely banned by the European Union, atrazine residue had a uniform limit of 0.1 µg L^{-1} for drinking water and groundwater[3,6]. Worldwide the limits set for atrazine presence are the following: 100 µg L^{-1} maximum concentration allowed by WHO for atrazine and its chloro-s-triazine metabolites in drinking water[7], 20 µg L^{-1} by the Australian government, 3 µg L^{-1} in the United States and 2 µg L^{-1} in the Brazil for freshwater, considering the use of the water for human consumption and the protection of aquatic life[8-10].

Even though in some countries the use of atrazine has been banned, the control of the presence of this compound in water and also food samples is of major importance due to the harmful effects it can have on the aquatic environment and human health. The classical chromatographics methods[11-15] for the determination of atrazine are expensive, long time analysis and require high reagent samples and qualified personnel. Due to these limitations in recent years the electrochemical methods had known a continuous development in the pesticides detection[16,17]. The following paper presents on overview of the electrochemical sensors for atrazine detection reported in the last five years.

2. Electrochemical detection of atrazine

The development of methods and techiques for the atrazine detection is an important matter in order to ensure the water and food safety. The classical chromatographic methods of detection are used for the atrazine and pesticides analysis for the validation of the methods by legislation of the regulatory agencies . Even if these methods are very sensitive and

reproducible they still suffer from many disadvantages like the very expensive and sophisticated laboratory instruments, complicated sample preparation that includes steps of extraction and purification with large amount of organic solvents, the requirment of supervision by an analytical chemist and the incapacity of an *on-site* and real-time detection. Consequently, the electrochemical methods have known a increasingly progress in the analysis of pesticides, due to their advantages presented towards the classical ones: low cost, reduced size and miniaturized equipment, portability, high sensitivity, rapid detection time, selectivity and accuracy. In the following we shall present the recent developments regarding the electrochemical detection of atrazine.

Guan et al presented a biosensor for the atrazine detection build on the inhibition of tyrosine. They incubated the biosensor in an atrazine containing PBS solution for 15 minutes, then the singal of the inhibited biosensor to 5.0 μM of phenol solution was recorded. A linear range was obtained in the range of 50 ppb - 3.0 ppm and a limit of detection of 10 ppb. The biosensor presented good operational stability and recoverability. The authors tested the practical application of the biosesnsor analyzing real water samples from a river, a lake and a farmland waste water spiked with various concentratons of atrazine, obtaining gratifying recoveries in the range of 93.0 – 106.2 %[18].

Medina-Sanchez et al developed a lab-on-chip (LOC) platform for the electrochemical and degradation of atrazine based on boron-doped diamond modified with platinum nanoparticles. The LOC device has integrated two BDD electrodes: one whose surface was covered with platinum nanoparticles for the detection of atrazine through magneto-enzyme immunoassay and another bare BDD for degradation of atrazine by anodic oxidation. The detection has the advantage that it is completely automated and guarantees the atrazine detection down to a 3.5 pM limit of detection.[19]

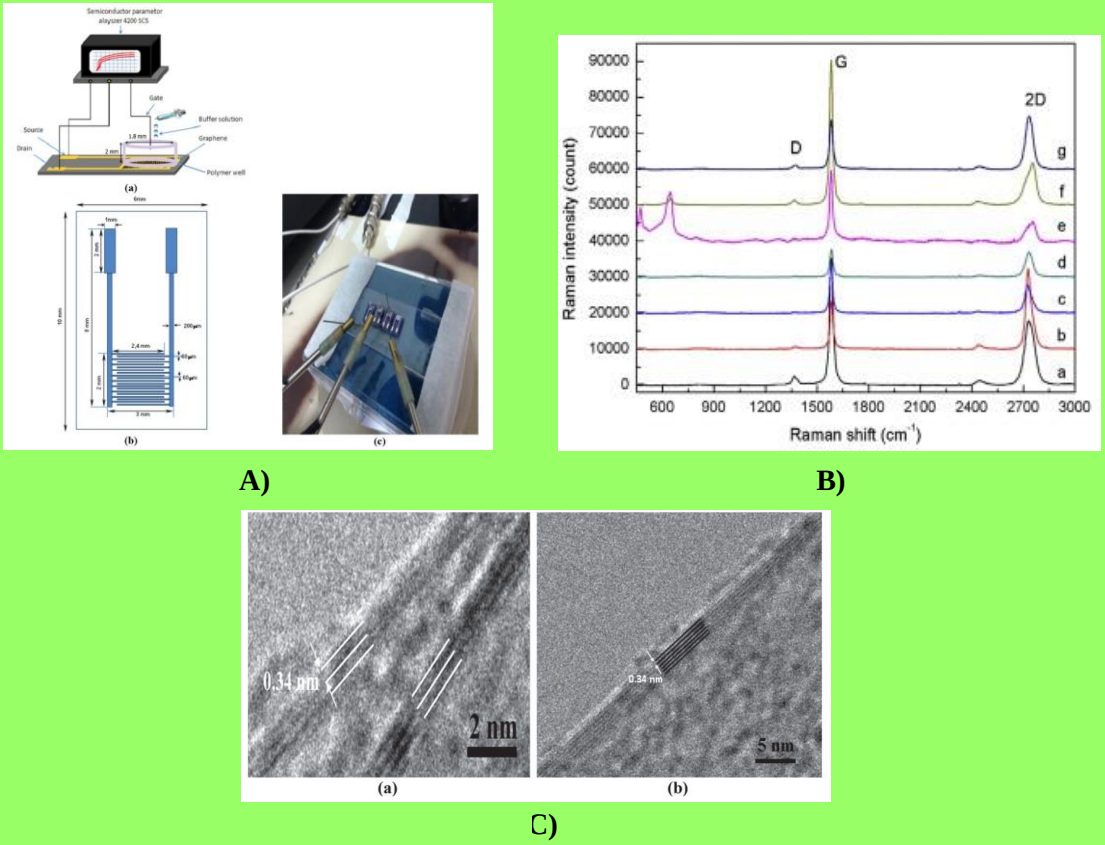

Figure 3. A) Schematic illustration of a FET device configuration (a) and the experimental setup (b) and (c) for electrolyte-gate GFETs. **B)** Raman spectra (a to g) of the graphene/ FLG film measured on the Cu substrate at the different correcponding locations. **C)** Typical HRTEM images of graphene/FLG film measured at two different locations: the film thicknesses are three (A) and six (B) layers. Adapted from Ref [20], an open acces article distrubuited under the Creative Commons Attribution license

Cao and collaborators reported the elaboration of a graphene based field effect transistor for atrazine detection. They immobilized urease molecules in a few-layered graphene (FLG) channel between S and D electrodes[20]. The detection mechanism of atrazine is based on the enzymatic hydrolysis reaction of urea followed by the measurement of changes in drain– source current of the FET sensor. In the FET type sensors/biosensors it is important the conductivity of electrode surface to measure some parameters like: the position, the intensity and the width of minimum conductance point. When atrazine is introduced in the system, it decreases the current signal because it acts as an inhibitor by reducing the activity of enzyme and therefore lowers the concentrations of ions at the electrodes. The decrease of the differential drain–source current (ΔIds) with increasing atrazine concentrations it taked place in the range 2×10^{-4}–20 ppb (figure 4C). Accordingly, the FET device proposed by the authors showed good linearity in the range before mentioned with a 0.98 coefficient of determination (R^2) and 0.05 ppt limit of detection [20].

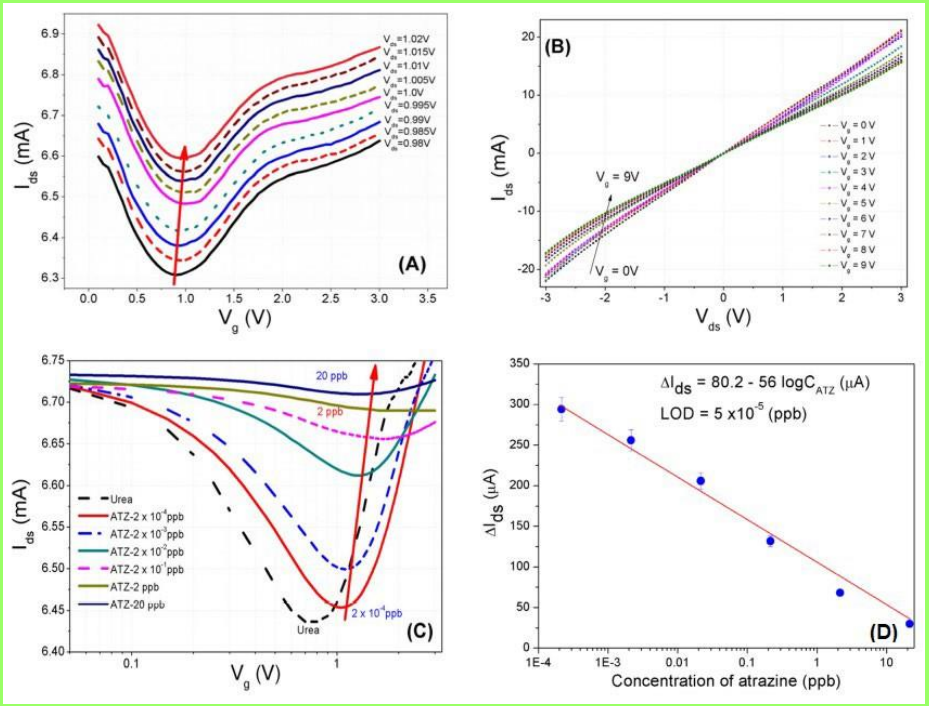

Fig.4 Electrical characteristics of the fabricated sensor**. A)** Ids as a function of Vg for different Vds from 0.98 to 1.02 V with a step of 0.05 V**; B)** Ids as a function of Vds for different Vg from 0 to 9 V with a step of 1.0 V. The dotted arrow shows the direction of the shift in the minimum of Ids; and **C)** Ids versus Vg curves measured for different atrazine concentrations at Vds = 1.0 V. As the atrazine concentration increases, from 2 × 10−4 to 20 ppb, the minimum of Ids is shifted towards higher Vg. Adapted from Ref. [20] an open acces article distrubuited under the Creative Commons Attribution license

The group of Van Chuc reported a method of depositing a multilayer-film of graphene on top of a pre-existing polyaniline electrode[21]. The group prepared platinum (Pt) working electrodes and chromium (Cr) counter electrodes on silicon oxide wafer using the planar microeletronic technology. Then the following step was the electrodeposition of polyaniline(PANI) onto the Pt working electrode by cyclic voltammetry between – 200 mV and + 800 mV at a scan rate of 50 mV/s. The aniline monomer 0.05 mol/L was prepared 0.1 mol/L H_2SO_4. The graphene films were obtained using the CVD method (chemical vapor deposition) on a Cu tape: in the first stage an argon flow of 1000 sccm and a temperature of 1000˚C was reached in the CVD chamber that was being kept constant, after was added hydrogen to the CVD chamber. After 30 minutes in the CVD system was introduced a methane flow to start growing the graphene on the Cu tape, a process that was mentained for another 30 minutes. After this CVD procedure the graphene films were let to cool down at room temperature under an Ar flow. The CVD process for graphene film synthesis was described in detail in another paper of the Van Chuc group[22]. Thus, the synthesized graphene layer was detached from the Cu tape and transferred to the working electrode (Pt/PANI)

using as a sacrificial layer polymethyl methacrylate (PMMA). And the final step of immobilization of anti-atrazine antibodies on the PANI/Gr films was done using glutaraldehyde as cross linker. The new immuosensor had reached a LOD of 43×10^{-12} g/L [21].

Bhardwaj et al[23] proposed for the first time a simple electrochemical way to grow glycine doped polyaniline nanofilms on a silicon substrate in one-step. Polyaniline was electrochemically deposited using bulk electrodeposition method at a constant potential of 0.7 V for 5 minutes using the monomer aniline of 0.1 M concentration doped with a suitable amount of glycine (5%) prepared in 10^{-3} M HCl . Before immobilization of the anti-antrazine antibodies the Glycine-PANI electrodes were incubated 30 minutes with 10 mL of 0.05 M EDC and 0.01 M NHS (1:1) prepared in MES buffer pH=5. Thus, the formed glycine PANI thin films have been easily and directly bioconjugated with the anti-atrazine antibodies. Then the response of the new electrode based on Ab/Gly/PANI was recorded against the varying atrazine concentration and a linear range of 0.1 ng/L – 1 µg/L was reached, and a 0.07 ng/L LOD was obtained. Thus the proposed immunosensor has an easy mode of fabrication and is using glycine, a natural amino-acid as sensing platform that is facilitating immobilization of the specific antibodies on conductive substrate[23].

Kardaș and others developed a CuO NPs/ILs carbon paste electrode for atrazine analysis from wastewater samples. They synthesized the CuO nanoparticles and 2-(3-acetoxy-4-methoxybenzylidenamino)-thiophenol (AMT) ionic liquid, and after the TEM, EDX and XRD characterization of CuO nanoparticles they prepared the sensor by mixing the ionic liquid (AMT) with CuO NPs, graphite powder and paraffin oil until a uniformly paste was obtained. The modified sensor was then characterized by CV and EIS showing his catalytic ability compared with the bare electrode. The new CuO NPs/ILs/CPE showed a very low limit of detection of 2×10^{-12} M and very good recoveries rates from wastewater samples[24].

The Yang group proposed for the atrazine detection an electrochemical platform based on Nb_2O_5 nanotube arrays modified with chitosan (CS) and carboxyl-Fe_3O_4 nanoparticles and atrazine monoclonal antibody. Nb_2O_5 nanotube arrays were grown from Nb substrate by anodization method. The schematic illustration of the proposed sensor is shown in the figure 5A. The carboxylated Fe_3O_4 NPs have been chosen for increasing antibody immobilization and also for enhancing the electrochemical signal responses and by chitosan addition the research group succeded to assure a secure attachment without agglomeration of the Fe_3O_4 NPs on the Nb_2O_5 surface. The electrochemical performance of the platform was measured

after each adjustment with Nb_2O_5 arrays by CV in 0.1 M PBS with 5.0 mM $[Fe(CN)_6]^{3-/4-}$ and 0.1 M KCl. Further the ATZ could be quantified by anti-ATZ/Fe_3O_4/CS/Nb_2O_5 nanotube electrode using DPV method in a linear range of 0.04 ng/mL – 0.60 ng/mL[25].

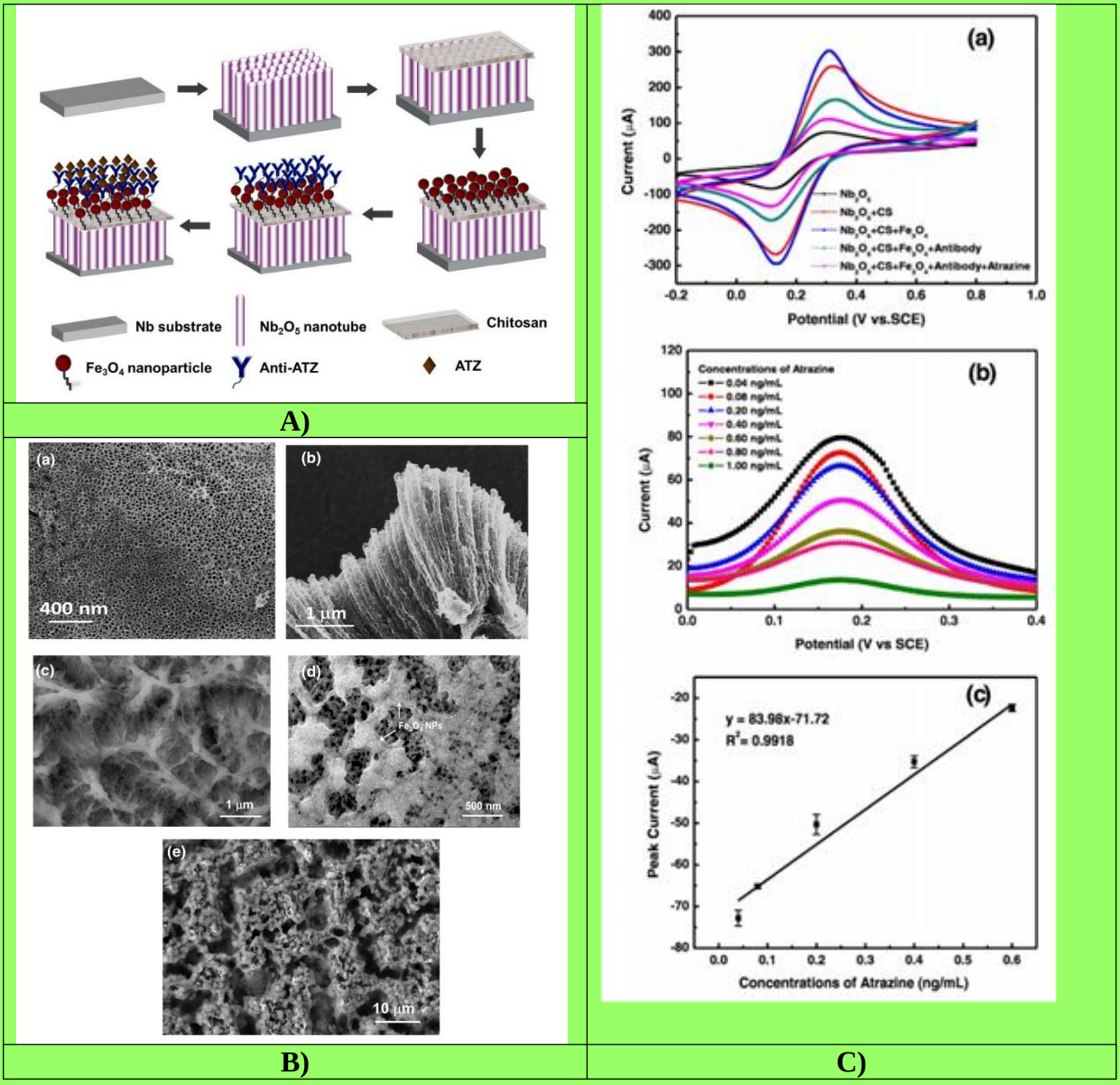

Fig.5 A.) Schematic illustration of fabrication processes on Fe_3O_4NPs modified Nb_2O_5 nanotube arrays. **B)** SEM images of (a) surface view of the self-ordered Nb_2O_5 nanotube arrays; (b) cross-section view of Nb_2O_5 nanotube arrays; (c) CS/ Nb_2O_5 electrode; (d) Fe_3O_4/CS/Nb_2O_5 electrode; (e) anti- anti-ATZ/Fe_3O_4/CS/Nb_2O_5 electrode. **C)** a) Cyclic voltammograms (CVs) of bare Nb_2O_5electrode, CS/ Nb_2O_5 electrode, Fe_3O_4/CS/Nb_2O_5 electrode, anti-ATZ/Fe_3O_4/CS/Nb_2O_5 electrode and ATZ/anti-ATZ/ Fe_3O_4/CS/Nb_2O_5 electrode performed in 0.1 M PBS (pH 7.5) containing 5.0 mM $[Fe(CN)_6]^{3-/4-}$ and 0.1 M KCl. (b) Differential pulse voltammetric (DPV) responses obtained from the same electrolyte with various concentrations of ATZ solutions: 0.04, 0.08, 0.2, 0.4, 0.6, 0.8, and 1.0 ng/mL. (c) Linear relationship between the peak current intensities and atrazine concentrations in ranges of 0.04 ng/mL–0.6 ng/mL. Adaptaed from Ref [25]

Yola and Atar have reported a molecular imprinting polymer and platinum nanoparticles/carbon nitride nanotubes nanocomposites based electrode (Pt NPs/C_3N_4 NTs) for atrazine analysis[26]. In their study the first step in developing the new sensor was the Pt NPs/C_3N_4 NTs preparation using hydrothermal treatment. Afterwards the Pt NPs/C_3N_4 NTs suspensions were dropped onto the clean GCE. The ATR imprinted electrode (MIP/Pt NPs/C_3N_4 NTs/GCE) was formed on Pt NPs/C_3N_4 NTs/GCE using cyclic voltammetric (CV) method for 10 cycles in 100 mM phenol in the presence of 25 nM ATR (0.1 M, pH 7.0 PBS). The nanostructures were characterized by the following techniques: SEM, TEM, EDX, XPS and XRD. The modified electrode was characterized by CV and EIS and the surface area was calculated to be 0.822 cm^2 compared to 0.070 cm^2 for the bare GCE. The obtained results highlights the enhanced performances of the MIP/Pt NPs/C_3N_4 NTs/GCE electrode. The authors optimized the working condition in terms of pH, monomer concentration, elution time and scan cycle for the electrodeposition of the monomer. Thus, the MIP/Pt NPs/C_3N_4 NTs/GCE showed a linear range towards detection of atrazine in the 1.0×10^{-12} – 1.0×10^{-10} M range and reached a 1.5×10^{-13} M limit of detection. The sensor also showed high selectivity and sensitivity in wastewater samples[26].

The paper of Ahmad team describes the a MIP based sensor for the detection of atrazine. Using the bulk polymerization process they prepared MIPs with different ratios of monomer:template and crosslonker: template. Thus they optimized the ratio of the crosslinker:monomer:atrazine to 5:25:1 for the recognition of atrazine. The MIP system can detect atrazine in water up to a concentration of 40 mg/L[27, 28].

Madianos and co-workers[29] succeded to develop an impedimetric aptasensor based on PtNPs for the detection of atrazine and acetamipirid. The aptasensor was build by the fusion of self-ssembled PtNPs two-dimensional films (which were formed by magnetron sputtering technique) and target specific nucleic acids showed higly sensitivity and selective detection of two pesticides: atrazine and acetamipirid[29].

Calfuman and collaborators showed the design, construction and characterization of a glassy carbon electrodes modified with tetrarutenated metalloporphyrin (M=Ni(II) and Zn (II) and 1-butyl-3-methylimidazolium bis(trifluoromethylsulfonyl)imide, BMIMNTF_2. They proposed a simple and quick method for the preparation of two modified electrode : 8 µL of a mixture of the ionic liquid and 1 mM of the tetrarutenated metalloporphyrin (1:9) was drop coated on the surface of the glassy carbon electrode and afterwards left at room temperature

to dry. The new modified sensors reached good response characteristics (**table 1**), are very stable and reproducible, and presents the advantages of an easy and fast way of preparation [30].

In 2019 Supraja and her group developed two very sensitive immunosensors based on metal oxide nanofibers for the detection of atrazine. The first article reported the use of the manganese oxide nanofibers (Mn_2O_3) as the transducing material[31], and in their second article [32] they detailed the use of tin oxide nanofibers (SnO_2) as the sensing material, which is opposite to the semiconducting action of Mn_2O_3. Due to its semiconducting nature, Mn_2O_3 has a higher ability for transfering electrons at electrode/electrolyte interface compared to other high bandgap metal oxide nanomaterials, emerging an excellent sensitivity and a low limit of detection. Previously, the group reported the detection of Dengue virus specific consensus primers using Mn_2O_3 nanofibers obtaining a limit of detection of 10^{-21} order of magnitude[33]. Mn_2O_3 were synthesized employing the electrospinning method. Afterwards the anti-atrazine antibody were immobilize on the Mn_2O_3 nanofiber modfified glassy carbon electrode. The detection of atrazine was accomplished with electrochemical impedance spectroscopy. The linear range obtained with GCE/MNF/EDC-NHS/Ab/BSA electrode for atrazine detection was 1 zg/mL-1µg/mL in the frequency range of 0.001 Hz – 10 kHz, and the limit of detection was calculated to be 0.22 zg/mL, the lowest limit of detection so far, for the electrochemical detection of atrazine[31]. The second article in which they report the electrochemical detection of atrazine using electrospun SnO_2 nanofibers the limit of detection was established at 0.9 zM, even smaller than the previously reported. The fabrication of the modified SnO_2 sensor is following the same steps as the Mn_2O_3 nanofiber modfified glassy carbon electrode. The electrochemical analysis of the new modified anti-atrazine sensor was done using CV and DPV, and the research team evaluated the practical application of the sensor by analyzing spiked ground and mineral water in order to detect atrazine. To conclude, an ultrasensitive sensor for the detection of atrazine in water that it reaches a 0.9 zM detection limit, the lowest limit of detection recorded ever for this compund with an electrochemical method was established with SnO_2 nanofibers [32].

Recently the same group proposed an electrochemical platform based on MWCNT-ZnO nanofibers for the detection of atrazine [34]. The protocol of fabrication of the modified sensor follows the same steps as previously reported studies and it is represented in figure 6. MWCNT-ZnO nanofibers were obtained by the electro-spinning method followed up by the

high-temperature calcination. Morphological studies have been made during the proccess of acquisition of the nanofibers (SEM, TEM before and after calcination) -figure 6.

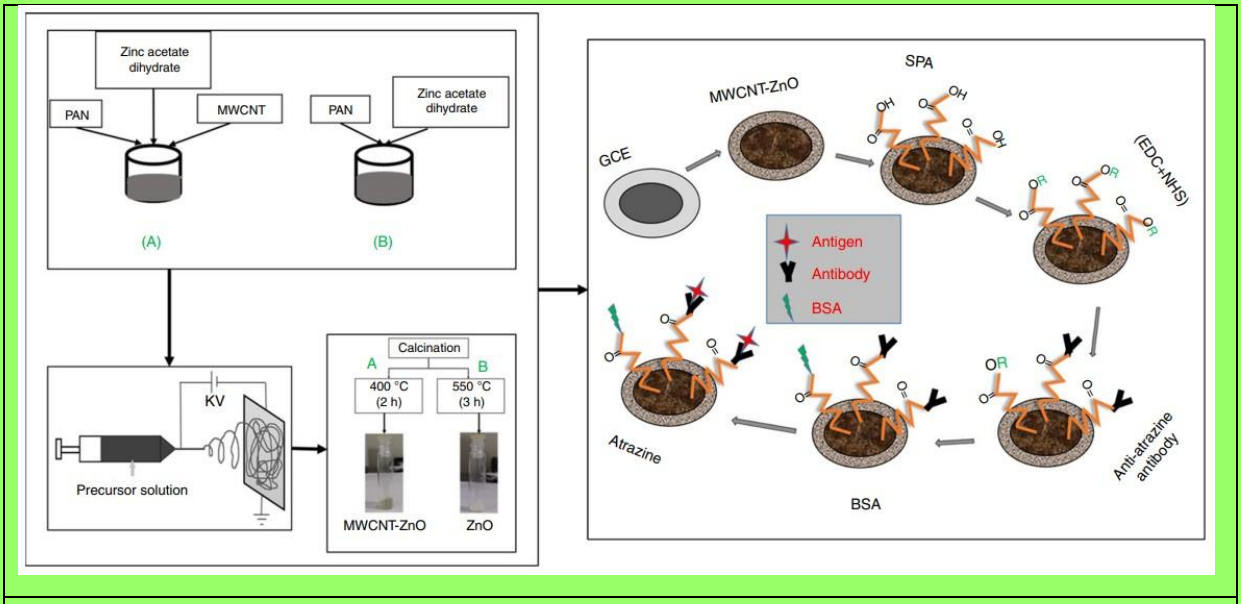

A)

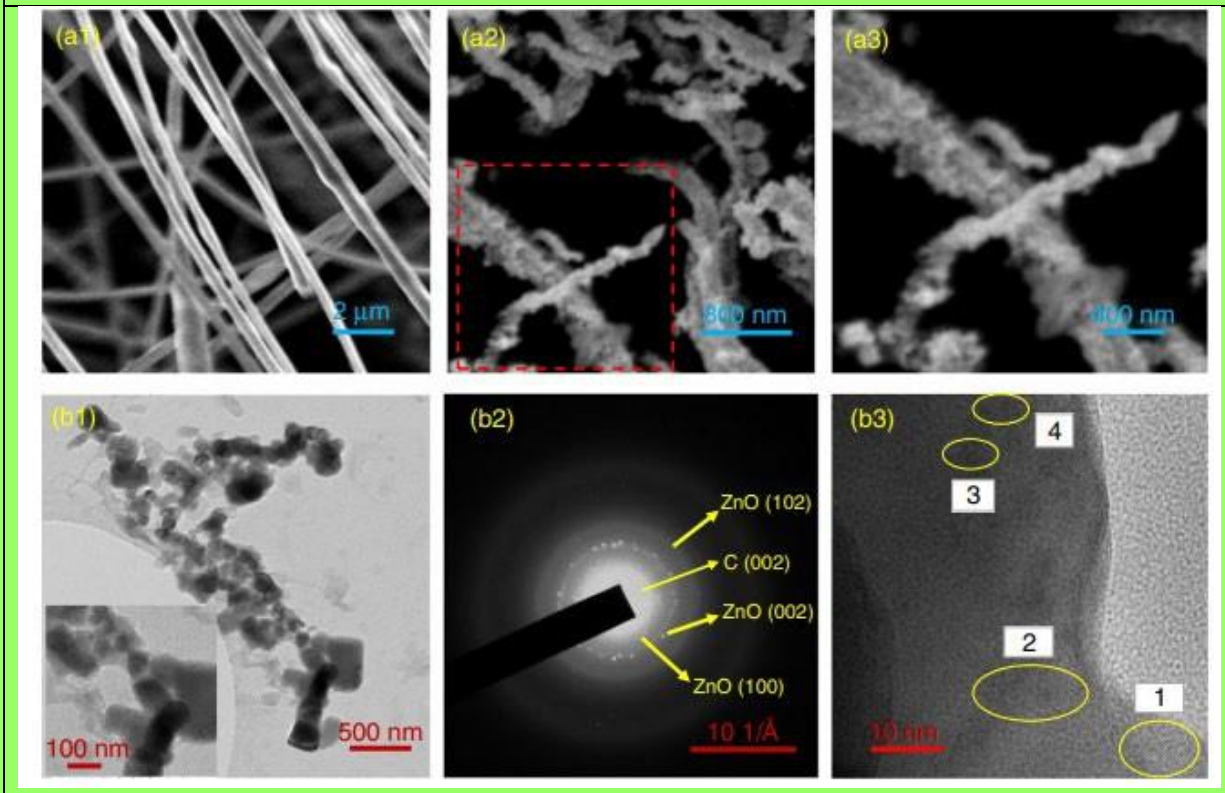

B)

Fig.6 A) Schematic representation of synthesis of ZnO nanofibers and preparation of the electrode. **B)** Morphological study of electrospun MWCNT embedded ZnO nanofibers using SEM and TEM. SEM images of MWCNT-ZnO nanofibers (a1) before calcination, (a2) after calcination at 400°C, and (a3) high-resolution image of calcinated nanofiber. TEM images of MWCNT-ZnO nanofibers (b1) after calcination with an inset showing high-resolution magnified image (b2) SAED

pattern and (b3) HRTEM showing an interface of polycrystalline MWCNT-ZnO nanofibers. Adapted from Ref. [34] an open acces article distrubuited under the Creative Commons Attribution license

Ultimately, the MWCNT-ZnO were drop-casted (20 mg/mL solution) on a cleaned GCE and dried at 60°C in an incubator for a 120 minutes period of time. Before the immobilization of the ATZ antibodies, the MWCNT-ZnO/GCE was funtionalized with SPA and EDC-NHS (EDC-coupling agent and NHS-activator). Afterwards the modified sensor was characterized by EIS and CV techiques (figure 7A). The electrochemial response of the anti-ATZ- MWCNT-ZnO/GCE was tested for various concentrations of ATZ by EIS technique (figure 7B). Thus, this platform succeded to reach a LOD of 5.358 zM and a wide linear detection range of 10 zM - 1µM. The proposed device presents good stability, selectivity, reproductibility and repetability.

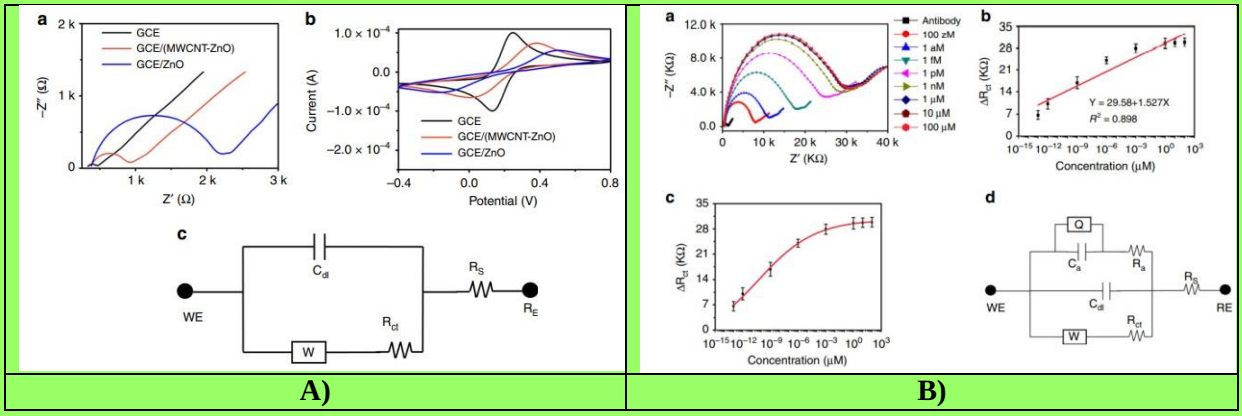

A) **B)**

Fig. 7. A) Electrochemical characterization of MWCNT-ZnO by a) EIS, b) CV **B)** Electrochemical analysis of the anti-ATZ-MWCNT-ZnO/GCE: a) EIS analysis of anti-ATZ-MWCNT-ZnO/GCE for various concentrations of ATZ, b) calibration curve with linear fitting, c)logistic sigmoidl curve fitting of data , d) electrical modeling of detection mechanism. Adapted from Ref. [34], an open acces article distrubuited under the Creative Commons Attribution license

Table 1. Sensors used for the electrochemical detection of atrazine

NR CRT	SENSOR MATERIAL	METHOD	LINEAR RANGE (nM)	LOD (nM)	SAMPLES	REF.
1	poly(L-DOPA)-tyrosinase (PDM-Tyr)/NAFION/Au	Inhibition measurement	231.82 - 13090	46.36	River water, lake water, waste water	18
2	PtNPs-BDD	CA	0.0045 – 45	3.5×10^{-3}	-	19
3	GRAPHENE FET (GFET)	FET	9.273×10^{-4} – 92.73	0.2388	-	20
4	PANi/Gr- α-ATZ	SWV	9.273×10^{-3} – 92.73	1.994×10^{-4}	-	21
5	Glycine-PAni	Conductometry	5×10^{-8} – 4.63	3×10^{8}	-	23
6	CuO NPs/ILs/CPE	DPV+CV	0.01 – 2	0.002	Wastewater	24
7	anti-ATZ/Fe_3O_4/CS/Nb_2O_5 nanotube electrode	DPV	0.185 – 2.78	0.083	-	25
8	MIP/Pt NPs/C_3N_4 NTs/GCE	DPV	0.001 – 0.1	0.00015	Wastewater	26
9	(Atr:EGDMA:MAA)MIP	CV	-	1.85×10^{5}	Water	27
10	Pt NP film/ SiO_2 substrates	EIS	0.6 – 1000	0.04	-	29
11	GC/BMIMNTF2/ZnTRP	DPV	212 – 2500	230	-	30
12	GC/BMIMNTF2/NiTRP	DPV	76.8 – 3500	540	-	
13	GCE/MNF/ EDC-NHS/Ab/BSA	EIS	4.64×10^{-5} – 4636.5	2.22×10^{-13}	Spiked water samples	31
15	GCE/SnO_2/EDC-NHS/Antibody/ BSA	DPV+CV	10^{-12} – 1000	9×10^{-12}	-	32
16	MWCNT-ZnO NANOFIBERS	EIS, CV	10×10^{-12}– 1000	5.368×10^{-12}	-	34
17	DOM/AgNP/GC-AgNP aggregation	SWASV	92.73 − 1020	89.48	River water	35
18	DOM/AgNP/GC-AgNP NON-aggregation	SWASV	46.36 – 649.10	63.05		
19	CLs/PGE	SWV	0.023 – 1.483	3.71×10^{-5}	Drinking water	36
20	CC125/CB-SPE	CA	100 - 5000	1	River water	37
21	Al_2NiCoO_5 (ANCO)/GCE	DPV	0.0023 – 0.463	0.00139	Blood serum samples	38

22	AIRGOC- SPE	SWV	1.2 – 23	0.4	Sugarcane juice, river water samples	39

The study of Zahran et al[35], describes the synthesis of AgNPs by direct chemical reduction technique and their application for the detection of atrazine from water samples. After their synthesis AgNPs were capped with DOM (dissolved organic matter, in this case humic acid) and transferred to a glassy carbon electrode by sticking method for 30 minutes. The sticking coefficient and the stability of AgNPs at the GCE surface were optimized before the sensor was used for the atrazine detection. The applicability of the sensor was studied in river water samples with good recoveries values (96-109%). The analytical parameters like linear range and limit of detection obtained with the DOM/AgNPs/GC sensor are displayed in the table.

Annu and collaborators prepared a cellulose modified pencil graphite (PGE) sensor for the atrazine detection. For this purpose, the celullose was obtained by hydrolization from isolated plant at optimized conditions (temperature, time and H_2SO_4 concentration), then was dispersed in *N*,*N*-dimethylformamide, and after was drop-casted on the surface on the cleaned PGE and kept at the room temperature till the solvent evaporated and a stable film appeared. Electrochemical repsonse characteristics were obtained using SWV technique, the linear range was founded to be 5.0 – 360.0 ng/mL and the limit of detection was calculated to be 0.008 ng/mL. The sensor was evaluated in terms of accuracy, precision, reproducibility repetability and stability showing very good results. The applicability of the method was evaluated by the detection of atrazine from tap water with very good recovery values (98.3-99.1)[36].

A novel amperometric algae-based biosensor was designed by Attaallah et al, for the atrazine detection from river water. The green photosynthetic algae Chlamydomonas reinhardtii was immobilized on carbon black modified screen-printed electrodes in order to monitor the changes in algae oxygen evolution during the photosynthetic process. The decrease of oxygen evolution, that it is taking place in the presence of atrazine, produce a decrease of current signals by means of amperometric measurements, in an analyte concentration dependent manner. Atrazine was found to have a linear response in the domain 0.1 – 5 µM and a 1 nM limit of detection. The proposed sensor was tested for the detection of atrazine from river water obtaining good recovery values (96-107%) and also has proven to be stable during a 10 h period of work and as well as 3 weeks of storage [37].

Ahmed and his team succeded to develop an atrazine imprinted graphene-oxide composite-modified screen-printed electrode (AIRGOC-SPE) for the atrazine detection in

aqueous matrices[39]. As a first step, they prepared the imprinted reduced graphene oxide composite (AIRGOC): graphene oxide (GO) was obtained by the modified Hummer`s method[40], then reduced to RGO by the Amarnath method[41]. In the next stage they prepared a porous imprinted composite by modification of RGO with $[BMIM]BF_4$, an ionic liquid. In the final step, the imprinted composite was prepared as follows: a pre-polymerization complexation was done by the addition of a certain amount of atrazine to the $[BMIM]BF_4$ – modified graphene composite, and afterwards to this mixture was added a solution containing pyrrole, $FeCl_2$ and H_2O_2 and let them to polymerize. The final product was washed intensively with deionized water, followed by a mixture solution formed by methanol and acetic acid (9:1) until the complete discharge of ATZ from the composite. AIRGOC-SPE was prepared by coating the circular black dotted surface of the unmodified SPE with the newly prepared AIRGOC and then air dried at room temperature, after the optimization of the parameters like amount of the composite to be deposited, type of the binding reagent and also the ratio between AIRGOC and the binding agent. The sensor thus modified was evaluated for the atrazine detection using the SWV technique obtaining the following results (table 2). To demonstrate the applicability of the AIRGOC-SPE the authors determined Atrazine from sugarcane and river water samples. The results showed that the modified SPE are efficient in detecting ATZ in real samples (recovery values are in the 90 – 108 % range) [39].

Table 2. Parameters of the calibration curve for the detection of ATZ using AIIRGOC-SPE

Parameters	**Values**
Linear range (nM)	1.2 – 23
Linearity (r^2)	0.9999
Slope (µM/nM)	0.16
Intercept (µA)	6.8
LOD (nM)	0.4
LOQ (nM)	1.2

Durai and Badhulika[38] proposed for the detection of atrazine from blood samples a glassy carbon electrode modified with a lead-free double perovskite Al_2NiCoO_5 (ANCO). They presented for the first time the synthesis and morfology characterization by SEM, XRD, Raman and FTIR techniques of Al_2NiCoO_5 nanoflakes. The sensor was prepared with a simple drop-casting technique, after the synthesis of Al_2NiCoO_5. The improved sensing

ability of the ANCO/GCE it is due to the presence of electrocatalytic active sites with $Ni^{2+/}Ni^{3+}$ and $Co^{2+/}Co^{3+}$ redox couples at the octahedral sites of the Al_2NiCoO_5 nanoflakes. The performances of this sensor (table 1), and the fact that it succeded to detect atrazine in biological samples shows it can be a promising platform for a variety of bioanalytical applications.

3. Conclusions

We can conclude that in the last five years the domain of the environmental electrochemical methods knowed an active advancement, and several studies achieved low limits of detection and very good sensitivity regarding the atrazine detection. Different methods have been tested and applied to achieve this target: immobilizing antibodies at the electrode surface, molecular imprinting polymers, the modification of the electrode surfaces with nanomaterials or metal oxides nanofibers. A part of the reported sensors were not tested in real samples, where other possible interferences can be investigated for a proper and accurate analysis, and were investigated only in laboratory standards solutions. This it is an important parameter that will have to be taken into consideration in the future studies. Altough the electrochemical sensors presented here appear to promise a strong option for a reliable, fast, accurate, sensitive, selective and portable device for real field application.

References

1. The WHO recommended classification of pesticides by hazard and guidelines to classification. World Health Organization, Geneva, WHO. 2012.
2. K.R. Solomon, D.B. Baker, R.P. Richards, K.R. Dixon, S.J. Klaine, T.W. La Point, R.J. Kendall, C.P. Weisskopf, J.M. Giddings, J.P. Giesy, L.W. Hall Jr. and W.M. Williams, *Environ. Toxicol. Chem*., **15**, 31 (1996).
3. F.P. de Albuquerque, J.L. de Oliveira, V. Moschini-Carlos and L.F. Fraceto, *Sci. Total Environ*., **700**, 134868 (2020).
4. E.U. Commission Decision of 10 March 2004 concerning the non inclusion of atrazine in Annex I to Council Directive 91/414/EEC and the withdrawal of authorisations for plant protection products containing this active substance, EC 2004.
5. K. Nödler, T. Licha and D Voutsa, *Mar. Pollut. Bull*., **70**, 112 (2013).
6. F. Ackerman, *Int. J. Occup. Environ. Health*, **13**, 437 (2007).

7. World Health Organization. Guidelines for Drinking Water Quality, p. 1. Available: (11 jun. 2019). WHO, 2017

8. Australian Drinking Water Guidelines. Paper 6 National Water Quality Management Strategy. National Health and Medical Research Council, National Resource Management Ministerial Council, Common wealth of Australia, Canberra. NHMRC/NRMMC 2011.

9. United States Environmental Protection Agency. National Primary Drinking Water Regulations, USEPA, 2009.

10. IBAMA – Instituto Brasileiro do Meio Ambiente. Available: (21 jun. 2019).CONAMA, 2005. Resolução no 357, de 17 de março de 2005. Conselho Nacional do Meio Ambiente, Brasil, 2019.

11. T. Zhang, Z. Q, B. Li, and Z. Yang, *Food Analytical Methods*, **12**, 1179 (2019).

12. S.H. Guan, M.W. Huang, X. Li and Q. Cai, *Anal. Lett*., **51**, 613 (2018).

13. L. Jia, M.Su, X. Wu and H. Sun, *Journal of Separation Science*, **39**, 4512 (2016).

14. Huang, Y.; Shi, T.; Luo, X.; Xiong, H.; Min, F.; Chen, Y. *Food Chem*., **275**, 255 (2019).

15. Song, N.; Lee, J.Y.; Mansur, A.R.; Jang, H.W.; Lim, M.; Lee, Y. *Food Chem*., **298**, 125050 (2019).

16. J.S. Noori, J. Mortensen and Alemnew Geto, *Sensors*, **20**, 2221 (2020).

17. B. Perez-Fernandez, A. Costa-Garcia and A. de la Escosura-Muniz, *Biosensors*, **10**, 32 (2020).

18. Y. Guan, L. Liu, C. Chen, X. Kang and Q. Xie, *Talanta*, **160**, 125 (2016).

19. M. Medina-Sanchez, C.C. Mayorga-Martinez, T. Watanabe, T.A. Ivandini, Y. Honda, A. Nakata, A. Fujishima, Y. Einaga and A. Merkoci, *Biosens. Bioelectron*., **75**, 365 (2016).

20. T.T. Cao, V.C. Nguyen, H.B. Nguyen, H.T. Bui, T.T. Vu, N.H. Phan, B.T. Phan, L. Hoang, M. Bayle, M. Paillet, J.L. Sauvajol, N.M. Phan and D.L. Tran, *Adv. Nat. Sci.: Nanosci. Nanotechnol*., **7**, 035007 (2016).

21. N. Van Chuc, N.H. Binh, C.T. Thanh, N. Van Tu, N. Le Huy, N.T. Dzung, P.N. Minh, V.T. Thu, and T.D. Lam, *J. Mat. Sci. Technol.*, **32**, 539 (2016).

22. N.V. Chuc, C.T. Thanh, N.V. Tu, V.T.Q. Phuong, P.V. Thang, N.T.T. Tam, *J. Mater. Sci. Technol*., **31**, 479 (2015).

23. S.K. Bhardwaj, A.L. Sharma, K.-H. Kim and A. Deep, *Mater. Res. Express*, **4**, 125022 (2017).

24. Kardaș, M. Beytur, O. Akyildirim, H. Yuksek, M.L. Yola and N. Atar, *Journal of Molecular Liquids*, **248**, 360 (2017).

25. M. Yang, X. Zhao, S. Zheng, X. Liu, B. Jin, H. Li and Y. Gan, *Journal of Electroanalytical Chemistry*, **791**, 17 (2017).

26. M.L. Yola and N. Atar, *Ind. Eng. Chem. Res*., **56**, 7631 (2017).

27. A.L. Ahmad, N.F.C. Lah and S.C. Low, *Journal of Polymer Research*, **25**, 243 (2018).

28. A.L. Ahmad, N.F.C. Lah and S.C. Low, *Journal of Physical Science*, **29**, 33 (2018)

29. L. Madianos, E. Skotadis, G. Tsekenis, L. Patsiouras, M. Tsigkourakos and D. Tsoukalas, *Microelectronic Engineering*, **189**, 39 (2018).

30. K. Calfuman, J. Honores, M. Isaacs, D. Quezada, J. Valdebenito and M. Urzua, *Electroanalysis*, **31**, 671 (2019).

31. P. Supraja, S. Tripathy, S.R.K. Vanjari, V. Singh and S.G. Singh, *Sens. Actuat.B*, **285**, 317 (2019).

32. P. Supraja, S. Tripathy, S.R.K. Vanjari, V. Singh, S.G. Singh, *Biosens. Bioelectron*., **141**, 111441 (2019).

33. S. Tripathy, S.R. Krishna Vanjari, V. Singh, S. Swaminathan, and S.G. Singh, *Biosens. Bioelectron.*, **90**, 378 (2017).

34. P. Supraja, V. Singh, S.R.K. Vanjari and S.G. Singh, *Microsyst. Nanoeng***., 6**, 3 (2020).

35. M. Zahran, Z. Khalifa, M. A.-H. Zahran and M.A. Azzem, *ACS Applied Nano Materials*, **3**, 3868 (2020).

36. Annu, S. Sharma, A. Nitin and R. Jain, *Diamond and Related Materials*, **105**, 107788 (2020).

37. R. Attaallah, A. Antonacci, V. Mazzaracchio, D. Moscone, G. Palleschi, F. Arduini, A. Amine and V. Scognamiglio, *Biosens. Bioelectron*., **159**, 112203 (2020).

38. L. Durai and S. Badhulika, *Sensors and Actuators B*, **325**, 128792 (2020).

39. S. Ahmed, H. Shaikh, A. Solangi, J. Barek, Sirajuddin, A. Denizli and M.H. Agheem, *Monatsh. Chem.*, **151**, 1271 (2020).

40. L. Shahriary and A.A. Athawale, *Int. Journal of Renewable Energy Environ. Eng.*, **2**, 58 (2014).

41. C.A. Amarnath, C.E. Hong, N.H. Kim, B.C. Ku, T. Kuila and J.H. Lee, *Carbon*, **49**, 3497 (2011)

Review. Recent Trends on the Electrochemical Sensors Used for the Determination of Tartrazine and Sunset Yellow FCF from Food and Beverage Products

Abstract

Synthetic dyes were widely used in food industry due to their advantages such as good stability to oxygen, light and pH, reproducibility, bright color, low sensitivity to storage conditions and technological processing, and of course, low cost. Unfortunately, some of them have potential harmful effect to human health (the presence of azo group in the molecular structure of azo dyes has carcinogenic and mutagenic effects in the human health), thus, their detection in various food and beverage products became essential. Therefore, this review presents the latest development in sensors design used for the determination of two commonly used azo dyes – tartrazine and sunset yellow in real food and beverage samples, revealing that there is a variety of efficient sensors with low limits of detection, wide linear concentration ranges, high selectivities and sensitivities.

Introduction

Over the past centuries, food dyes have been used in foods and beverages due to their unique characteristics such as color return during processing, improving food color and uniformity of the color of the resulted produce.[1] The food dyes are categorized into natural and synthetic. The majority of natural dyes are extracted from plant sources like β-carotene, betanin, anthocyanins and chlorophyll, while other dyes such as carmine come from animal sources. [1,2] However, these natural dyes are easily to degrade, more sensitive to temperature, light, pH and are very expensive.[3] Therefore, synthetic food dyes are widely used in food industry due to their high stability to oxygen, light, pH, and due to the fact they are more reproducible and have brighter color, lower sensitivity to storage conditions and technological processing, and also lower cost.[2,4] The largest group of synthetic food dyes is the azo dyes. The most used azo dyes in food industry are yellow dyes (tartrazine and sunset yellow) and red dyes (amaranth, allura red and others).[2] They contain the azo group (─N═N─) as the chromophore and ─OH group on aromatic ring in their chemical structure.[2]

Due to their widespread use, a number of negative effects on human health have been identified.[2]

In recent years, numerous teams of researchers have centered their attention on developing and improving of more sensitive and more fast electrochemical methods for the determination of tartrazine and sunset yellow FCF in food, beverage, pharmaceutical,[5-7] water[8,9] and cosmetics samples.[10] The electrochemical techniques are based on the preparation of sensors or biosensors and can determine the following parameters, such as: the intensity of the current throughout the electrochemical cell (amperometry or voltammetry), the potential of the electrode (potentiometry), the resistance and time needed for the development of the electrode (electrical conductance), the quantity of electricity entering the cell (coulometry), and the opposition force to electric current in a circuit (electrochemical impedance spectroscopy). Among the methods mentioned above, the voltammetric techniques are mostly utilized for the determination of tartrazine and sunset yellow, respectively, from food and beverage samples. The types of voltammetric methods used can be: cyclic voltammetry (CV), square-wave voltammetry (SWV), differential pulse voltammetry (DPV), and linear sweep voltammetry (LSV).

This review is focused on the most recent research papers (up to five years old) regarding electrochemical sensors used for the detection of tartrazine and sunset yellow FCF from food and beverage products.

Electrochemical sensors used for the determination of tartrazine

Tartrazine (Tz) is a synthetic organic food dye,[11,12] water soluble, orange-colored used in various food products (such as soft drinks, candies, cakes, soups and other products), pharmaceutical, textiles and cosmetics.[1] Tartrazine is one of the most frequently used synthetic azo-dyes in the world. The IUPAC name of tartrazine is trisodium 5-hydroxy-1-(4-sulfonatophenyl)-4-[(*E*)-(4-sulfonatophenyl)diazenyl]-1*H*-pyrazole-3 carboxylate. It is also known as Food Yellow No. 4 with European Community (EC) number E 102 and as Food Drug & Cosmetic (FD&C) Yellow No. 5, C.I. No. 19140.[1]

The presence of the azo group in the molecular structure of tartrazine (Fig. 1) has carcinogenic and mutagenic effects in the human health.[13] Thus, many studies reported that high concentration levels of tartrazine can be harmful to health and can cause various diseases like cancer, asthma, allergies, childhood hyperactivity and dermal toxicity.[13-15] The acceptable daily intake (ADI) of tartrazine has been established at 7.5 mg kg^{-1} body weight

per day by Joint United Nations Food and Agricultural Organization (FAO) and World Health Organization (WHO) Expert Committee on Food Additive (JECFA), and EU Scientific Committee for Food (SCF). In soft drinks, the maximum content of tartrazine should not exceed 0.01 g mL^{-1}.[1] In conclusion, it is very important to detect the tartrazine level in food and beverages for improving food safety in the world.

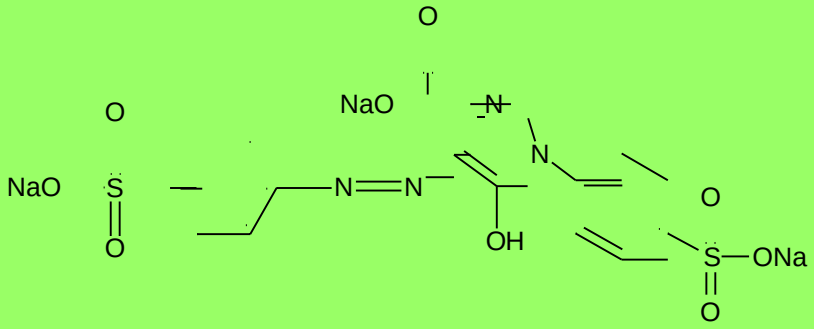

Figure 1. Chemical structure of tartrazine.

Numerous analytical methods have been reported for the determination of tartrazine including capillary electrophoresis (CE),[12,16] high performance liquid chromatography (HPLC),[17-20] thin layer chromatography (TLC)[21,22] and spectrophotometry.[23,24] Although these methods are used with high accuracy, most of them are expensive, complicated and have long testing time.[25,26] Nevertheless, electrochemical methods are more promising due to their simplicity, good sensitivity, high selectivity, low cost, easy sample preparation and short analysis time.[2,26]

Lately, the electrochemical determination of tartrazine in food and beverage products has been performed using different types of modified electrodes (Table I). The chemically modified electrodes represent a future trend in analytical chemistry.[2]

Rovina et al.[1] published a comprehensive review about different analytical methods for the detection of tartrazine that could be useful for regulatory authorities and food analysts to control and check the tartrazine level in food and beverage products. Also, Lipskikh et al.[2] in their review article presented the comparison of the electrochemical sensors and measuring protocols by voltammetric determination of most commonly used azo dyes in food.

Table I. Electrochemical sensors used for the detection of tartrazine in food and beverage products.

Sensor	Method	Linear range (μmol L^{-1})	Limit of detection (μmol L^{-1})	Sample	Ref.
g-C_3N_4/PGE	DPV	0.1 – 10.0	0.21	saffron fake powder	13
Gr/PLPA/PGE	DPV	2 – 100	1.54	orange juice	14
N-PC-G/CS/GCE	DPV	0.05 – 15.00	0.036	soft drink	15
MIP-PmDB/PoPD-GCE	DPV	0.005 – 1.1	0.0035	soft drink	25
PEDOT@TbHCF/GCE	DPV	0.1 – 206 .0	0.032	soft drink, chips, candy and jelly	26
PTH/MWCNT-G/GCE	SWV	1 – 100 250 – 450	0.25 0.303	soft drink	27
N-grap/Graphite	SWV	2.0 – 50.0	0.02	commercial sport drink	28
CHIT/GO/MWCNTs/AuNPs/ GCE	DPV	0.02 – 0.19	0.003	candy, jelly and soft drinks	29
PGMCPE	CV	1 – 27 35 – 87	0.28	candy and soft drink	30
PLA-ERGO/GCE	DPV	1 – 250	0.25	carbonated beverage and fruit juice	31
MIP/MWCNTs/GCE	DPV	0.08 – 1.00 1 – 10	0.027	fanta, milk flavored and pineapple grain drink	32
Pp-ABSA/ZnO NPs-CPE	DPV	0.0349 – 1.246 1.246 – 5.440	0.08	orange powder and coolak drink	33
Co_C/CPE	SWV	0.12 – 3.00	0.3	flavored gelatin powder	34
Au/(AuNPs-PAH/NiTsPc)$_5$	DPV	0 – 3 4 – 9	0.055 0.122	juice	35
SDSMCPE	DPV	20 – 50 60 – 110	5.2	lemon yellow powder	36
Microspheres-laccase/AuNPs/SPE	DPV	0.2 – 14.0	0.04	candy coated chocolate and mango juice	37
TiO_2-ErGO-GCE	SDLSV	0.02 – 20.00	0.008	carbonated beverage	38

g-C_3N_4/PGE – graphitic carbon nitride/ graphite pencil electrode;
Gr/PLPA/PGE – graphene/ poly(L-phenylalanine) modified pencil graphite electrode;
N-PC-G/CS/GCE – N-doped graphene natively grown on hierarchical porous carbon nanocomposite/ chitosan/ glassy carbon electrode;
MIP-PmDB/PoPD-GCE – molecularly imprinted copolymer-m-dihydroxybenzene/ o-phenylenediamine modified glassy carbon electrode;

PEDOT@TbHCF/GCE – poly(3,4-ethylenedioxythiophene)@terbium hexacyanoferrate composite/ glassy carbon electrode.
PTH/MWCNT-G/GCE – polythiophene/ multi-walled carbon nanotube-graphene/ glassy carbon electrode;
N-grap/Graphite – colorless nail polish film/ graphite;
CHIT/GO/MWCNTs/AuNPs/GCE – chitosan/ graphene oxide/ multi-walled carbon nanotubes/ gold nanoparticles/ glassy carbon electrode;
PGMCPE – poly (glycine) modified carbon paste electrode;
PLA-ERGO/GCE – poly(L-arginine)-electrochemically reduced graphene oxide modified glassy carbon electrode;
MIP/MWCNTs/GCE – molecularly imprinted polymer/ multi-walled carbon nanotubes/ glassy carbon electrode;
Pp-ABSA/ZnO NPs-CPE – poly (p-aminobenzenesulfonic acid)/ zinc oxide nanoparticles – carbon paste electrode;
Co$_C$/CPE – carbon paste electrode decorated with cobalt complex microcomposite;
Au/(AuNPs-PAH/NiTsPc)$_5$ – nickel (II) phthalocyanine-tetrasulfonic-Au nanoparticles nanocomposite film;
SDSMCPE – sodium dodecyl sulfate modified carbon paste electrode;
Microspheres-laccase/AuNPs/SPE – laccase conjugated microspheres/ gold nanoparticles coated on a carbon-paste screen-printed electrode;
TiO$_2$-ErGO-GCE – TiO_2-electrochemically reduced graphene oxide composite modified glassy carbon electrode;
SDLSV – second-order derivative linear scan voltammetry;

Karimi et al.[13] proposed a sensitive sensor for the electrochemical detection of tartrazine in food samples built on graphite pencil electrode modified with graphitic carbon nitride (g-C_3N_4) which was synthesized by direct pyrolysis of the melamine. The researchers investigated first the electrochemical activity of Tz using the CV and DPV. The Tz concentration range covered was from 0.1 – 10.0 µmol L^{-1} with a limit of detection of 0.21 µmol L^{-1} obtained under optimal conditions. The proposed sensor showed good stability and reproducibility with relative standard deviation (RSD) value of 2.5%. The g-C_3N_4/graphite pencil electrode was successfully used to detect Tz levels from two saffron fake powder samples.[13]

Tahtaisleyen et al.[14] developed a sensor platform for the tartrazine detection, using graphene and poly(L-phenylalanine) which were connected to the surface of the pencil graphite electrode. By differential pulse voltammetry, the tartrazine exhibited a limit of detection of 1.54 µmol L^{-1} and oxidation peak currents in the linear concentration range between 2 and 100 µmol L^{-1}. The modified sensor showed satisfactory results for the determination of tartrazine in orange juice samples. A recovery percentage in the range of 98.71% and 104.44% was obtained.[14]

For the determination of tartrazine, An et al.[15] described a novel electrochemical sensor platform based on chitosan (CS) and N-doped graphene natively grown on hierarchical porous carbon (N-PC-G) nanocomposite. The proposed sensor showed a linear current response for the electrochemical oxidation of tartrazine in the range between 0.05 – 15.00 μmol L^{-1} with a lower detection limit of 0.036 μmol L^{-1}, obtained in optimal experimental conditions. Moreover, the prepared electrode also exhibited a good sensitivity and selectivity towards the oxidation of Tz. The applicability of N-PC-G/CS/GCE was tested in soft drinks in order to check the effectiveness of the sensor.[15]

Zhao et al.[25] developed for the first time a novel sensor based on molecularly imprinted copolymers (MIPs) used for direct and rapid analysis of tartrazine. The MIPs were immobilized directly on the surface of the glassy carbon electrode (GCE) by electrochemical polymerization of m-dihydroxybenzene (m-DB) and o-phenylenediamine (o-PD) used as monomers. The linear relation between the Tz concentration and the peak current signal was from 0.005 – 1.1 μmol L^{-1} and with a limit of detection of 0.0035 μmol L^{-1}. The selectivity of the developed electrode was investigated using six types of interfering species which revealed no significant difference in the peak current for the detection of Tz. The proposed sensor displayed many advantages, like good stability, high sensitivity, is cheap and offers the opportunity of in-situ examination. The MIP-PmDB/PoPD-GCE sensor was able to determine Tz in soft drinks without sample pretreatment. In order to study the accuracy of this modified electrode, the content of Tz was also determined by HPLC. The results obtained by the developed sensor were comparable with those obtained by HPLC, indicating that the MIP-PmDB/PoPD-GCE sensor was feasible and accurate.[25]

Sakthivel and co-workers[26] proposed an electrochemical method for the fabrication of poly(3,4-ethylenedioxythiophene) (PEDOT)@Terbium hexacyanoferrate (TbHCF) composite onto glassy carbon electrode for sensitive detection of tatrazine. Their results are detailed in Fig. 2.[26] The PEDOT@TbHCF composite was investigated by scanning electron microscopy (SEM), energy dispersive X-ray spectroscopy (EDX), X-ray diffraction (XRD), Fourier transformed infrared spectra (FT-IR), EIS and Raman Spectroscopy. The electrochemical behavior of Tz was tested using CV and DPV. The proposed sensor exhibited good electrocatalytic activity towards the detection of Tz. The developed sensor exhibited wide linear concentration range between 0.1 – 206.0 μmol L^{-1} and high sensitivity. The limit of detection was 0.032 μmol L^{-1}. Different food samples such as soft drink, chips, candy and

jelly were used for the practical applicability of the developed sensor and satisfactory recoveries were obtained for tartrazine detection.[26]

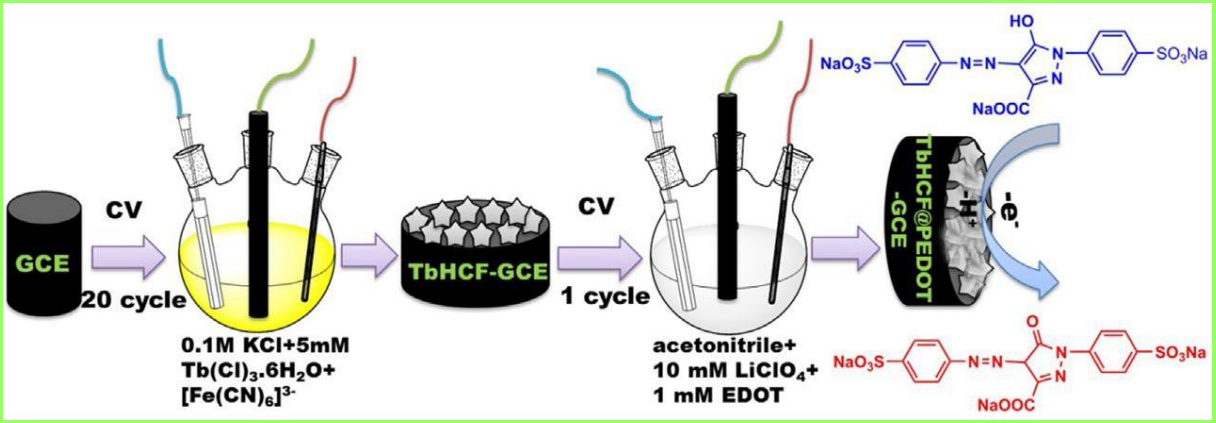

(A)

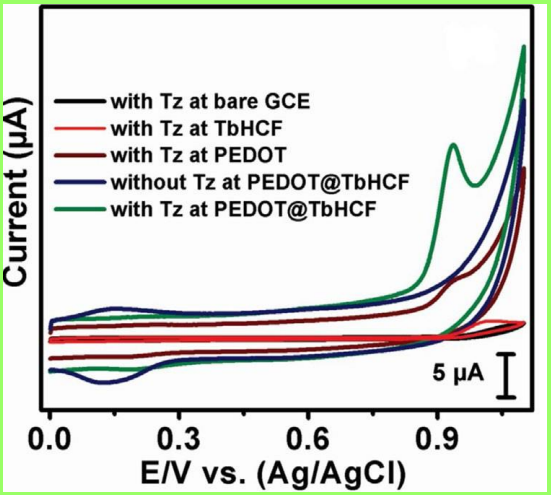

(B)

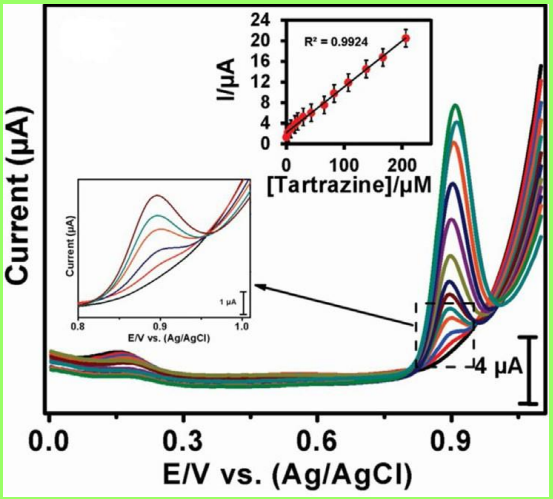

(C)

Figure 2. (A) Schematic representation of the PEDOT@TbHCF/GCE sensor preparation process and the redox mechanism for the electrooxidation of Tz; **(B)** CVs of bare GCE, TbHCF/GCE, PEDOT/GCE and TbHCF@PEDOT/GCE with and without presence of Tz (99 µmol L^{-1}) in N_2 saturated 0.05 mol L^{-1} PBS (pH 5), scan rate of 50 mV s^{-1}; **(C)** DPVs of TbHCF@PEDOT/GCE in N_2 saturated PBS (pH 5) containing different concentrations of Tz from 0.1 µmol L^{-1} to 206 µmol L^{-1}.[26]

AL-Refai et al.[27] described a selective and sensitive voltammetric sensor for the detection of tartrazine based on polythiophene nanocomposite and mixed multi-walled carbon nanotube - graphene (PTH/MWCNT-G) which was obtained by chemical oxidative polymerization. The PTH/MWCNT-G was characterization using the FT-IR and XRD and

the morphology was investigated by SEM, transmission electron microscope (TEM) and energy dispersive X-ray analyses. Under optimum conditions, the effect of the scan rate suggested that the electrochemical oxidation of Tz on the surface of the proposed sensor was irreversible with diffusion process. The electrocatalytic behavior of the developed sensor was examined by square wave voltammetry (SWV), and the results exhibited two linear ranges: 1 – 100 µmol L^{-1} and 250 – 450 µmol L^{-1}. The detection limit was 0.25 µmol L^{-1} and 0.303 µmol L^{-1}, respectively. The modified electrode also showed a good stability and reproducibility. For the evaluation of the practical application, soft drink samples were spiked with various concentrations of Tz, and the recovery rates in the ranges 97.87% – 106.7% were obtained.[27]

Lima et al.[28] proposed a new method to prepare a disposable and low-cost electrochemical device based on graphite and colorless nail polish (N-grap) as presented in Fig. 3[28] for the determination of tartrazine by square-wave voltammetry. Scanning electron microscopy indicated that the N-grap composite electrode showed high porosity. For the electrochemically characterization of the electrode the authors used cyclic voltammetry and electrochemical impedance spectroscopy methods. The linear range of the developed sensor was 2.0 – 50.0 µmol L^{-1} with a LOD of 0.02 µmol L^{-1}. The N-grap device was successfully applied for the detection of Tz in sports drinks samples. The obtained outcomes were comparable with those obtained by the UV-Vis technique suggesting the accuracy of the developed method.[28]

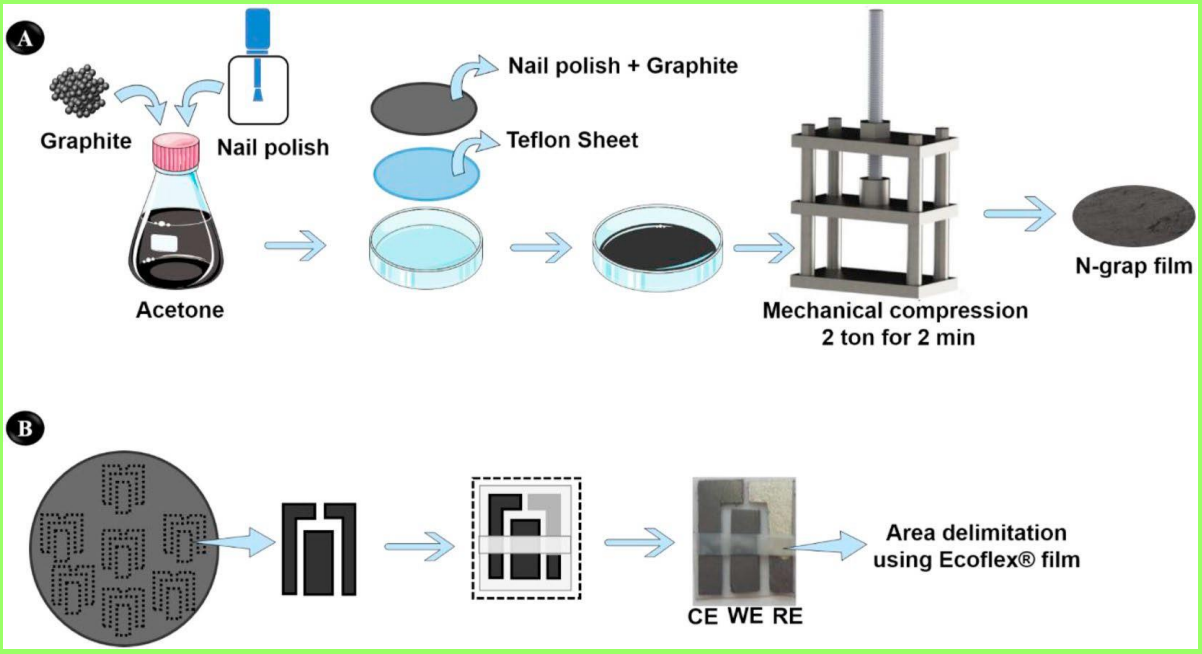

Figure 3. Overall illustration of the N-grap device preparation procedure.[28]

In 2021, Rovina and co-workers[29] used an electrochemical sensor based on glassy carbon electrode (GCE) modified with chitosan (CHIT), graphene oxide (GO), multi-walled carbon nanotubes (MWCNTs) and gold nanoparticles (AuNPs) for the tartrazine determination. Using the DPV, the anodic peak currents linearly depended on Tz concentrations in the range 0.02 – 0.19 μmol L^{-1}, with a limit of detection of 0.003 μmol L^{-1}. The CHIT/GO/MWCNTs/AuNPs/GCE presents good stability, an acceptable reproducibility, a high selectivity and it was successfully used for the determination of the Tz in different commercial food products. The levels of Tz in food samples were also analyzed by HPLC method. The outcomes obtained by both methods were in good agreement.[29]

In the paper of Manjunatha[30] a sensor based on CPE modified with poly (glycine) was developed for the detection of tartrazine. The CV and DPV methods were used to test the electrochemical behavior of Tz on the sensor surface. The obtained outcomes demonstrated that the polymer film on the electrode presented a good electrocatalytic activity for the oxidation of Tz in phosphate buffer solution (PBS) pH = 7.0. The proposed sensor displayed two linear concentration ranges 1 – 27 μmol L^{-1} and 35 – 87 μmol L^{-1} with a detection limit of 0.28 μmol L^{-1} and a quantification limit of 0.94 μmol L^{-1}. The practical applicability of the PGMCPE for the determination of Tz in various food samples such as candy and soft drink was investigated. The recovery rate for the two samples was 94.5% and 98.2%, respectively, and RSD value was lower than 1.0%. These results demonstrated the good accuracy of the proposed method.[30]

Wang and co-authors[31] reported a rapid electrochemical method for the determination of tartrazine in carbonated beverage and fruit juice samples, using GCE modified with poly(L-arginine)-electrochemically reduced graphene oxide. The modified electrode exhibited a higher oxidation peak than that of the unmodified electrode due to increased electrochemical active surface area and conductivity. The anodic peak current showed a linear relation against Tz concentration in the range of 1 – 250 μmol L^{-1} with a limit of detection of 0.25 μmol L^{-1}. The selectivity of the sensor was examined using the influence of different interfering species on the detection of Tz. The results indicated that the sensor presented a good selectivity. The proposed method was successfully applied for to detection Tz in carbonated beverage and fruit juice samples and the obtained recovery values were between 98.2% and 99.6%.[31]

Wang et al.[32] prepared a sensitive electrochemical sensor based on glassy carbon electrode modified with multi-walled carbon nanotubes and molecularly imprinted polymer (MIP) film for the determination of tartrazine. The MIP was used in the construction of the

sensor due its advantages like high selectivity, low cost and simple operation. The performance of the modified electrode was analyzed by CV, electrochemical impedance spectroscopy and DPV. The results indicated that the MIP film enhanced the electrochemical response for the detection of Tz. The DPV study showed a limit of detection of 0.027 μmol L^{-1} (S/N = 3) for tartrazine with two linear concentration ranges between 0.08 – 1.00 μmol L^{-1} and 1 – 10 μmol L^{-1}. The MIP/MWCNTs/GCE exhibited good selectivity towards electrochemical oxidation of Tz. The proposed sensor was successfully applied to determine Tz in different soft drinks. The recovery rate was between 94.8% and 101.9% with RSD value less than 4.5%, demonstrating the accuracy of the proposed method.[32]

For the electrochemical determination of tartrazine in soft drinks, a carbon paste electrode modified with zinc oxide nanoparticles (ZnO NPs) and p-aminobenzenesulfonic acid (p-ABSA) was developed by Karim-Nezhad and collaborators.[33] The results are presented in Fig. 4.[33] The modified electrode showed a good electrocatalytic activity on Tz oxidation by obtaining much higher peak currents. The anodic peak current exhibited two linear relations against Tz concentration in the ranges of 0.0349 – 1.246 μmol L^{-1} and 1.246 – 5.440 μmol L^{-1}, with a detection limit of 0.08 μmol L^{-1} and a good sensitivity of 2.2034 μA/μmol L^{-1}. The proposed sensor was able to detect Tz in some soft drinks and orange powder. The contents of Tz were investigated by standard addition method. The authors demonstrated the accuracy of their method by HPLC technique.[33]

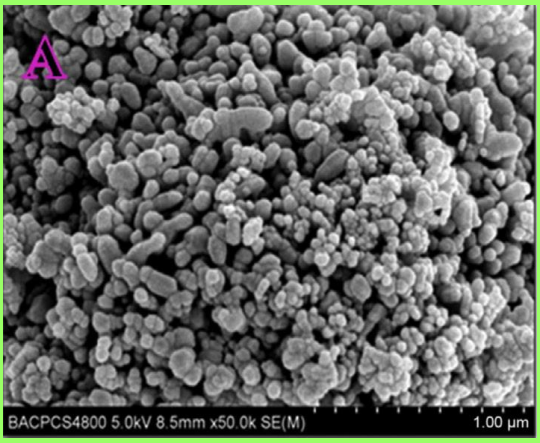

(A)

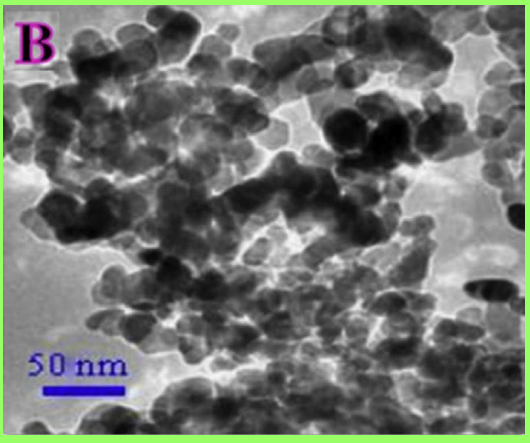

(B)

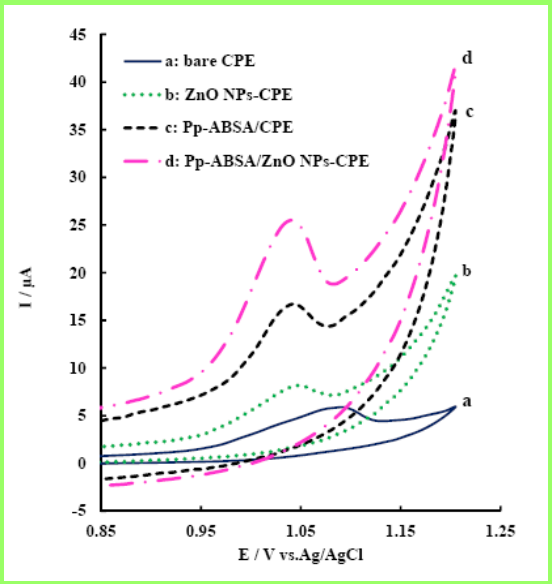

(C)

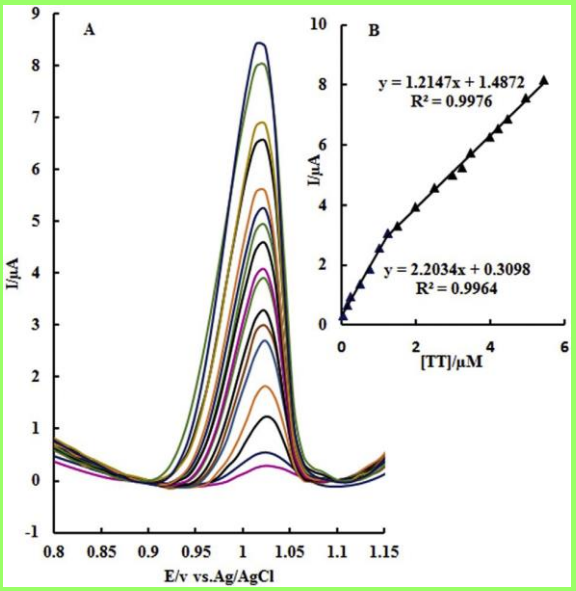

(D)

Figure 4. (A) SEM image of zinc oxide nanopaticles; **(B)** TEM image of zinc oxide nanopaticles; **(C)** CVs recorded with bare CPE (curve a), ZnO NPs-CPE (curve b), Pp-ABSA/CPE (curve c) and Pp-ABSA/ZnO NPs-CPE (curve d) in 0.1 mol L^{-1} PBS (pH 3.0) and 5.98 µmol L^{-1} tartrazine; **(D)** Differential pulse voltammograms of Pp-ABSA/ZnO NPs-CPE in 0.1 mol L^{-1} PBS (pH 3.0) containing different concentration of tartrazine. Inset: the concentration calibration curve for tartrazine.[33]

Penagos-Llanos et al.[34] described a sensitive, simple and cheap sensor based on carbon paste modified with cobalt complex microcomposite (Co_C) for the simultaneous determination of pairs of synthetic food dyes: tartrazine-sunset yellow (Tz-SY) and tatrazine- allura red (Tz-AR). The electrochemical characterization of the carbon paste electrode decorated with Co complex was investigated by EIS. The obtained results demonstrated that the modification of CPE with Co complex was successfully performed and that the applied method is efficient in increasing both the electrochemical signal and the electrical conductivity of the electrode. The linear concentration range and the limit of detection of Tz was 0.12 – 3.00 µmol L^{-1} and 0.3 µmol L^{-1}, respectively. The reproducibility of the modified CPE was tested by successive measurements (n = 6) using two sensors for a period of 3 days. The validation of the method was achieved for a standard of unflavored gelatin spiked with different concentrations of Tz-SY and Tz-AR and indicated a recovery rate more than 90%.[34]

In 2020, Lima et al.[35] used gold nanoparticles (AuNPs) and nickel(II)-phthalocyanine-tetrasulfonic (NiTsPc) for the electrochemical sensing of tartrazine by DPV. The Layer-by-

Layer (LBL) film was prepared using the Au-(AuNPs-PAH/NiTsPc)$_5$ architecture. The analytical signal for the anodic peak current and Tz concentrations were obtained in two linear ranges between 0 – 3 μmol L^{-1} and 4 – 9 μmol L^{-1}, respectively. The limit of detection was 0.055 μmol L^{-1} for the first linear concentration range and 0.122 μmol L^{-1} for the second linear concentration range. The selectivity study of the sensor was examined in the presence of various interfering substances, indicating that these foreign species didn't interfere in the detection of tartrazine. The Au/(AuNPs-PAH/NiTsPc)$_5$ electrode was utilized for the Tz detection in juice samples with recoveries between 97.74% and 108.26%.[35]

Raril and Manjunatha[36] prepared a sensor based on CPE modified with sodium dodecyl sulfate for the determination of tartrazine. The modified electrode showed a significantly improvement of the electrocatalytic activity compared to the unmodified electrode. The sensor was employed for the electrochemical determination of Tz, indicating two linear ranges between 20 – 50 μmol L^{-1} and 60 – 110 μmol L^{-1}. The limit of detection was 5.2 μmol L^{-1}. The SDSMCPE exhibited a good sensitivity, selectivity, acceptable stability and repeatability. The recovery study carried out in lemon yellow powder sample showed good recovery, ranging from 91.1% to 104%.[36]

In the research performed by Mazlan et al.,[37] a new biosensor was developed for the first time by modifying a screen-printed electrode (SPE) with laccase enzyme and gold nanoparticles for the detection of tartrazine. This biosensor is based on the immobilization of laccase enzyme on poly(glycidyl methacrylate-co-n-butyl acrylate) (poly(GMA-co-nBA)) microspheres. The anodic peak current exhibited a linear relationship against Tz concentration in the range of 0.2 – 14.0 μmol L^{-1} with a LOD of 0.04 μmol L^{-1}. The microspheres-laccase/AuNPs/SPE was evaluated for the detection of Tz in drink and food samples. The recovery percentage was between 94.75% and 108.00% and RSD% was smaller than 5%. The results exhibited that the biosensor method had a good correlation with the HPLC method suggesting that the proposed material was reliable and validated.[37]

He et al.[38] used TiO_2 reduced graphene oxide composite in order to modify a glassy carbon electrode obtained by hydrothermal and electrochemical reduction for the determination of tartrazine. The morphology of the synthesized materials was analyzed by TEM and XRD. After the sensor was electrochemically modified, the oxidation peak current on the surface of electrode increased. The electrochemical results demonstrated that the oxidation of Tz was an adsorption-controlled process involving one proton and one electron. The TiO_2-ErGO-GCE sensor detected Tz in a wide range (0.02 – 20.00 μmol L^{-1}) and reached

a LOD of 0.008 μmol L^{-1}. Thus, the modified GCE was successfully applied to detect tartrazine from carbonated beverage.[38]

Electrochemical sensors used for the determination of Sunset Yellow FCF

Sunset Yellow (SY) (Fig. 5.) is a synthetic food dye, an orange-red colored powder and is soluble in water. This azo-dye is found in cosmetics, drugs and food industry field due to its advantages such as improving the color, texture and appearance of products.[5,39] It is one of the most commonly synthetic dyes used in food and beverage products under the trade name E110.[40] Sunset Yellow is also known as Orange Yellow S and CI Food Yellow 3, INS No.110 according to Joint FAO/WHO Expert Committee on Food Additives (JECFA). The chemical name of sunset yellow is disodium 2-hydroxy-1-(4- sulphonatophenylazo)naphthalene-6-sulphonate.[39]

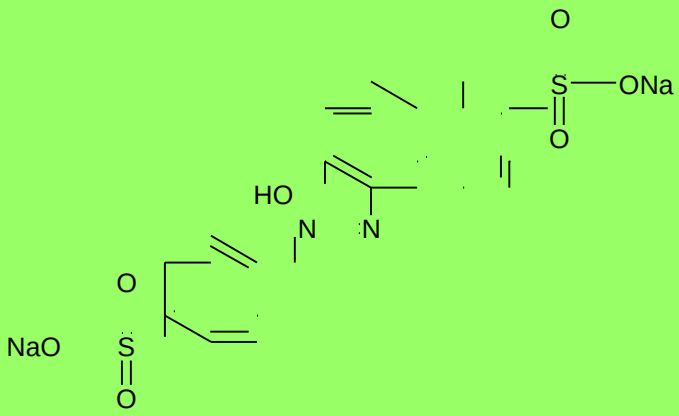

Figure 5. Chemical structure of Sunset Yellow FCF.

Many studies have reported that the excessive consumption of sunset yellow could cause some adverse effects on human health including asthmatic reaction, allergies, diarrhea, eczema and anxiety.[5,41,42] Therefore, the use of sunset yellow in food, beverage and pharmaceutical products should be strictly verified. The maximum value of acceptable daily intake (ADI) for sunset yellow was established at 2.5 mg/kg body weight. However, some countries have allowed a maximum value of 100 μg mL^{-1} of SY in soft drinks.[5,42]

Thus, for the assurance of consumer health from the whole world, it is very important to determine Sunset Yellow content in food and beverage products by developing a simple, fast and cheap analytical technique. Up to now, numerous analytical methods such as high performance liquid chromatography,[43,44] spectrophotometry,[45,46] capillary electrophoresis,[47] fluorescence,[48] and electrochemical methods have been developed for the detection of sunset yellow, but many of these electrochemical methods have especially attracted attention due to

their simplicity, rapidity, high sensitivity, selectivity, low cost, good handling and short testing time.

In recent years, different types of electrochemical sensors were developed as shown below in Table II based on glassy carbon electrodes, carbon paste electrodes, screen-printed carbon electrodes and pencil graphite electrodes which were modified with novel materials for the electrochemical sensing of sunset yellow from food and beverage samples. From this table it can be seen that the linear concentration ranges of electrochemical sensors were very wide. Until now, every year novel materials, substances, and their combinations have been used for the development of new, reliable, sensitive, and selective sensors for electrochemical determination of sunset yellow.

Table II. Electrochemical sensors used for the detection of sunset yellow in food and beverage products.

Sensor	Method	Linear range (μmol L^{-1})	Limit of detection (μmol L^{-1})	Sample	Ref.
Dy_2O_3NPs/MWCNTs/GCE	SWV	0.001 – 0.140	0.00035	powder aromatic drink	5
ZnO-Pd/[C4mim]-[PF6]/PE	LSW	0.001 – 280	0.0004	orange juice and fruit juice	9
IL/$NiFe_2O_4$/rGO/CPE	DPV	0.05 – 30.00 30 – 500	0.03	orange juice powder	10
ERGO/GCE	DPV	0.05 – 1.00	0.0192	soft drinks	40
GO/AgNPs–MIPs/GCE	CV	0.1 – 0.6 0.6 – 12.0	0.02	soft drinks	41
rGO-g-CN/ZnO-AuNPs/GCE	SWV	0.005 – 0.085	0.0013	candy, fruit juice and red wine	42
SiO_2@MIP-PDA/CPE	DPV	0.0045 – 9.1	0.0015	fanta, orange flavored candy, orange flavored jelly powder, cheese snack and orange juice	49
EGO-PGE	DPV	0.5 – 10.0	0.057	orange juice	50
GCE/MWCNT@MIP-PDA	DPV	0.0022 – 4.64	0.0014	jelly, fanta, mirinda, chocolate, instant juice powder, ice cream and candy	51
AuNPs/PANI-co-PoAN-co-PoT/GO/Au elctrode	SWV	5 – 500	0.0142	candy, instant juice powder and soft drink	52

PDDA-Gr-Pd/GCE	DPV	0.01 – 10.0	0.002	soft drinks	53
GO/MWCNTs/GCE	LSW	0.09 – 8.00	0.025	orange juice	54
ZnO/Cysteic acid/GCE	DPV	0.1 – 3.0	0.03	soft drinks and peach gelatin	55
rGO/CPE	DPV	0.05 – 10.00	0.027	fanta, mirinda, cheese snack and cheetoz	56
CHIT/GO/MWCNTs/AuNPs/ GCE	DPV	0.02 – 0.2	0.0001	candy, jelly and soft drinks	57
PLC/PGE	DPV	1 – 1000	0.125	cake, jelly, orange juice and mixed fruit juice	58
Au-Pd-RGO/GCE	DPV	0.69 – 331.00	0.0015	soft drinks	59
ERGO-AuNRs/GCE	DPV	0.01 – 3.00	0.0024	orange juice, orange soda and jelly	60
PDDA-Gr-(Pt-Cu)/GCE	DPV	0.02 – 10.00	0.006	soft drinks	61
PDDA-Gr-(Pd-Pt)/GCE		0.02 – 10.00	0.004		
PDDA-Gr-(Co-Ni)/GCE		0.008 – 10.00	0.002		
Fe_3O_4–MWCNTs/GCE	DPV	0.2 – 3.5	0.0014	soft drinks	62
M-NCS/GCE	SWV	0.001 – 2.5	0.00095	mirinda, sports drink, candy and chocolate	63
GC/EGr-1	LSV	6 – 100	1.8	orange juice	64
GC/EGr-2		1 – 100	0.3		
rGO/NiBTC/SPCE	DPV	0.05 – 5.0	0.025	orange sport drink and yellow sport drink	65
ZnONF/CPE	SWV	0.001 – 0.022 0.022 – 0.154	0.0002	soft drinks	66
MIP/f-MWCNTs/GCE	DPV	0.05 – 100.00	0.005	candy, candy coated chocolate, orange flavored jelly powder, peach juice powder and beverage	67
Sparked Mo-SPE	DPV	0.005 – 0.25	0.002	orange sweetie and cocktail Margarita	68
MGO/*β*-CD/IL/AuNPs/GCE	DPV	0.005 – 2.000	0.002	minute maid and mirinda drink	69
ZnO/RGO/ZnO@Zn	DPV	0.01 – 5.00	0.003	soft drinks	70

Dy_2O_3NPs/MWCNTs/GCE – dysprosium oxide nanoparticles/ multi-walled carbon nanotubes / glassy carbon electrode;

ZnO-Pd/[C4mim]-[PF6]/PE – zinc oxide nanoparticles doped with palladium/ 1-butyl-3-methylimidazolium hexafluoro phosphate/ paste electrode;

IL/$NiFe_2O_4$/rGO/CPE – ionic liquid/ $NiFe_2O_4$/ reduced graphene oxide/ carbon paste electrode;
ERGO/GCE – exfoliated graphene oxide onto a glassy carbon electrode; **GO/AgNPs–MIPs/GCE** – graphene oxide decorated with silver nanoparticles–molecular imprinted polymers/ glassy carbon electrode;
rGO-g-CN/ZnO-AuNPs/GCE – reduced graphene oxide-graphitic carbon nitride/ ZnO-Au nanoparticles/ glassy carbon electrode;
SiO_2@MIP-PDA/CPE – molecular imprinted polydopamine-coated silica nanoparticles/ carbon paste electrode;
EGO-PGE – electrochemically prepared graphene oxide-pencil graphite electrode;
GCE/MWCNT@MIP-PDA – glassy carbon electrode/ molecularly imprinted polydopamine-coated multi-walled carbon nanotubes;
AuNPs/PANI-co-PoAN-co-PoT/GO/Au electrode – gold nanoparticles/ poly(aniline-co-o-anisidine-co-o-toluidine)/graphene oxide nanocomposite/ gold electrode;
PDDA-Gr-Pd/ GCE – poly (diallyldimethylammonium chloride)-dispersed graphene and palladium nanoparticle composite/ glassy carbon electrode;
GO/MWCNTs/GCE – graphene oxide/ multi-walled carbon nanotubes/ glassy carbon electrode;
ZnO/Cysteic acid/GCE – ZnO/ cysteic acid/ glassy carbon electrode;
rGO/CPE – reduced graphene oxide/ carbon paste electrode;
CHIT/GO/MWCNTs/AuNPs/GCE – chitosan/ graphene/ multiwall carbon nanotubes/ gold nanoparticles/ glassy carbon electrode;
PLC/PGE – poly(L-cysteine) modified pencil graphite electrode;
Au-Pd-RGO/GCE – Au-Pd-reduced graphene oxide nanocomposites modified glassy carbon electrode;
ERGO-AuNRs/GCE – nanohybrid of gold nanorods decorated graphene oxide nanosheets/ glassy carbon electrode;
PDDA-Gr-(Pd-Pt)/GCE – poly(diallyldimethylammonium chloride)-dispersed graphene -(Pd-Pt)/ glassy carbon electrode;
PDDA-Gr-(Pt-Cu)/GCE – poly(diallyldimethylammonium chloride)-dispersed graphene -(Pt-Cu)/ glassy carbon electrode;
PDDA-Gr-(Co-Ni)/GCE – poly(diallyldimethylammonium chloride)-dispersed graphene -(Co-Ni)/ glassy carbon electrode;
Fe_3O_4–MWCNTs/GCE – Fe_3O_4 nanoparticles - multiwalled carbon nanotubes/ glassy carbon electrode;
M-N CS/GCE – M-nitrogen-doped carbon nanospheres/ glassy carbon electrode;
GC/EGr-1, GC/EGr-2 – graphene modified glassy carbon electrodes;
rGO/NiBTC/SPCE – screen-printed carbon electrode modified with reduced graphene oxide and NiBTC frameworks;
ZnONF/CPE – zinc oxide nanoflower/ carbon paste electrode;
MIP/f-MWCNTs/GCE – molecularly imprinted polymer / functionalized multi-walled carbon nanotubes/ glassy carbon electrode;
Sparked Mo-SPE – molybdenum-sparked screen-printed graphite electrode;
MGO/*β*-CD/IL/AuNPs/GCE – β-cyclodextrin/ ionic liquid/ gold nanoparticles functionalized magnetic graphene oxide/ glassy carbon electrode;
ZnO/RGO/ZnO@Zn – zinc oxide/ graphene-based and binder-free electrochemical nonenzymatic sensor.

In the work of Baytak et al.[5] a novel voltammetric platform based on glassy carbon electrode modified with dysprosium oxide (Dy_2O_3) nanoparticles and multi-walled carbon nanotubes was reported. The Dy_2O_3NPs/MWCNTs/GCE platform was used for the determination of sunset yellow in the presence of tartrazine. For the absorption studies the authors concluded that SY is absorbed on the surface of the modified electrode after a period of 200 s. The modified electrode showed good electrocatalytic activity. The proposed platform presented an improved anodic peak at 0.705 V and a cathodic peak at 0.690 V for SY. The peak current signal was linear with concentration of SY in a wide concentration range of 0.001 – 0.140 μmol L^{-1} and reached a limit of detection of 0.00035 μmol L^{-1}. These results were obtained by square wave voltammetry. The proposed platform exhibited a high accuracy and precision for the quantification of SY. The experimental results demonstrated that the developed voltammetric platform could be adequately utilized for the detection of SY in different food and pharmaceuticals samples.[5]

Motahharinia et al.[9] determined sunset yellow in real samples using an electroanalytical sensor amplified with Pd-ZnO nanoparticles. Pd-ZnO was obtained by chemical precipitation method and was further used to modify the paste electrode in the presence of 1-butyl-3-methylimidazolium hexafluoro phosphate, ([C4mim]-[PF6]) and paraffin oil. The as obtained ZnO-Pd/[C4mim]-[PF6]/PE had an oxidation signal almost 2.6 times higher than the unmodified electrode. Also, the proposed sensor proved to be efficient in the determination of SY in the concentration range of 0.001 – 280 μmol L^{-1}, with a LOD of 0.0004 μmol L^{-1}. The recovery rate in various food samples was between 97.84% – 104.73%.[9]

An electrochemical sensor based on the modification of carbon paste electrode with $NiFe_2O_4$-rGO nanocomposite and 1-ethyl-3-methylimidazolium chloride used as ionic liquid (IL) was developed by Darabi et al.[10] for sunset yellow determination when tartrazine (Tz) and allura red (AR) are present. The detection of SY was achieved by differential pulse voltammetry resulting a low limit of detection of 0.03 μmol L^{-1} and a wide linear concentration range between 0.05 – 500 μmol L^{-1}. The diffusion coefficient value being 3.9×10^{-5} cm^2 s^{-1}. The proposed sensor (IL/$NiFe_2O_4$/rGO/CPE) was successfully tested to detect SY, Tz and AR in real samples such as orange juice and shampoo samples. The obtained results were compared with the outcomes obtained by HPLC. The RSD value was lower than 5%, indicating that the developed sensor was accurate and efficient for examination in various real samples.[10]

In 2019, Tran and co-authors[40] developed an electrochemical sensor for the sensitive detection of Sunset Yellow using an efficient and simple approach. They prepared the ERGO/GCE sensor by electrodepositing electrochemically reduced graphene oxide (ERGO) on the surface of GCE and characterized them using CV and field emission scanning electron spectroscopy (FE-SEM). This sensor showed a good electroactive surface area which permit effective adsorption of SY. Under optimum conditions, the proposed sensor had a good linear relationship at concentrations ranging from 0.05 – 1.00 μmol L^{-1}, a detection limit of 0.0192 μmol L^{-1} and a sensitivity of 9 μA/μmol L^{-1}. The stability of the modified electrode was investigated for 2 days, observing a slight decrease of 15% from the initial response. The advantages of this developed sensor were good stability, high sensitivity, selectivity, and high reusability. The ERGO/GCE sensor was employed for the detection of SY in different soft drinks samples with recovery rates between 93.35% and 107.7%. The results suggested that the proposed method exhibited good accuracy. The authors proved the applicability and accuracy of their method using HPLC. The results obtained by both methods were comparable.[40]

In the research performed by Qin et al.,[41] an electrochemical sensor was obtained by modifying a glassy carbon electrode with graphene oxide decorated with silver nanoparticles–molecular imprinted polymers (GO/AgNPs–MIPs) for the selective recognition of sunset yellow. The GO/AgNPs were synthesized by self-assembly technology and GO/AgNPs–MIPs were obtained with surface imprinted technology through using SY as the template and GO/AgNPs as the substrate, respectively. The resultant sensor was prepared by a drop-casting technique at room temperature. The developed GO/AgNPs–MIPs/GCE sensor exhibited two linear dynamic ranges between 0.1 – 0.6 μmol L^{-1} and 0.6 – 12.0 μmol L^{-1} and a limit of detection of 0.02 μmol L^{-1}. The selectivity of modified GCE was investigated by testing the electrochemical signal of 5 μmol L^{-1} SY in the presence of the same concentration of interfering substances, like brilliant blue G, amaranth, ascorbic acid and tartrazine. The results suggested that the proposed sensor has high selectivity toward SY. For the reproducibility, the authors constructed five modified electrodes by the same way obtaining the relative standard deviation of 8.33%. Also, the stability of the GO/AgNPs–MIPs/GCE was tested for a month and it was observed that the sensor still retained 85.2% of the initial current response. These results showed good reproducibility and stability of the modified sensor. The proposed sensor was successfully applied for the determination of SY in various soft drinks.[41]

Vilian et al.[42] developed a reduced graphene oxide-graphitic carbon nitride on ZnO-Au nanoparticles (rGO-g-CN/ZnO-AuNPs) sensor for sunset yellow determination. The process of the formation of the rGO-g-CN/ZnO-AuNPs composite is illustrated in Fig. 6.[42] The proposed sensor was prepared by hydrothermal route. They obtained a linear concentration range of 0.005 to 0.085 μmol L^{-1}, a limit of detection of 0.0013 μmol L^{-1} and sensitivity of 0.5898 μA nm^{-1} cm^2. The authors checked SY oxidation in real samples using SWV and concluded that the proposed sensor is efficient even when interferents are present, demonstrating good recoveries.[42]

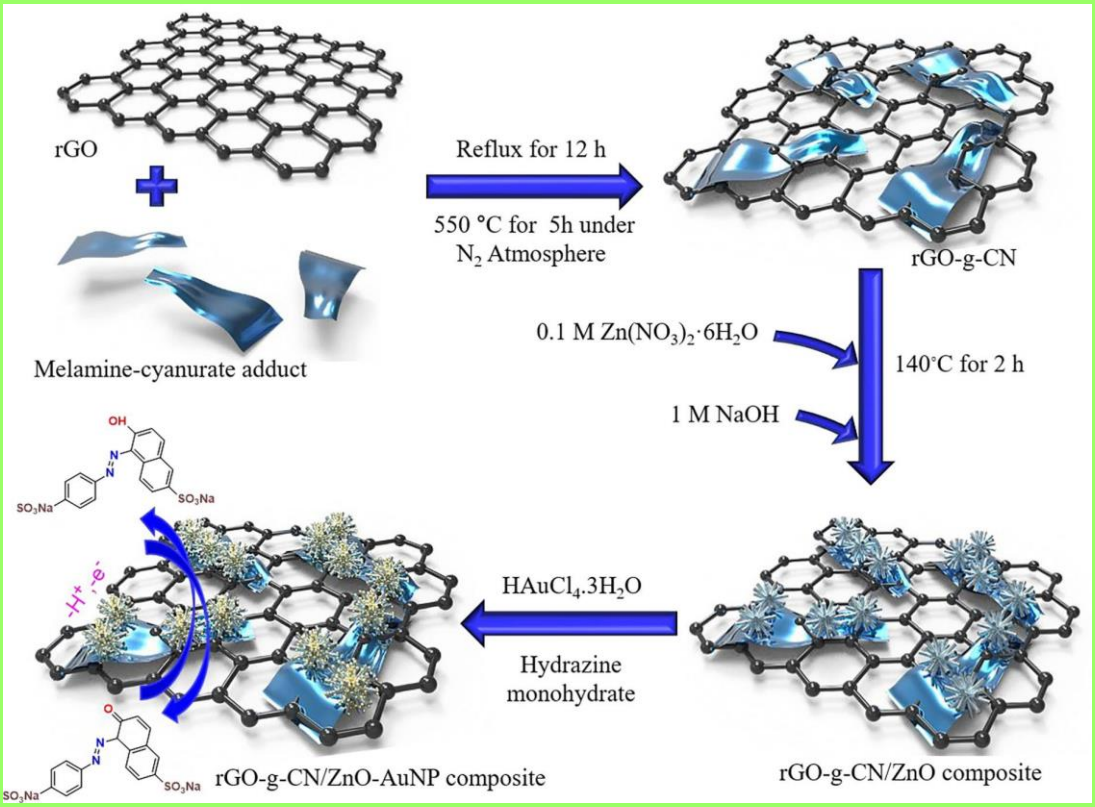

Figure 6. Schematic illustration of the construction process of the rGO-g-CN/ZnO-AuNPs composite.[42]

In 2021, Bonyadi and Ghanbari[49] developed a selective and sensitive sensor based on molecular imprinted polydopamine-coated silica nanoparticles for the electrochemical sensing of sunset yellow in different food samples. The authors synthesized SiO_2@MIP-PDA NPs by means of a green method in a one step using surface imprinted technology and analyzed it by field emission scanning electron microscopy, atomic force microscopy, high resolution transmission electron microscopy (HRTEM), Fourier transform infrared spectroscopy and thermal gravimetric analysis (TGA) methods. This was used to modify the

carbon paste electrode. The preparation process of the SY-imprinted SiO_2@MIP-PDA NPs is illustrated in Fig. 7.[49] The developed sensor demonstrated good sensitivity, high selectivity, good stability, and adequate reproducibility. The SiO_2@MIP-PDA/CPE exhibited a high linear dynamic range from 0.0045 µmol L^{-1} to 9.1 µmol L^{-1} and a lower limit of detection of 0.0015 µmol L^{-1} (S/N = 3). The applicability of the modified sensor was tested in various food samples like orange juice, orange-flavored jelly powder, candy, fruit drink and cheese snack. The recovery percentages were higher than 96.19%. The precision of the used method was evaluated by comparison with the reference spectrophotometric method. The obtained results by the proposed sensor are in agreement with the outcomes obtained by the spectrophotometric technique.[49]

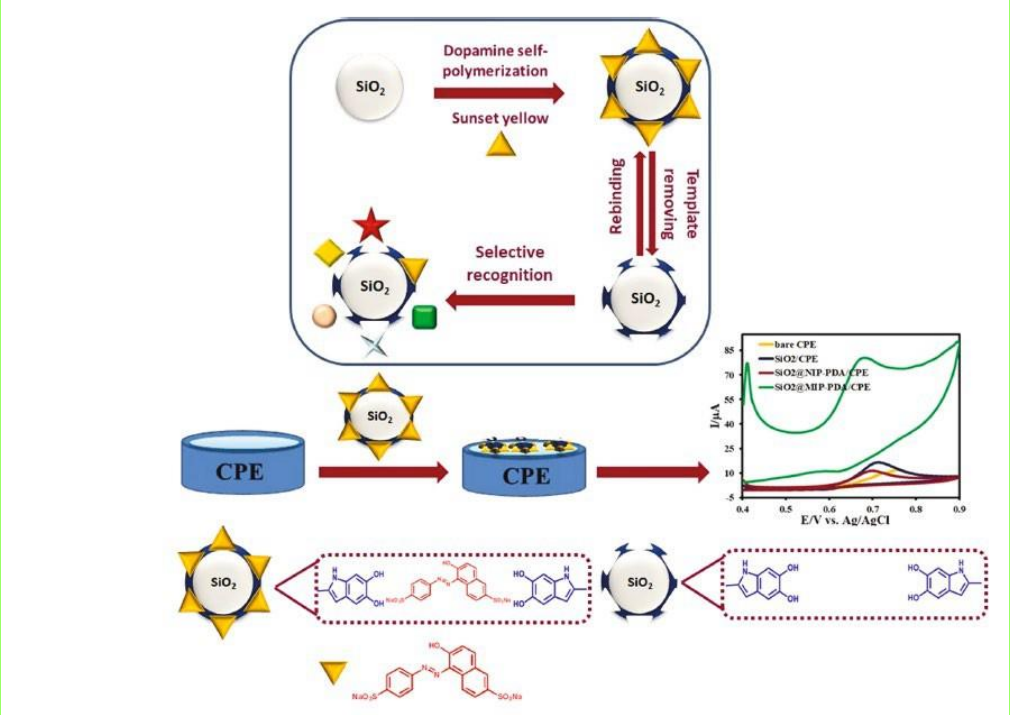

Figure 7. Schematic representation of the SY-imprinted SiO_2@MIP-PDA NPs preparation process.[49]

S. Tahtaisleyen et al.[50] developed a graphene oxide modified – pencil graphite electrode for sunset yellow determination. By means of chronoamperometry, the authors obtained a graphene oxide modified pencil graphite electrode in one-step by applying + 1.9 V constant potential for 60 seconds in 5.0 mol L^{-1} sulfuric acid. CV and DPV were used in a pH 9 PBS containing 1.0 mmol L^{-1} SY over the potential range from + 0.4 V to + 1.0 V. The proposed sensor proved to be highly stable showing good reproducibility and no interferences from other substances. Their experiments revealed a limit of detection of 0.057 µmol L^{-1} and a

limit of quantitation equal to 0.19 μmol L^{-1}. This EGO-PGE sensor was further used successfully in orange juice analysis.[50]

Yin et al.[51] used a sensor based on molecularly imprinted polydopamine (MIP)-coated multi-walled carbon nanotubes (MWCNTs) in order to determine sunset yellow. They obtained the electrochemical sensor by dropping a suspension of MWCNT@MIP-PDA on a previously polished GCE, thus obtaining GCE/MWCNT@MIP-PDA. The preparation process of SY-imprinted MWCNT@MIP-PDA is presented in Fig. 8.[51] This sensor showed a highly selective and ultra sensitive electrochemical response to SY under optimized conditions due to its superficial imprinted cavities on the electrocatalytic matrix of MWCNTs and due to the electronic barrier of the non-imprinted polydopamine to outside molecules. Therefore, the obtained sensor possessed a linear relationship to SY concentrations from 0.0022 μmol L^{-1} to 4.64 μmol L^{-1} with a detection limit of 0.0014 μmol L^{-1}. It also had good stability, selectivity and reproducibility and detected sunset yellow in real spiked samples. A recovery percentage in the range of 96.0% to 103.6% was obtained.[51]

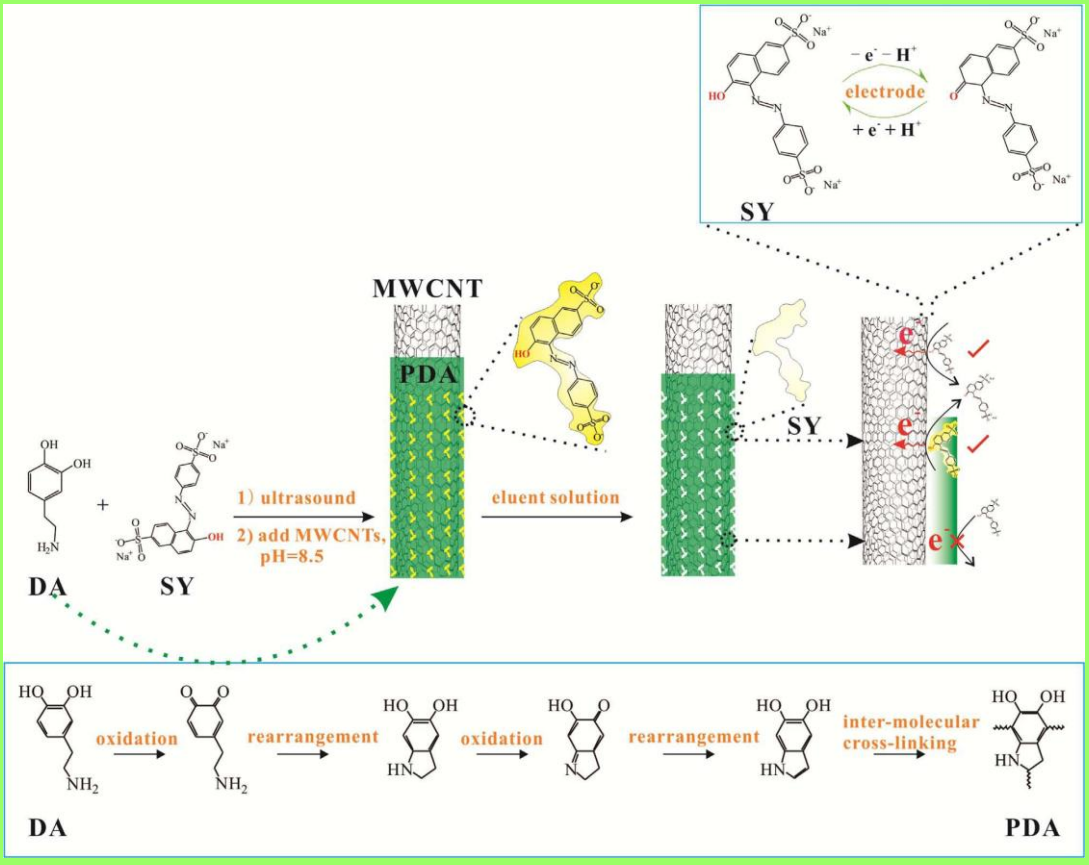

Figure 8. The fabrication procedure of MWCNT@MIP-PDA. (Lower) The formation process of PDA by spontaneous oxidative polymerization. (Upper) The redox mechanism of SY.[51]

Sunset yellow was also successfully determined by Alqarni et al.[52] using a terpolymer poly(aniline-co-o-anisidine-co-o-toluidine)/graphene oxide nanocomposite (PANI-co-PoAN-co-PoT/GO) doped with gold nanoparticles. They synthesized the mentioned nanocomposite by *in situ* oxidative polymerization process with ultrasonic assistance. Afterwards the electrochemical sensor was obtained by coating an Au electrode with PANI-co-PoAN-co-PoT/GO and Au nanoparticles. The electrochemical behavior of the newly obtained sensor, AuNPs/PANI-co-PoAN-co-PoT/GO/Au, was investigated by CV and SWV and showed a linear calibration curve for sunset yellow over the range of 5 – 500 μmol L^{-1} and a limit of detection of 0.0142 μmol L^{-1}, thus proving good selectivity, low detection limit, high sensitivity, and excellent stability of the proposed sensor. The proposed sensor was able to detect SY in different food products based on its rapid response and easy preparation.[52]

The simultaneous determination of SY and Tz was studied by Yu et al.[53] using an electrochemical sensor based on poly (diallyldimethylammonium chloride) (PDDA)-dispersed graphene (Gr) and palladium nanoparticles (Pd NP) composite. The modified sensor showed high sensitivity and good selectivity due to synergistic effect of increased surface active area and improved electron transfer efficiency of Gr and Pd nanoparticles. The electrochemical behavior of SY and Tz on the surface sensor was examined by CV and DPV. The anodic peak current exhibited a linear relation against SY concentration in the range from 0.01 to 10.0 μmol L^{-1} with a limit of detection of 0.002 μmol L^{-1}, obtained in optimal experimental conditions. The accuracy and reliability of PDDA-Gr-Pd/GCE in real samples were analyzed by standard addition method. The developed method was successfully used for simultaneous detection of SY and Tz in soft drink samples with acceptable recovery values.[53]

Qiu et al.[54] managed to determine sunset yellow and tartrazine simultaneously using a GO/MWCNT nanocomposite. They prepared nano graphite oxide sheets from graphite flakes by sonicating the GO solution and then centrifuging it at 16000 RPM. Then they added MWCNT to the obtained GO solution followed by centrifugation. The obtained composite was subjected to sonication, thus resulting GO/MWCNT. The authors observed that under optimum conditions the peak current enhanced in the range 0.09 – 8.00 μmol L^{-1} for tartrazine and SY detection, also having a limit of detection of 0.025 μmol L^{-1} for sunset yellow and 0.01 μmol L^{-1} for tartrazine. The sensor was validated successfully for SY and Tz determination in orange juice.[54]

Dorajji and Jalali[55] determined simultaneously sunset yellow and tartrazine using a glassy carbon electrode modified with ZnO and cysteic acid. DPV was used as investigation

method. The authors acquired linear calibration curves in the of 0.1 – 3.0 μmol L^{-1}, and 0.07 – 1.86 μmol L^{-1} range and a limit of detection of 0.01 μmol L^{-1} and 0.03 μmol L^{-1} for sunset yellow and tartrazine respectively. Good recovery (>95%) and RSD% (<5%) were obtained for SY and Tz determination in processed soft drinks.[55]

Vatandost et al.[56] used a modified CPE with reduced graphene oxide (rGO) to monitor SY in various food products. The rGO was prepared via an environmentally friendly method using green tea extract as reducing agent. The authors obtained after optimizing conditions when using the proposed sensor, a linear range between 0.05 and 10.00 μmol L^{-1} with a detection limit of 0.027 μmol L^{-1} and also a high sensitivity. The rGO/CPE showed very good electro-catalytic activity as well as high electrical conductivity, demonstrating excellent stability of the modified electrode. The authors also studied the selectivity of the sensor by investigating the influence of different foreign substances towards SY detection. It was observed that allura red interfere, while amaranth interfere slightly in the SY determination. Testing on real samples (beverages and food) revealed fast analysis time and good recoveries and overall good performance for SY detection in food products. The experimental results were compared with results recorded by UV-Vis spectroscopy as a reference method, using F-test and Student's t-test for precision and accuracy, respectively, and no differences between the methods were observed.[56]

Rovina and co-authors[57] used a sensitive and simple electrochemical sensor based on glassy carbon electrode modified with graphene oxide (GO), multiwall carbon nanotubes, gold nanoparticles and nanocomposite membrane of chitosan (CHIT) to determine the content of sunset yellow in commercial products. DPV was preferred as analysis method. Thus, the authors concluded the CHIT/GO/MWCNTs/AuNPs/GCE enhanced the electrochemical signals towards SY detection. The calibration curves revealed a linear correlation from 0.02 to 0.2 μmol L^{-1}, while the limits of detection and quantification were 0.0001 μmol L^{-1} (0.032 mg mL^{-1}) and 0.0002 μmol L^{-1} (0.096 mg mL^{-1}), respectively. They also observed that interfering species does not obviously change the oxidation peak current, proving good selectivity as well. The prepared sensor was used to the determination of SY in various food and beverages samples. The RSD% was less than 5%, suggesting a good precision of the prepared sensor. Furthermore, the recovery test of the CHIT/GO/MWCNTs/AuNPs/GCE sensor was investigated using spiked the samples with precise concentration of SY. The proposed sensor demonstrated good applicability and reliability for the detection of sunset yellow.[57]

Koyun and Sahin[58] determined sunset yellow in food and beverages using a poly(L-cysteine) modified pencil graphite electrode (PLC/PGE) by differential pulse voltammetry method. They observed that the modified electrode had an enhanced electrochemical response than bare PGE. The linear response for the electrochemical oxidation of SY of the proposed sensor was in the concentration range of 1.0 – 1000 μmol L^{-1} with a detection limit of 0.125 μmol L^{-1} (S/N = 3). This proposed sensor was successfully tested in food and beverage samples such as jelly, cake, mixed fruit juice and orange juice.[58]

The electrochemical detection of sunset yellow was also studied by Wang et al.[59] using a GCE modified with Au-Pd and reduced graphene oxide (RGO) nanocomposites. This sensor was fabricated by a one-step facile synthesis method. The presence of RGO improved the correlation between Au-Pd nanocomposites and also accelerated the charge transfer between the electrolyte and the surface of the sensor. The modified electrode showed good electrocatalytical activity with a wide linear concentration range between 0.69 – 331.00 μmol L^{-1} and a lower limit of detection of 0.0015 μmol L^{-1}. The Au-Pd-RGO/GCE sensor exhibited high sensitivity, stability and repeatability. The practicability of the prepared sensor was evaluated by measuring the concentration of SY in soft drinks. The recovery rate was obtained between 98.82% and 102.47%.[59]

Deng et al.[60] used GCE modified with nanohybrid of gold nanorods (AuNRs) decorated graphene oxide (GO) nanosheets for simultaneous determination of sunset yellow and tartrazine. The developed sensor exhibited very good analytical performances with a lower limit of detection of 0.0024 μmol L^{-1} and a wide linear range between 0.01 – 3.00 μmol L^{-1} for SY. The ERGO-AuNRs/GCE showed that it can be applied for the detection of SY in orange juice, orange soda and jelly samples. The recoveries of SY in food samples were from 89.4% and 106.5%.[60]

Li and collaborators[61] prepared three electrochemical sensors using Co-Ni bimetallic nanoflowers, Pd-Pt bimetallic nanocages, Pt-Cu bimetallic nanoframes and poly (diallyldimethylammonium chloride) (PDDA)-dispersed graphene (Gr) for the detection of sunset yellow. The unique morphology of the PDDA-Gr-(Pt-Cu), PDDA-Gr-(Pd-Pt) and PDDA-Gr-(Co-Ni) nanocomposites endows the constructed electrochemical electrodes with excellent electrical conductivity and wide active surface areas, which contribute more active sites for the target substance and also, improves the sensitivity of the sunset yellow determination. The morphologies of these nanocomposites as well as the morphologies of Pd-Pt bimetallic nanocages, Pt-Cu bimetallic nanoframes and Co-Ni bimetallic nanoflowers were

characterized by TEM (Fig. 9).[61] The proposed sensors were examined by CV and DPV methods, and were compared with others for the detection of SY. The anodic current intensity of SY on three modified sensors was linear with the SY concentration in the ranges between 0.02 – 10.00 μmol L^{-1}, 0.02 – 10.00 μmol L^{-1}, 0.008 – 10.00 μmol L^{-1}, respectively. The detection limits obtained were 0.006 μmol L^{-1}, 0.004 μmol L^{-1} and 0.002 μmol L^{-1}. The outcomes exhibited that the PDDA-Gr-(Co-Ni)/GCE was more sensitive with a low cost and a large linear dynamic range compared to the other two sensors, which has demonstrated that the metal can realize better and similar property. Furthermore, the three modified electrodes were successfully applied for the determination of SY in soft drinks with the RSD less than 5%.[61]

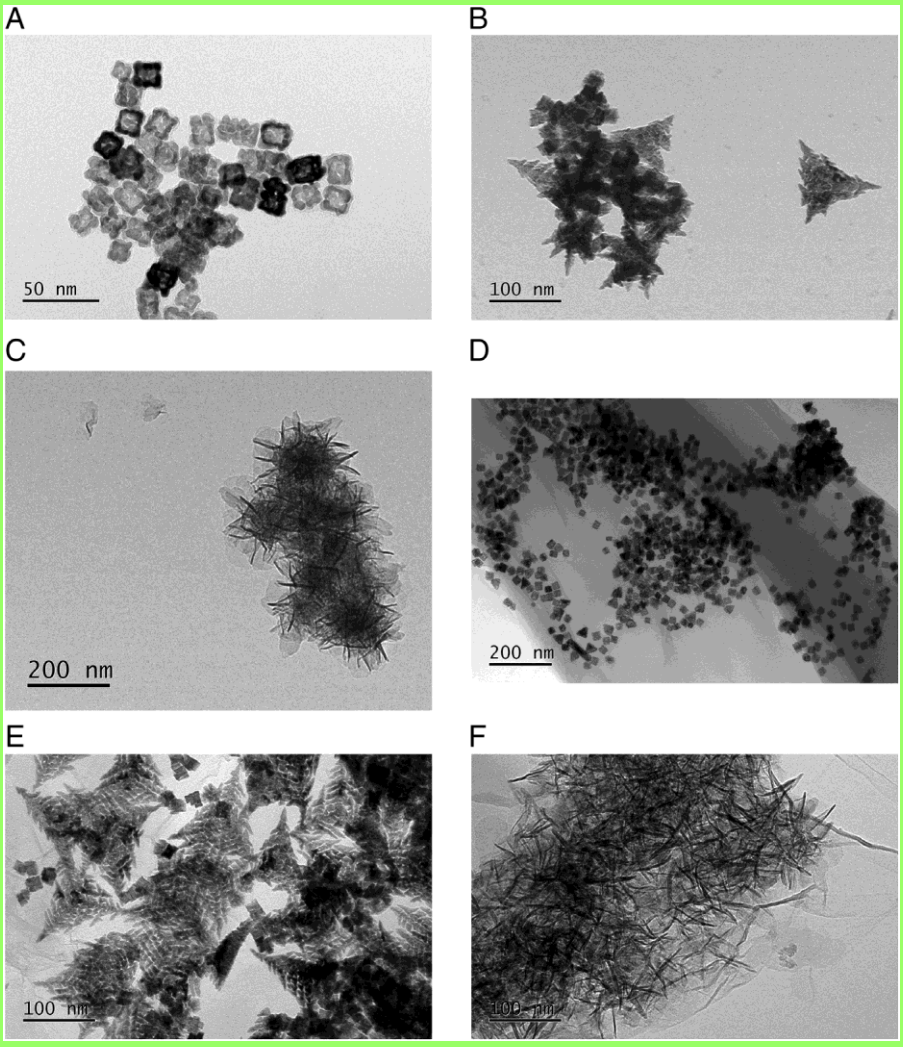

Figure 9. (A)TEM images of Pd-Pt bimetallic nanocages, **(B)** Pt-Cu bimetallic nanoframes and **(C)** Co-Ni bimetallic nanoflowers. **(D)** TEM images of PDDA-Gr-(Pd-Pt) composite, **(E)** PDDA-Gr-(Pt-Cu) composite and **(F)** PDDA-Gr-(Co-Ni) composite.[61]

Recently, Shaikshavali et al.[62] developed a selective and sensitive sensor based on glassy carbon electrode modified with Fe_3O_4–MWCNTs for the detection of sunset yellow. The synthesis of Fe_3O_4–MWCNTs nanocomposites was performed by a simple one-step hydrothermal technique. The FE-SEM, EDS and XRD studies confirmed the cubic structure and the purity of synthesized nanocomposites. The electrochemical performance of SY was evaluated by CV, DPV and EIS methods. The modified electrode showed larger surface area, high conductivity and improved electrocatalytic activity on the detection of SY. The differential pulse voltammetry analysis shows a detection limit of 0.0014 μmol L^{-1} with a linear concentration range of 0.2 – 3.5 μmol L^{-1}. The selectivity study was tested using the influence of different interfering substances towards the determination of SY. The experimental results indicated that the proposed sensor has high selectivity, good repeatability, reproducibility and stability. The applicability of the Fe_3O_4–MWCNTs/GCE sensor was examined in soft drinks. The recovery values were reached between 90% and 101% proving that the proposed method was suitable to determine SY in soft drink samples, obtaining good precision and accuracy.[62]

In 2019, Wang and co-authors[63] developed a “green nano” approach to manufacture monodisperse polypyrrole (PPy) nanospheres with adjustable dimensions by simply modifying the pyrrol concentration. It was obtained a linear model and after was used to anticipate the size of polypyrrole nanospheres. The synthesis of nitrogen-doped carbon nanospheres (NCSs) with well-controlled sizes was performed by direct carbonzilation of harvested PPy nanospheres, which proved a facile way for the fabrication of highly dispersible NCSs of controlled dimensions. The preparation procedure of the PPy nanosphere and NCSs is displayed in Fig. 10.[63] The electrochemical response of prepared nitrogen-doped carbon nanospheres on SY was investigated. NCSs with medium size (M-NCSs) exhibited the best electrochemical performance, a wide linear range from 0.001 μmol L^{-1} to 2.5 μmol L^{-1}, a lower limit of detection of 0.00095 μmol L^{-1} and very high sensitivity of 679.16 Amol L^{-1} cm^{-2}. The built sensor was applied to determine SY using the standard addition method in food samples such as sport drinks, Mirinda, chocolate and candy. The recovery rate was between 91.7% and 102.3%.[63]

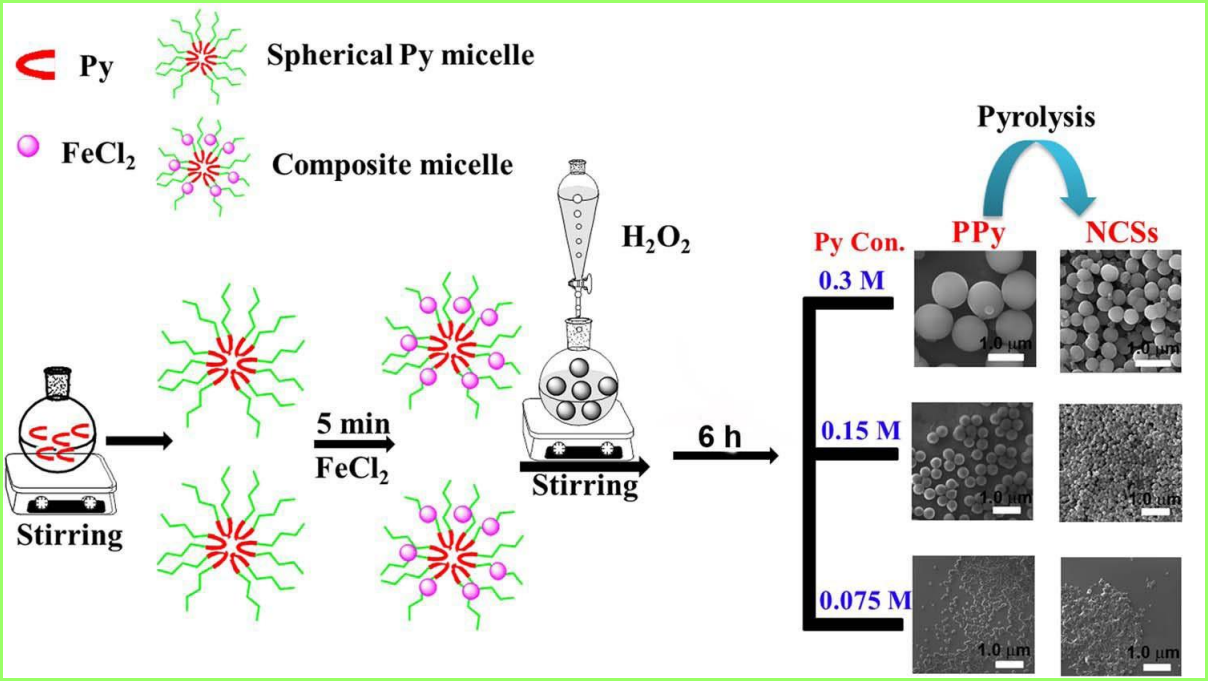

Figure 10. Schematic representation of the fabrication process of size-controlled PPy nanosphere and NCSs.[63]

Pogacean et al.[64] used 2 graphene based materials as modifiers of glassy carbon electrodes in order to determine sunset yellow. Pulses of current were used to exfoliate graphite rods to obtain the graphene modifiers. One of them (EGr-1) was exfoliated in a solution of H_2SO_4 and HNO_3, while the second (EGr-2) was exfoliated in H_3BO_3 and NaCl, eventually obtaining 2 sensors: GC/EGr-1 and GC/EGr-2, which were used for SY determination. The authors obtained different sensitivities, linear ranges and the limits of detection for each electrode as follows: for GC/EGr-1 the sensitivity was 0.017 μA/mol L^{-1}, the linear range between 6 and 100 mol L^{-1}, and the limit of detection was 1.8 mol L^{-1}, while for the second the sensitivity was higher (0.021 μA/mol L^{-1}), the linear range was between 1
– 100 mol L^{-1} and the LOD was 0.3 mol L^{-1}, concluding that the latter was the best performing for SY detection among the two developed. The applicability of the GC/EGr-2 electrode was evaluated in two orange juice samples. The results proved the proposed sensor was able to detect content of SY in real samples.[64]

Wu and Lee[65] developed a sensor based on screen printed carbon electrode (SPCE) modified with a combination of hydrothermally prepared rGO and metal–organic frameworks of NiBTC used for simultaneous determination of sunset yellow and tartrazine. The modification process of SPCE with the rGO and NiBTC is described in Fig. 11.[65] The as

modified sensor had an electrochemical response increased by 36.5 and 33.4 times for SY and Tz detection, respectively versus the unmodified electrode. Thus, after experiments the authors obtained linear ranges of 0.05 – 5.0 μmol L^{-1} for SY and 0.075 – 5.0 μmol L^{-1} for Tz and detection limits of 0.025 and 0.05 μmol L^{-1} for sunset yellow and tartrazine, respectively making them suitable for SY and Tz detection in soft drinks.[65]

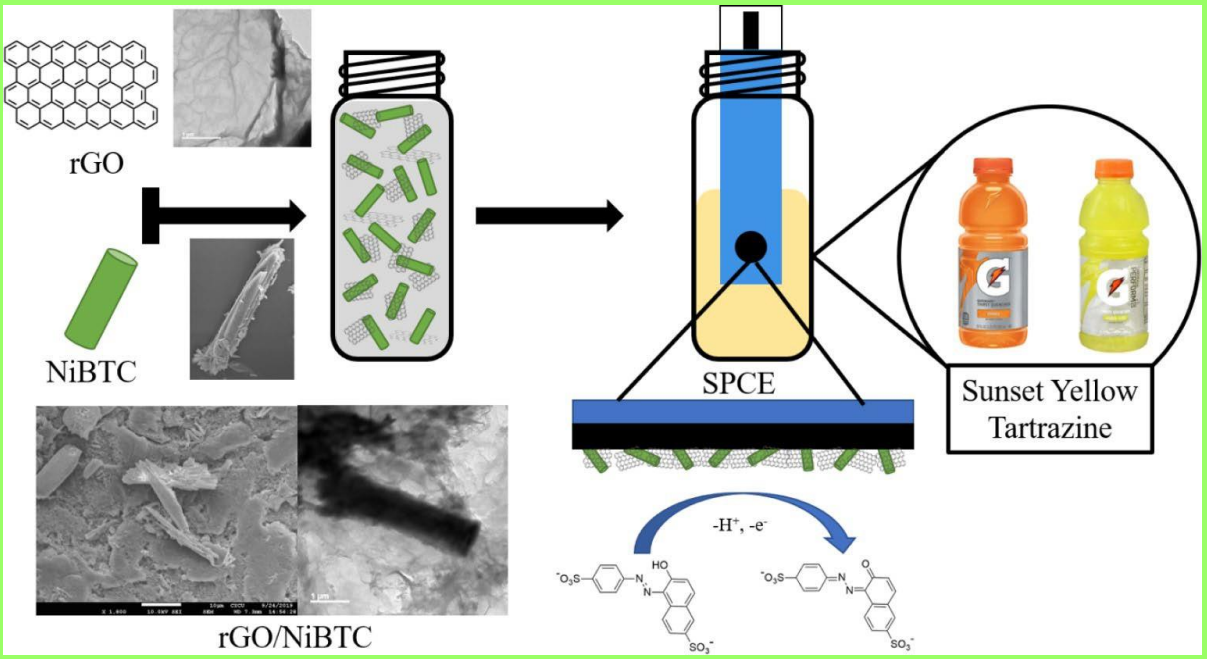

Figure 11. The process for preparation of the rGO/NiBTC/SPCE sensor.[65]

Ya and collaborators[66] developed a zinc oxide nanoflower (ZnONF) based electrochemical sensor to detect sunset yellow. Thus, the ZnONF synthesized by a simple method, was used to modify a carbon paste electrode (CPE). In optimized condition, the authors obtained a linear concentration in the range of 0.001 – 0.022 μmol L^{-1} and 0.022 –
0.154 μmol L^{-1}, and a limit of detection of 0.0002 μmol L^{-1} (0.10 μg/L) (S/N = 3). The reproducibility of the proposed sensor was investigated by using six modified electrodes obtained in the same way. Also, the stability of the modified CP electrode was examined after long-term storage in a refrigerator for seven days, and a decrease up to 93.7% of the initial current response was observed. To study the selectivity of the sensor in the detection of SY, the influence of potential interfering substances was tested. The experimental results indicated good stability, reproducibility and high selectivity of the ZnONF/CPE. The proposed sensor was used for SY determination in soft drinks with recoveries of 97.5% – 103%, results that were confirmed by HPLC.[66]

A molecularly imprinted polymers on functionalized multi-walled carbon nanotubes (MIP/f-MWCNTs) sensor was proposed by Arvand et al.[67] for sunset yellow determination in food samples. In this study electropolymerization was used to obtain the MIP sensor. Thus, acrylamide was electropolymerized on f-MWCNTs/GCE surface, while sunset yellow was present as template molecule. After SY extraction the remained imprints proved viable to selectively reattach SY molecules. The developed sensor was employed for the electrochemical determination of SY, showing a wide linear concentration range of 0.05 – 100.00 μmol L^{-1} and a detection limit of 0.005 μmol L^{-1}, obtained in optimal conditions. Interference studies confirmed that various added interferents don't interfere with SY detection. The MIP/f-MWCNTs/GCE was successfully applied in different food samples such as candy, candy coated chocolate, orange flavored jelly powder, peach juice powder and beverage. The recoveries between 91.4% and 105.9% were obtained. Also, the authors investigated the accuracy of the developed method by using reference spectrophotometric method. The results exhibited that the values acquired by the electrochemical method are in agreement with those obtained by UV-Vis spectrophotometric method.[67]

In 2020, Kolozof et al.[68] developed for the first time a screen-printed graphite electrode modified with sparked generated molybdenum (Mo-SPE) used for simultaneous determination of sunset yellow and tartrazine. The Mo-SPEs were obtained by applying 40 sparking cycles at ambient conditions delivered at 1.2 kV, the Mo being connected to the "+" pole while the SPE to the "–" pole. Under optimum conditions, the modified SPE showed a linear concentration range between 0.005 and 0.25 μmol L^{-1} and a detection limit of 0.002 μmol L^{-1}. Interference studies were performed and exhibited satisfactory results. When using the Sparked Mo-SPE sensor in real samples, recoveries in the range 94% to 109% were obtained, proving its efficiency in simultaneous determination of SY and Tz.[68]

Li et al.[69] modified a glassy carbon electrode with magnetic graphite oxide (MGO) functionalized with *β*-cyclodextrin, ionic liquid and gold nanoparticles in order to determine sunset yellow. The authors obtained this molecularly imprinted sensor in multiple steps, starting by co-precipitating magnetite particles on the surface of graphene oxide, resulting the MGO. Afterwards, β-cyclodextrin (*β*-CD) and the ionic liquid (IL) were adsorbed on MGO followed by the addition of gold nanoparticles (AuNPs) on the previously obtained MGO/*β*-CD/IL. In the end the MIPs were obtained by precipitation polymerization. Thus, after the development of the mentioned sensor for SY detection the authors obtained under optimal conditions, a wide linear concentration range between 0.005 and 2.000 μmol L^{-1} and a lower

limit of detection of 0.002 μmol L^{-1}. Due to their synergetic approach, the prepared sensor showed high sensitivity, good selectivity and rapid response on sunset yellow detection. In order to examine its feasibility and applicability, the MGO/*β*-CD/IL/AuNPs/GCE was utilized in the detection of sunset yellow in various real samples like Mirinda drink, minute mead and spiked water. The obtained recoveries were between 97% − 105%, making it suitable for SY determination.[69]

Sunset yellow was successfully detected in soft drinks by Wu et al.[70] which developed a nonenzymatic sensor based on zinc oxide and graphene oxide. Thus, the ZnO/RGO/ZnO was grown on a Zn foil through a hydrothermal technique, where the zinc foil acts both a support for zinc oxide and reductant for graphene oxide and also as a source for zinc in the lower layer. The obtained ZnO/RGO/ZnO@Zn proved to be efficient on SY determination with the following characteristics: good reproducibility and stability, a sensitivity of 20.25 μA μmol L^{-1} cm^{-2}, a limit of detection equal to 0.003 μmol L^{-1} and a linear range from 0.01 to 5.00 μmol L^{-1}.[70]

Conclusions

Given the harmful effects that tartrazine and sunset yellow have on human health, there is an essential need for continuous enhancement of highly sensitive methods for the detection of these two food azo dyes. So, it is extremely important to determine tartrazine and sunset yellow contents from food and beverages products in order to improve food safety in the whole world.

Therefore, this review described the recent trends in the development of electrochemical sensors and methods used for the determination of tartrazine and sunset yellow in food and beverages samples. It was showed that there is a variety of modified sensors that possess low limits of detection, wide linear concentration ranges, high selectivities and sensitivities. In general, best results were obtained on glassy carbon electrode modified with various metal nanoparticles, multi-walled carbon nanotubes and lately with molecular imprinted polymers, used as single modifiers or in different combinations. Also, there seem to be a trend to develop electrochemical sensors that determine sunset yellow and tartrazine simultaneously. Given the importance of the described matter it is reasonable to expect that more accurate sensors and fast and sensitive methods will be developed in the future for various food dyes detection in real commercial samples.

References

1. K. Rovina, S. Siddiquee, and S. M. Shaarani, *Crit. Rev. Anal. Chem.*, **47**, 309 (2017).
2. O. I. Lipskikh, E. I. Korotkova, Ye. P. Khristunova, J. Barek, and B. Kratochvil, *Electrochim. Acta*, **260**, 974 (2018).
3. K. Rovina, P. P. Prabakaran, S. Siddiquee, and S. M. Shaarani, *Trends Anal. Chem.*, **85**, 47 (2016).
4. K. Rovina, S. Siddiquee, and S. M. Shaarani, *Trends Food Sci. Technol.*, **65**, 68 (2017)
5. A. K. Baytak, E. Akbaş, and M. Aslanoglu, *Anal. Chim. Acta*, **1087**, 93 (2019).
6. E. Blanco, L. Hristova, R. Martínez-Moro, L. Vázquez, G. J. Ellis, L. Sánchezd, M. del Pozo, M. D. Petit-Domínguez, E. Casero, and C. Quintana, *Sens. Actuators B Chem.*, **324**, 128731 (2020).
7. J. Penagos-Llanos, O. García-Beltrán, E. Nagles, and J. J. Hurtado, *Electroanalysis*, **32**, 2174 (2020).
8. L. Magerusan, F. Pogacean, M. Coros, C. Socaci, S. Pruneanu, C. Leostean, and I. O. Pana, *Electrochim. Acta*, **283**, 578 (2018).
9. M. Motahharinia, H. A. Zamani, and H. Karimi-Maleh, *Eurasian Chem. Commun.*, **2**, 760 (2020).
10. R. Darabi and M. Shabani-Nooshabadi, *Food Chem.*, **339**, 127841 (2021).
11. L. Zhao, B. Zeng, and F. Zhao, *Electrochim. Acta*, **146**, 611 (2014).
12. J. Yi, L. Zeng, Q. Wu, L. Yang, and T. Xie, *Food Anal. Methods*, **11**, 1608 (2018).
13. M. A. Karimi, V. H. Aghaei, A. Nezhadali, and N. Ajami, *Food Anal. Methods*, **11**, 2907 (2018).
14. S. Tahtaisleyen, O. Gorduk, and Y. Sahin, *Anal. Lett.*, **53**, 1683 (2020).
15. Z.-Z. An, Z. Li, Y.-Y. Guo, X.-L. Chen, K.-N. Zhang, D.-X. Zhang, Z.-H. Xue, X.-B. Zhou, and X.-Q. Lu, *Chin. Chem. Lett.*, **28**, 1492 (2017).
16. M. A. Prado, L. F. V Boas, M. R. Bronze, and H. T. Godoy, *J. Chromatogr. A*, **1136**, 231 *(***2006**).
17. W. de A. S. Bento, B. P. Lima, and A. P. S. Paim, *Food Chem.*, **183**, 154 (2015).
18. D. Chen, M. Wu, S. Xie, X. Li, Y. Tao, X. Wang, L. Huang, Y. Pan, D. Peng, and Z. Yuan, *J. Chromatogr. Sci.*, **57**, 462 (2019).

19. E. Dinç, A. H. Aktaş, D. Baleanu, and Ö. Üstündağ, *J. Food Drug Anal.*, **14**, 284 (2006).
20. M. Vidal, R. Garcia-Arrona, A. Bordagaray, M. Ostra, and G. Albizu, *Talanta*, **184**, 58 (2018).
21. F. Soponar, A. C. Moţ, and C. Sârbu, *J. Chromatogr. A*, **1188**, 295 (2008).
22. T.-X. Tang, X.-J. Xu, D.-M. Wang, Z.-M. Zhao, L.-P. Zhu, and D.-P. Yang, F*ood Anal. Methods*, **8**, 459 (2015).
23. R. Li, Z.-T. Jiang, and Y.-H. Liu, *J. Food Drug Anal.*, **16**, 91 (2008).
24. R. Sahraei, A. Farmany, and S. S. Mortazavi, *Food Chem.*, **138**, 1239 *(***2013)**.
25. X. Zhao, Y. Liu, J. Zuo, J. Zhang, L. Zhu, J. Zhang, *J. Electroanal. Chem.*, **785**, 90 (2017).
26. M. Sakthivel, M. Sivakumar, S.-M. Chen, and K. Pandi, *Sens. Actuators B*, **256**, 195 (2018).
27. H. H. AL-Refai, A. A. Ganash, and M. A. Hussein, *Synth. Met.*, **280**, 116875 (2021).
28. L. F. de Lima, A. L. Ferreira, C. C. Maciel, M. Ferreira, and W. R. de Araujo, *Talanta*, **227**, 122200 (2021).
29. K. Rovina, S. Siddiquee, and S. Md Shaarani, *Drug Chem. Toxicol.*, **44**, 447 (2021).
30. J. G. Manjunatha, *Heliyon*, **4**, e00986 (2018).
31. P. Wang, X. Liu, Q. Hu, H. Gao, and W. Ma, *Int. J. Electrochem. Sci.*, **15**, 8901 (2020).
32. Z. Wang, Y. Shan, L. Xu, G. Wu, and X. Lu, *Int. J. Polym. Anal. Charact.*, **22**, 83 (2017).
33. G. Karim-Nezhad, Z. Khorablou, M. Zamani, P. S. Dorraji, and M. Alamgholiloo, *J. Food Drug Anal.*, **25**, 293 (2017).
34. J. Penagos-Llanos, O. García-Beltrán, J. A. Calderón, J. J. Hurtado-Murillo, E. Nagles, and J. J. Hurtado, *J. Electroanal. Chem.*, **852**, 113517 (2019).
35. L. F. de Lima, C. C. Maciel, A. L. Ferreira, J. C. de Almeida, and M. Ferreira, *Mater. Lett.*, **262**, 127186 (2020).
36. C. Raril and J. G. Manjunatha, *Port. Electrochim. Acta*, **39**, 59 (2021).
37. S. Z. Mazlan, Y. H. Lee, and S. A. Hanifah, *Sensors*, **17**, 2859 (2017).
38. Q. He, J. Liu, X. Liu, G. Li, P. Deng, J. Liang, and D. Chen, *Sensors*, **18**, 1911 (2018).

39. K. Rovina, L. A. Acung, S. Siddiquee, J. H. Akanda, and S. M. Shaarani, *Food Anal. Methods*, **10**, 773 (2017)
40. Q. T. Tran, T. T. Phung, Q. T. Nguyen, T. G. Le, and C. Lagrost, *Anal. Bioanal. Chem.*, **411**, 7539 (2019).
41. C. Qin, W. Guo, Y. Liu, Z. Liu, J. Qiu, and J. Peng, *Food Anal. Methods*, **10**, 2293 (2017).
42. A. T. E. Vilian, S.-M. Kang, S. Y. Oh, C. W. Oh, R. Umapathi, Y. S. Huh, and Y.-K. Han, *Food Chem.*, **323**, 126848 (2020).
43. Ş. D. Zor, B. Aşçı, Ö. A. Dönmez, and D. Y. Küçükkaraca, *J. Chromatogr. Sci.*, **54**, 952 (2016).
44. S. P. Alves, D. M. Brum, É. C. B. de Andrade, and A. D. P. Netto, *Food Chem.*, **107**, 489 (2008).
45. A. Benvidi, S. Abbasi, S. Gharaghani, M. D. Tezerjani, and S. Masoum, *Food Chem.*, **220**, 377 (2017).
46. M. S. El-Shahawi, A. Hamza, A. A. Al-Sibaai, A. S. Bashammakh, and H. M. Al-Saidi, *J. Ind. Eng. Chem.*, **19**, 529 (2013).
47. H.-Y. Huang, Y.-C. Shih, and Y.-C. Chen, *J. Chromatogr. A*, **959**, 317 (2002).
48. Y. Yuan, X. Zhao, M. Qiao, J. Zhu, S. Liu, J. Yang, and X. Hu, *Spectrochim. Acta A Mol. Biomol. Spectrosc.*, **167**, 106 (2016).
49. S. Bonyadi and K. Ghanbari, *Microchem. J.*, **167**, 106322 (2021).
50. S. Tahtaisleyen, O.Gorduk, and Y. Sahin, *Anal. Lett.*, **54**, 394 (2021).
51. Z.-Z. Yin, S.-W. Cheng, L.-B. Xu, H.-Y. Liu, K. Huang, L. Li, Y.-Y. Zhai, Y.-B. Zeng, H.-Q. Liu, Y. Shao, Z.-L. Zhang, and Y.-X. Lu, *Biosens. Bioelectron.*, **100**, 565 (2018).
52. S. A. Alqarni, M. A. Hussein, and A. A. Ganash, *ChemistrySelect*, **3**, 13167 (2018).
53. L. Yu, H. Zheng, M. Shi, S. Jing, and L. Qu, *Food Anal. Methods*, **10**, 200 (2017).
54. X. Qiu, L. Lu, J. Leng, Y. Yu, W. Wang, M. Jiang, and L. Bai, *Food Chem.*, **190**, 889 (2016).
55. P. S. Dorraji and F. Jalali, *Food Chem.*, **227**, 73 (2017).
56. E. Vatandost, A. G.-H. Saraei, F. Chekin, S. N. Raeisi, and S.-A. Shahidi, *Food Chem. X*, **6**, 100085 (2020).
57. K. Rovina, S. Siddiquee, and S. M. Shaarani, *Food Control*, **82**, 66 (2017).
58. O. Koyun and Y. Sahin, *Int. J. Electrochem. Sci.*, **13**, 159 (2018).

59. J. Wang, B. Yang, K. Zhang, D. Bin, Y. Shiraishi, P. Yang, and Y. Du, *J. Colloid Interface Sci.*, **481**, 229 (2016).
60. K. Deng, C. Li, X. Li, and H. Huang, *J. Electroanal. Chem.*, **780**, 296 (2016).
61. L. Li, H. Zheng, L. Guo, L. Qu, and L. Yu, *J. Electroanal. Chem.*, **833**, 393 (2019).
62. P. Shaikshavali, T. M. Reddy, A. L. Narayana, O. M. Hussain, G. Venkataprasad, and T. V. Gopal, *J. Food Meas. Charact.*, **14**, 3319 (2020).
63. M. Wang, H. Shi, M. Cui, W. Liu, and X. Liu, *J. Electrochem. Soc.*, **166**, B13 (2019).
64. F. Pogacean, M. Coros, V. Mirel, L. Magerusan, L. Barbu-Tudoran, A. Vulpoi, R.-I. Stefan-van Staden, and S. Pruneanu, *Microchem. J.*, **147**, 112 (2019).
65. J.-H. Wu and H.-L. Lee, *Microchem. J.*, **158**, 105133 (2020).
66. Y. Ya, C. Jiang, T. Li, J. Liao, Y. Fan, Y. Wei, F. Yan, and L. Xie, *Sensors*, **17**, 545 (2017).
67. M. Arvand, M. Zamani, and M. S. Ardaki, *Sens. Actuators B Chem.*, **243**, 927 (2017).
68. P.-A. Kolozof, A. B. Florou, K. Spyrou, J. Hrbac, and M. I. Prodromidis, *Sens. Actuators B Chem.*, **304**, 127268 (2020).
69. J. Li, X. Wang, H. Duan, Y. Wang, Y. Bu, and C. Luo, *Talanta*, **147**, 169 (2016).
70. X. Wu, X. Zhang, C. Zhao, and X. Qian, *Talanta*, **179**, 836 (2018).

Rapid and Sensitive Electrochemical Determination of Tartrazine in Commercial Food Samples Using IL/$AuTiO_2$/GO Composite Modified Carbon Paste Electrode

Abstract

A novel electrochemical sensor based on the modification of carbon paste electrode with an ionic liquid (1-butyl-2,3-dimethylimidazolium tetrafluoroborate) and $AuTiO_2$/GO composite (IL/$AuTiO_2$/GO/CPE) was developed for rapid and sensitive determination of tartrazine by differential pulse voltammetry. Under the optimum experimental conditions, the peak current was linear to concentration of tartrazine in the ranges of 1 – 400 µmol L^{-1} and 400 – 1000 µmol L^{-1}, with sensitivities of 0.008 µA µmol L^{-1} and 0.002 µA µmol L^{-1}, respectively, and with a limit of detection of 0.33 µmol L^{-1} (S/N = 3). To demonstrate the performance of the method, the reproducibility was studied and the obtained values of RSD% were 2.72%. The method was applied to the sensitive determination of tartrazine in isotonic drink, mustard and yellow egg dye samples with recovery rates between 98.55% and 103.62%.

Introduction

Tartrazine (Tz, E102) is a synthetic organic food dye that can be found in various food products like dairy products, beverage, candies, etc.[1-3] The synthetic food dyes presents some advantages such as reproducible and brighter color, lower sensitivity to technological processing, lower costs of production and high stability to light.[4-5]

The chemical structure of Tz contains the azo group (─N═N─) and ─OH group on aromatic ring. However, the content of Tz must be controlled due to its potential harmfulness to human health;[1,6] so, the amount of used tartrazine should be monitored constantly. Joint FAO/WHO Expert Committee on Food Additive (JECFA) and EU Scientific Committee for Food (SCF) established the acceptable daily intake (ADI) for tartrazine at 7.5 mg kg^{-1} body weight per day.[4,7] The high concentrations of Tz can cause childhood asthma, allergies, anxiety, migraines, eczema, and dermal toxicity.[2,5,6,8] Therefore, the detection of tartrazine content in food products is very important to improve food safety in the world.

Until now, numerous analytical methods, such as high performance liquid chromatography (HPLC),[9-12] capillary electrophoresis (CE)[13,14] and spectrophotometry[15,16]

have been reported for the determination of tartrazine. These methods are widely used with high accuracy. However, most of them need expensive equipments, large quantities of organic solvents, pre-treatment involving extraction, separation and adsorption with high costs and long analysis time. On the other hand, electrochemical methods have attracted more attention due to their simplicity, fast response, high sensitivity and selectivity, and relatively low cost. In recent years, different modified electrodes (Table I)[1-3,5,6,8,17-24] have been developed for the electrochemical determination of tartrazine.

Table I. Comparison of different electrodes used for the detection of tartrazine.

Electrode	Method	Linear concentration range ($\mu mol\ L^{-1}$)	LOD ($\mu mol\ L^{-1}$)	Ref.
MIP-MWNTs-IL@PtNPs/GCE[a]	DPV	0.03 – 5.0 5.0 – 20.0	0.008	1
Gr/PLPA/PGE[b]	DPV	2 – 100	1.54	2
CHIT/GO/MWCNTs/AuNPs/GCE[c]	DPV	0.02 – 0.19	0.003	3
g-C_3N_4/PGE[d]	DPV	0.1 – 10.0	0.21	5
MIP-PmDB/PoPD-GCE[e]	DPV	0.005 – 1.1	0.0035	6
Pp-ABSA/ZnO NPs-CPE[f]	DPV	0.0349 – 1.246 1.246 – 5.440	0.08	8
N-PC-G/CS/GCE[g]	DPV	0.05 – 15.0	0.036	17
PGMCPE[h]	CV	1 – 27 35 – 87	0.28	18
PLA-ERGO/GCE[i]	DPV	1 – 250	0.25	19
MIP/MWCNTs/GCE[j]	DPV	0.08 – 1.00 1 – 10	0.027	20
Au/(AuNPs-PAH/NiTsPc)$_5$[k] Au/(AuNPsP-PAH/NiTsPc)$_5$[k]	DPV	0.5 – 3.0 4.0 – 9.0	0.055 0.122	21
TiO_2-ErGO-GCE[l]	SDLSV	0.02 – 20.00	0.008	22
Exfoliated graphite-GCE[m]	DPV	0.009 – 0.374	0.0028	23
PEDOT@TbHCF/GCE[n]	DPV	0.1 – 206 .0	0.032	24
IL/AuTiO_2/GO/CPE	DPV	1 – 400 400 – 1000	0.33	This work

[a]Molecularly imprinted polymer – multiwalled carbon nanotubes - ionic liquid supported Pt nanoparticles composite film coated glassy carbon electrode; [b]Graphene/poly (L-phenylalanine) modified pencil graphite electrode; [c]Chitosan/graphene oxide/multi-walled carbon nanotubes/gold nanoparticles/glassy carbon electrode; [d]Graphitic carbon nitride/graphite pencil electrode; [e]Molecularly imprinted copolymer-m-dihydroxybenzene/o-phenylenediamine modified glassy carbon electrode; [f]Poly (p-aminobenzenesulfonic acid)/zinc oxide nanoparticles – carbon paste electrode; [g]Chitosan/N-doped graphene natively grown on hierarchical porous carbon nanocomposite/glassy carbon electrode; [h]Poly (glycine) modified carbon paste electrode; [i]Poly(L-arginine)-electrochemically reduced graphene oxide modified glassy carbon electrode; [j]Molecularly imprinted polymer/multi-walled carbon nanotubes/glassy carbon electrode; [k]Nickel (II) phthalocyanine-tetrasulfonic-Au nanoparticles nanocomposite film; [l]TiO_2-electrochemically reduced graphene oxide composite modified glassy carbon electrode; [m]Exfoliated graphite modified glassy carbon electrode; [n]Poly(3,4-ethylenedioxythiophene)@terbium hexacyanoferrate composite/glassy carbon electrode.

The carbon paste electrodes (CPEs) became very popular as electrode materials in electrochemical research, due to their easily modification, low background current, fast regenerative surface, low ohmic resistance and low cost, as well as to their versatility and ease with which they can be functionalized by the direct incorporation of various modifiers into the preparation of the carbon paste.[25,26]

The use of nanometric titania (TiO_2) for electrochemical sensors has multiple advantages compared to other materials including low costs, good adsorption capacity, good electrical conductivity, etc. TiO_2 has a tendency to form aggregates if a surfactant is not used, thus diminishing the stability and sensitivity of the sensor. Therefore there is necessary to anchor TiO_2 on graphene oxide to improve the dispersion and to fasten TiO_2 on the carbon paste electrode.[27]

Moreover, nanoparticle synthesis with controlled morphology and high dispersion on supports with large specific surfaces facilitates composition control and size of the catalytic active phase. Nanoparticles with controlled morphology and desired properties has experienced remarkable development over the last years because of their vast potential in nanotechnology.[28] Gold nanoparticles were preferred as modifiers in this study because they are capable to amplify the sensitivity of the electrochemical sensors.[3]

Recently, room-temperature ionic liquids (ILs) are non-molecular ionic compounds which have been developed and are widely used in many fields of electrochemistry, biophysical chemistry, material science, etc. due to their applications and unique properties such as high conductivity, electrochemical stability, their affinity to interact with various substances, wide electrochemical range and low toxicity.[29,30]

In this work, a novel IL/$AuTiO_2$/GO composite modified carbon paste electrode was developed for the fast and sensitive determination of tartrazine in real samples. The proposed sensor, IL/$AuTiO_2$/GO/CPE shows a good response for the electrochemical oxidation of tartazine in commercial food samples, like isotonic drink, mustard and yellow egg dye.

Experimental

Materials and reagents

Tartrazine, 1-butyl-2,3-dimethylimidazolium tetrafluoroborate, graphite powder (< 20 µm, synthetic), graphene oxide powder (15-20 sheets, 4-10% edge-oxidized), monosodium phosphate, disodium phosphate, iron(III) nitrate, copper(II) sulfate pentahydrate, manganese(II) chloride, magnesium chloride, potassium sulfate, potassium chloride, sodium chloride, sodium nitrate, potassium nitrate, ascorbic acid, D-glucose, sucrose, sunset yellow FCF and allura red AC were purchased from Sigma Aldrich, paraffin oil (d_4^{20}, 0.86 g cm^{-1}) from Fluka (Buchs, Sweden) and titanium dioxide nanopowder (TiO_2) (Degussa, P25) from Wako Chemicals. Polyvinylpyrrolidone, M.W. 8000 and chloroauric acid ($HAuCl_4$) were purchased from Alfa-Aesar (Germany).

Phosphate buffer solution (PBS, 0.1 mol L^{-1}) was prepared by using monosodium phosphate and disodium phosphate. The pH of the buffer solution was adjusted using different amounts of 0.1 mol L^{-1} sodium hydroxide solution to obtain different pH (2.0, 3.0, 4.0, 5.0, 6.0 and 7.0). The stock solution of 10^{-2} mol L^{-1} tartrazine was prepared in deionized water. The working solutions were daily prepared and protected from sun light.

Apparatus and methods

The cyclic voltammetry (CV) and differential pulse voltammetry (DPV) analysis were carried out using a mini potentiostat EmSTAT Pico (software PsTrace 5.7 PalmSens) connected to a laptop for data acquisition. The electrochemical impendence spectroscopy (EIS) measurements were achieved using an IVIUM COMPACTSTAT potentiostat connected to a laptop with IVIUM 2.025 software. All electrochemical experiments were carried out at around 22 °C. The results were recorded using an electrochemical cell containing three electrodes: the modified carbon paste electrode, Ag/AgCl (0.1 mol L^{-1} KCl) and Pt-wire as working, reference and auxiliary electrodes. The pH adjustment was done using a Mettler Toledo pH meter.

The morphology of the sensors was investigated by scanning electron microscopy (SEM). The SEM images were taken by a FEI Company's Quanta Inspect F microscope with field emission electron beam gun (FEG) and a resolution of 1.2 nm equipped with EDAX (Mn = 129 eV).

Synthesis of Au nanoparticles

Au nanoparticles surrounded by polyvinylpyrrolidone (PVP) were obtained by alkaline polyol method. A modified synthesis method adapted from previous studies described in detail in a previous publication[31] was conducted for producing monodisperse nanoparticles. More exactly, 5 mL of 5 mmol L^{-1} $AuHCl_4 \times 3H_2O$ Roth solution in ethylene glycol (EG) was added dropwise at 100 mL alkaline solution 25 mmol L^{-1} NaOH and 5 mmol L^{-1} PVP held at 120 °C in hydrogen flow (25 cm^3 min^{-1}) under stirring in a three-neck flask. In this so-called alkaline polyol synthesis, EG serves both as reducing agent and solvent. The temperature is kept at 120 °C for 60 minutes in order to obtain the nucleation process and grow of the metallic particles due to the fact that the metallic precursor is reduced by EG to its metallic phase. The as obtained suspension of metal nanoparticles contains uniformly distributed particles having nano dimension. The solutions were then cooled down to room temperature maintaining all this time the inert atmosphere.

The AuNPs were separated by adding acetone to the colloidal suspensions. The mixture was then cooled to -16 °C for 24 hours; the precipitates were repeatedly washed with acetone and separated by centrifugation at 14000 rpm to remove any traces of PVP and EG. Afterward it was dried in oven at 100 °C for a period of 4 h.

Preparation of $AuTiO_2$/GO composite

For the synthesis of the $AuTiO_2$/GO composite, 50 mg graphene oxide and 50 mg TiO_2 were dispersed in deionized water and ultrasound for 30 minutes each. The two solutions were mixed and ultrasound for 4 hours at 80 °C until the water was removed. The obtained material was dried for 24 hours at 100 °C and then heated in a stream of inert gas to 300 °C. Afterwards it was reduced using a reduction mixture of 5% H_2/Ar for 1 hour at 300 °C and then was cooled to room temperature. Finally, the Au/TiO_2/GO composite was obtained by impregnating the previously synthetised Au nanoparticles on the TiO_2/GO powder, thus resulting a new composite material with 5% metal loading (5%Au@TiO_2/GO).

Preparation of IL/AuTiO$_2$/GO/CPE

For the preparation of the IL/AuTiO$_2$/GO/CPE electrochemical sensor, 90 mg of graphite powder and 10 mg of AuTiO$_2$/GO composite were used, over which was added 40 μL paraffin oil and mixed for 20-30 min to form a homogenous paste. Then, 30 μL from a solution of 1-butyl-2,3-dimethylimidazolium tetrafluoroborate as ionic liquid (IL) (10^{-3} mol L^{-1} stock solution in methanol) was added to carbon paste to form the modified carbon paste electrode. The obtained paste was inserted into a plastic tube. The electrical contact was realized by introducing a silver wire into the paste. The surface of the modified sensor was refreshed by polishing on an aluminum foil. When not used, the IL/AuTiO$_2$/GO/CPE was kept at room temperature, in a dry place, protected from light. Utilization of TiO2 and Au nanoparticles improved the conductivity of the sensors. The ionic liquid was used as electrocatalyst.

Samples preparation

To test the practical application, the proposed electrochemical sensor was used to determine tartrazine in various commercial food samples: isotonic drink, mustard and yellow egg dye, which were purchased from a local supermarket. The isotonic drink and yellow egg dye samples were diluted in PBS pH = 2.0, in a ratio of 1:1 (v/v) and spiked with different concentrations of the tartrazine. The mustard samples were weighed, then were diluted 10 times with PBS pH = 2.0, then were stirred for 15 min and then were filtered, after that were spiked with various concentrations of the tartrazine. The samples were freshly prepared immediately before analysis.

Results and Discussions

SEM-EDX characterization

SEM technique was utilized to characterize the surface morphologies of the prepared electrodes. Fig. 1 presents the SEM images of CPE, IL/CPE, AuTiO$_2$/GO/CPE, IL/AuTiO$_2$/GO/CPE and EDAX spectrum of IL/AuTiO$_2$/GO/CPE. A dense porous surface can be seen for CPE and IL/CPE, adding that for the latter the surface is more homogenous. When AuTiO$_2$/GO and IL/AuTiO$_2$/GO composite were added to the carbon paste electrode, the microstructure changes. The CPE modified with AuTiO$_2$/GO composite shows a denser and uniform surface, augmenting the surface area and thus improving the signal. In Figs. 1c

and d, the presence of Au/TiO_2 is confirmed from the lighter zones in the SEM images and from the EDAX spectrum (Fig. 1e).

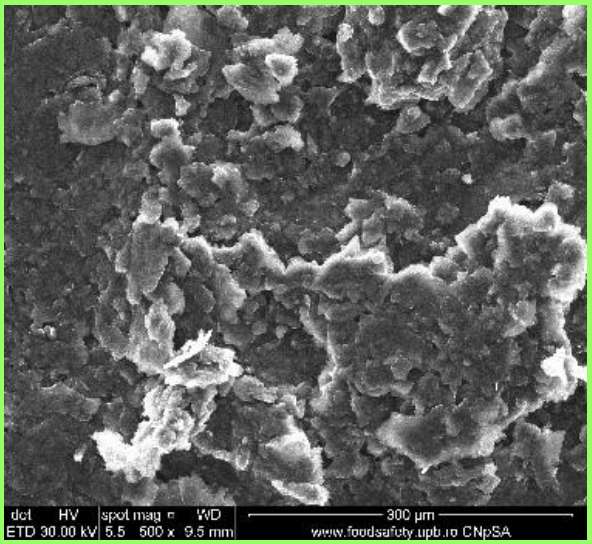

(a)

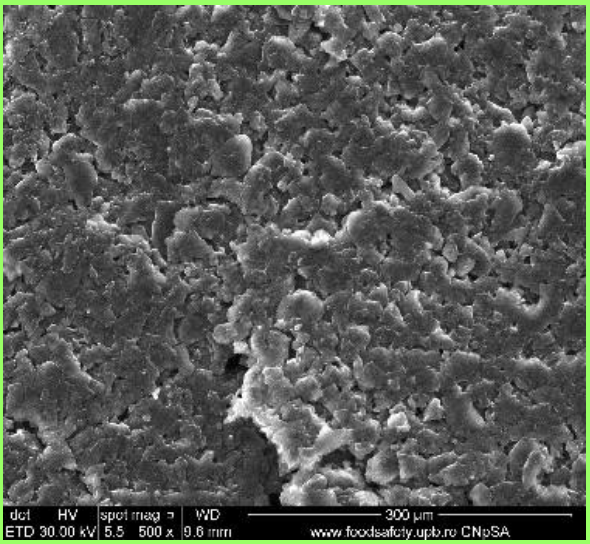

(b)

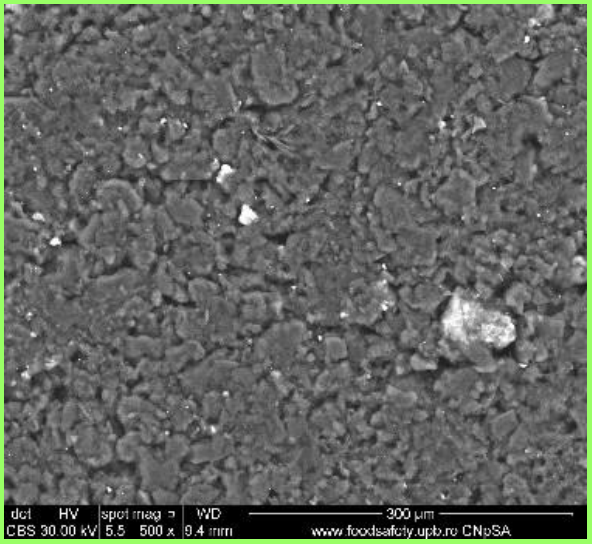

(c)

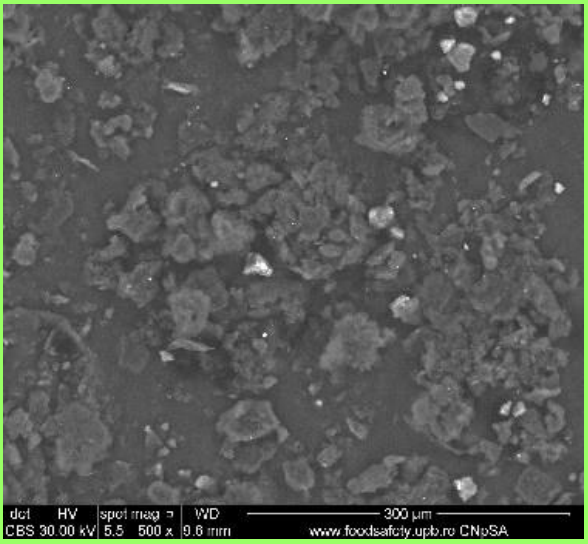

(d)

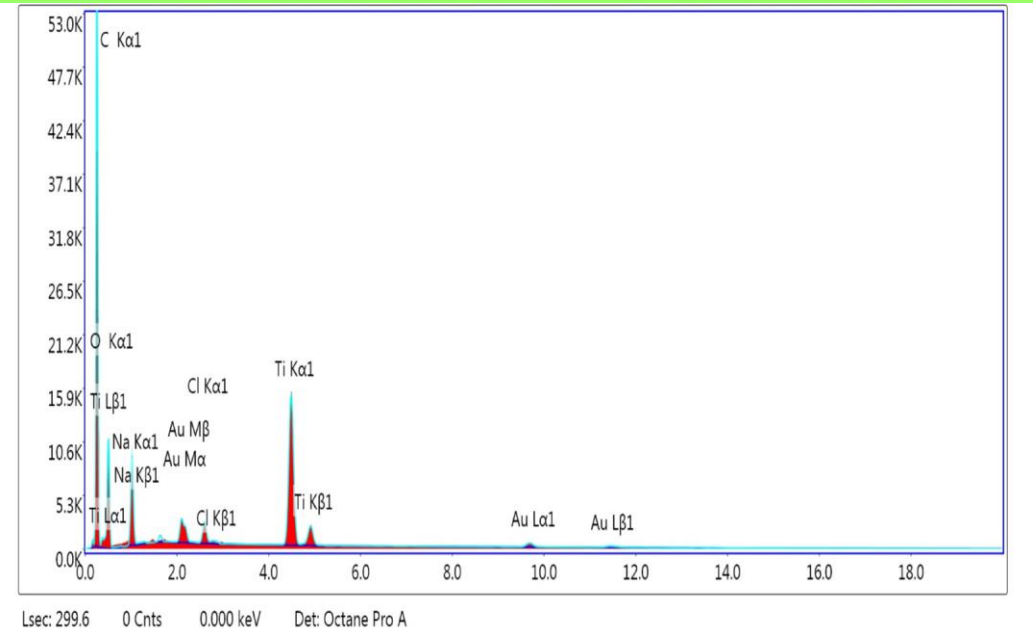

(e)

Figure 1. SEM images of (a) CPE, (b) IL/CPE, (c) $AuTiO_2$/GO/CPE, and (d) IL/$AuTiO_2$/GO/CPE; (e) EDAX spectrum of IL/$AuTiO_2$/GO/CPE.

The presence of $AuTiO_2$/GO composite was proved by SEM mapping also. Fig. 2 shows the SEM mapping of $AuTiO_2$/GO/CPE. It was observed that gold/titania was distributed throughout the whole sample.

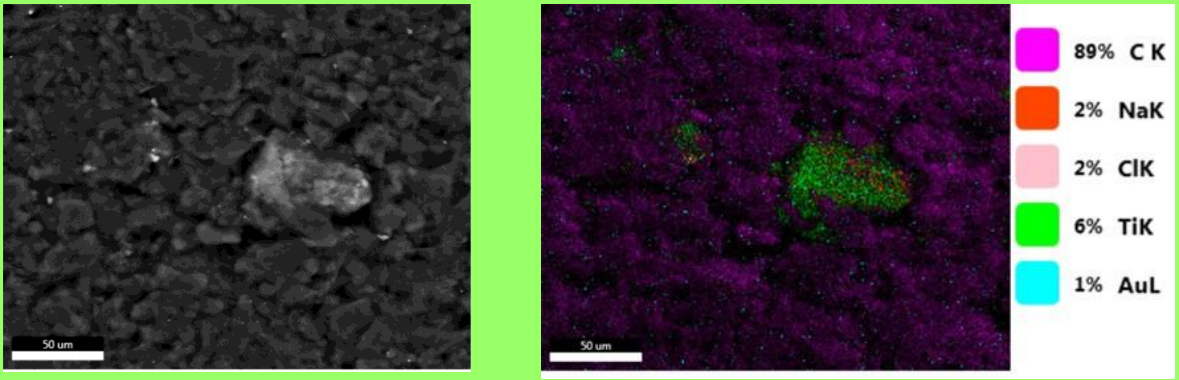

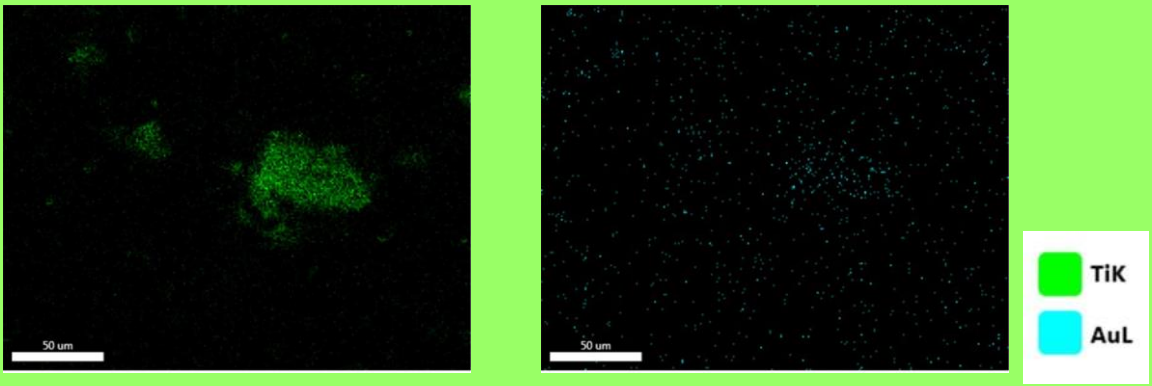

Figure 2. SEM mapping of Au/TiO_2/GO/CPE.

Electrochemical characterization of the sensors

The electrochemical characterization of the sensors: carbon paste electrode (CPE), carbon paste electrode modified with IL (IL/CPE), carbon paste electrode modified with $AuTiO_2$/GO ($AuTiO_2$/GO/CPE) and carbon paste electrode modified with IL/$AuTiO_2$/GO (IL/$AuTiO_2$/GO/CPE) was performed using the following methods: cyclic voltammetry (CV) and electrochemical impedance spectroscopy (EIS).

The CV was used to study the electrochemical response of the modified sensor. The CVs were performed in a solution of 5.0×10^{-3} mol L^{-1} $K_3[Fe(CN)_6]$ (0.1 mol L^{-1} KCl) in a potential range between -0.6 V and 1.0 V, using as working electrodes, the CPE, IL/CPE, $AuTiO_2$/GO/CPE and IL/$AuTiO_2$/GO/CPE (Fig. 3a). It can be observed that after the modification of the CP electrode with IL, $AuTiO_2$/GO and IL/$AuTiO_2$/GO, the conductivity of the sensor increased. Therefore, this has indicated that the modification was done and the electrochemical response was improved.

The EIS study was achieved to examine the interface of the sensors in a frequency range between 1.0×10^5 and 1.0×10^{-1} Hz. All the measurements of EIS were performed in a solution of 5.0×10^{-3} mol L^{-1} $K_3[Fe(CN)_6]$ (0.1 mol L^{-1} KCl). The Nyquist plots are illustrated in the Fig. 3b. As can be seen from Fig. 3b, CPE showed a large well-defined semicircle in a low frequency range which corresponds to a high electrical resistance R_{ct} = 1.250×10^5 Ω. After the modification process of CPE with IL, the semicircle diameter decreased ($R_{ct} = 2.818 \times 10^4$ Ω). The same behavior was observed afterwards for CPE modified with $AuTiO_2$/GO ($R_{ct} = 1.392 \times 10^4$ Ω). In the case of IL/$AuTiO_2$/GO/CPE, a much smaller quasi-semicircle is observed ($R_{ct} = 5.714 \times 10^3$ Ω). In conclusion, the CPE modified

with $AuTiO_2$/GO and IL, respectively, showed a smaller semicircle and a R_{ct} value lower than the R_{ct} value of the unmodified carbon paste electrode. The EIS results showed that are in good agreement with the results obtained by CV in a solution of 5.0×10^{-3} mol/L $K_3[Fe(CN)_6]$ (0.1 mol L^{-1} KCl).

The electrochemical behavior of the CPE, IL/CPE, $AuTiO_2$/GO/CPE and IL/$AuTiO_2$/GO/CPE was tested using also the CV method. In Fig. 3c the recorded cyclic voltammograms for all the sensors in PBS pH 2.0 containing 100 µmol L^{-1} Tz are presented. Comparing the four electrodes (Fig. 3c), the IL/$AuTiO_2$/GO/CPE gave the best results for the oxidation of tartrazine. Thus, this sensor was further characterized and investigated for the electrochemical detection of Tz in real food samples.

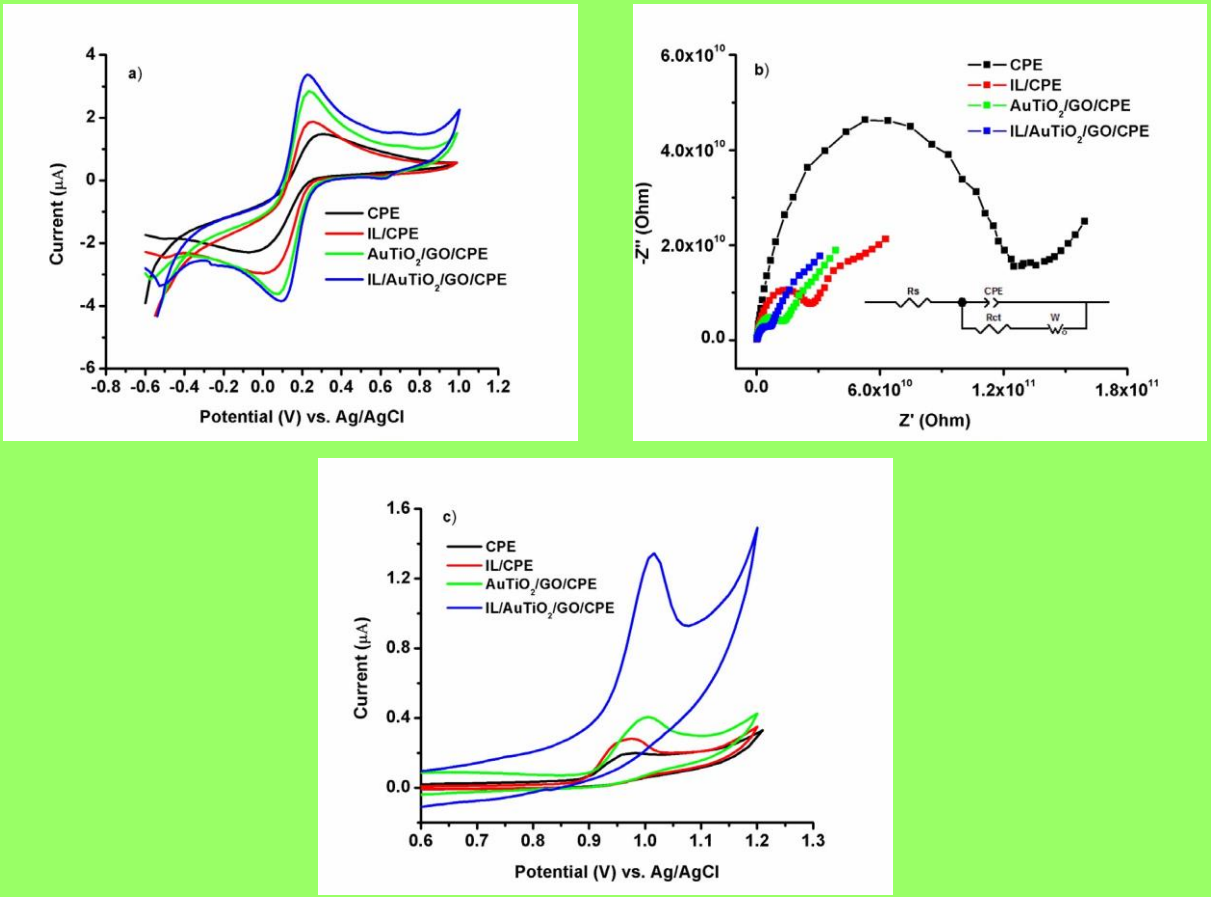

Figure 3. (a) Cyclic voltammograms of the current plotted against the potential (Working conditions: step potential 0.025 V; scan rate 0.1 V s^{-1}) in a solution of 5.0×10^{-3} mol L^{-1} $K_3[Fe(CN)_6]$ in 0.1 mol L^{-1} KCl using the CPE (black line), IL/CPE (red line), $AuTiO_2$/GO/CPE (green line), and IL/$AuTiO_2$/GO/CPE (blue line); **(b)** Electrochemical impedance spectra recorded for CPE (black line), IL/CPE (red line), $AuTiO_2$/GO/CPE (green

line), and IL/$AuTiO_2$/GO/CPE (blue line) in a solution of 5.0×10^{-3} mol L^{-1} $K_3[Fe(CN)_6]$ in 0.1 mol L^{-1} KCl (Conditions: frequency range between 1.0×10^5 to 1.0×10^{-1} Hz). Inset: equivalent circuit diagram of the electrochemical interface used to fit the impedance spectra where R_s is the solution resistance, CPE is the constant phase element, R_{ct} is the electron-transfer resistance, and Z_w is the Warburg diffusion resistance; **(c)** The recorded cyclic voltammograms in pH 2.0 PBS containing 100 µmol L^{-1} tartrazine for the CPE (black line), IL/CPE (red line), $AuTiO_2$/GO/CPE (green line), and IL/$AuTiO_2$/GO/CPE (blue line).

The electrocatalytic activity of the four sensors was investigated by calculating the electroactive surface area using the Randles-Sevcik equation[32] for quasi-reversible processes. The peak current intensity equation can be described as follows:

$$Ip_a = \pm (2.69 \times 10^5)\, n^{3/2} A C_0 D_R^{1/2} \nu^{1/2} \quad (1)$$

where: Ip_a - anodic peak current (A), n - number of transferred electrons (in this case, n = 1), A - active surface area of the electrode (cm^2), C_0 - concentration of $K_3[Fe(CN)_6]$ (mol cm^{-3}), D_R - diffusion coefficient (7.60×10^{-6} cm^2 s^{-1}), and ν - scan rate (V s^{-1}). The study was performed in a solution of 5.0×10^{-3} mol L^{-1} $K_3[Fe(CN)_6]$ (0.1 mol L^{-1} KCl). By the variation of the scan rate from 0.010 to 0.100 V s^{-1}, the anodic and cathodic peaks (Ip_a and Ip_c) showed a linear dependency on the square root of the scan rate, suggesting that the redox process was controlled by diffusion. Fig. 4a shows the trend between the increase of the scan rate and intensity of the current. The linear dependences for both peaks Ip_a *vs.* $\nu^{1/2}$ and Ip_c *vs.* $\nu^{1/2}$ are presented in Fig. 4b. The values of the surface area were determined from Eq. (1). The IL/$AuTiO_2$/GO/CPE presents a bigger active area, 0.0036 cm^2 compared to 0.0015 cm^2 for the CPE, 0.0019 cm^2 for the IL/CPE, and respectively, 0.0030 cm^2 for the $AuTiO_2$/GO/CPE.

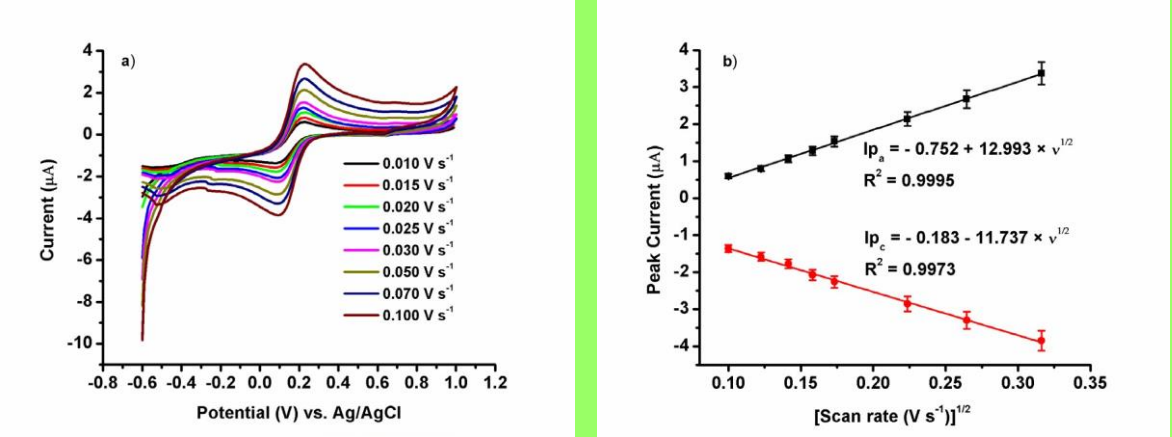

Figure 4. (a) Cyclic voltammograms in a solution of 5.0×10^{-3} mol L^{-1} $K_3[Fe(CN)_6]$ in 0.1 mol L^{-1} KCl at different scans rate from 0.010 to 0.100 V s^{-1} using the IL/$AuTiO_2$/GO/CPE (Working conditions: potential range from -0.6 V to1.0 V; step potential 0.025 V); **(b)** Dependence of the peak current on the square root of the scan rate, using the IL/$AuTiO_2$/GO/CPE; all data points were the mean value of 3 measurements.

Influence of the scan rate on the oxidation of tartrazine

The electrochemical behavior of tartrazine was investigated by cyclic voltammetry technique, using the IL/$AuTiO_2$/GO/CPE at different scan rates between 0.01 and 0.70 V s^{-1}. This study was carried out in PBS pH = 2.0 containing 100 µmol L^{-1} tartrazine. The anodic peak currents increased with the increase of the scan rate (Fig. 5a).

A linear relation between the peak current and the square root of the scan rate ($\nu^{1/2}$) (Fig. 5b) was observed, given by the following regression equation: Ip_a (µA) = - 0.029 + 2.871 × $\nu^{1/2}$ (R^2 = 0.9938), which showed that the oxidation of Tz on the IL/$AuTiO_2$/GO/CPE was a typical diffusion-controlled process.[33,34]

The linear dependence obtained by plotting the logarithm of peak current and the logarithm of scan rate is illustrated in Fig. 5c. The relationship between them is given by the equation: Log (Ip_a) (µA) = 0.434 + 0.483 × log (ν). If the value of the slope is 0.500, it indicates a process controlled by diffusion, while if it is close to 1, it is controlled by adsorption. Thus, the obtained slope value was calculated to be 0.483 which confirmed that the electrochemical process of Tz on the IL/$AuTiO_2$/GO/CPE is controlled by diffusion. These results are in agreement with the results obtained from Fig. 5b.

The Laviron equation[35] was used to calculate the heterogeneous rate constant:

$$Ep_a = E^0 - \left(\frac{RT}{\alpha nF}\right)\ln\left(\frac{RTk_s}{\alpha nF}\right) + \left(\frac{RT}{\alpha nF}\right)\ln\upsilon \quad (2)$$

where E^0 - formal potential (V), R - universal gas constant (8.314 J mol^{-1} K^{-1}), T - absolute temperature (298.15 K), α - electron transfer coefficient of the oxidation of Tz, n - number of electrons transferred, k_s - heterogeneous rate constant of the electrochemical reaction (s^{-1}), F - Faraday's constant (96.485 C mol^{-1}), and ν - scan rate (V s^{-1}). The formal potential of Tz (E^0 = 0.988) was found as the value of the intercept from relation: Ep_a (V) = 0.988 + 0.661× ν, which was associated with the peak potential and the scan rate (Fig. 5d). In Fig. 5d, the oxidation peak potential (Ep_a) was positively shifted with the increase of the scan rate (ν).

Fig. 5e illustrates the linear relationship between anodic peak potential *vs.* natural logarithm of scan rate. The heterogeneous rate constant of the electrochemical reaction was calculated to be 0.443 s^{-1} using the intercept and the slope values from equation: Ep_a (V) = 1.070 + 0.017 × Ln(ν). According to this equation, the two kinetic parameters α and n were determined to be 0.5 and 0.8 (~ 1 electron), respectively.

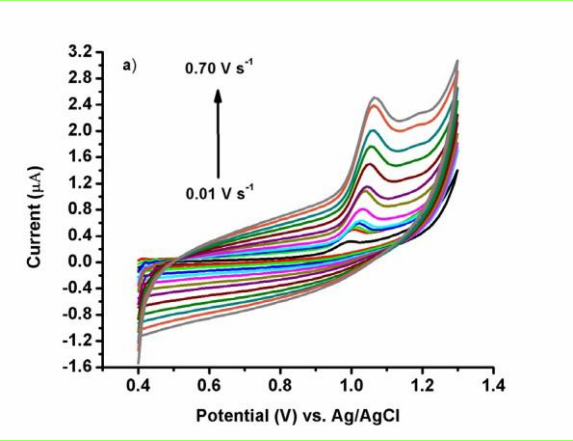

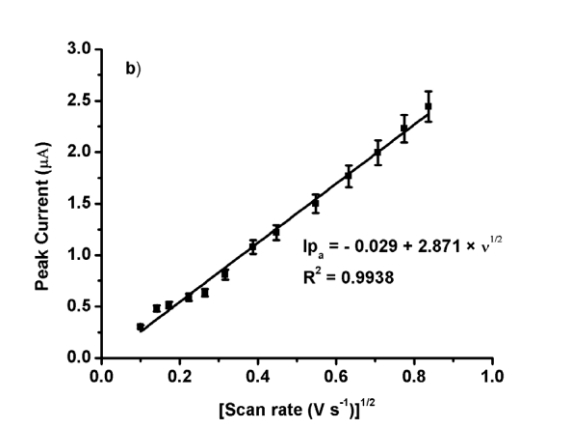

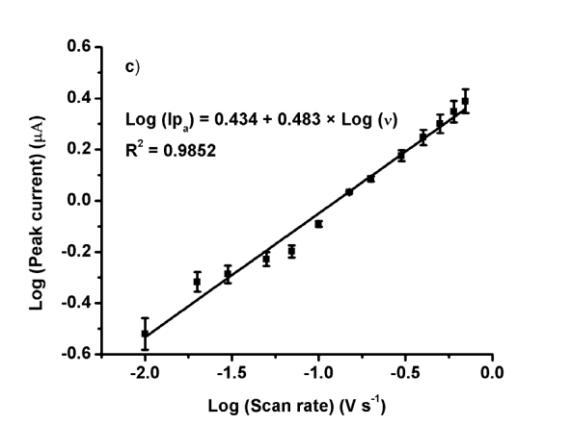

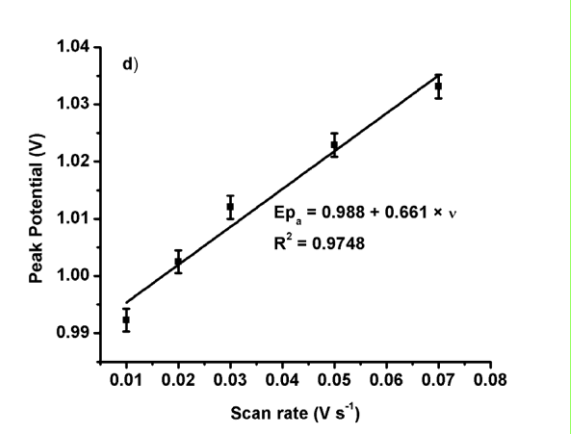

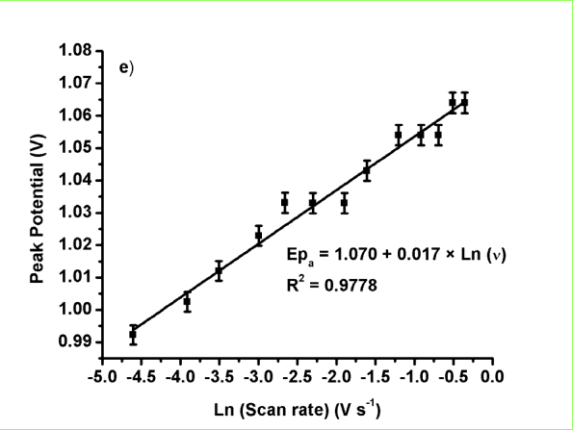

Figure 5. (a) Cyclic voltammograms recorded at different scan rates between 0.01 and 0.70 V s^{-1} in PBS pH = 2.0 containing 100 µmol L^{-1} tartrazine, using the IL/$AuTiO_2$/GO/CPE; **(b)** Linear dependence of the peak current on the square root of the scan rate; **(c)** Dependence between logarithm of peak current and logarithm of scan rate; **(d)** Linear dependence between peak potential and scan rate; **(e)** Linear correlation of peak potential *vs.* natural logarithm of scan rate; all data points were the mean value of 3 measurements.

Thus, one electron was involved in the oxidation process of tatrazine which is situated on the aromatic ring. Scheme 1 described the possible electrochemical oxidation mechanism of tartrazine.

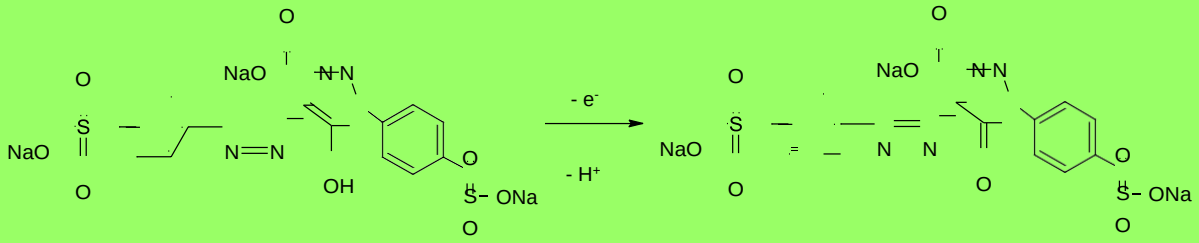

Scheme 1. The possible mechanism of the electrooxidation of tartrazine on the IL/$AuTiO_2$/GO/CPE in acidic medium (pH = 2.0).

Influence of the pH

The pH value of the buffer solution is an essential parameter, which has a major influence on the electrochemical behavior of tartrazine. The influence of pH on the electrochemical oxidation of a 100 µmol/L solution of tartrazine in PBS at different pH values (2.0, 3.0, 4.0, 5.0, 6.0 and 7.0) at the surface of IL/$AuTiO_2$/GO/CPE was investigated by differential pulse voltammetry method, as shown in Fig. 6a. The current intensity decreased from pH = 2.0 to 4.0 with a slight increment at pH = 5.0, and then, it started to

decrease until pH = 7.0 was achieved (Fig. 6b). As can be seen in Fig. 6b, the highest current intensity of tartrazine was observed when the pH was 2.0. It is known that tartrazine is a protic aromatic molecule and turns into cations at low pH by deprotonation. The optimum pH of 2.0 was lower than the acid dissociation constant of tartrazine ($pK_a = 9.4$).[36] Thus, for pH solution < pK_a, molecules of tartrazine exist in a cationic form.[37] Therefore, the pH 2.0 PBS was selected as the supporting electrolyte for further experiments. As the pH increased, a slightly negative potential shift was observed. Fig. 6b shows the relationship between the peak potential (Ep_a) and the pH values. The linear relations: Ep_a (V) = 1.019 – 0.062 × pH with regression coefficient (R^2) of 0.9844 and the slope value of 0.062 V pH^{-1}, which is close to the Nernstian theoretical value of 0.059 V pH^{-1}, indicated that the number of protons is equal to the number of the electrons involved in the oxidation process.

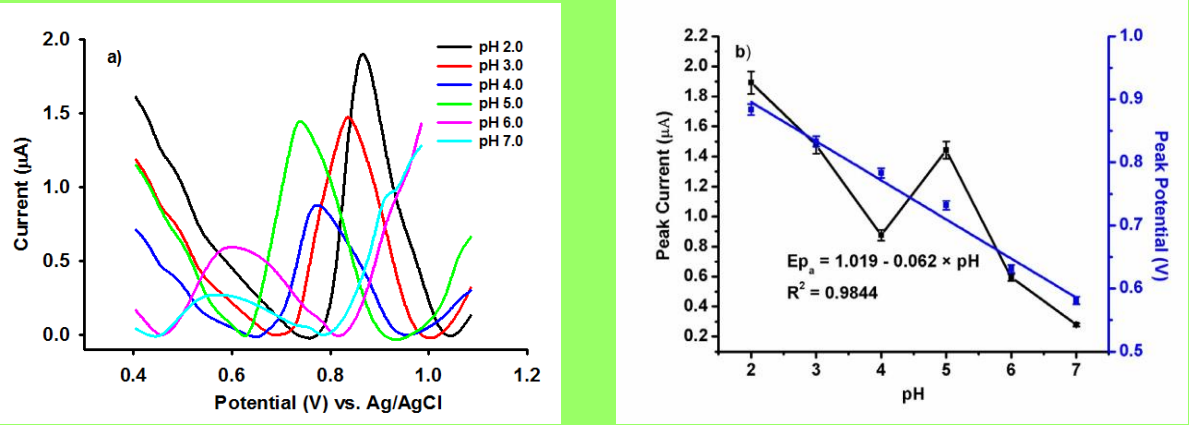

Figure 6. (a) Differential pulse voltammograms of 100 µmol L^{-1} tartrazine at the IL/$AuTiO_2$/GO/CPE in PBS at pH values of 2.0, 3.0, 4.0, 5.0, 6.0 and 7.0; **(b)** The effect of the pH on the peak current (black dots) and the linear dependence of the peak potential with the pH (blue line). Working conditions: step potential of 0.025 V and scan rate of 0.025 V s^{-1}

Response characteristics of IL/$AuTiO_2$/GO/CPE on the oxidation of tartrazine

The response characteristics of the tartrazine oxidation on the surface of IL/$AuTiO_2$/GO/CPE were also studied. The differential pulse voltammetry method (Fig. 7a) was used, in PBS pH = 2.0 containing different concentrations of tartrazine. In Fig. 7b the peak current response versus concentration of tartrazine was plotted and exhibited a linear dependence on two concentration ranges: from 1 to 400 µmol L^{-1} and from 400 to 1000 µmol L^{-1}, with the correlation coefficients of 0.9992 and 0.9929, respectively. The limit of detection (LOD) was 0.33 µmol L^{-1}, which was calculated by using the following equation:

LOD = 3s/m,[38] where *s* - standard deviation of the current intensity response (3 runs) of the blank (PBS) and *m* - slope of the calibration curve. The corresponding linear regression equation was: Ip_a (µA) = 0.070 + 0.008 × $C_{tartrazine}$. According to this equation the sensitivity of the proposed sensor was 0.008 µA µmol L^{-1}.

The LOD value of the IL/AuTiO$_2$/GO/CPE was comparable with those previously reported in the literature for the determination of tartrazine using various sensors (Table I). Although, in most cases (Table I), a lower detection limit and a wide linear range and was observed. Thus, the prepared electrode showed many advantages, such as high sensitivity, easy surface update, simple modification process and good stability. Although the limit of detection reported in this paper is higher with two magnitude ordered, and the proposed sensor can be used at higher concentrations than the sensor proposed before,[22] the advantages of the proposed sensor versus the one published earlier[22] are: the samples do not need any dilution before measurement, as the concentration of tartrazine in the samples analyzed is withing the linear concentration range of the proposed sensor; the design of the proposed sensor is highly reliable; the cost of the sensor proposed by us is very low, and the utilization time longer. Furthermore, the method can be carried out using inexpensive equipment in a relatively short time.

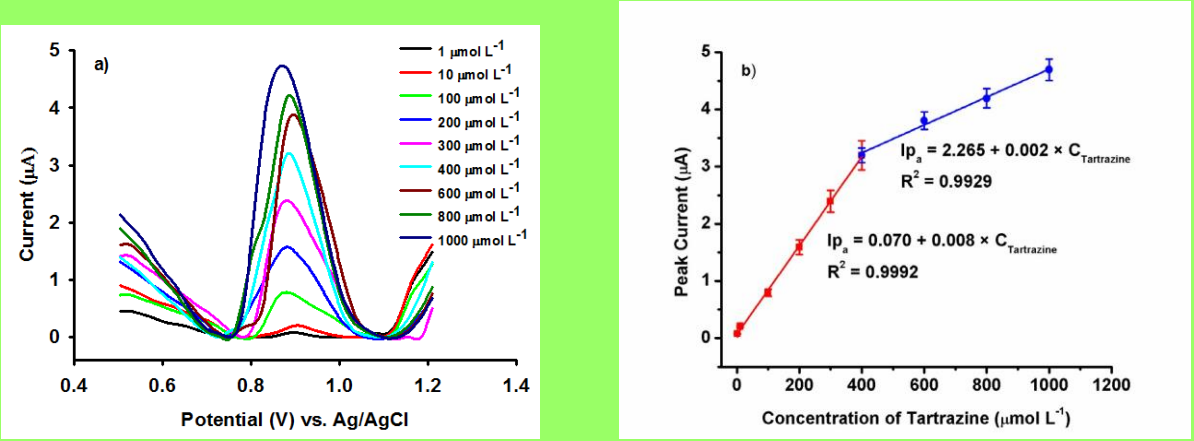

Figure 7. (a) Differential pulse voltammograms recorded with the IL/AuTiO$_2$/GO/CPE in PBS pH = 2.0 containing different concentrations of tartrazine (1 to 1000 µmol L^{-1}); **(b)** Calibration curves obtained with the IL/AuTiO$_2$/GO/CPE, in two linear ranges, from 1 to 400 µmol L^{-1} (red line) and from 400 to 1000 µmol L^{-1} (blue line). Working conditions: step potential of 0.025 V and scan rate of 0.025 V s^{-1}.

Interference studies

For selectivity study, several inorganic ions such as Fe^{3+}, Cu^{2+}, Mg^{2+}, Na^{+}, K^{+}, Mn^{2+}, Cl^{-}, NO_3^{-}, SO_4^{2-}, and organic species like sucrose, glucose, ascorbic acid, allura red and sunset yellow were tested as possible interferences in the determination of tartrazine. The possible interfering species were chosen from the substances commonly found with tartrazine in food samples. The tolerance limit was defined as the maximum concentration of interference that caused a current intensity variation in terms of a relative error (± 5% acceptance level), and bias (%). All the assessed solutions were obtained in optimal conditions, pH = 2.0 PBS with a constant concentration of tartrazine (10 µmol L^{-1}). The experimental results exhibited no obvious influence on the detection of tartrazine when an excess of 10-fold of ascorbic acid, sunset yellow, and allura red; 25-fold of SO_4^{2-}, and glucose; 50-fold of K^{+}, Mn^{2+}, and Fe^{3+}, 100-fold of Cu^{2+}, Mg^{2+}, Na^{+}, Cl^{-}, NO_3^{-}, and sucrose was added (Table II), which indicate that the proposed sensor presented a high selectivity on the determination of tartrazine.

Table II. The influence of coexisting species on the detection of tartrazine (n = 5)

Coexisting species	Concentration of coexisting species (µmol L^{-1})	Tolerance limit	Relative error (%)	Bias (%)
Cu^{2+}	1000	100	3.22	2.43
Mg^{2+}	1000	100	-2.50	1.18
Na^{+}	1000	100	1.69	-2.28
Cl^{-}	1000	100	-3.87	6.36
NO_3^{-}	1000	100	0.33	-1.97
Sucrose	1000	100	3.72	-1.33
K^{+}	500	50	0.73	2.64
Mn^{2+}	500	50	3.26	1.99
Fe^{3+}	500	50	1.68	0.87
SO_4^{2-}	250	25	-0.56	-3.33
Glucose	250	25	0.94	-0.35
Ascorbic acid	100	10	-3.66	-3.27
Sunset yellow	100	10	-4.21	-7.28
Allura red	100	10	-4.21	-3.92

Reproducibility, repeatability and stability

Under the optimal experimental conditions, the reproducibility, repeatability and stability of the IL/$AuTiO_2$/GO/CPE were tested using a solution of 10 µmol L^{-1} tartrazine in PBS pH = 2.0 by DPV. To evaluate the reproducibility, 3 new modified electrochemical electrodes were fabricated in the same way. For all the modified electrodes, the relative standard deviation (RSD%) was found to be 2.72% (n = 5); after 5 runs each, the obtained outcome was correlated with repeatability. For the same sensors, the inter-day repeatability was calculated at 3.85% for 5 repetitive measurements. Then, the long-term stability of the IL/$AuTiO_2$/GO/CPE was examined by keeping the modified electrode at room temperature for two weeks. After this period, the current intensity of the tartrazine was retained around 96.23% ± 2.19% from the initial current response. The above results have demonstrated good stability and reproducibility and of the proposed sensor in the detection of tartrazine.

Analytical application

The applicability of the developed method was tested by carrying out recovery tests of tartrazine from different commercial food samples, such as isotonic drink, mustard and yellow egg dye. The IL/$AuTiO_2$/GO/CPE was used to perform DPV measurements in real samples for the detection of tartrazine. The food samples were prepared as mentioned before. The samples were inserted into the electrochemical cell; afterwards the height of the peak current was recorded. The values obtained were introduced into the equation of calibration shown above and the concentrations/amounts of the tartrazine. The values of the recovery, RSD and Bias (%) are summarized in Table III. The recoveries were found in the range 98.55-103.62%, with RSD% and Bias (%) values lower than 5.00%, respectively 2.00%. The results confirmed that the developed sensor can be accurately and reliably used for the assay of tartrazine in food samples.

Table III. Determination of tartrazine levels in isotonic drink, mustard and yellow egg dye using IL/$AuTiO_2$/GO/CPE

Samples	Amount added (µmol L^{-1})	Amount found (µmol L^{-1})	Recovery (%)	RSD (%)	Bias (%)
Isotonic	1.00	0.99	98.96	2.03	1.05
Drink	5.00	5.05	101.00	0.07	-0.99
	10.00	10.02	100.20	0.94	-0.20
	40.00	40.19	100.48	1.98	-0.48
Mustard	1.00	0.99	98.55	0.96	1.48
	5.00	5.01	100.16	0.67	-0.16
	10.00	9.94	99.35	0.62	0.65
	40.00	39.47	98.68	4.30	1.34
Yellow egg	1.00	1.00	99.99	4.85	0.01
Dye	5.00	4.98	99.51	3.38	0.50
	10.00	10.36	103.62	4.00	-3.49
	40.00	40.44	101.10	1.90	-1.08

Conclusions

This paper reported for the first time an electrochemical sensor used for the sensitive determination of tartrazine based on carbon paste electrode modified with IL and $AuTiO_2$/GO composite, respectively. The modified electrode showed a good electrochemical activity towards the oxidation of tartrazine in acidic medium at pH 2.0, a high selectivity, sensitivity, reproducibility and a good stability. The IL/$AuTiO_2$/GO/CPE was successfully applied to detect tartrazine from isotonic drink, mustard and yellow egg dye samples with recoveries values higher than 98.55% and with RSD and Bias values lower than 5.00%, respectively 2.00%, indicating the reliability of the method.

References

1. L. Zhao, B. Zeng, and F. Zhao, *Electrochim. Acta*, **146**, 611 (2014).
2. S. Tahtaisleyen, O. Gorduk, and Y. Sahin, *Anal. Lett.*, **53**, 1683 (2020).
3. K. Rovina, S. Siddiquee, and S. Md Shaarani, *Drug Chem. Toxicol.*, **44**, 447 (2021).
4. O. I. Lipskikh, E. I. Korotkova, Ye. P. Khristunova, J. Barek, and B. Kratochvil, *Electrochim. Acta*, **260**, 974 (2018).

5. M. A. Karimi, V. H. Aghaei, A. Nezhadali, and N. Ajami, *Food Anal. Methods*, **11**, 2907 (2018).
6. X. Zhao, Y. Liu, J. Zuo, J. Zhang, L. Zhu, J. Zhang, *J. Electroanal. Chem.*, **785**, 90 (2017).
7. K. Rovina, S. Siddiquee, and S. Md Shaarani, *Crit. Rev. Anal. Chem.*, **47**, 309 (2017).
8. G. Karim-Nezhad, Z. Khorablou, M. Zamani, P. S. Dorraji, and M. Alamgholiloo, J. *Food Drug Anal.*, **25**, 293 (2017).
9. S. Bonan, G. Fedrizzi, S. Menotta, and C. Elisabetta, *Dyes Pigm.*, **99**, 36 (2013).
10. E. Dinç, A. H. Aktaş, D. Baleanu, and Ö. Üstündağ, *J. Food Drug Anal.*, **14**, 284 (2006).
11. D. Chen, M. Wu, S. Xie, X. Li, Y. Tao, X. Wang, L. Huang, Y. Pan, D. Peng, and Z. Yuan, *J. Chromatogr. Sci.*, **57**, 462 (2019).
12. W. de A. S. Bento, B. P. Lima, and A. P. S. Paim, *Food Chem.*, **183**, 154 (2015).
13. J. Yi, L. Zeng, Q. Wu, L. Yang, and T. Xie, *Food Anal. Methods*, **11**, 1608 (2018).
14. M. A. Prado, L. F. V Boas, M. R. Bronze, and H. T. Godoy, *J. Chromatogr. A*, **1136**, 231 *(***2006**).
15. R. Sahraei, A. Farmany, and S. S. Mortazavi, *Food Chem.*, **138**, 1239 *(***2013)**.
16. R. Li, Z.-T. Jiang, and Y.-H. Liu, *J. Food Drug Anal.*, **16**, 91 (2008).
17. Z.-Z. An, Z. Li, Y.-Y. Guo, X.-L. Chen, K.-N. Zhang, D.-X. Zhang, Z.-H. Xue, X.-B. Zhou, and X.-Q. Lu, *Chin. Chem. Lett.*, **28**, 1492 (2017).
18. J. G. Manjunatha, *Heliyon*, **4**, e00986 (2018).
19. P. Wang, X. Liu, Q. Hu, H. Gao, and W. Ma, *Int. J. Electrochem. Sci.*, **15**, 8901 (2020).
20. Z. Wang, Y. Shan, L. Xu, G. Wu, and X. Lu, *Int. J. Polym. Anal. Charact.*, **22**, 83 (2017).
21. L. F. de Lima, C. C. Maciel, A. L. Ferreira, J. C. de Almeida, and M. Ferreira, *Mater. Lett.*, **262**, 127186 (2020).
22. Q. He, J. Liu, X. Liu, G. Li, P. Deng, J. Liang, and D. Chen, *Sensors*, **18**, 1911 (2018).
23. X. Song, Z. Shi, X. Tan, S. Zhang, G. Liu, and K. Wu, *Sens. Actuators B*, **197**, 104 (2014).
24. M. Sakthivel, M. Sivakumar, S.-M. Chen, and K. Pandi, *Sens. Actuators B*, **256**, 195 (2018).
25. S. G. Hernández-Vargas, C. A. Cevallos-Morillo, and J. C. Aguilar-Cordero, *Electroanalysis*, **32**, 1938 (2020).

26. C. O. Chikere, E. Hobben, N. H. Faisal, P. Kong-Thoo-Lin, and C. Fernandez, *Microchem. J.*, **160**, 105668 (2021).
27. Z. Qin, J. Zhang, Y. Liu, J. Wu, G. Li, J. Liu, and Q. He, *Chemosensors*, **8**, 70 (2020).
28. O. V. Salata, *J. Nanobiotechnology*, 2, 3 (2004).
29. R. Darabi and M. Shabani-Nooshabadi, *Food Chem.*, **339**, 127841 (2021).
30. S. Šekuljica, V. Guzsvány, J. Anojčić, T. Hegedűs, M. Mikov, and K. Kalcher, *J. Mol. Liq.*, **306**, 112900 (2020).
31. F. Papa, C. Negrila, A. Miyazaki, and I. Balint, *J. Nanopart. Res.*, **13**, 5057 (2011).
32. P. Zanello, Inorganic electrochemistry: theory, practice and application, *RSC Adv.*, (2003).
33. X. Ye, Y. Du, D. Lu, and C. Wang, *Anal. Chim. Acta*, **779**, 22 (2013).
34. T. Gan, J. Sun, S. Cao, F. Gao, Y. Zhang, and Y. Yang, *Electrochim. Acta*, **74**, 151 (2012).
35. E. Laviron, *J. Electroanal. Chem.*, **101**, 19 (1979).
36. G. L. Dotto, M. L. G. Vieira, V. M. Esquerdo, and L. A. A. Pinto, *Brazilian J. Chem. Eng.*, **30**, 13 (2013).
37. S. Sahnoun, M. Boutahala, C. Tiar, and A. Kahoul, *C. R. Chim.*, **21**, 391 (2018).
38. S. A. Ozkan, J. M. Kauffmann, and P. Zuman, in: F. Scholz (Ed.), Chapter 8, Electroanalytical Method Validation in Pharmaceutical Analysis and Their Applications in Electroanalysis in Biomedical and Pharmaceutical Sciences, Springer Publishing House, 252 (2015).

Recent trends in ibuprofen and ketoprofen electrochemical quantification – a review

Abstract

Non-steroidal anti-inflammatory drugs are intensively manufactured and used. Therefore, is a need for simple, cost-effective, sensitive and selective detection methods that could improve their quality of analyses. The aim of this review is to present the construction, analytical performances and applicability of recently developed electrochemical sensors for the determination of ibuprofen and ketoprofen.

Introduction

Ibuprofen and ketoprofen are propionic acid derivatives, a subclass of non-steroidal anti-inflammatory drugs (NSAIDs). By inhibiting the enzyme cyclooxygenase, NSAIDs hinder the synthesis of pro-inflammatory prostaglandins, thus exhibiting their anti-inflammatory, analgesic and antipyretic features.[1] That is why they are used in conditions such as mild to moderate pain, musculoskeletal disorders, gout flares, fever and dysmenorrhea. Although NSAIDs are a well-established, widely used and effective class of drugs, they are not without side effects. Mainly, these active pharmaceutical ingredients affect the gastrointestinal, cardiovascular and renal systems.[2,3] Recent studies have shown that widespread consumption of NSAIDs has led to their emergence as environmental contaminants. Even in low concentrations or as residues or metabolites, the NSAIDs bear ecotoxicological effects on the aquatic biota (e.g. plants, bacteria and animals), producing DNA damage, cyto and genotoxicity, alterations on the oxidative stress enzymes, and haematological alterations.[4]

As compendial methods, the European Pharmacopoeia indicates the use of titrimetry and potentiometric titration to determine ibuprofen and ketoprofen, while the United States Pharmacopoeia recommends HPLC and titrimetry.[5-7] A literature survey revealed several chromatographic techniques used for the quantification of ibuprofen and ketoprofen such as high-performance liquid chromatography (HPLC) with UV-Vis,[8] reversed-phase HPLC (RP- HPLC) with fluorescence detection[9] or UV-Vis detection,[10,11] ultra-performance liquid chromatography-tandem mass spectrometry (UPLC-MS/MS),[12] gas chromatography-mass spectrometry (GC-MS)[13] and gas chromatography-tandem mass spectrometry (GC–MS/MS);[14] other categories of methods like spectrofluorimetry[15] and capillary electrophoresis (CE)[16,17] have also been identified in the literature. These determination methods were performed on various types of real or spiked samples such as biological samples (human serum and plasma, equine urine) or pharmaceutical dosage forms (tablets and gels). Although sensitive, reliable and accurate, the above-mentioned techniques bear a series of drawbacks as they are time- consuming, expensive, require sample pretreatment and separation and specialized personnel supervision.

Electrochemical methods such as chronoamperometry (CA), potentiometry, cyclic voltammetry (CV), differential pulse voltammetry (DPV) and square wave voltammetry (SWV) represent an appealing alternative to conventional techniques as they are simple, inexpensive and highly sensitive. Another advantage of these methods is that their principle is based on a surface phenomenon that allows the use of small amounts of samples, thus enabling miniaturization.[18] Moreover, the sensors used in these methods are easily designed and provide a rapid response that can be further improved through addition of chemical modifiers or surface functionalization.

This review is focused on the research activity aimed at developing new sensors with applicability in the determination of ibuprofen and ketoprofen conducted in the last five years.

1. Electrochemical sensors used for determination of ibuprofen

Ibuprofen (IBP), chemically denoted (RS)-2-(4-(2-methylpropyl)phenyl)propanoic acid, was previously electrochemically determined from water and biological samples, pharmaceutical formulations and aqueous solutions using electrochemical sensors such as boron-doped diamond electrode,[19,20] screen printed graphite electrode,[21] two types of silver-functionalized carbon nanofiber composite electrodes,[22] silver-doped zeolite-expanded graphite composite electrode[23] and a sensing platform comprising an aptamer attached by covalent bond to gold nanoparticles and deposited on the surface of a glassy carbon electrode.[24]

The following recently developed electrochemical sensors (Table 1) used in the determination of ibuprofen are classified in two categories, 3D sensors and disposable sensors. The 3D sensors class is subsequently sorted into glassy carbon based electrodes, carbon paste electrodes and other types of electrodes.

Table 1. Analytical characteristics of different electrochemical sensors used for the detection of ibuprofen and ketoprofen reported in the literature.

Analyte	Electrode	Detection method	Linear range (μmol L^{-1})	Detection limit	Sample matrix	Reference
Ibuprofen	pretreated GCE	SWSV	1.45 – 3.87	0.96	pharmaceutical tablets	25
	SD-MWCNT/GCE	FIA-AMP	10 – 1000	1.9	pharmaceutical tablets	27
	polyaniline nanofiber/GCE	DPSV	0.96 – 1.94	0.48	pharmaceutical liquid	28
	MB/Apt/nanocomposite/GCE	DPV	7×10^{-5} – 6	2×10^{-5}	pharmaceutical tablets pharmaceutical oral suspension blood serum wastewater	29
	Apt/AuNPs@N-GQDs/GCE	DPV	1×10^{-10} – 0.2	33.33×10^{-12}	pharmaceutical tablets blood serum wastewater	30
	P(L-Asp)/GCE	SWV	1 – 150	0.22	pharmaceutical tablets urine	31
	AgNPs@Af-GO-MIP/GCE	DPV	1 – 100	8.7×10^{-3}	pharmaceutical tablets human urine	32
	Cu_3TeO_6/GCE	DPV	0.02 – 5 9 – 246	1.7×10^{-2}	infected human urine human urine blood serum	33
	Mt–CPE	DPV	0.1 – 10000	6.8×10^{-2}	pharmaceutical tablets river water	34
	Pd–PdO/Mt–CPE	DPV	1.0×10^{-2} – 1	2.85×10^{-3}	human blood	35
	MWCNT–CPE	DPV	2.36 – 242	9.1	pharmaceutical tablets	36
	Clay–CPE	DPV	1 – 1000	83.5×10^{-2}	pharmaceutical tablets human blood	37
	CPE–Clay/Al_2O_3	DPV	1 – 1000	1.95×10^{-2}	human blood	38
	HKUST-CNF	CV CA	4.84 – 29.08 9.69 – 48.47	0.1_{-4} 6.3×10	—	39

		MPA	9.69 – 58.17	1.93×10^{-2}	pharmaceutical tablets pharmaceutical liquid human urine	40
	BDDE	DPV SWV	0.95 – 66.9	0.41 0.93		
	ITO|{PAH|PB/SWCNTs}$_3$	CV	4.7×10^{-2} – 0.23	——	——	41
	CNF/SPCE	DPV	0.8 – 30	0.35	pharmaceutical tablets	42
	SPCE	DPV	18.42 – 489.14	5.33	tap water	43
	SPCNTE		9.21 – 155.12	2.90		
	SPCNFE		19.39 – 114.40	5.81		
	SPGPHE		30.54 – 86.29	9.21		
	aSPCE	DPV	0.5 – 20 20 – 500	5.9×10^{-2}	pharmaceutical tablets	44
Ketoprofen	GCE	DPV	9 – 5000	11.4	——	51
	ITO-LMR	ITO-LMR probe	1 – 1000	500	——	52
	CPS	DPV	0.088 – 1.96 1.96 – 6.02	0.11 ± 0.01 0.21 ± 0.05	wastewater fish	53

GCE = glassy carbon electrode
SD-MWCNT/GCE = short diameter multi-walled carbon nanotubes modified glassy carbon electrode
MB/Apt/nanocomposite/GCE = methylene blue intercalated onto immobilized ibuprofen specific aptamer on multiwalled carbon nanotubes/ionic liquid/chitosan nanocomposite modified glassy carbon electrode
Apt/AuNPs@N-GQDs/GCE = ibuprofen specific aptamer bound with nitrogen-doped graphene quantum dots and gold nanoparticles nanocomposite modified glassy carbon electrode
P(L-Asp)/GCE = poly(L-aspartic acid) modified glassy carbon electrode
AgNPs@Af-GO-MIP/GCE = molecular imprinted polymer-wrapped silver nanoparticles decorated acid-functionalized graphene oxide modified glassy carbon electrode
Cu_3TeO_6/GCE = 3D stone-like copper tellurate modified glassy carbon electrode
Mt–CPE = montmorillonite-doped carbon paste electrode
Pd–PdO/Mt–CPE = palladium particles-impregnated sodium montmorillonite modified carbon paste electrode
MWCNT–CPE = multiwalled carbon nanotube composite modified carbon paste electrode

Clay–CPE = clay particles modified carbon paste electrode
CPE–Clay/Al_2O_3 = aluminum oxide particles supported on clay modified carbon paste electrode
HKUST-CNF = [Cu_3(1,3,5-benzentricarboxilate)$_2$] metal-organic framework carbon nanofiber-epoxy composite electrode
BDDE = boron-doped diamond electrode
ITO|{PAH|PB/SWCNTs}$_3$ = self-assembled layer-by-layer Prussian blue nanoparticles, single-walled carbon nanotubes and poly-allylamine hydrochloride nanostructured films deposited on indium tin oxide
CNF/SPCE = carbon nanofibers modified screen-printed carbon electrode
SPCE = carbon screen-printed electrode
SPCNTE = carbon nanotubes modified screen-printed electrode
SPCNFE = carbon nanofibers modified screen-printed electrode
SPGPHE = graphene modified screen-printed electrode
aSPCE = activated screen-printed carbon electrode
ITO-LMR = optical fiber sensor coated with indium tin oxide overlay based on the lossy-mode resonance
CPS = carbon paper sensor

1.1. 3D sensors used for determination of ibuprofen

1.1.1. Glassy carbon based electrodes used for determination of ibuprofen

Senthil Kumar et al.[25] employed a pretreated glassy carbon electrode (GCE) using square wave voltammetry for the determination of IBP in different tablets. Two pretreatment methods were applied to the electrode: mechanical polishing using alumina suspension and electrochemical treatment at 1.5 V potential for 2 seconds. While using the square wave stripping voltammetric (SWSV) method, the sensor recorded a detection limit (LOD) of 0.96 μmol L^{-1} and a linear concentration range between 1.45 and 3.87 μmol L^{-1}. The relative standard deviation (RSD) based on five identical measurements performed at an analyte concentration of 1.94 μmol L^{-1} was 2.5%.[25] Later that year, Senthil Kumar's group[26] successfully used the same pretreated GCE for simultaneous determination of paracetamol and IBP in commercial tablets through differential pulse stripping voltammetry (DPSV) and SWSV. The sensor's response was linear between the concentration range 1.45 and 3.39 μmol L^{-1} while using DPSV and SWSV with a LOD of 0.96 μmol L^{-1} for DPSV and 0.48 μmol L^{-1} for SWSV. The observed RSD for seven successive measurements carried out at 1.45 μmol L^{-1} were 2.7% for DPSV and 2.4% for SWSV.[26]

Montes and co-authors[27] studied the quantification of IBP and naproxen from tablets and liquid pharmaceutical samples using GCEs modified with two types of multi-walled carbon nanotubes (MWCNTs), presenting larger (LD-MWCNT) and shorter diameters (SD-MWCNT). The electrochemical oxidation of the two compounds was studied using CV and further verified in amperometric experiments. The mechanism of electrochemical oxidation of IBP is presented in Figure 1. The SD-MWCNT-modified electrode proved superior detection sensitivity (Figure 2),

especially when it was employed in amperometric detection, because of a higher electrocatalytic activity of the material. This is due to a higher packing density of the carbon nanotubes confirmed through Raman spectroscopic measurements, which is in correlation with a higher electron transfer rate confirmed through electrochemical impedance spectroscopic (EIS) measurements. While determining IBP with the amperometric method using the SD-MWCNT- modified electrode, a linear range of 10 to 1000 μmol L^{-1} and a LOD of 1.9 μmol L^{-1} were obtained. The RSD for 15 measurements of 50 μmol L^{-1} IBP was 4.2%. Pharmaceutical formulations containing IBP were assayed using the SD-MWCNT-modified electrode in a flow- injection analysis (FIA) system with amperometric detection and the results were similar with those obtained by CE.[27]

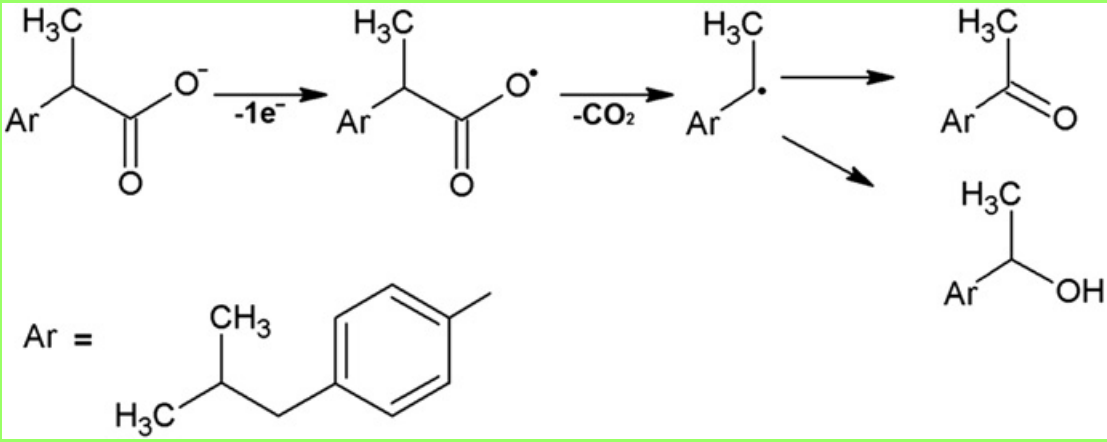

Figure 1. Mechanism of the electrochemical oxidation of ibuprofen. Adapted from[27] an open access article distributed under the Creative Commons Attribution license.

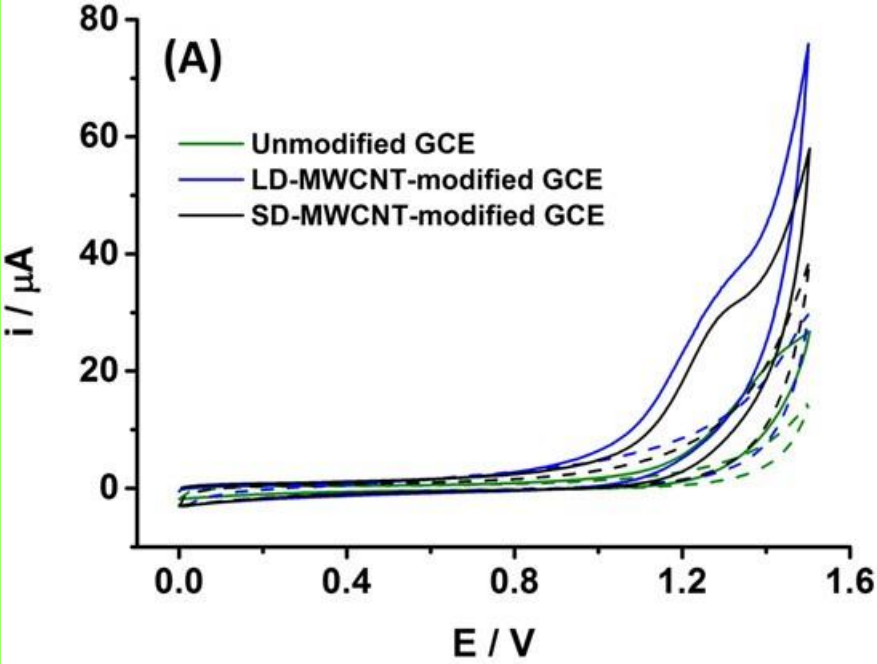

Figure 2. Cyclic voltammogram for 1 mmol L^{-1} ibuprofen in 0.1 mol L^{-1} phosphate buffer solution (pH 7.5) at LD-MWCNT-modified (black lines) and SD-MWCNT-modified (blue lines) and unmodified (green lines) GCE and the respective blanks (dashed lines). The scan rate was 50 mV s^{-1}. Adapted from[27] an open access article distributed under the Creative Commons Attribution license.

Kavitha et al.[28] fabricated a polyaniline nanofiber modified glassy carbon electrode for the detection of IBP from pharmaceutical tablets using DPSV and the obtained results were in agreement with those reported by the manufacturing companies. The GCE was modified through addition of a small quantity of a solution, prior obtained by stirring chemically prepared nanostructured polyaniline in water. A linear concentration range 0.96 to 1.94 μmol L^{-1} and a low LOD (0.48 μmol L^{-1}) were obtained. The RSD calculated for 7 identical determinations at a concentration of 1.21 μmol L^{-1} was 2.1%.[28]

Roushani and Shahdost-fard[29] developed an aptasensor for selective and sensitive detection of IBP in pharmaceutical formulations (tablets and oral suspension) and spiked human serum and waste water. The electrode was produced by applying a layer of a nanocomposite paste containing MWCNTs, ionic liquid (IL) and chitosan (Chit) on the surface of a GCE. The

nanocomposite increases the surface area of the electrode, accelerates electron transfer processes and provides a stable matrix for the aptamer. The above-mentioned electrode denoted MWCNTs/IL/Chit/GCE was coupled with terephthalaldehyde through the free amino groups and then a 3′-amine-terminated capture probe (ssDNA1) was attached covalently by amide coupling to the terephthalaldehyde. An IBP-specific aptamer (ssDNA2) was linked to the ssDNA1 through hybridization and afterwards methylene blue (MB) was intercalated into the ssDNA2 as an electrochemical marker for redox processes. The aptasensor (denoted MB/Apt/nanocomposite/GCE) detects IBP by binding specifically to it and forming an aptamer/IBP complex while the MB detaches from the aptamer and the current decreases so the MB can indicate the IBP concentrations. The aptasensor was used for the determination of IBP by DPV technique and it provided a linear concentration range between 7×10^{-5} and 6 μmol L^{-1}, a LOD of 2×10^{-5} μmol L^{-1} and a RSD of 2.7% (obtained from four measurements conducted of four different MB/Apt/nanocomposite/GCEs for an IBP concentration of 2×10^{-4} μmol L^{-1}). The recovery values ranged from 96.62 to 105.152 %.[29]

In 2018, Roushani and Shahdost-fard[30] designed a novel aptasensing platform based on a GCE modified with a nanocomposite containing nitrogen-doped graphene quantum dots (N-GQDs) and gold nanoparticles (AuNPs) that enables the aptamer (Apt) to bind with the nanocomposite. Firstly, on the bare GCE was applied a layer of in-house synthetized N-GQDs, obtaining the N-GQDs/GCE. AuNPs were electrodeposited over the surface of the electrode from a solution of $HAuCl_4$ and H_2SO_4, thus obtaining the AuNPs@N-GQDs/GCE. An amino capture probe (NH_2-ssDNA1) covalently bonded to the AuNPs was used as the linking agent between the nanocomposite and the IBP specific Apt (ssDNA2). The prepared aptasensor, denoted Apt/AuNPs@N-GQDs/GCE, quantifies the IBP concentration by forming IBP-Apt complexes

while the relative signal response decreases as the IBP concentration at the platform level increases. Calibration curves were attained through DPV, the measurements showing a linear IBP concentration range between 1×10^{-10} and 0.2 μmol L^{-1} and a 33.33×10^{-12} μmol L^{-1} LOD. Codeine, sodium diclofenac, paracetamol and sodium valproate in concentrations 10^3-fold higher than IBP (5×10^{-5} μmol L^{-1}) were chosen as potential interfering substances and analyzed. The affinity of the Apt for IBP was much stronger compared to the affinity of the Apt for the other substrates, proving the aptasensor detects IBP with high selectivity. Pharmaceutical tablets, spiked wastewater and human serum samples were assessed with the fabricated aptasensor, obtaining good recovery values (97 – 102%).[30]

Mekassa and co-authors[31] obtained a poly(L-aspartic acid) modified GCE (P(L-Asp)/GCE) via electropolymerization using CV (20 cycles, 0.1 V s^{-1} scan rate). The sensor showed a good electrocatalytic activity toward IBP oxidation, being able to improve the peak current and to decrease the overpotential in comparison with the bare GCE. Square wave voltammetric (SWV) method at the P(L-Asp)/GCE electrode was applied in optimized conditions, obtaining a linear IBP concentration within the range 1 – 150 μmol L^{-1} and a LOD of 0.22 μmol L^{-1}. The electrode was employed for eight successive measurements in 100 μmol L^{-1} IBP, achieving a RSD of 3.1% which indicates a good repeatability of the sensor. In order to study the influence of potential interfering substances in the quantification of IBP (100 μmol L^{-1}), substances such as ascorbic acid, uric acid, caffeine, glucose, lactose, Mg^{2+} and Na^{+} were chosen. Even at equimolar concentrations, caffeine exhibited a notable interference, which can be attributed to the caffeine and IBP redox peaks overlapping, while uric acid displayed a minor interference at concentrations of 10 fold or higher than IBP. The other substances did not interfere. Recovery

values between 90.0% and 108.0% were obtained after the analysis of pharmaceutical tablets and spiked urine samples using the P(L-Asp)/GCE.[31]

Nair and Sooraj[32] proposed an electrode based on a novel molecular imprinted polymer (MIP) for electrochemical sensing of IBP. The fabrication of the sensor involves a series of steps. In- house synthetized silver nanoparticles (AgNPs) and acid functionalized graphene oxide (Af-GO) were mixed with *Caesalpinia sappan* leaf extract to obtain AgNPs-decorated Af-GO (AgNPs@Af-GO) and then AgNPs@Af-GO was firstly treated with a mixture of IBP (as template), acrylamide (as monomer), ethylene glycol dimethacrylate (as cross-linker) and methanol; afterwards, 2,2'-azobisisobutyronitrile (as radical initiator) was added to the mixture in order to obtain a polymer. Methanol was used to detach IBP from the polymer, developing the AgNPs@Af-GO-MIP, which was applied for the modification of a GCE. When CV technique was used to compare the AgNPs@Af-GO-MIP-modified GCE with a GCE-modified with AgNPs@Af-GO-NIP (a polymerization product obtained by the same method only without IBP as template), the AgNPs@Af-GO-MIP-modified GCE exhibited an oxidation peak corresponding to IBP, while the other electrode showed no redox peak. This confirmed the formation of IBP template memory cavities on the AgNPs@Af-GO-MIP polymer surface. When studied by DPV, the AgNPs@Af-GO-MIP-modified GCE employed for IBP analysis showed a linear response in the concentration range 1 – 100 μmol L^{-1} and a LOD of 8.7×10^{-3} μmol L^{-1}. Sensor repeatability was evaluated in 100 μmol $L^{-}1$ IBP by DPV for eight cycles, achieving a RSD value of 1.9%. Interference studies were conducted by simultaneous determinations of IBP and selected substances such as ascorbic acid, uric acid, glucose and lactose of 100 μmol L^{-1} concentration each. The AgNPs@Af-GO-MIP-modified GCE had a 7 times higher current

response for IBP compared to potential interferences, whereas the AgNPs@Af-GO-NIP-

modified GCE exhibited a similar response for both IBP and selected substances, meaning the MIP sensor is highly sensitive to IBP. Samples (tablets, spiked human urine and infected human urine) were analyzed using DPV method and the recovery results of IBP ranged from 97.8 to 100.6%.[32]

Mutharani et al.[33] modified a GCE with 3D stone-like copper tellurate (Cu_3TeO_6) for the electrochemical determination of IBP. The team produced in-house a Cu_3TeO_6 nanostructure that was drop coated on a GCE. The electrochemical behavior of Cu_3TeO_6/GCE was explored using EIS and CV; the results proved a superior electron transfer rate and redox peaks when compared to a bare GCE. Electrocatalytic activity studies conducted on Cu_3TeO_6/GCE, TeO_2/GCE, CuO/GCE and bare GCE through CV showed the highest anodic peak for Cu_3TeO_6/GCE, significantly increased peak for TeO_2/GCE and CuO/GCE, while the bare GCE exhibited no observable peak for IBP oxidation. DPV measurements applied on different IBP concentrations expressed two linear concentration ranges from 0.02 to 5 μmol L^{-1} and from 9 to 246 μmol L^{-1} and a LOD of 1.7×10^{-2} μmol L^{-1}. The selectivity of the sensor was analyzed in 15 μmol L^{-1} IBP along with potential interfering agents such as theophylline, dopamine, uric acid, ascorbic acid, naproxen, glucose, and chlorpromazine in 20-fold excess concentrations than IBP. The current response of the interfering substances showed slight changes in the detection of IBP. For the reproducibility of the sensor 5 modified electrodes were assayed by CV in 60 μmol L^{-1} IBP, obtaining a RSD value of 3.7%. Spiked biological samples (human urine and blood serum) were used for the determination of IBP with the Cu_3TeO_6/GCE and the recovery results were in the range of 96 to 98.6%.[33]

1.1.2. Carbon paste electrodes used for determination of ibuprofen

Loudiki and collaborators[34] used a montmorillonite-doped carbon paste electrode (Mt–CPE) to explore the electrochemical oxidation of IBP. The electrode was manufactured by mixing sodium montmorillonite clay with graphite powder and then the paste was inserted into the cavity of a plastic pipette tip with a bar of carbon establishing the electrical contact. Comparative CV measurements performed on Mt–CPE and an unmodified carbon paste electrode (CPE) revealed that the modified sensor displayed a well-defined anodic peak corresponding to IBP electrooxidation. The electrocatalytical activity of the electrode was further confirmed through CA technique and EIS. DPV measurements showed a linear concentration range of IBP from 0.1 to 10000 μmol $L^{-1}$and a LOD of 6.8×10^{-2} μmol L^{-1}. RSD values of 1.24% and 1.07% were obtained after eight measurements performed in 1 μmol L^{-1} and 0.4 μmol L^{-1}, respectively. Interference studies of IBP quantification using Ni^{2+}, NO_3^-, Sr^{2+}, Ba^{2+}, Li^+, Cr^{2+}, NH_4^+, Ca^{2+}, Co^{2+}, Cu^{2+}, Mg^{2+}, Na^+, and K^+ in 1000-fold concentration and paracetamol, uric acid, ascorbic acid and dopamine in 100-fold concentrations revealed no significant influence on the current response (<2% signal change), whilst ions like SO_4^{2-}, Cl^- and PO_4^{3-} in 100-fold concentration slightly increased the signal (2%). Real samples (tablets and river water) were analyzed with the proposed sensor and compared to HPLC, obtaining corresponding recovery values in the range 98.50 – 99.25%.[34]

Later in 2016, Loudiki et al.[35] produced a palladium particles-impregnated sodium montmorillonite modified carbon paste electrode (Pd–PdO/Mt–CPE) for IBP quantification. The sensor was obtained by mixing sodium montmorillonite impregnated with palladium particles (Pd–PdO/Mt) with carbon powder and incorporating the paste in an electrode cavity. A carbon

bar was used as the electrical contact. Voltammetric activity of IBP at various sensors such as unmodified CPE, Mt–CPE and Pd–PdO/Mt–CPE studied through CV revealed a high and distinct oxidation peak at the Pd–PdO/Mt–CPE which demonstrates a rapid electron transfer rate, proving the electrode has reliable electrooxidation capacities. DPV method was employed for the calibration curve, obtaining a linear range between 1.0×10^{-2} and 1 μmol L^{-1} and a LOD of 2.85×10^{-3} μmol L^{-1}. The proposed sensor was applied for the determination of IBP in human blood samples with recovery values between 95.65 and 99.07%. When compared with HPLC, the proposed method provided similar results regarding linearity, LOD, accuracy and specificity.[35]

Rivera-Hernández and collaborators[36] designed a multiwalled carbon nanotube composite modified carbon paste electrode. The paste obtained by mixing graphite powder and multiwalled carbon nanotubes with mineral oil was inserted in a plastic tube with a copper rode as electrical contact. When comparing the modified electrode to an unmodified one, the cyclic voltammograms (CVs) performed in 1000 μmol L^{-1} IBP exhibited an anodic peak three times larger for the multiwalled carbon nanotube composite – carbon paste electrode. DPV measurements revealed concentration linearity between 2.36 and 242 μmol L^{-1} and a LOD of 9.1 μmol L^{-1}. The electrode was used for six successive measurements in 400 μmol L^{-1} IBP in order to assess the repeatability of the sensor, obtaining a 1.93% RSD. Interference studies conducted using NO_3^-, oxalate, ascorbic acid, povidone, polyethylene glycol, silicon oxide, sucrose, sorbitol, and microcelulose in equimolar, 10-fold and 100-fold concentrations than IBP revealed that NO_3^-, oxalate and ascorbic acid interfered with IBP detection while the other selected potential interfering species did not interfere. The sensor applicability was tested on pharmaceutical tablets, obtaining recovery values ranging from 101.24 to 104.67%.[36]

Hammami and co-authors[37] proposed a graphite electrode modified with clay particles (Clay–CPE). Surface characterization and electrochemical behavior of Clay–CPE and unmodified CPE toward IBP oxidation were observed via CV, Tafel plots and EIS, the collected results indicated an elevated electron transfer rate and a decreased anodic overvoltage for the Clay–CPE. When using DPV, the linear concentration range was 1 – 1000 μmol L^{-1} with a LOD of 83.5×10^{-2} μmol L^{-1}. Reproducibility of the Clay–CPE was evaluated based on eight successive measurements in 10 μmol L^{-1} IBP, the RSD was 2.31%. Interference studies were performed using mixt solution method. A solution of IBP (10 μmol L^{-1}) and solutions of various concentrations of selected potential interferences (dopamine, catechol, ascorbic acid, phenol, 3- aminophenol, paracetamol, resorcinol, 4-nitrophenol, salicylic acid and hydroquinone) were used. Paracetamol, ascorbic acid, phenol and 10-fold concentrations of resorcinol, 4-nitrophenol and salicylic acid decreased the current response for IBP, while 50-fold 3-aminophenol, hydroquinone, catechol and dopamine and equimolar resorcinol, 4-nitrophenol and salicylic acid had no influence in IBP oxidation. IBP determined by DPV from pharmaceutical tablets provided recovery values of 99.56% and 100.82% while analyzed spiked human blood samples yielded a linear response in the range 1 – 1000 μmol L^{-1} IBP, the calibration curve slope decreased by 80.16% comparing to the slope obtained in phosphate buffer.[37]

EL Ouafy and co-authors[38] modified a carbon paste electrode with aluminum oxide particles supported on clay (CPE–Clay/Al_2O_3) in order to evaluate its electrocatalytic activity on IBP oxidation. Electrochemical behavior of IBP studied on CPE, CPE–Clay and CPE–Clay/Al_2O_3 in 1000 μmol L^{-1} IBP solution in 0.1 mol L^{-1} phosphate buffer provided CVs that show an oxidation peak in the potential range 0.5 – 1.4 V, describing an irreversible redox process.

Furthermore, the voltammograms depict an increased peak current and a lowered peak potential

on the CPE–Clay/Al_2O_3 in comparison with CPE and CPE–Clay, which indicates an enhanced electrocatalytic performance. DPV measurements applied in IBP provided a linear concentration range from 1 to 1000 μmol L^{-1} and a LOD of 1.95×10^{-2} μmol L^{-1}. Repeatability studies conducted in 10 μmol L^{-1} IBP yielded a 3.4% RSD after nine measurements. The selectivity of the proposed sensor was evaluated through interference studies accomplished in a solution containing 100 μmol L^{-1} IBP and a mixture of the selected interfering molecules (equimolar ascorbic acid and 0.1-fold resorcinol and salicylic acid); the voltammogram illustrated that the IBP current density in not influenced by the presence of selected interfering compounds. Spiked human blood samples analyzed by DPV employing CPE–Clay/Al_2O_3 presented a 8.81×10^{-2} μmol L^{-1} LOD and a 4.08% RSD value after nine measurements performed in 10 μmol L^{-1} IBP solution.[38]

1.1.3. Other types of electrodes used for determination of ibuprofen

Motoc and Manea's team[39] developed an electrochemically synthesized [Cu_3(1,3,5-benzentricarboxilate)$_2$] metal-organic framework (HKUST-1)-carbon nanofiber-epoxy composite electrode (HKUST-CNF) for simultaneous quantification of IBP and diclofenac (DCF). CV, CA and multiple-pulsed amperometric (MPA) measurements provided an IBP concentration linear range of 4.84 – 29.08 μmol L^{-1}, 9.69 – 48.47 μmol L^{-1} and 9.69 – 58.17 μmol L^{-1} respectively and a LOD of 0.1 μmol L^{-1}, 6.3×10^{-4} μmol L^{-1} and 1.93×10^{-2} μmol L^{-1}. The scanning electron microscope (SEM), CV, CA and MPA results are depicted in Figure 3. The calculated RSD based on three measurements was 2.05% for CV, 0.81% for CA and 1.14 for MPA. The sensor was tested through CV, CA and MPA for simultaneous detection of IBP and DCF in order to

assess a potential mutual interference, the results indicating the possibility to selectively detect the two compounds by switching the potential.[39]

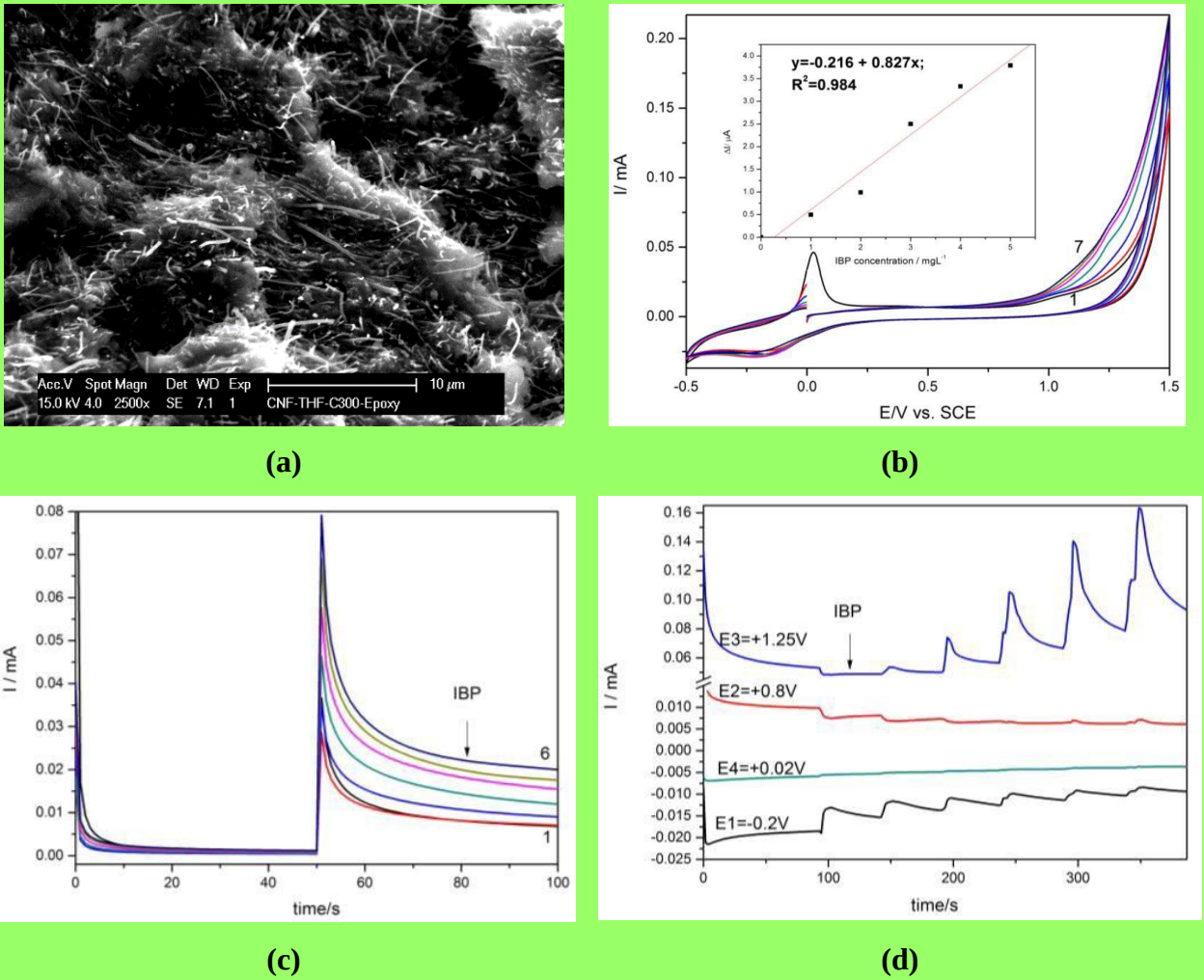

(a) **(b)**

(c) **(d)**

Figure 3. (a) SEM image of the HKUST-CNF composite electrode, **(b)** Cyclic voltammogram recorded on HKUST-CNF electrode in 0.1 M Na_2SO_4 supporting electrolyte (curve 1) and in the presence of various ibuprofen concentrations: curves 2–7: 1–6 mg L^{-1} ibuprofen; potential scan rate: 0.05 V s^{-1}; potential range: −0.5 to +1.5 V/SCE. Inset: Calibration plots of the currents recorded at E = +1.25 V vs. SCE versus ibuprofen concentrations, **(c)** CA recorded under two potential levels of +0.8 V and +1.25 V vs. SCE at the HKUST-CNF electrode in 0.1 M Na_2SO_4 supporting electrolyte (curve 1) and in the presence of 2 mg L^{-1} ibuprofen (curve 2), 4 mg L^{-1} ibuprofen (curve 3), 6 mg L^{-1} ibuprofen (curve 4), 8 mg L^{-1} ibuprofen (curve 5), 10 mg L^{-1} ibuprofen (curve 6), **(d)** Multiple-pulsed amperograms recorded by HKUST-CNF electrode in 0.1 M Na_2SO_4 supporting electrolyte and adding consecutively and continuously 2 mg L^{-1} ibuprofen, recorded at E1 = −0.2 V/SCE, E2 = +0.8 V/SCE, E3 = +1.25 V/SCE, E4 = +0.02 V/SCE. Adapted from[39] an open access article distributed under the Creative Commons Attribution license.

Švorc et al.[40] employed a bare boron-doped diamond electrode (BDDE) for the detection of IBP. DPV and SWV measurements were used for the calibration curves, obtaining a similar linear concentration range of 0.95 – 66.9 μmol L^{-1}, whereas a lower LOD of 0.41 μmol L^{-1} was achieved through DPV compared to 0.93 μmol L^{-1} attained by SWV. RSD values below 5% (3.6% for DPV and 4.6% for SWV) were attained from six measurements in 10 μmol L^{-1} IBP. For the interference studies were studied substances such as magnesium stearate, starch, cellulose, benzoic acid, sodium benzoate, glucose, ascorbic acid, uric acid, dopamine and caffeine in various concentration ratios (1:1, 1:10, 1:100) with IBP (10 μmol L^{-1}). Magnesium stearate, starch, cellulose, benzoic acid, sodium benzoate, glucose, dopamine, 20-fold uric acid and equimolar caffeine did not interfere with the IBP detection, whereas 10-fold ascorbic acid and 100-fold uric acid decrease the current response for IBP with about 20%. Overlapping signals that impeded IBP detection were recorded for 100-fold ascorbic acid, 10-fold and 100- fold caffeine. Pharmaceutical dosage forms (tablets and liquid) and human urine samples were analyzed employing DPV and SWV with recovery results ranging from 99.8 to 107.5% (DPV) and 99.8 to 105% (SWV) for pharmaceuticals and from 95 to 107% (DPV) and 97 to 103% (SWV) for urine.[40]

Carvalho and collaborators[41] constructed an electrode based on Prussian blue nanoparticles (PB NPs), single-walled carbon nanotubes (SWCNTs) and poly-allylamine hydrochloride (PAH) nanostructured films deposited on indium tin oxide (ITO). The PB NPs were first synthesized and then three bilayers of nanostructured films were deposited onto ITO using the self-assembly method layer-by-layer, by alternate immersion of the substrate into aqueous solutions charged negatively (PB NPS or PB/SWCNTs) and positively (PAH). Depending on the negatively charged solutions, two electrodes were obtained: “blank” ITO|{PAH|PB}$_3$ when the PB NPS was

used and ITO|{PAH|PB/SWCNTs}$_3$ when the PB/SWCNTs was used. The ITO|{PAH|PB}$_3$ electrode measurements in KCl electrolyte solution exhibited two redox processes on the CVs, the first peak recorded at 160 mV (vs. SCE) corresponding to the transformation of Prussian white to PB and the second peak appeared at 850 mV (vs. SCE) attributed to the conversion of PB to Berlin green, whereas at the ITO|{PAH|PB/SWCNTs}$_3$ were observed the two redox processes with highly elevated current densities, 0.12 and 0.87 V (vs. SCE), a characteristic that is due to enhanced electrical conductivity of carbon nanotubes. CVs performed in the presence of IBP reveal an inhibition of current densities peaks of PB species that is proportional with IBP concentrations, signifying an interaction between the components. It has been proposed that PB interacts through its Fe^{3+} sites with the COO^- functional group present in IBP structure in neutral pH conditions. The first cathodic process demonstrated a linear concentration range of 4.7×10^{-2} to 0.23 μmol L^{-1} IBP and a good sensitivity (2532.37 ± 69.05 μA μmol^{-1} L cm^{-2}), while the second anodic process exhibited a broader linear range, 0.047 – 0.37 μmol L^{-1} but a diminished sensitivity (~592.54±1.49 μA μmol^{-1} L cm^{-2}). These results suggest the first redox process is more suitable and reliable for the IBP detection.[41]

1.2. Disposable sensors used for determination of ibuprofen

Apetrei et al.[42] described a carbon nanofibers modified screen-printed carbon electrode (CNF/SPCE) for IBP electrochemical quantification. The sensor was obtained through the dispersion of carbon nanofibers onto a commercial screen printed electrode. CVs of the CNF/SPCE performed in 0.2 mol L^{-1} acetate buffer (pH 4.5) and 10 μmol L^{-1} IBP in 0.2 mol L^{-1} acetate buffer (pH 4.5) revealed the lack of redox peaks when employed in support electrolyte solution, whilst the measurements in IBP solution displayed an irreversible oxidation peak at

+1.19 V. DPV analyses produced an IBP oxidation peak at +1.08 V vs. Ag, a linear concentration range between 0.8 and 30 μmol L^{-1} and a 0.35 μmol L^{-1} LOD. The repeatability of the CNF/SPCE determined by ten DPV successive determinations in 10 μmol L^{-1} IBP solution in 0.2 mol L^{-1} acetate buffer (pH 4.5) was expressed through calculated RSD of 1.8%. Interference studies performed by DPV in solutions containing equimolar IBP (10 μmol L^{-1}) and various potential interfering substances (paracetamol, ascorbic acid and glucose) showed no significant interference (values of the relative deviations of IBP peak current below 4%). CNF/SPCE was employed in recovery study using tablets samples, the results obtained were close to 100%.[42]

Serrano and co-authors[43] employed four commercial screen-printed electrodes for simultaneous determination of IBP, paracetamol and caffeine. Carbon screen-printed electrode (SPCE), multi-walled carbon nanotubes modified screen-printed electrode (SPCNTE), carbon nanofibers modified screen-printed electrode (SPCNFE), and graphene modified screen-printed electrode (SPGPHE) used in individual DPV measurements (Figure 4) provided the following linear concentration ranges for IBP: 18.42 – 489.14 μmol L^{-1} at SPCE, 9.21 – 155.12 μmol L^{-1} at SPCNTE, 19.39 – 114.40 μmol L^{-1} at SPCNFE and 30.54 – 86.29 μmol L^{-1} at SPGPHE; the LOD calculated values were 5.33, 2.90, 5.81 and 9.21 μmol L^{-1} at SPCE, SPCNTE, SPCNFE and SPGPHE, respectively. Simultaneous calibration of IBP, paracetamol and caffeine was performed by DPV using SPCNFE (Figure 5) in order to assess the influence of coexisting molecules on individual analytical behavior, the obtained results displaying narrower linear ranges (10.66 – 49.44, 0.59 – 5.29 and 1.03 – 5.66 μmol L^{-1} for IBP, paracetamol and caffeine) and diminished LODs (2.9, 0.19 and 0.25 μmol L^{-1} for IBP, paracetamol and caffeine). The individual and simultaneous voltammograms are presented in Figures 4 and 5. For IBP, sensitivities calculated based on calibration curves slopes were 0.0380, 0.0404, 0.082 and 0.051

μA V mg^{-1} L for SPCE, SPCNTE, SPCNFE and SPGPHE. Simultaneous quantification of IBP, paracetamol and caffeine in spiked tap water samples was carried out by DPV using SPCNFE obtaining recovery values ranging from 97.6 to 103.1%. [43]

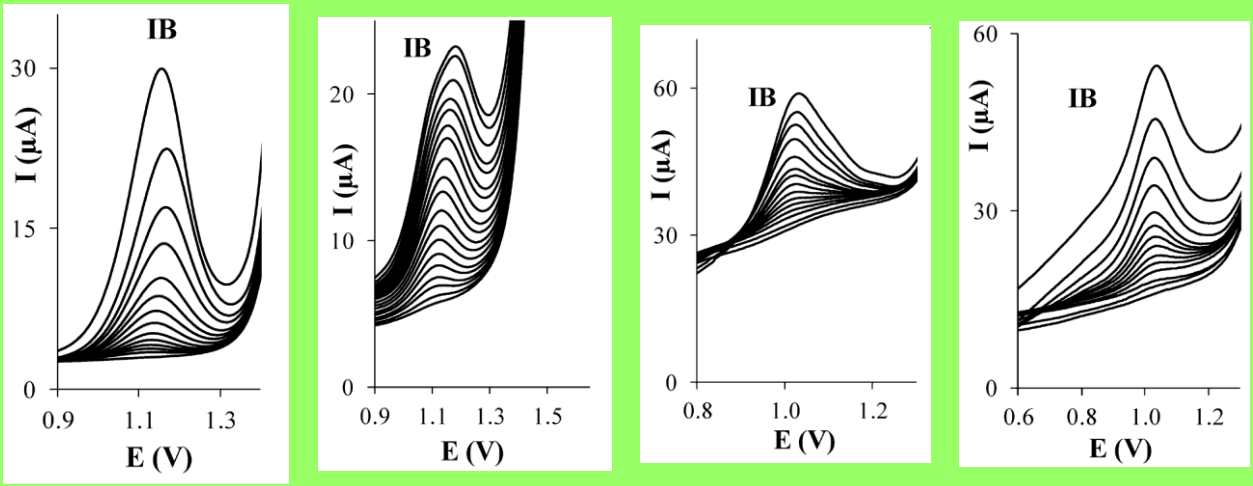

Figure 4. Separate differential pulse voltammograms of ibuprofen in 0.1 mol L^{-1} acetate buffer (pH 5.5) using a: **(a)** carbon screen-printed electrode (SPCE), **(b)** carbon nanotubes modified screen-printed electrode (SPCNTE), **(c)** carbon nanofibers modified screen-printed electrode, **(d)** graphene screen-printed electrode (SPGPHE). Adapted from[43] an open access article distributed under the Creative Commons Attribution license.

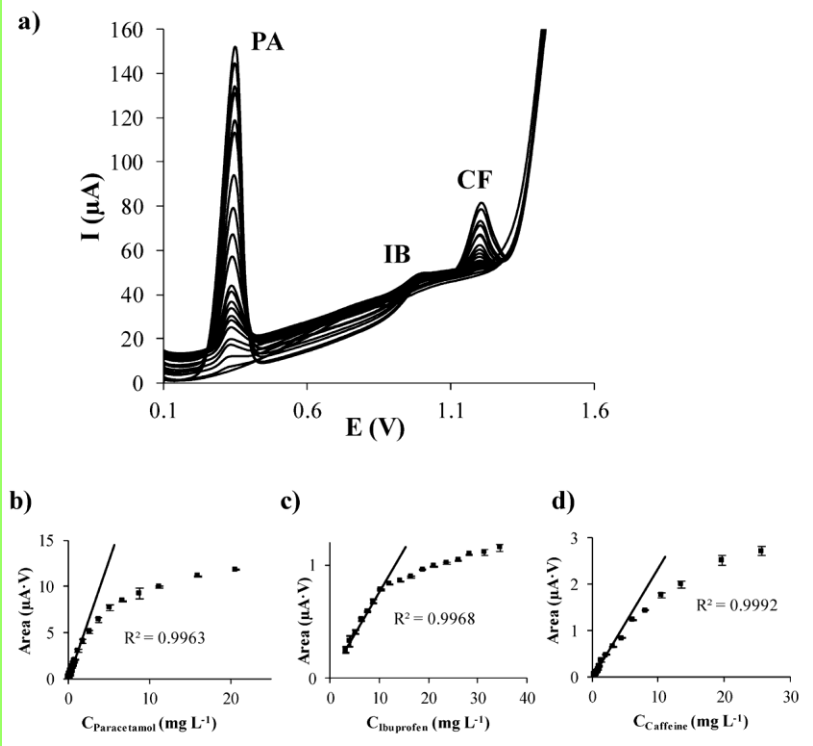

Figure 5. (a) differential pulse voltammograms of a mixture of paracetamol, ibuprofen and caffeine; and their respective calibration plots **(b)**, **(c)** and **(d)** in 0.1 mol L^{-1} acetate buffer (pH 5.5) using a carbon nanofibers modified screen-printed electrode (SPCNFE). Adapted from[43] an open access article distributed under the Creative Commons Attribution license.

Tyszczuk-Rotko and collaborators[44] proposed an electrochemically activated screen-printed carbon electrode (aSPCE) for IBP detection. The electrochemical activation involves five voltammetric cycles from 0 to 2 V at a 100 mV s^{-1} scan rate in a NaOH solution (0.1 mol L^{-1}) and then the electrode is rinsed with deionized water. In order to assess the electrochemical behavior of IBP at aSPCE, CV at different scan rates ranging from 5 to 500 mV s^{-1} was applied in a 0.1 mmol L^{-1} IBP prepared in acetate buffer solution (0.25 mol L^{-1}) of pH 4.5 ± 0.1; the voltammograms presented an anodic peak at around 0.9V and no peak on the cathodic run. DPV measurements in optimal conditions performed on IBP provided two linear concentration ranges from 0.5 to 20 µmol L^{-1} and 20 to 500 µmol L^{-1} and a LOD of 5.9×10^{-2} µmol L^{-1}. Repeatability tests were carried out by ten successive measurements in 20 µmol L^{-1} IBP and a RSD of 3.5%

was obtained; for reproducibility assay, three independently prepared aSPCE used in 20 μmol L^{-1} IBP presented a RSD value of 4.5%. In interference studies, paracetamol and glucose (50-fold excess) did not interfere on IBP (20 μmol L^{-1}) signal. The applicability of aSPCE was evaluated by applying DPV on pharmaceutical tablets; the results were consistent with the quantitative composition provided by the manufacturer while the calculated relative error was between 3.1 and 4.7%.[44]

2. Electrochemical sensors used for determination of ketoprofen

Prior to 2016, ketoprofen (KTP), 2-(3-benzoylphenyl)propanoic acid, was detected from pharmaceutical dosage forms (capsules, tablets, suppositories and solutions for injection) and human plasma using the dropping mercury electrode and polymeric electrode.[45-48] Furthermore, enantioselective, potentiometric membrane electrodes were reported for the enantioanalysis of KTP.[49,50]

Cebula et al.[51] employed a GCE in order to detect ketoprofen. CVs carried out 100 mV s^{-1} scan rate in KTP solution containing 0.01 mol L^{-1} phosphate buffer (pH 7.0) displayed a cathodic peak at -1.3 V that corresponds to an irreversible reduction process. DPV measurements provided a linear concentration range from 9 to 5000 μmol L^{-1} and a LOD of 11.4 μmol L^{-1}.[51]

Bogdanowicz et al.[52] developed an optical fiber sensor coated with a ITO overlay based on the lossy-mode resonance (LMR) phenomenon. The sensor, denoted ITO-LMR, was produced by reactive magnetron sputtering of ITO onto a polymer-clad silica fiber and then KTP was electrodeposited onto the electrode. The electrode enables simultaneous optical and electrochemical monitoring of the changes that occur during the electrochemical process and its

spectral response is based on the KTP electrodeposition process. ITO-LMR sensor registered a KTP concentration linear range from 1 to 1000 μmol L^{-1} and a LOD of 500 μmol L^{-1}.[52]

Torrinha and co-authors[53] used disposable carbon paper sensors (CPS) for electrochemical detection of KTP. CV measurements of KTP in 0.1 mol L^{-1} Britton-Robinson buffer (BRB) pH 5.5 revealed a diffusion-controlled process and CVs displayed two reduction peaks at -1.05 and -1.1 V vs. Ag/AgCl, the most pronounced being the one at -1.1 V. DPV in optimal conditions was selected for KTP detection, achieving two dynamic linear concentration ranges, from 0.088 to 1.96 μmol L^{-1} and from 1.96 to 6.02 μmol L^{-1} and a LOD of 0.11 ± 0.01 μmol L^{-1} or 0.21 ± 0.05 μmol L^{-1}, depending on the calibration curve. Reproducibility tests employing five sensors obtained a RSD in the range 10 – 16%, whereas repeatability assessed through five successive measurements yielded a RSD from 6 to 15%. High concentrations (500 μmol L^{-1}) of sulphates, nitrites, phosphates, glucose, lactose and ascorbic acid and 10 μmol L^{-1} paracetamol, aspirin, ibuprofen and diclofenac showed no alteration of the KTP peak at -1.1 V. Spiked real samples (wastewater and fish) evaluated through DPV using CPS provided good recovery values.[53]

Conclusions

This review outlines some recent trends in electrochemical detection of ibuprofen and ketoprofen. The described sensors provide reliable alternative methods of determination for standard methods proposed in Pharmacopoeias, as they are remarkably sensitive, highly selective, easily reproducible and cost effective. They were successfully employed for the determination of ibuprofen and ketoprofen from various types of samples such as pharmaceutical formulations, biological samples and water resources with good recovery values.

In case of ketoprofen, although it is widely used as an efficient NSAID in various pharmaceutical dosage forms, there was a limited interest for developing electrochemical sensors for its analysis in various samples.

References

1. J. R. Vane and R. M. Botting, *Scand. J. Rheumatol.*, **25**, 9–21 (1996).
2. M.-J. Domper Arnal, G. Hijos-Mallada, and A. Lanas, *Expert Opinion on Drug Safety*, 1–12 (2021).
3. S. Harirforoosh and F. Jamali, *Expert Opin. Drug Saf.*, **8**, 669–681 (2009).
4. A. Mejía-García, H. Islas-Flores, L. M. Gómez-Oliván, N. SanJuan-Reyes, J. M. Ortega-Olvera, and M. D. Hernández-Navarro, *Handb. Environ. Chem.*, 41–53 (2020).
5. *European pharmacopoeia, Council of Europe*, 10th ed., Strasbourg (2017), p. 2921–2923.
6. *European pharmacopoeia, Council of Europe*, 10th ed., Strasbourg (2017), p. 3035–3037.
7. *The United States Pharmacopeia USP 34-NF 29*, (2011).
8. E. Ameyibor and J. T. Stewart, *J. Pharm. Biomed. Anal.*, **17**, 83–88 (1998).
9. Y. Y. Lau, *J. Liq. Chromatogr. Relat. Technol.*, **19**, 2143–2153 (1996).
10. S. Ravisankar, M. Vasudevan, M. Gandhimathi, and B. Suresh, *Talanta*, **46**, 1577–1581 (1998).
11. D. K. Bempong and L. Bhattacharyya, *J. Chromatogr. A*, **1073**, 341–346 (2005).
12. A. Szeitz, A. N. Edginton, H. T. Peng, B. Cheung, and K. W. Riggs, *Am. J. Anal. Chem.*, **01**, 47–58 (2010).
13. J. Y. Kim, S. J. Kim, K.-J. Paeng, and B. C. Chung, *J. Vet. Pharmacol. Ther.*, **24**, 315–319 (2001).

14. E. Waraksa, M.K. Woźniak, E. Kłodzińska, R. Wrzesień, B. Bobrowska-Korczak, J. Namieśnik, *J. Sep. Sci.*, **41**, 3881–3891 (2018).

15. P. C. Damiani, M. Bearzotti, and M. A. Cabezón, *J. Pharm. Biomed. Anal.*, **25**, 679–683 (2001).

16. J. Sádecká, M. Čakrt, A. Hercegová, J. Polonský, and I. Skačáni, *J. Pharm. Biomed. Anal.*, **25**, 881–891 (2001).

17. M. Friedberg and Z. K. Shihabi, *J. Chromatogr. B: Biomed. Sci. Appl.*, **695**, 193–198 (1997).

18. A. C. Power and A. Morrin, *IntechOpen* (2013) https://www.intechopen.com/chapters/42956.

19. A. B. Lima, E. O. Faria, R. H. Montes, R. R. Cunha, E. M. Richter, R. A. Munoz, and W. T. dos Santos, *Electroanalysis*, **25**, 1585–1588 (2013).

20. A. B. Lima, L. M. Torres, C. F. Guimarães, R. M. Verly, L. M. Silva, Á. D. Carvalho Júnior, and W. T. dos Santos, *J. Braz. Chem. Soc.*, **25**, 478–483 (2014).

21. S. Amin, M. T. Soomro, N. Memon, A. R. Solangi, T. Qureshi, and A. R. Behzad, *Environ. Nanotechnol. Monit. Manag.*, **1-2**, 8–13 (2014).

22. F. Manea, S. Motoc, A. Pop, A. Remes, and J. Schoonman, *Nanoscale Res. Lett.*, **7**, 331 (2012).

23. S. Motoc, F. Manea, A. Pop, R. Pode, and G. Burtica, *Adv. Sci., Eng. Med.*, **3**, 7–12 (2011).

24. M. Roushani and F. Shahdost-fard, *Talanta*, **144**, 510–516 (2015).

25. E. Suresh, K. Sundaram, B. Kavitha, and N. Senthil Kumar, *Int. J. PharmTech Res.*, **9**, 182–188 (2016).

26. E. Suresh, K. Sundaram, B. Kavitha, S. Maria Rayappan, and N. Senthil Kumar, *J. Adv. Chem. Sci.*, **2**, 369–372 (2016).

27. R. H. O. Montes, A. P. Lima, R. R. Cunha, T. J. Guedes, W. T. P. dos Santos, E. Nossol, E. M. Richter, and R. A. A. Munoz, *J. Electroanal. Chem.*, **775**, 342–349 (2016).

28. E. Suresh, K. Sundaram, B. Kavitha, and N. Senthil Kumar, *Int. J. Curr. Pharm. Res.*, **8**, 44 (2016).

29. M. Roushani and F. Shahdost-fard, *Mater. Sci. Eng. C*, **68**, 128–135 (2016).

30. M. Roushani and F. Shahdost-fard, *Bioelectrochemistry*, **126**, 38–47 (2019).

31. B. Mekassa, M. Tessema, B. S. Chandravanshi, and M. Tefera, *IEEE Sens. J.*, **18**, 37–44 (2018).

32. A. S. Nair and M. P. Sooraj, *J. Mater. Sci.*, **55**, 3700–3711 (2019).

33. B. Mutharani, R. Rajakumaran, S.-M. Chen, P. Ranganathan, T.-W. Chen, D. A. Al Farraj, M. Ajmal Ali, and F. M. A. Al-Hemaid, *Microchem. J.*, **159**, 105378 (2020).

34. A. Loudiki, H. Hammani, W. Boumya, S. Lahrich, A. Farahi, M. Achak, M. Bakasse, and M. A. El Mhammedi, *Appl. Clay Sci.*, **123**, 99–108 (2016).

35. A. Loudiki, W. Boumya, H. Hammani, H. Nasrellah, Y. El Bouabi, M. Zeroual, A. Farahi, S. Lahrich, K. Hnini, M. Achak, M. Bakasse, and M. A. El Mhammedi, *Mater. Sci. Eng. C*, **69**, 616–624 (2016).

36. S. I. Rivera-Hernández, G. A. Álvarez-Romero, S. Álvarez-Romero, M. E. Páez-Hernández, C. A. Galán-Vidal, and M. Romero-Romo, *Instrum. Sci. Technol.*, **44**, 483–494 (2016).

37. H. El Ouafy, H. Hammani, A. Farahi, S. Lahrich, M. Bakasse, and M. A. El Mhammedi, *ChemistrySelect*, **4**, 11282–11287 (2019).

38. H. El Ouafy, T. El Ouafy, M. Oubenali, A. El Haimouti, A. Gamouh, and M. Mbarki, *Methods Objects Chem. Anal.*, **16**, 81–87 (2021).

39. S. Motoc, F. Manea, A. Iacob, A. Martinez-Joaristi, J. Gascon, A. Pop, and J. Schoonman, *Sensors*, **16**, 1719 (2016).

40. Ľ. Švorc, I. Strežová, K. Kianičková, D. M. Stanković, P. Otřísal, and A. Samphao, *J. Electroanal. Chem.*, **822**, 144–152 (2018).

41. C. L. Carvalho, G. de Andrade Rodrigues, J. L. Magalhães, R. A. de Sousa Luz, E. T. da Silva, and W. Cantanhêde, *Surf. Interfaces*, **25**, 101276 (2021).

42. I. M. Apetrei, A. A. Bejinaru, M. Boev, C. Apetrei, and O. Dumitriu Buzia, *Farmacia*, **65**, 790–795 (2017).

43. N. Serrano, Ò. Castilla, C. Ariño, M. Diaz-Cruz, and J. Díaz-Cruz, *Sensors*, **19**, 4039 (2019).

44. K. Tyszczuk-Rotko, J. Kozak, and A. Węzińska, *Appl. Sci.*, **11**, 9908 (2021).

45. M. M. Ghoneim and A. Tawfik, *Can. J. Chem.*, **81**, 889–896 (2003).

46. L. Amankwa and L. G. Chatten, *Analyst*, **109**, 57–60 (1984).

47. K. Emara, A. Ali, and N. Maali, *Talanta*, **41**, 639–645 (1994).

48. J. Lenik, C. Wardak, and B. Marczewska, *Acta Pol. Pharm.*, **63**, 239–244 (2006).

49. R.-I. Stefan-van Staden, N. Suzan Nhlapo, J. Frederick van Staden, and H. Y. Aboul-Enein, *Anal. Lett.*, **42**, 764–774 (2009).

50. R.-I. Stefan-van Staden and R. G. Bokretsion, *Anal. Methods*, **4**, 1492 (2012).

51. Z. Cebula, P. Niedziałkowski, and T. Ossowski, *Special Issue Conference Abstract Book CNS 2018*, **1**, 7–8 (2018).

52. R. Bogdanowicz, P. Niedziałkowski, M. Sobaszek, D. Burnat, W. Białobrzeska, Z. Cebula, P. Sezemsky, M. Koba, V. Stranak, T. Ossowski, and M. Śmietana, *Sensors*, **18**, 1361 (2018).

53. Á. Torrinha, M. Martins, M. Tavares, C. Delerue-Matos, and S. Morais, *Talanta*, **226**, 122111 (2021).

Aflatoxines

The main aflatoxins were identified to bbe determined from raw and cooked food. A selection of literature is shown bellow:

References

1. Van der Zijden ASM, Blanche Koelensmid W A A, Boldingh J, Barrett C B, Ord W O and Philp J. Aspergillus flavus and turkey X disease. Isolation in crystalline form of a toxin responsible for turkey X disease. Nature, 195, 1060-10621, 962.

2. Nesbitt B F, O'Kelly J, Sargeant K and Sheridan A. Aspergillus flavus and turkey X disease. Toxic metabolites of Aspergillus flavus. Nature, 195, 1062-1063, 1962.

3. Dvorackova I. Aflatoxins and Human Health, CRC Press, Boca Raton, FL, 1990.

4. Betina V. Mycotoxins, Bioactive Molecules, Vol. 9, Elsevier, Amsterdam, 1989.

5. Hall A J, Wild C P. Epidemiology of aflatoxin-related disease. In Eaton D L and Groopman J D (Eds). The Toxicology o f Aflatoxins, Academic Press, San Diego, CA, 1994, 233-258.

6. ***IARC. (2002). Some traditional herbal medicines, some mycotoxins, naphthalene and styrene. 8 Summary of data reported and evaluation. IARC Monographs on the eval- uation of the carcinogenic risk to humans. International Agency for Research on Cancer, Lyon, France.

7. Frisvad, J. C., Smedsgaard, J., Larsen, T. O., & Samson, R. A. (2004). Mycotoxins, drugs and other extrolites produced by species in Penicillium subgenus Penicillium. Studies in Mycology, 49, 201-241.

8. Asao, T., Buchi, G. H., Abdel-Kader, M. M., Chang, S. B., Wick, E. L., & Wogan, G. N. (1965). The structures of aflatoxins B1 and G1. Journal of the American Chemical Society, 87-882.

9. D'Mello, J. P. F., & Macdonald, A. M. C. (1997). Mycotoxins. Animal Feed Science and Technology, 69(1997), 155-166.

10. Strosnider, H., Azziz-Baumgartner, E., Banziger, M., Bhat, R. V., Breiman, R., & Wil- son, D. (2006). Public Health Strategies for Reducing Aflatoxin Exposure in Develop- ing Countries: A Workgroup Report. Environmental Health Perspectives, 114(12), 1898-1903.

11. Gimeno. (2004). Aflatoxina M1 no leite. Riscos para a saúde pública, prevenção e con- trolo Alimentação Animal. Revista de la Associação Portuguesa dos Industriais de Alimen- tos Compostos para Animais, 49, 32-44.

12. Wild, C. P., & Gong, Y. Y. (2010). Mycotoxins and human disease: A largely ignored global health issue. Carcinogenesis, 31(1), 71-82.

13. Copetti, M. V., Iamanaka, B. T., Pereira, J. L., Lemes, D. P., Nakano, F., & Taniwaki, M. H. (2012). Co-occurrence of ochratoxin A and aflatoxins in chocolate marketed in Brazil. Food Control, 26(1), 36-41.

14. Betina V. Mycotoxins, Bioactive Molecules, Vol. 9, Elsevier, Amsterdam, 1989

15. Zain, M.E. Impact of mycotoxins on humans and animals. J. Saudi Chem. Soc. 2011, 15, 129–144.

16. ***International Agency for Research on Cancer (IARC). IARC Monographs on the Evaluation of Carcinogenic Risks to Humans; IARC: Lyon, France, 2002; Volume 82, p. 171.

17. Mejri Omrani, N.; Hayat, A.; Korri-Youssoufi, H.; Marty, J.L. Electrochemical biosensors for food security: Mycotoxins detection. In Biosensors for Security and Bioterrorism Applications; Nikolelis, D.P., Nikoleli, G.-P., Eds.; Springer: Berlin, Germany, 2016; pp. 469–490.

18. Wilson, D.M.; Mubatanhema, W.; Jurjevic, Z. Biology and ecology of mycotoxigenic aspergillus species as related to economic and health concerns. In Mycotoxins and Food Safety; DeVries, J.W., Trucksess, M.W., Jackson, L.S., Eds.; Kluwer Academic/Plenum Publ.: New York, NY, USA, 2002; Volume 504, pp. 3–17.

19. Shephard, G.S. Aflatoxin analysis at the beginning of the twenty-first century. Anal. Bioanal. Chem. 2009, 395, 1215–1224.

20. Bennett, J.W.; Klich, M. Mycotoxins. Clin. Microbiol. Rev. 2003, 16, 497–516.

21. Prandini, A.; Tansini, G.; Sigolo, S.; Filippi, L.; Laporta, M.; Piva, G. On the occurrence of aflatoxin M1 in milk and dairy products. Food Chem. Toxicol. 2009, 47, 984–991.

22. Alshannaq, A.; Yu, J.-H. Occurrence, toxicity, and analysis of major mycotoxins in food. Int. J. Environ. Res. Public Health 2017, 14, 632.

23. Campagnollo, F.B.; Ganev, K.C.; Khaneghah, A.M.; Portela, J.B.; Cruz, A.G.; Granato, D.; Corassin, C.H.; Oliveira, C.A.F.; Sant'Ana, A.S. The occurrence and effect of unit operations for dairy products processing on the fate of aflatoxin M1 : A review. Food Control 2016, 68, 310–329.

24. Santini, A.; Raiola, A.; Ferrantelli, V.; Giangrosso, G.; Macaluso, A.; Bognanno, M.; Galvano, F.; Ritieni, A. Aflatoxin m-1 in raw, uht milk and dairy products in sicily (Italy). Food Addit. Contam. Part B 2013, 6, 181–186.

25. Murphy, P.A.; Hendrich, S.; Landgren, C.; Bryant, C.M. Food mycotoxins: An update. J. Food Sci. 2006, 71, R51–R65.

26. Bartoszek, A. Genotoxic food components. In Carcinogenic and Anticarcinogenic Food Components; CRC Press: Boca Raton, FL, USA, 2005.

27. Troxel, C.M.; Reddy, A.P.; O'Neal, P.E.; Hendricks, J.D.; Bailey, G.S. In vivo aflatoxin B1 metabolism and hepatic DNA adduction in zebrafish (danio rerio). Toxicol. Appl. Pharmacol. 1997, 143, 213–220.

28. Marin, S.; Ramos, A.J.; Cano-Sancho, G.; Sanchis, V. Mycotoxins: Occurrence, toxicology, and exposure assessment. Food Chem. Toxicol. 2013, 60, 218–237.

29. Ketney, O.; Ovidiu, T.; Tifrea, A. Structural diversity and biochemical and microbiological characteristics of aflatoxins. In Acta Universitatis Cibiniensis. Series E: Food Technology; De Gruyter Open: Warsaw, Poland, 2014; Volume 18, p. 3.

30. Peers, F.G.; Linsell, C.A. Dietary aflatoxins and liver cancer—A population based study in kenya. Br. J. Cancer 1973, 27, 473–484.

31. Vanrensburg, S.J.; Cookmozaffari, P.; Vanschalkwyk, D.J.; Vanderwatt, J.J.; Vincent, T.J.; Purchase, I.F. Hepatocellular-carcinoma and dietary aflatoxin in mozambique and transkei. Br. J. Cancer 1985, 51, 713–726.

32. Jalili, M.; Scotter, M. A review of aflatoxin M1 in liquid milk. Iran. J. Health Saf. Environ. 2015, 2, 283–295.

33. El-Tras, W.F.; El-Kady, N.N.; Tayel, A.A. Infants exposure to aflatoxin M1 as a novel foodborne zoonosis. Food Chem. Toxicol. 2011, 49, 2816–2819. [CrossRef] [PubMed]

34. Gürbay, A.; Sabuncuo ˘glu, S.A.; Girgin, G.; ¸Sahin, G.; Yi ˘git, ¸S.; Yurdakök, M.; Tekinalp, G. Aflatoxin M1 levels in breast milk samples from ankara, turkey. Toxicol. Lett. 2010, 196, S345. [CrossRef]

35. De Roma, A.; Rossini, C.; Ritieni, A.; Gallo, P.; Esposito, M. A survey on the aflatoxin M1 occurrence and seasonal variation in buffalo and cow milk from southern italy. Food Control 2017, 81, 30–33. [CrossRef]

36. Neal, G.E.; Eaton, D.L.; Judah, D.J.; Verma, A. Metabolism and toxicity of aflatoxins M1 and B1 in human-derived in vitro systems. Toxicol. Appl. Pharmacol. 1998, 151, 152–158.

37. International Agency for Research on Cancer (IARC). IARC Monographs on the Evaluation of Carcinogenic Risks to Humans; IARC: Lyon, France, 2002; Volume 82, p. 171.

38. Hall A J, Wild C P. Epidemiology of aflatoxin-related disease. In Eaton D L and Groopman J D (Eds). The Toxicology o f Aflatoxins, Academic Press, San Diego, CA, 1994, 233-258.

39. Eaton D L, Ramsdell H S and Neal G E. Biotransformation of aflatoxins. In Eaton D L and Groopman J D (Eds). The Toxicology of Aflatoxins, Academic Press, San Diego, CA, 1994, 45-72.

40. Groopman J D. Molecular dosimetry methods for assessing human aflatoxin exposures. In Eaton D L and Groopman J D (Eds). The Toxicology o f Aflatoxins, Academic Press, San Diego, CA, 1994, 259- 279.

41. Roebuck B D and Maxuitenko Y Y. Biochemical mechanisms and biological implications of the toxicity of aflatoxins as related to aflatoxin carcinogenesis. In Eaton D L and Groopman J D (Eds). The Toxicology o f Aflatoxins, Academic Press, San Diego, CA, 1994, 27- 43.

42. Olsen J H, Dragsted L and Autrup H. Cancer risk and occupational exposure to aflatoxins in Denmark. Br. J. Cancer, 58 (1988), 392- 396.

43. McLaughlin J K, Malker HSR, Malker B K, Stone B J, Ericsson J L E, Blot W J, Weiner J A and Fraumeni J F Jr. Registry-based analysis of occupational risks for primary liver cancer in Sweden. Cancer Res., 47(1987), 287-291.

44. Hayes R B, van Nieuwenhuize J P, Raatgever J W and ten Kate F J W. Aflatoxin exposures in the industrial setting, an epidemiological study of mortality. Food Chem. Toxicol., 22 (1984), 39-43

45. Mintzlaff HJ, Lotzsch R, Tauchmann F, Meyer W, Leistner L. Aflatoxin residues in the liver of broiler chicken given aflatoxin-containing feed. Fleischwirtschaft; 1974, 54: 774- 778.

46. Guengerich FP. Cytochrome P450s and other enzymes in drug metabolism and toxicity. The AAPS Journal ; 2006, 8 (1).

47. Patterson DSP, Allcroft R. Metabolism of aflatoxins in susceptible and resistant animal species. Fd. Cosmet. Toxicol 1970, 8: 43.

48. Dhanasekaran D, Shanmugapriya S, Thajuddin N Panneerselvam A. Aflatoxins and aflatoxicosis in human and animals. In aflatoxins - biochemistry and molecular biology, Guevara-Gonzalez, R.G. (editor), ISBN 978-953-307-395-8, InTech, Published, 2011, PP.221-254.

49. Special Nutrients Inc., TARGET ORGANS - The key to an effective mycotoxins adsorbent, 2009

50. Ball R W, Huie J M and Coulombe R A Jr. Comparative activation of aflatoxin Bi by mammalian pulmonary tissues. Toxicol. Lett., 75 (1995), 119-125.

51. Larsson P, Pettersson H and Tjälve H. Metabolism of aflatoxin Bi in the bovine olfactory mucosa. Carcinogenesis, 10 (1989), 1113-1118.

52. Pitt, J.I. Toxigenic fungi: Which are important? Med. Mycol. 2000, 38, 17–22.

53. Rodricks, J.V. Mycotoxins in Human and Animal Health; Pathotox Publishers: Park Forest South, IL, USA, 1977; p. 656, ISBN 0930376005, 9780930376000. 12. Stoloff, L. Aflatoxin as a cause of primary liver-cell cancer in the united states: A probability study. Nutr. Cancer 1983, 5, 165–186.

54. Ueno, Y. Trichothecenes: Chemical, Biological, and Toxicological Aspects; Kodansha: New York, NY, USA, 1983; ISBN 0444996613. 14. Niessen, L. Pcr-based diagnosis and quantification of mycotoxin producing fungi. Int. J. Food Microbiol. 2007, 119, 38–46.

55. Wicklow D T and Shotwell O L. IntrafUngal distribution of aflatoxins among conidia and sclerotia of Aspergillus flavus and Aspergillus parasiticus. Can. J. Microbiol., 29 (1983), 1-5.

56. Ellis W O, Smith J P, Simpson B K and Oldham J H. Aflatoxins in food: occurrence, biosynthesis, effects on organisms, detection, and methods of control. Crit. Rev. Food Sci. Nutr., 30 (1991), 403-439.

57. Wilson D M and Payne G A. Factors affecting Aspergillus flavus group infection and aflatoxin contamination of crops. In Eaton D L and Groopman J D (Eds). The Toxicology o f Aflatoxins, Academic Press, San Diego, CA, 1994, 309-325.

58. Stoloff L. Aflatoxins-an overview. In Rodricks J V, Hesseltine C W and Mehlman M A (Eds). Mycotoxins in Human and Animal Health. Pathotox, Park Forest South, IL, 1977, 7-28.

59. Gamer R C, Whattam M M, Taylor P J L and Stow M W. Analysis of United Kingdom purchased spices for aflatoxins using an immunoaffinity column clean-up procedure followed by highperformance liquid chromatographic analysis and post-column derivatisation with pyridinium bromide perbromide. J. Chromatogr., 648 (1993), 485-490.

60. Pettersson H, Holmberg T, Larsson K and Kaspersson A. Aflatoxins in acid-treated grain in Sweden and occurrence of aflatoxin Mi in milk. J. Sci. FoodAgric., 48 (1989), 411-420.

61. Bennett, J.W.; Klich, M. Mycotoxins. Clin. Microbiol. Rev. 2003, 16, 497–516.

62. European Commission. Commission Regulation (EC) No. 466/2001 Setting Maximum Levels for Certain Contaminants in Foodstuffs; EU Law Publication: Luxembourg, 2001.

63. Alshannaq, A.; Yu, J.-H. Occurrence, toxicity, and analysis of major mycotoxins in food. Int. J. Environ. Res. Public Health 2017, 14, 632.

64. ***FAO, Worldwide Regulations for Mycotoxins in Food and Feed. Food and Nutrition Paper 81, Food and Agriculture Organization of the United Nations, Rome, 2003.

65. ***Food and Drug Administration (FDA), Compliance guidance manual, 2004.

66. Diaz-Rios L, Jaffe S., Standards, Competitiveness, and Africa's groundnut Exports to Europe: Barrier, Catalyst, or Distraction, Agriculture & Rural Development Department, 39, 2008.

67. Fallah, A. A., Rahnama, M., Jafari, T., and Saei-Dehkordi, S. S. (2011). Seasonal variation of aflatoxin M1 contamination in industrial and traditional Iranian dairy products. *Food Control* 22, 1653–1656.

68. Tabari, M., Karim, G., Ghavami, M., and Chamani, M. (2011). Method validation for aflatoxin M1 determination in yoghurt using immunoaffinity column clean-up prior to high-performance liquid chromatography. *Toxicol.*

69. Sulyok, M., Beed, F., Boni, S., Abass, A., Mukunzi, A., and Krska, R. (2015). Quantitation of multiple mycotoxins and cyanogenic glucosides in cassava samples from Tanzania and Rwanda by an LC-MS/MS-based multi-toxin method. *Food Addit. Contam. Part A Chem. Anal. Control, Expo. Risk Assess.* 32, 488–502.

70. Costa-Fernandez, J. M., and Sanz-Medel, A. (2000). Room temperature phosphorescence biochemical sensors. *Quim. Anal.* 19, 189–204.

71. Li, G. R., Wu, J. J., Jin, W. J., and Xie, J. W. (2003). Antioxygen quenching room temperature phosphorescence stabilized by deoxycholate aggregate.

72. Gurban A., Epure P., Achievements and Prospects in Electrochemical-Based Biosensing Platforms for Aflatoxin M1 Detection in Milk and Dairy Products, December 2017.

73. Fukayama, M.; Winterlin, W.; Hsieh, D.P. Rapid method for analysis of aflatoxin M1 in dairy products. J. Assoc. Off. Anal. Chem. 1980, 63, 927–930. [PubMed]

74. Gauch, R.; Leuenberger, U.; Baumgartner, E. Rapid and simple determination of aflatoxin M1 in milk in the low parts per 1012 range. J. Chromatogr. A 1979, 178, 543–549.

75. Bakirci, I. A study on the occurrence of aflatoxin M1 in milk and milk products produced in van province of turkey. Food Control 2001, 12, 47–51.

76. Bijl, J.; van Peteghem, C. Rapid extraction and sample clean-up for the fluorescence densitometric determination of aflatoxin M1 in milk and mil powder. Anal. Chim. Acta 1985, 170, 149–152.

77. Andreou, V.G.; Nikolelis, D.P.; Tarus, B. Electrochemical investigation of transduction of interactions of aflatoxin M1 with bilayer lipid membranes (blms). Anal. Chim. Acta 1997, 350, 121–127.

78. Micheli, L.; Grecco, R.; Badea, M.; Moscone, D.; Palleschi, G. An electrochemical immunosensor for aflatoxin M1 determination in milk using screen-printed electrodes. Biosens. Bioelectron. 2005, 21, 588–596.

79. Badea, M.; Micheli, L.; Messia, M.C.; Candigliota, T.; Marconi, E.; Mottram, T.; Velasco-Garcia, M.; Moscone, D.; Palleschi, G. Aflatoxin M1 determination in raw milk using a flow-injection immunoassay system. Anal. Chim. Acta 2004, 520, 141–148.

80. Vdovenko, M.M.; Lu, C.C.; Yu, F.Y.; Sakharov, I.Y. Development of ultrasensitive direct chemiluminescent enzyme immunoassay for determination of aflatoxin M1 in milk. Food Chem. 2014, 158, 310–314.

81. Chunlei Y., Qi W., Recent Advances in Aflatoxins Detection Based on Nanomaterials, Nanomaterials, 10, 1626, 2020.

82. Jans, H.; Huo, Q. Gold nanoparticle-enabled biological and chemical detection and analysis. Chem. Soc. Rev. 2012, 41, 2849–2866.

83. Dykman, L.; Khlebtsov, N. Gold nanoparticles in biomedical applications: Recent advances and perspectives. Chem. Soc. Rev. 2012, 41, 2256–2282.

84. Sun, J.; Xianyu, Y.; Jiang, X. Point-of-care biochemical assays using gold nanoparticle-implemented microfluidics. Chem. Soc. Rev. 2014, 43, 6239–6253.

85. Ruchika, C.; Jay, S.; Pratima, R.S.; Basu, T.; Richard, O.K.; Malhotra, B.D. Electrochemical piezoelectric reusable immunosensor for aflatoxin B1 detection. Biochem. Eng. J. 2015, 103, 103–113.

86. Reverté, L.; Prieto-Simón, B.; Campàs, M. New advances in electrochemical biosensors for the detection of toxins: Nanomaterials, magnetic beads and microfluidics systems. A review. Anal. Chim. Acta 2015, 908, 8–21.

87. Gan, N.; Zhou, J.; Xiong, P.; Hu, F.; Cao, Y.; Li, T.; Jiang, Q. An Ultrasensitive Electrochemiluminescent Immunoassay for Aflatoxin M1 in Milk, Based on Extraction by Magnetic Graphene and Detection by Antibody-Labeled CdTe Quantumn Dots-Carbon Nanotubes Nanocomposite. Toxins 2013, 5, 865–883.

88. Srivastava, S.; Ali, M.A.; Umrao, S.; Parashar, U.K.; Srivastava, A.; Sumana, G.; Malhotra, B.D.; Pandey, S.S.; Hayase, S. Graphene Oxide-Based Biosensor for Food Toxin Detection. Appl. Biochem. Biotechnol. 2014, 174, 960–970.

89. Rijian, M.; Lei, H.; Xiemin, Y.; Tiantian, S.; Chunxia, Z.; Zhe, W.; Pengzhi, H.; Shengli, S.; Chengyong, L. A novel aflatoxin B1 biosensor based on a porous anodized alumina membrane modified with graphene oxide and an aflatoxin B1 aptamer. Electrochem. Commun. 2018, 95, 9–13.

90. Goud, K.Y.; Hayat, A.; Catanante, G.L.; Satyanarayana, M.; Gobi, K.V.; Marty, J.L. An electrochemical aptasensor based on functionalized graphene oxide assisted electrocatalytic signal amplification of methylene blue for aflatoxin B1 detection. Electrochim. Acta 2017, 244, 96–103.

91. Shadjou, R.; Hasanzadeh, M.; Heidar Oor, M.; Shadjou, N. Electrochemical monitoring of aflatoxin M1 in milk samples using silver nanoparticles dispersed on α-cyclodextrin-GQDs nanocomposite. J. Mol. Recognit. 2018, 31, e2699.

92. Wang, D.; Hu, W.; Xiong, Y.; Xu, Y.; Li, C. Multifunctionalized reduced graphene oxide-doped polypyrrole/pyrrolepropylic acid nanocomposite impedimetric immunosensor to ultra-sensitively detect small molecular aflatoxin B1. Biosens. Bioelectron. 2015, 63, 185–189.

93. Singh, C.; Srivastava, S.; Ali, M.A.; Gupta, T.K.; Sumana, G.; Srivastava, A.; Mathur, R.B.; Malhotra, B.D. Carboxylated multiwalled carbon nanotubes based biosensor for aflatoxin detection. Sens. Actuators B Chem. 2013, 185, 258–264

94. Wang Z., Li J., Xu, L. *et al.*, Electrochemical sensor for determination of aflatoxin B_1 based on multiwalled carbon nanotubes-supported Au/Pt bimetallic nanoparticles. *J Solid State Electrochem* 18, 2487–2496, 2014.

95. Ricci, F.; Volpe, G.; Micheli, L.; Palleschi, G. A review on novel developments and applications of immunosensors in food analysis. Anal. Chim. Acta 2007, 605, 111–129.

96. Karczmarczyk, A.; Baeumner, A.J.; Feller, K.-H. Rapid and sensitive inhibition-based assay for the electrochemical detection of ochratoxin a and aflatoxin M1 in red wine and milk. Electrochim. Acta 2017, 243, 82–89.

97. Atul S. Kotagiri Y., Recent Advances in Electrochemical-Based Sensing Platforms for Aflatoxins Detection, Biosensor Lab, Department of Chemistry, Zuarinagar, India, 2016.

98. Ammida, N.H.S.; Micheli, L.; Palleschi, G. Electrochemical immunosensor for determination of aflatoxin B1 in barley. Anal. Chim. Acta 2004, 520, 159–164.

99. Parker, C.O.; Tothill, I.E. Development of an electrochemical immunosensor for aflatoxin M1 in milk with focus on matrix interference. Biosens. Bioelectron. 2009, 24, 2452–2457.

100. Zhang, X.; Li, C.-R.; Wang, W.-C.; Xue, J.; Huang, Y.-L.; Yang, X.-X.; Tan, B.; Zhou, X.-P.; Shao, C.; Ding, S.-J.; et al. A novel electrochemical immunosensor for highly sensitive detection of aflatoxin B1 in corn using single-walled carbon nanotubes/chitosan. Food Chem. 2016, 192, 197–202.

101. Gan, N.; Zhou, J.; Xiong, P.; Hu, F.; Cao, Y.; Li, T.; Jiang, Q. An ultrasensitive electrochemiluminescent immunoassay for aflatoxin M1 in milk, based on extraction by magnetic graphene and detection by antibody-labeled cdte quantumn dots-carbon nanotubes nanocomposite. Toxins 2013, 5, 865–883.

102. Wang, D.; Hu, W.; Xiong, Y.; Xu, Y.; Li, M.C. Multifunctionalized reduced graphene oxide-doped polypyrrole/pyrrolepropylic acid nanocomposite impedimetric immunosensor to ultra-sensitively detect small molecular aflatoxin B1. Biosens. Bioelectron. 2015, 63, 185–189.

103. Yugender Goud K., Suresh Kumar K., Progress on nanostructured electrochemical sensors and their recognition elements for detection of mycotoxins, Biosensors and Bioelectronics, 121, 205-222, 2018,

104. C. L. Morgan, D. J. Newman, and C. P. Price, “Immunosensors: technology and opportune

105. A.-L. Valimaa, A. T. Kivist ¨ o, P. I. Leskinen, and M. T. Karp, ¨ “A novel biosensor for the detection of zearalenone family mycotoxins in milk,” Journal of Microbiological Methods, vol. 80, no. 1, pp. 44–48, 2010.

106. J. H. Owino, O. A. Arotiba, N. Hendricks et al., “Electrochemical immunosensor based on polythionine/gold nanoparticles for the determination of aflatoxin B1,” Sensors, vol. 8, no. 12, pp. 8262–8274, 2008.

107. Z. Linting, L. Ruiyi, L. Zaijun, X. Qianfang, F. Yinjun, and L. Junkang, “An immunosensor for ultrasensitive detection of aflatoxin B1 with an enhanced electrochemical performance based on graphene/conducting polymer/gold nanoparticles/the ionic liquid composite film on modified gold electrode with electrodeposition,” Sensors and Actuators B: Chemical, vol. 174, pp. 359–365, 2012.

108. Wacoo Alex P., Wendiro D., Methods for Detection of Aflatoxins in Agricultural Food Crops, Uganda Industrial Research Institute, Uganda , 2014.

109. Park, D. L., Effect of processing on aflatoxin. *Adv. Exp. Med. Biol.* 504, 173–179, 2002.

110. Awasthi, V., Bahman, S., Thakur, L. K., Singh, S. K., Dua, A., and Ganguly, S. (2012). Contaminants in milk and impact of heating: an assessment study. *Indian J. Public Health* 56, 95–99

111. Yazdanpanah, H., Mohammadi, T., Abouhossain, G., and Cheraghali, A. M.. Effect of roasting on degradation of aflatoxins in contaminated pistachio nuts. *Food Chem. Toxicol.* 43, 1135–1139. 2005.

112. Torres, P., Guzman-Ortiz, M., and Ramirez-Wong, B., Revising the role of pH and thermal treatments in aflatoxin content reduction during the tortilla and deep frying processes. *J. Agric. Food Chem.* 49, 2825–2829, 2001.

113. Hameed, H. G., *Extrusion and Chemical Treatments for Destruction of Aflatoxin in Naturally-Contaminated Corn.* Ph.D. thesis, University of Arizona, Tucson, AZ, 1993.

114. Cheftel, J. C., “Extrusion cooking and food safety,” in *Extrusion Cooking*, eds C. Mercier, P. Linko, and J. M. Harper (Eagan, MN: American Association of Cereal Chemists), 435–461,1989.

115. Saalia, F. K., and Phillips, R. D., Degradation of aflatoxins by extrusion cooking: effects on nutritional quality of extrudates. *LWT Food Sci. Technol.* 44, 1496–1501, 2011a.

116. Saalia, F. K., and Phillips, R. D., Reduction of aflatoxins in peanut meal by extrusion cooking in the presence of nucleophiles. *LWT Food Sci. Technol.* 44, 1511–1516, 2011b.

117. Paterson, R., and Lima, N., How will climate change affect mycotoxins in food? *Food Res. Int.* 43, 1902–1914, 2010.

118. Paterson, R., and Lima, N., Further mycotoxin effects from climate change. *Food Res. Int.* 44, 2555–2566, 2011.

119. Paterson, R., and Lima, N., “Climate change, fumonisins and animal feed,” in *Nutrieconomics: Balancing Global Nutrition and Productivity*, ed. E. M. Binder (Tulln: BiominWorld Nutrition Forum), 241–247, 2012.

120. Magan, N., and Aldred, D., Post-harvest control strategies: minimizing mycotoxins in the food chain. *Int. J. Food Microbiol.* 119, 131–139, 2007.

121. Magan, N., Aldred, D., Hope, R., and Mitchell, D., Environmental factors and interactions with mycoflora of grain and grapes: effects on growth and deoxynivalenol and ochratoxin production by *Fusarium culmorum* and *Aspergillus carbonarius*. *Toxins* 2, 353–366, 2010.

122. Magan, N., Medina, A., and Aldred, D., Possible climate change effects on mycotoxin contamination of food crops pre- and post-harvest. *Plant Pathol.* 60, 150–163, 2011.

123. Schmidt-Heydt, M., Rufer, C. E., Abdel-Hadi, A., Magan, N., and Geisen, R., The production of aflatoxin B1 or G1 by *Aspergillus parasiticus* at various combinations of temperature and water activity is related to the ratio of aflS to aflR expression. *Mycotoxin Res.* 26, 241–246, 2010.

124. Medina, A., Rodriguez, A., and Magan, N., Effect of climate change on aspergillus flavus and aflatoxin B1 production. *Front. Microbiol.* 5:348, 2014.

125. Abdel-Hadi, A., Carter, D., and Magan, N., Temporal monitoring of the nor-1 (aflD) gene of *Aspergillus flavus* in relation to aflatoxin B1 production during storage of peanuts under different environmental conditions. *J. Appl. Microbiol.* 109, 1914–1922, 2010.

126. Gallo, A., Solfrizzo, M., Epifani, F., Panzarini, G., and Perrone, G., Effect of temperature and water activity on gene expression and aflatoxin biosynthesis in *Aspergillus flavus* on almond medium. *Int. J. Food Microbiol.* 217, 162–169, 2016.

127. Hell, K., & Mutegi, C., Aflatoxin control and prevention strategies in key crops of Sub-Saharan Africa. African Journal of Microbiology Research, 5(5), 459-466, 2011.

128. Shakerardekani, A., & Karim, R., Effect of different types of plastic packaging films on the moisture and aflatoxin contents of pistachio nuts during storage. Journal of Food Science and Technology In Press , 1-3, 2012.

129. Hell, K., Cardwell, K. F., Setamou, M., & Poehling, H. M., The influence of storage practices on aflatoxin contamination in maize in four agro- ecological zones of Benin, West Africa. Journal of Stored Products Research, 36(4), 365-382, 2000.

130. Udoh, J. M., Cardwell, K. F., & Ikotun, T., Storage structures and aflatoxin con- tent of maize in five agroecological zones of Nigeria. Journal of Stored Products Re- search, 36(2), 187-201, 2000.

131. Bastioli, C., Global status of the production of biobased packaging materials. Starch/Starke, 53(8), 351-355, 2001.

132. Devlieghere, F., Vermeulen, A., & Debevere, J. (2004). Chitosan: antimicrobial activi- ty, interactions with food components and applicability as a coating on fruit and veg- etables. Food Microbiology ., 21(6), 703-714.

133.Miranda-Castro, S.P. (2000). La quitina y su potencial aplicación industrial. Revista Investigación y Desarrollo. Periodismo de Ciencia y tecnología,

134.Miranda-Castro, S.P. (2004). Películas compuestas de quitosano y esponjas para usos biomédicos y alimentarios. (A Chitosan and/or porous solids film for Biomedical and/or Food Uses, a process for the obtention thereof and use of the same). Instituto Mexicano de la Propiedad Industrial, México.

135. Miranda, S. P., Miranda, E., & Serrano, J. (2007). Chitosan and gamma irradiated chi- tosan against Aspergillus flavus in maize. Asian Chitin Journal, 3-37.

136. Rivero, D., Cruz, A., Martínez, B., Ramírez, M. A., Rodríguez, A. T., & Cárdenas, R. M. (2004). Efecto protector de la quitosana en semillas de arroz frente a Fusarium sp. Revista de Protección Vegetal, 19(2), 140-144

137. Alam T, Anco DJ, Rustgi S., Management of Aflatoxins in Peanut. Clemson (SC): Clemson Cooperative Extension, Land-Grant Press by Clemson Extension, 2020.

Hormons and steroids

Some of the hormons and steroids were identified to be assayed especially from chicken meet. A selection of literature is shown below:

References

1. N. VanHoof, D. Courtheyn, D. J. P. Antignac et al., “Multiresidue liquid chromatography/tandem mass spectrometric analysis of beta agonists in urine using molecular imprinted polymers,” Rapid Communication in Mass Spectrometer, vol. 19, no. 19, pp. 2801–2808, 2005.

2. H. Noppe, B. Le Bizec, K. Verheyden, and H. F. De Brabander, “Novel analytical methods for the determination of steroid hormones in edible matrices,” Analytica Chimica Acta, vol. 611, no. 1, pp. 1–16, 2008.
3. H. Galbraith, “Hormones in international meat production: biological, sociological and consumer issues,” Nutrition Research Reviews, vol. 15, no. 2, pp. 243–314, 2002.
4. P. Annamaria, “Steroid hormones in food producing animals,” in A Bird’s-Eye View of Veterinary MedicineIntechOpen, London, UK, 2012.
5. D. Courtheyn, B. Le Bizec, G. Brambilla et al., “Recent developments in the use and abuse of growth promoters,” Analytica Chimica Acta, vol. 473, no. 1-2, pp. 71–82, 2002.
6. A. A. M. Stolker and U. A. T. Brinkman, “Analytical strategies for residue analysis of veterinary drugs and growth-promoting agents in food-producing animals-a review,” Journal of Chromatography A, vol. 1067, no. 1-2, pp. 15–53, 2005.
7. E. S. E. Hafez, M. R. Jainudeen, and Y. Rosnina, “Hormones and growth factors in reproduction,”“Hormones and growth factors in reproduction,” in Reproduction in Farm Animals, B. Hafez and E. Hafez, Eds., pp. 108–120, Wiley-Blackwell, Lindon, UT, USA, 7th edition, 2013
8. P. Fernandes, J.M.S. Cabral, Bioresour. Technol. 98 (2007) 2335.
9. V. Piironen, D.G. Lindsay, T.A. Miettinen, J. Toivo, A.-M. Lampi, J. Sci. Food Agric. 80 (2000) 939.
10. S.L. Abidi, J. Chromatogr. A 935 (2001) 173.
11. M.J. Lagarda, G. Garc´ıa-Llatas, R. Farre, J. Pharmaceut. ´ Biomed. Anal. 41 (2006) 1486.
12. H.S.M. Ahmida, P. Bertucci, L. Franzo, R. Massoud, C. ` Cortese, A. Lala, G. Federici, J. Chromatogr. B 842 (2006) 43.
13. S. Rozner, N. Garti, Colloid Surf. A 282–283 (2006) 435.
14. R. Santos, E. Limas, M. Sousa, M. da Conceic¸ao Castilho, F. ˜ Ramos, M.I.N. da Silveira, Food Chem. 102 (2006) 113.
15. Y.-T. Lin, S.-S. Wu, H.-L. Wu, J. Chromatogr. A 1156 (2007) 280.
16. R.E. Ostlund, Curr. Opin. Lipidol. 15 (2004) 37.
17. R. Draisci, R. Merlanti, G. Ferretti, L. Fantozzi, C. Ferranti, F. Capolongo, S. Sefato, C. Montesissa, Anal. Chim. Acta 586 (2007) 171.
18. S. Poelmans, K. De Wasch, Y. Martele, R. Schilt, N. Van Hoof, ´ H. Noppe, T. Verlsycke, C.R. Janssen, D. Courtheyn, H.F. De Brabander, Proceedings EuroFoodChem XIII, Bruges, Belgium, 2003, p. 74.
19. K. Verheyden, H. Noppe, V. Mortier, J. Vercruysse, E. Claerebout, F. Van Immerseel, C.R. Janssen, H.F. De Brabander, Anal. Chim. Acta 586 (2007) 163.
20. M.J. Tikkanen, Handb. Exp. Pharmacol. 170 (2005) 215.
21. S. Impens, The use of gas chromatography–tandem mass spectrometry (GC–MS-MS) for optimization of targeted research on residues in matrices of animal origin, Ph.D. Thesis, Ghent University, Ghent, Belgium, 2002, p. 201, ISBN 90-5864-025-6.
22. M. E. Dikeman, “Effects of metabolic modifiers on carcass traits and meat quality,” Meat Science, vol. 77, no. 1, pp. 121–135, 2007.
23. H. F. De Brabander, B. Le Bizec, G. Pinel et al., “Past, present and future of mass spectrometry in the analysis of residues of banned substances in meat-producing animals,” Journal of Mass Spectrometry, vol. 42, no. 8, pp. 983–998, 2007.
24. EU/EC, “Pharmacologically active substances and their classification regarding maximum residue limits in foodstuffs of animal origin,” Official Journal of European Commissions, vol. 37, pp. 1–72, 2010.

25. EU/EC, “Amending council directive 96/22/EC concerning the prohibition on the use in stockfarming of certain substances having hormonal or thyreostatic action and of beta agonists,” European Community Council (ECC) Directive 2003/74/EC of 22 September 2003, Official Journal of European Commissions, vol. 262, pp. 17–21, 2003.
26. D. Courtheyn, B. Le Bizec, G. Brambilla et al., “Recent developments in the use and abuse of growth promoters,” Analytica Chimica Acta, vol. 473, no. 1-2, pp. 71–82, 2002.
27. U S–FDA, “Tolerances for residue of new animal drugs in food,” in Animal Drugs, Feeds, and Related Products, Implantation or Injectable Dosage form New Animal Drugs, Code of Federal Regulation (CITE: 21CFR 522)Vol. 6, FDA, Silver Spring, MD, USA, 2017.
28. U S–FDA, “Implantation or injectable dosage form new animal drugs, zeranol,” in Animal Drugs, Feeds, and Related Products, Code of Federal Regulation (CITE 21CFR 556.760) Vol. 6, FDA, Silver Spring, MD, USA, 2017.
29. U S–FDA, “Tolerances for residue of new animal drugs in food, trenbolone,” in Animal Drugs, Feeds, and Related Products, Code of Federal Regulation (CITE: 21CFR 556.739) Vol. 6, FDA, Silver Spring, MD, USA, 2017.
30. U S–FDA, “Oral dosage form new animal drugs, clenbuterol syrup,” in Animal Drugs, Feeds, and Related Products, Code of Federal Regulation (CITE 21CFR 520.452)Vol. 6, FDA, Silver Spring, MD, USA, 2017.
31. EU/EC, “Pharmacologically active substances and their classification regarding maximum residue limits in foodstuffs of animal origin,” Official Journal of European Commissions, vol. 37, pp. 1–72, 2010.
32. CAC, “Maximum residue limits (MRLs) and risk management recommendations for residues of veterinary drugs in foods,” in Codex Alimentarius Commission (CAC)/MRL 2-2017, pp.
33. JECFA, “Evaluation of certain veterinary drug residues in food,” in Joint FAO/WHO Expert Committee on Food Additives (JECFA)vol. 52, WHO Technical Report Series893 pages, WHO Technical Report Series, Geneva, Switzerland, 2000. 1–84, CAC, Japan, 2017.`
34. D. Courtheyn, B. Le Bizec, G. Brambilla, H.F. De Brabander, E. Cobbaert, M. Van de Wiele, J. Vercammen, K. De Wasch, Anal. Chim. Acta 473 (2002) 71.
35. J.-P. Antignac, B. Bizec, F. Monteau, F. Poulain, F. Andre, J. ´ Chromatogr. B 757 (2001) 11.
36. J.-P. Antignac, F. Monteau, J. Negrolli, F. Andr ´ e, B. Le Bizec, ´ Chromatographia 59 (2004) 1. [29] B. Shao, R. Zhao, J. Meng, Y. Xue, G. Wu, J. Hu, X. Tu, Anal. Chim. Acta 548 (2005) 41.
37. H.F. De Brabander, B. Le Bizec, G. Pinel, J.-P. Antignac, K. Verheyden, V. Mortier, D. Courtheyn, H. Noppe, J. Mass Spectrom. 42 (2007) 983.
38. H. Noppe, K. Verheyden, W. Gillis, D. Courtheyn, P. Vanthemsche, H.F. De Brabander, Anal. Chim. Acta 586 (2007) 22.
39. A.A.M. Stolker, U.A.Th. Brinkman, J. Chromatogr. A 1067 (2005) 15.
40. A. Daxenberger, D. Ibarreta, H.H.D. Meyer, Hum. Reprod. Update 7 (2001) 340.
41. U S–FDA, “Tolerances for residue of new animal drugs in food,” in Animal Drugs, Feeds, and Related Products, Implantation or Injectable Dosage form New Animal Drugs, Code of Federal Regulation (CITE: 21CFR 522)Vol. 6, FDA, Silver Spring, MD, USA, 2017.
42. P. E. Strydom, L. Frylinck, J. L. Montgomery, and M. F. Smith, “*e comparison of three β-agonists for growth performance, carcass characteristics and meat quality of feedlot cattle,” Meat Science, vol. 81, no. 3, pp. 557–564, 2009.

43. U S–FDA, “Implantation or injectable dosage form new animal drugs, zeranol,” in Animal Drugs, Feeds, and Related Products, Code of Federal Regulation (CITE 21CFR 556.760) Vol. 6, FDA, Silver Spring, MD, USA, 2017.
44. Hassan MALEKINEJAD, Aysa REZABAKHSH, Hormones in Dairy Foods and Their Impact on Public Health, Iran J Public Health, Vol. 44, No.6, Jun 2015, pp.742-758.
45. Collier RJ, Miller MA, Hildebrandt JR, Torkelson AR, White TC, Madsen KS, Vicini JL, Eppard PJ, Lanza GM (1991). Factors affecting insulin-like growth factor-I concentration in bovine milk. J Dairy Sci, 74 (9):2905-2911.
46. Atroshi F, Rizzo A, Osterman T, Parantainen J (1989). Free fatty acids and lipid peroxidation in normal and mastitic bovine milk. Zentralbl Veterinarmed,A 36 (5):321-330.
47. Hansel W, Hixon J, Shemesh M, Tobey D (1976). Concentrations and activities of prostaglandins of the F series in bovine tissue, blood and milk. J Dairy Sci, 59 (7):1353-1365.
48. Schams D, Karg H (1986). Hormones in milk. Ann N Y Acad Sci, 464:75-86.
49. Foulkes JA, Cookson AD, Sauer MJ (1982). Artificial insemination of cattle based on daily enzyme immunoassay of progesterone in whole milk. Vet Rec, 111 (13):302-303.
50. Atroshi F, Parantainen J, Kangasniemi R, Osterman T (1987). Milk prostaglandins and electrical conductivity in bovine mastitis. Vet Res Commun, 11 (1):15-22.
51. Andersson AM, Skakkebaek NE (1999). Exposure to exogenous estrogens in food: possible impact on human development and health. Eur J Endocrinol, 140 (6):477-485.
52. Vadgama JV, Wu Y, Datta G, Khan H, Chillar R (1999). Plasma insulin-like growth factor-I and serum IGF-binding protein 3 can be associated with the progression of breast cancer, and predict the risk of recurrence and the probability of survival in African-American and Hispanic women. Oncology, 57 (4):330-340.
53. Hoffmann B, Hamburger R, Hollwich W (1977). Determination of progesterone directly in milk fat as an improved method for fertility control in cattle. Zuchthygiene, 2 (1):1-7.
54. Rioux P, Rajotte D (2004). Progesterone in milk: a simple experiment illustrating the estrous cycle and enzyme immunoassay. Adv Physiol Educ, 28 (1-4):64-67.
55. Hoffmann B, Hamburger R, Karg H (1975). Natural occurrence of progesterone in commercial milk products (author's transl). Z Lebensm Unters Forsch, 158 (5):257-259.
56. Hassan MALEKINEJAD, Aysa REZABAKHSH, Hormones in Dairy Foods and Their Impact on Public Health, Iran J Public Health, Vol. 44, No.6, Jun 2015, pp.742-758.
57. Directive 81/206/EEC, Off. J. Eur. Comm., L222 (1981) 32.
58. Directive 88/146/EEC, Off. J. Eur. Comm., L70 (1988) 16.
59. Directive 88/299/EEC, Off. J. Eur. Comm., L128 (1988) 36.
60. Commission Regulation 2377/90, Off. J. Eur. Comm., L224 (1990) 1.
61. Council Directive 96/22/EC, Off. J. Eur. Comm., L125 (1996) 3.
62. Council Directive 96/23/EC, Off. J. Eur. Comm., L125 (1996) 10
63. Commission Decision 2002/657/EC, Off. J. Eur. Comm., L221 (2002) 8.
64. Commission Decision 93/256/EEC, Off. J. Eur. Comm., L118 (1993) 64.
65. Commission Decision 93/257/EEC, Off. J. Eur. Comm., L118 (1993) 75.
66. F. Andre, K. De Wasch, H.F. De Brabander, S. Impens, L.A.M. ´ Stolker, L. Van Ginkel, R. Stepahny, R. Schilt, D. Courtheyn, Y. Bonnaire, P. Furst, P. Gowik, G. Kennedey, T. Kuhn, J.-P. ¨ Moretain, M. Sauer, Trends Anal. Chem. 20 (2001) 435.
67. J.-P. Antignac, B. Le Bizec, F. Monteau, F. Andre, Anal. Chim. ´ Acta 483 (2003) 325.
68. S. Impens, The use of gas chromatography–tandem mass spectrometry (GC–MS-MS) for optimization of targeted research on residues in matrices of animal origin, Ph.D. Thesis, Ghent University, Ghent, Belgium, 2002, p. 201, ISBN 90-5864-025-6.

69. A.A.M. Stolker, U.A.Th. Brinkman, J. Chromatogr. A 1067 (2005) 15.
70. B. Shao, R. Zhao, J. Meng, Y. Xue, G. Wu, J. Hu, X. Tu, Anal. Chim. Acta 548 (2005) 41.
71. S. Hartmann, H. Steinhart, J. Chromatogr. B 704 (1997) 105.
72. E. Daeseleire, R. Vandeputte, C. Van Peteghem, Analyst 123 (1998) 2595.
73. S. Impens, K. De Wasch, M. Cornelis, H.F. De Brabander, J. Chromatogr. A 970 (2002) 235.
74. B. LeBizec, P. Marchand, C. Gade, D. Maume, F. Monteau, F. ´ Andre, Proceedings of the EuroResidue IV Conference, ´ Veldhoven, 2000, p. 226.
75. P. Marchand, B. Le Bizec, C. Gade, F. Monteau, F. Andre, J. ´ Chromatogr. A 867 (2000) 219.
76. J. Seo, H. Kim, B.C. Chung, J. Hong, J. Chromatogr. A 1067 (2005) 303.
77. C. Blasco, C. Van Poucke, C. Van Peteghem, J. Chromatogr. A 1154 (2007) 230.
78. H. Malekinejad, P. Scherpenisse, A.A. Bergwerf, J. Agric. Food Chem. 54 (2006) 9785
79. H.F. De Brabander, B. Le Bizec, G. Pinel, J.-P. Antignac, K. Verheyden, V. Mortier, D. Courtheyn, H. Noppe, J. Mass Spectrom. 42 (2007) 983.
80. C. Blasco, C. Van Poucke, and C. Van Peteghem, "Analysis of meat samples for anabolic steroids residues by liquid chromatography/tandem mass spectrometry," Journal of Chromatography A, vol. 1154, no. 1-2, pp. 230–239, 2007.
81. H. Noppe, B. Le Bizec, K. Verheyden, and H. F. De Brabander, "Novel analytical methods for the determination of steroid hormones in edible matrices," Analytica Chimica Acta, vol. 611, no. 1, pp. 1–16, 2008.
82. Z. Zeng, R. Liu, J. Zhang, J. Yu, L. He, and X. Shen, "Determination of seven free anabolic steroid residues in eggs by high-performance liquid chromatography-tandem mass spectrometry," Journal of Chromatographic Science, vol. 51, no. 3, pp. 229–236, 2013.
83. I. M. Zuchowska, B. Wozniak, and A. Posyniak, "Determination of hormone residues in milk by gas chromatographymass spectrometry," Food Analytical Methods, vol. 10, no. 3, pp. 727–739, 2017.
84. T. Gao, N. Ye, and L. Jian, "Determination of ractopamine and clenbuterol in beef by graphene oxide hollow fiber solid-phase microextraction and high-performance liquid chromatography," Analytical Letters, vol. 49, no. 8, pp. 1163–1175, 2016.
85. L. Giannetti, D. Barchi, F. Fiorucci et al., "High-performance liquid chromatography-tandem mass specrometry validation of medroxyprogesterone acetate in products of pork origin and serum," Journal of Chromatographic Science, vol. 43, no. 7, pp. 333–336, 2005.
86. K. Kureckova, B. Maralikova, and K. Ventura, "Supercritical fluid extraction of steroids from biological samples and first experience with solid-phase micro extraction–liquid chromatography," Journal of Chromatography B, vol. 770, no. 1-2, pp. 83–89, 2002
87. M.-R. Fuh, S.-Y. Huang, and T.-Y. Lin, "Determination of residual anabolic steroid in meat by gas chromatography-ion trap-mass spectrometer," Talanta, vol. 64, no. 2, pp. 408–414, 2004.
88. B. Socas-Rodr´ıguez, M. Asensio-Ramos, J. Hernandez-Borges, ´ A. V. Herrera-Herrera, and M. A. Rodr ´ ´ıguez-Delgado, "Chromatographic analysis of natural and synthetic estrogens in milk and dairy products," TrAC Trends in Analytical Chemistry, vol. 44, pp. 58–77, 2013.
89. Y. Shi, D.-D. Peng, C.-H. Shi, X. Zhang, Y.-T. Xie, and B. Lu, "Selective determination of trace 17β-estradiol in dairy and meat samples by molecularly imprinted solid-phase extraction and HPLC," Food Chemistry, vol. 126, no. 4, pp. 1916–1925, 2011.
90. S. Studzinska, B. Buszewski, Fast method for the resolution and determination of sex steroids in urine, J. Chromatogr. B Anal. Technol. Biomed. Life Sci. 927 (2013) 158–163.

91. N. Tagawa, H. Tsuruta, A. Fujinami, Y. Kobayashi, Simultaneous determination of estriol and estriol 3-sulfate in serum by column-switching semi-micro high-performance liquid chromatography with ultraviolet and electrochemical detection, J. Chromatogr. B 723 (1999) 39–45.
92. S. Wang, W. Huang, G. Fang, J. He, Y. Zhang, On-line coupling of solid-phaseextraction to high-performance liquid chromatography for determination of estrogens in environment, Anal. Chim. Acta 606 (2008) 194–201.
93. Z.L. Li, S. Wang, N.A. Lee, R.D. Allan, I.R. Kennedy, Development of a solid-phase extraction—enzyme-linked immune sorbent assay method for the determination of estrone in water, Anal. Chim. Acta 503 (2004) 171–177.
94. Y.P. Tang, S.Q. Zhao, Y.S. Wu, J.W. Zhou, M. Li, A direct competitive inhibition time-resolved fluoro immunoassay for the detection of unconjugated estriol inserum of pregnant women, Anal. Methods 5 (2013) 4068–4073.
95. S.H. Wang, S.L. Lin, L.Y. Du, H.S. Zhuang, Electrochemical enzyme-linked immunoassay for the determination of estriol using methyl red as substrate, Anal. Lett. 39 (2006) 947–956.
96. N.S. Lisboa, C.S. Fahning, G. Cotrim, J.P. Anjos, J.B. Andrade, V. Hatje, G.O. Rocha, A simple and sensitive UFLC-fluorescence method for endocrine disrupters determination in marine waters, Talanta 117 (2013) 168–175.
97. A.P. Fonseca, D.L.D. Lima, V.I. Esteves, Degradation by solar radiation of estrogenic hormones monitored by UV–visible spectroscopy and capillary electrophoresis, Water Air Soil Pollut. 215 (2011) 441–447.
98. S. Flor, S. Lucangioli, M. Contin, V. Tripodi, Simultaneous determination of nine endogenous steroids in human urine by polymeric-mixed micelle capillary electrophoresis, Electrophoresis 31 (2010) 3305–3313.
99. K.D. Santos, O.C. Braga, I.C. Vieira, A. Spinelli, Electroanalytical determination of estriol hormone using a boron-doped diamond electrode, Talanta 80 (2009) 1999–2006.
100. Hadi Beitollahi, Hassan Karimi-Maleh, Hojatollah Khabazzadeh, Epinephrine in the presence of norepinephrine using carbon paste electrode modified with carbon nanotubes and novel 2-(4-Oxo-3-phenyl-3,4-dihydro-quinazolinyl)-N′-phenyl-hydrazinecarbothioamide, Anal. Chem. 80 (2008) 9848–9851.
101. Somayeh Tajik, Mohammad Ali Taher, Hadi Beitollahi, Application of a new ferrocene-derivative modified-graphene paste electrode for simultaneous determination of isoproterenol, acetaminophen and theophylline, Sensors Actuators B Chem. 197 (2014) 228–236.
102. Zahra Taleat, Mohammad Mazloum Ardakani, Hossein Naeimi, Hadi Beitollahi, Maryam Nejati, Hamid Reza Zare, Electrochemical behavior of ascorbic acid at a 2,2¢-[3,6-Dioxa- 1,8-octanediylbis(nitriloethylidyne)]-bis-hydroquinone carbon paste electrode, Anal. Sci. 24 (2008) 1039–1044.
103. Mohammad Mehdi Foroughi, Hadi Beitollahi, Somayeh Tajik, Mozhdeh Hamzavi, Hekmat Parvan, Hydroxylamine Electrochemical sensor based on a modified carbon nanotube paste electrode: Application to determination of hydroxylamine in water samples, Int. J. Electrochem. Sci. 9 (2014) 2955–2965.
104. Mohammad Mazloum-Ardakani, Bahram Ganjipour, Hadi Beitollahi, Mohammad Kazem Amini, Fakhradin Mirkhalaf, Hossein Naeimi, Maryam Nejati-Barzoki, Simultaneous determination of levodopa, carbidopa and tryptophan using nanostructured electrochemical sensor based on novel hydroquinone and carbon nanotubes: application to the analysis of some real samples, Electrochim. Acta 56 (2011) 9113–9120.

105. S. Mohammadi, H. Beitollahi, A. Mohadesi, Electrochemical behaviour of a modified carbon nanotube paste electrode and its application for simultaneous determination of epinephrine, uric acid and folic acid, Sens. Lett. 11 (2013) 388–394.
106. Hadi Beitollahi, Jahan-Bakhsh Raoof, Hassan Karimi-Maleh, Rahman Hosseinzadeh, Electrochemical behavior of isoproterenol in the presence of uric acid and folic acid at a carbon paste electrode modified with 2,7-bis(ferrocenyl ethyl)fluoren-9-one and carbon nanotubes, J. Solid State Electrochem. 16 (2012) 1701–1707. [
107. Mohammad Reza Akhgar, Hadi Beitollahi, Mohammad Salari, Hassan KarimiMaleh, Hassan Zamani, Fabrication of a sensor for simultaneous determination of norepinephrine, acetaminophen and tryptophan using a modified carbon nanotube paste electrode, Anal. Methods 4 (2012) 259–264.
108. J.G. Manjunatha, M. Deraman, N.H. Basri, N.S.M. Nor, I.A. Talib, N. Ataollahi, Sodium dodecyl sulfate modified carbon nanotubes paste electrode as a novel sensor for the simultaneous determination of dopamine, ascorbic acid, and uric acid, C. R. Chimie 17 (2014) 465–476.
109. Y. Ohnuki, T. Ohsaka, H. Matsuda, N. Oyama, Permselectivity of films prepared by electrochemical oxidation of phenol and amino-aromatic compounds, J. Electroanal. Chem. 158 (1983) 55–67.
110. A. Volkov, G. Tourillon, P.C. Lacaze, J.E. Dubois, Electrochemical polymerization of aromatic amines: IR, XPS and PMT study of thin film formation on a Pt electrode, J. Electroanal. Chem. 115 (1980) 279–291. [
111. Protiva Rain Roy, Takeyoshi Okajima, Takeo Ohsaka, Simultaneous electroanalysis of dopamine and ascorbic acid using poly-(N,N-dimethylaniline) modified electrode, Bioelectrochemistry 59 (2003) 11–19.
112. G. Milczarek, A. Ciszewski, 2,2-bis(3-amino-4-hydroxyphenyl)hexafluoropropane modified glassy carbon electrodes as selective and sensitive voltammetric sensors, selective detection of dopamine and uric acid, Electroanalysis 16 (2004) 1977–1983.
113. Ahmadi, A., H. Shirazi, N. Pourbagher, A. Akbarzadeh, K. Omidfar (2014): An electrochemical immunosensor for digoxin using core-shell gold coated magnetic nanoparticles as labels. Mol. Biol. Rep. 41, 1659-1668.
114. Vidal, J. C., L. Bonel, A. Ezquerra, P. Duato, J. R. Castillo (2012): An electrochemical immunosensor for ochratoxin A determination in wines based on a monoclonal antibody and paramagnetic microbeads. Anal. Bioanal. Chem. 403, 1585-1593.
115. Ricci, F.; Volpe, G.; Micheli, L.; Palleschi, G. A review on novel developments and applications of immunosensors in food analysis. Anal. Chim. Acta 2007, 605, 111–129. [CrossRef]
116. Mishra Kumar, G.; Barfidokht, A.; Tehrani, F.; Kumar Mishra, R. Food Safety Analysis Using Electrochemical Biosensors. Foods 2018, 7, 141. [CrossRef]
117. Thakur, M.S.; Ragavan, K.V. Biosensors in food processing. J. Food Sci. Technol. 2013, 50, 625–641. [CrossRef]
118. Barfidokht, A.; Gooding, J.J. Approaches toward allowing electroanalytical devices to be used in biological fluids. Electroanalysis 2014, 26, 1182–1196. [CrossRef]
119. Ronkainen, N.J.; Halsall, H.B.; Heineman, W.R. Electrochemical biosensors. Chem. Soc. Rev. 2010, 39, 1747–1763. [CrossRef]
120. Chen, A.; Chatterjee, S. Nanomaterials based electrochemical sensors for biomedical applications. Chem. Soc. Rev. 2013, 42, 5425–5438. [CrossRef] 12. Curulli, A. Nanomaterials in Electrochemical Sensing Area: Applications and Challenges in Food Analysis. Molecules 2020, 25, 5759. [CrossRef]

121. Naresh, V.; Lee, N. Review on Biosensors and Recent Development of Nanostructured Materials-Enabled Biosensors. Sensors 2021, 21, 1109. [CrossRef]
122. Mishra, G.K.; Sharma, V.; Mishra, R.K. Electrochemical aptasensors for food and environmental safeguarding: A review. Biosensors 2018, 8, 28. [CrossRef]
123. Bartlett, P.N. Bioelectrochemistry 45: Fundamentals, Experimental Techniques, and Applications; John Wiley & Sons: Hoboken, NJ, USA, 2008.
124. Bonizzoni, M.; Anslyn, E.V. Combinatorial Methods for Chemical and Biological Sensors. J. Am. Chem. Soc. 2009, 131, 14597–14598. [CrossRef]
125. Suni, I.I. Impedance methods for electrochemical sensors using nanomaterials. TrAC Trends Anal. Chem. 2008, 27, 604–611. [CrossRef]
126. Katz, E.; Willner, I. Probing Biomolecular Interactions at Conductive and Semiconductive Surfaces by Impedance Spectroscopy: Routes to Impedimetric Immunosensors, DNA-Sensors, and Enzyme Biosensors. Electroanalysis 2003, 15, 913–947. [CrossRef]
127. Wang, J. Analytical Electrochemistry, 2nd ed.; Wiley/VCH: New York, NY, USA, 2000.
128. Diamanti-Kandarakis, E.; Bourguignon, J.-P.; Giudice, L.C.; Hauser, R.; Prins, G.S.; Soto, A.M.; Zoeller, R.T.; Gore, A.C. EndocrineDisrupting Chemicals: An Endocrine Society Scientific Statement. Endocr. Rev. 2009, 30, 293–342.
129. World Health Organization (WHO). State of the Science of Endocrine Disrupting Chemicals-2012; Bergman, Å., Heindel, J.J., Jobling, S., Kidd, K.A., Zoeller, R.T., Eds.; United Nations Environment Programme: Nairobi, Kenya; World Health Organization: Geneva, Switzerland, 2013.
130. Medeiros, A.S.; Silva, D.B.; Santos, A.O.; Castro, S.S.L.; Oliveira, T.M.B.F. Voltammetric sensing of E,E-dienestrol in fish tissue by combining a cathodically pretreated boron-doped diamond electrode and QuEChERS extraction method. Microchem. J. 2020, 155, 104718. [CrossRef]
131. Hazani Mat Zaid, M.; Abdullah, J.; Rozi, N.; Rozlan, A.A.M.; Hanifah, S.A. A Sensitive Impedimetric Aptasensor Based on Carbon Nanodots Modified Electrode for Detection of 17ß-Estradiol. Nanomaterials 2020, 10, 1346. [CrossRef]
132. Spychalska, K.; Baluta, S.; Swist, A.; Cabaj, J. Biosensors for ´ β17-estradiol detection based on graphene quantum dots (GQDs)/conducting polymer and laccase modified platinum/gold electrodes. Int. J. Electrochem. Sci. 2020, 15, 3127–3142. [CrossRef]
133. Sun, Y.; Zhao, J.; Liang, L. Recent development of antibiotic detection in food and environment: The combination of sensors and nanomaterials. Microchim. Acta 2021, 188, 21–43. [CrossRef] [PubMed]
134. Shen, Z.; He, L.; Cao, Y.; Hong, F.; Zhang, K.; Hu, F.; Lin, J.; Wu, D.; Gan, N. Multiplexed electrochemical aptasensor for antibiotics detection using metallic-encoded apoferritin probes and double stirring bars-assisted target recycling for signal amplification. Talanta 2019, 197, 491–499. [CrossRef]
135. Fuentes, N.; Silveyra, P. Estrogen receptor signaling mechanisms. Adv. Protein Chem. Struct. Biol. 2019, 116, 135–170.
136. Tran, T.K.A.; Yu, R.M.K.; Islam, R.; Nguyen, T.H.T.; Bui, T.L.H.; Kong, R.Y.C.; O'Connor, W.A.; Leusch, F.D.L.; Andrew-Priestley, M.; MacFarlane, G.R. The utility of vitellogenin as a biomarker of estrogenic endocrine disrupting chemicals in molluscs. Environ. Pollut. 2019, 248, 1067–1078. [CrossRef]

137. Zamfir, L.-G.; Puiu, M.; Bala, C. Advances in Electrochemical Impedance Spectroscopy Detection of Endocrine Disruptors. Sensors 2020, 20, 6443. [CrossRef]
138. Lu, X.; Sun, J.; Sun, X. Recent advances in biosensors for the detection of estrogens in the environment and food. TrAC Trends Anal. Chem. 2020, 127, 115882.
139. Medeiros, A.S.; Silva, D.B.; Santos, A.O.; Castro, S.S.L.; Oliveira, T.M.B.F. Voltammetric sensing of E,E-dienestrol in fish tissue by combining a cathodically pretreated boron-doped diamond electrode and QuEChERS extraction method. Microchem. J. 2020, 155, 104718.
140. Hazani Mat Zaid, M.; Abdullah, J.; Rozi, N.; Rozlan, A.A.M.; Hanifah, S.A. A Sensitive Impedimetric Aptasensor Based on Carbon Nanodots Modified Electrode for Detection of 17ß-Estradiol. Nanomaterials 2020, 10, 1346.
141. Spychalska, K.; Baluta, S.; Swist, A.; Cabaj, J. Biosensors for ´ β17-estradiol detection based on graphene quantum dots (GQDs)/conducting polymer and laccase modified platinum/gold electrodes. Int. J. Electrochem. Sci. 2020, 15, 3127–3142. [CrossRef]
142. J. D. Yager and N. E. Davidson, “Estrogen carcinogenesis in breast cancer,” New England Journal of Medicine, vol. 354, no. 3, pp. 270–282, 2006.
143. D. Ganmaa and A. Sato, “*e possible role of female sex hormones in milk from pregnant cows in the development of breast, ovarian and corpus uteri cancers,” Medical Hypotheses, vol. 65, no. 6, pp. 1028–1037, 2005.
144. F. Massart, J. C. Harrell, G. Federico, and G. Saggese, “Human breast milk and xenoestrogen exposure: a possible impact on human health,” Journal of Perinatology, vol. 25, no. 4, pp. 282–288, 2005.
145. A. Daxenberger, D. Ibarreta, and H. H. Meyer, “Possible health impact of animal oestrogens in food,” Human Reproduction Update, vol. 7, no. 3, pp. 340–355, 2001.
146. S. Hartmann, M. Lacorn, and H. Steinhart, “Natural occurrence of steroid hormones in food,” Food Chemistry, vol. 62, no. 1, pp. 7–20, 1998.
147. S. Liu and Y. C. Lin, “Transformation of MCF-10A human breast epithelial cells by zeranol and estradiol-17 beta,” Ee Breast Journal, vol. 10, no. 6, pp. 514–521, 2004.
148. JECFA, “Toxicological evaluation of certain veterinary drug residues in food: estradiol-17β, progesterone, and testosterone,” in Joint FAO/WHO Expert Committee on Food Additives (JECFA)Vol. 43, WHO Food Additives Series, Geneva, Switzerland, 2000.
149. P. E. Strydom, L. Frylinck, J. L. Montgomery, and M. F. Smith, “*e comparison of three β-agonists for growth performance, carcass characteristics and meat quality of feedlot cattle,” Meat Science, vol. 81, no. 3, pp. 557–564, 2009.
150. J. Y. Yang, Y. Zhang, H. T. Lei et al., “Development of an ultrasensitive chemiluminescence enzyme immunoassay for the determination of diethylstilbestrol in seafood,” Analytical Letters, vol. 46, no. 14, pp. 2189–2202, 2013.
151. F. Tas¸çi, “Determination of diethylstilbestrol residue in raw meat sold in Burdur, Turkey,” Journal of Applied Biological Sciences, vol. 8, no. 3, pp. 32–34, 2014.
152. D. L. Moyer, B. d. Lignieres, P. Driguez, and J. P. Pez, “Prevention of endometrial hyperplasia by progesterone during long-term estradiol replacement: influence of bleeding pattern and secretory changes ∗∗ supported in part by BesinsIscovesco laboratories, Paris, France,” Fertility and Sterility, vol. 59, no. 5, pp. 992–997, 1993.
153. M. J. Seraj, A. Umemoto, M. Tanaka, A. Kajikawa, and K. Monden, “DNA adduct formation by hormonal steroids in vitro,” Mutation Research/Genetic Toxicology, vol. 370, no. 1, pp. 49–59, 1996.

Mini-Review: Electrochemical Sensors Used for the Determination of Water- and Fat- Soluble Vitamins

Abstract

Vitamins are one of the most essential organic compounds that are necessary for the human body, in order for it to develop and grow in a healthy way. The aim of this review is to bring together a series of electrochemical sensors developed for the determination of vitamins from biological, pharmaceutical or food related samples. For this review, articles from 2016-2021 were taken into consideration.

Introduction

The human body requires a series of vitamins in order to fully develop in a healthy way. These vitamins can be found in food sources. There are two major types of vitamins: the water-soluble vitamins, which are not stored in the human body, and the fat-soluble vitamins, which are stored in the fatty tissue of the human body. From an early age, these organic compounds are needed so that men can develop in a healthy way. Some of the vitamins that are necessary for the human body are: vitamin B_2, vitamin B_6, vitamin B_9, vitamin B_{12}, vitamin D, and vitamin K. Vitamins D and K are fat-soluble, whereas the vitamins from group B are water-soluble.

Vitamin B_2, also known as riboflavin, is one of the vitamins that the human body requires in order to fully develop in a healthy way. Given the fact that it cannot be internally synthesized, it is recommended to be included in the diet in small quantities [1]. Vitamin B_2 is an important component of flavoenzyme, which helps with the catalysis of various biochemical reactions of protein, fat and carbohydrate in the human body. Some of the benefits of riboflavin are:

reducing fatigue, especially the eye one, induces a natural growth of hair, nails and skin and it reduces the inflammation of the tongue, lips and mouth [2,3]. The deficiency of vitamin B_2 can lead to some of the following symptoms: skin peeling, itchy eyes, photophobia and sore throat [4, 5]. There are various methods which are used for the detection of this type of vitamin, such as, chemiluminescence [6, 7], liquid chromatography [8, 9, 10], polarography [11], UV-vis [12] and fluorescence spectroscopy [13, 14].

Vitamin B_6, also known as pyridoxine, is a water-soluble vitamin, among the other B vitamins [15]. This type of vitamin plays an important role when it comes to reducing nausea at an early pregnancy stage [16 -18] and it is also involved in the response of the human body to more than 100 enzymes. Given the fact that pyridoxine is found mostly in food, such as tuna, potatoes, rice, onions, spinach, tofu, ground beef, salmon, watermelon and chicken breast analytical methods are used for the analysis food samples [19 - 23].

Vitamin B_9, which is more commonly known as folic acid, is part of the B group vitamins, which is soluble in water and it is mostly known for its important role when it comes to biological functions [24], the synthesis and repair of the DNA, the construction of healthy cells and the methylation of the DNA [25, 26]. Despite the fact that it can be found in food, such as cabbage, fruits nuts and many others, it is not possible for the human body to produce this vitamin. Serious complications which result in malformations of the skull, brain and spine of the fetus are caused by the deficiency of folic acid [27].

Vitamin B_{12}, which is also known as cobalamin, is a cobalt-containing vitamins, which is water-soluble. This type of vitamin helps with the formation of red blood cells, the synthesis of the DNA, and maintaining the neurological functions [28]. Due to the fact that bacteria from

the small intestine partially synthesize vitamin B_{12}, it is necessary for this type of vitamin to be ingested from food [29]. The main sources of cobalamin are: meat, eggs, clams, oysters, liver, fish and milk. A low intake of vitamin B_{12} can cause different health problems, such as fatigue, anemia, kidney failure, liver disease or neurotoxicity [30]. Some of the most used techniques used for the detection of cobalamin are: radioscopy, chemiluminescence, high performance liquid chromatography, mass spectrometry, atomic absorption spectrometry and capillary electrophoresis [31].

Vitamin D, a fat-soluble vitamin, is made out of two groups, ergocalciferol, also known as D_2, and cholecalciferol, known as D_3. Vitamin D_2 is obtained from chemical synthesis and plants, while vitamin D_3 is naturally present in the human body. These can be found in egg yolk (D_2 and D_3), shitake mushrooms (D_2), cod liver oil (D_3) AND fresh salmon (D_3) [32, 33]. This type of vitamin plays a major role in strengthening bones. The deficiency of vitamin D can cause osteomalacia in adults, rickets in children, cardiovascular, Parkinson's, hypertension and cancer diseases [34 - 40].

Vitamin K is a fat-soluble vitamin and it is also known as naphthoquinone compound. There are two forms, K_1 and K_2, respectively. Vitamin K_1 is produced by green vegetables and plants and it is the predominant form. Vitamin K_2 derives from eggs, fermented food, meat and curd cheese. This type of vitamin is important for the bone calcification [41, 42] and the coagulation of blood [43, 44]. The deficiency of the naphthoquinone compound can lead to hemorrhagic excessive bleeding tendencies and can cause the decrease of prothrombin [45, 46].

Compared with the analytical methods which are currently used for the determination of vitamins, the electrochemical sensors represent a fast, reliable and cheap alternative.

This review is focused on the electrochemical sensors which were used for the determination of vitamins from various types of samples (biological, pharmaceutical and food related samples).

Electrochemical Sensors Used for the Detection of Vitamin B_2

Li et al. [47] proposed an electrochemical sensor for the determination of vitamin B_2 from pharmaceutical samples. The proposed sensor, which is based on a glassy carbon electrode (GCE) and gold nanoparticles (AuNPs) and modified with a hybrid of reduced graphene and polydopamine (PDA-RGO), showed effectiveness when it came to the assay of pharmaceutical samples, thus proving that the obtained sensor could be potentially used for the therapeutic drug monitoring. In order to investigate the efficiency of the modified surface, and in order to obtain a comparison between the modified electrodes, cyclic voltammetry was used. Thus, a standard solution of quasi-reversible ferro/ferrocyanide, which contained 0.1 mol L^{-1} KCl was used. The potential range was from -0.3 to 0.8 V vs. Ag/AgCl and the scan rate was 0.05 $V \cdot s^{-1}$. For the bare electrode, the following can be observed: a weak redox peak, which had the peak-to-peak potential separations equal to 198 mV, was obtained. Due to the active sites and the area of the surface, the peak currents greatly increased when the dispersion of PDA-RGO was casted onto the surface of the bare electrode. Moreover, the peak-to-peak potential separations decreased to 145 mV. In comparison to the bare electrode, the peak currents were increased by 38.1% when the AuNPs were electrodeposited onto the GCE, due to the fact that AuNPs permitted more $[Fe(CN)_6^{3-/4-}]$ to reach the surface of the electrode with more ease. Given the fact that the peak-to-peak potential separations decreased by 53 mV, it is proved that

the AuNPs cand accelerate the transfer of the electrons between the electrode's surface and the solution. Among all of the modified electrodes, the lowest peak-to-peak potential separations and the highest current response were obtained when the GCE/AuNPs@PDA-RGO sensor was used, which suggests the possibility of a synergistic effect which exists between the AuNPs and the PDA-RGO. For the detection of vitamin B2 from pharmaceutical samples, the highest sensitivity was obtained when the sensor based on GCE/AuNPs@PDA-RGO was used. The recoveries for the B2 vitamin are ranged from 104.40 to 105.00% and the RSD are between 0.25-1.43%. They were assayed by using the differential pulse voltammetry (DPV). The proposed sensor showed high sensitivity with LOD of 0.0096 µmol L^{-1}, a wide linger range with the linear regression (R^2) of 0.9977 in 0.02−60.0 µmol L^{-1}.

Another group of researchers, led by Puangjan A. [48], designed an electrochemical sensor based on chemically functionalized multi-wall carbon nanotubes, on which cuprous oxide (Cu_2O) was deposited; onto the copper substrate, a composite of silver oxide (Ag_2O) was also deposited. The sensors used in this study are: multi-wall carbon nanotubes (MWCNTs), functionalized multi-walled carbon nanotubes (*f*-MWCNTs), *f*-MWCNTs-Cu_2Ocomposite, *f*-MWCNTs-Ag_2O composite and *f*-MWCNTs-Cu_2O-Ag_2O composite. For the determination of vitamin B_2, *f*-MWCNTs-Cu_2O-Ag_2O composite was used. Among these sensors, the *f*-MWCNTs-Cu_2O-Ag_2O composite electrode showed the best cycling stability. The proposed sensor showed high sensitivity, fast response, low detection limit, an extended stability and a wide linearity when it came to the detection of vitamin B_2. These results are given by the fact that the capacitive behavior of the *f*-MWCNTs-Cu_2O-Ag_2O composite is increased by the particles of Cu_2O and Ag_2O, which are strongly attached to the surface of the functionalized

nanotubes. Furthermore, the active surface area and the catalytic property of the integrated *f*-MWCNTs with Cu_2O and Ag_2O particles. The linear concentration range was 0.05-1752.65 µmol L^{-1} and the detection limit was 0.014 µmol L^{-1}. The following types of samples were used for this study: honey samples, orange juice samples and human urine samples.

Vijayaprasath et al. [49] proposed a novel gadolinium oxide nanosheet-modified glassy carbon electrode (Gs_2O_3-GCE) for the electrochemical detection of the B_2 vitamin. In order to investigate whether Gs_2O_3 could detect the vitamin of interest in the presence of various interferences, such as biotin, serotonin, dopamine, uric acid and epinephrin, the DPV technique was used. These interferences were added at a certain concentration, which was that of 0.5 mmol L^{-1}. The high selectivity of the proposed electrode was proved by the fact that there was no signal interference for the possible substances previously mentioned. The obtained results prove that the sensor which was newly made has good reproducibility and stability and it also has a high selectivity. Real samples, represented by commercial tablets and milk powder, were assayed for the determination of the B_2 vitamin. The sensor proposed by this group of researchers allows the sensitive detection of various concentrations of vitamin B_2 from pharmaceutical or food related samples, which can lead to its application in many areas.

Another type of nanoparticles, palladium-cooper (Pd-Cu), was used and placed on an activated carbon by Sangili et al. [50] in order to electrochemically sense this type of vitamin. For this study, a carbon electrode was modified with Pd-Cu alloy nanoparticles by deposition onto nutshell carbon (Pd-Cu@NSC). In order to investigate the electrocatalytic activity of the proposed electrode, CV and DPV were performed. Like the previous study[3], these researchers also used riboflavin tablets and milk powder in order to test and to prove the selectivity of the

sensor. For the assay of the samples, the Pd-Cu@NSC/SPCE was used. This electrode had an extraordinary electro-oxidation performance when it came to the sensing of this vitamin, given its surface functionality, large surface area, rapid electron transfers and good conductivity. The LOD value was that of 7.64 pmol L^{-1}, the linear concentration range was good (0.004-0.001 µmol L^{-1}) and the current sensitivity was that of 163.4 µA µmol L^{-1} cm^{-2}. Moreover, an exceptional selectivity, reproducibility and stability was achieved by using the proposed SCPE, thus, allowing it to be used for the sensing of the vitamin of interest in different types of samples.

Electrochemical Sensors Used for the Detection of Vitamin B_6

An electrochemical sensor was proposed by Sadeghi et al. [51] for the determination of vitamin B_6 from juice and water samples. This group of researchers designed an amplified sensor for which they used two conductive mediators, represented by NiO-CNTs and MOHFPE, respectively. The modified sensor, which contained the CPE and the two mediators, showed an improvement of the oxidation current (up to 2.5 times). Moreover, the recoveries obtained when the electrochemical sensor was used were of 97.33-103.8%, thus confirming the ability of the proposed sensor of detecting vitamin B_6 from real samples. The group of researchers studied the importance of the two mediators and the following results were obtained: the oxidation current of the vitamin of interest increased from 19.8 µA to 4.94 µA; also, a noticeable change could be seen for the relative potential, which decreased from 626 mV to 526 mV. The obtained results prove that by adding these two mediators, the conductivity of the CPE can be improved and thus, a good electrical condition can be created for the design of a sensitive sensor.

Electrochemical Sensors Used for the Detection of Vitamin B_9

Sharma and Arya [52] proposed an efficient and economical sensor for the determination of vitamin B_9 using a platinum electrode. In order to synthesize undoped, Ag doped and Pd-Ag co-doped tin dioxide (SnO_2) nanoparticles, a sol gel assisted hydrothermal technique was employed. In order to prove that Pd and Ag co-doped SnO_2 nanoparticles have a remarkable capacity of sensing the vitamin of interest, CV and DPV techniques were used. As a sensing agent, the modified platinum (Pt) electrode was used. The two synthesized nanoparticles were used in order to improve the catalytic activity of the Pt electrode. The proposed electrode had a low limit of detection and the linear detection ranges were wide. Moreover, the nanosensor was tested for the assay of the vitamin of interest and favorable and successful results were obtained. CV was the technique which was used in order to study the electrochemical behavior of vitamin B_9 for: the bare Pt electrode, the SnO_2/Pt, the Ag-SnO_2 and Pd and Ag-SnO_2/Pt. Compared to the bare electrode, the modified electrodes previously mentioned showed a noticeable increase in the redox peak current. For the assay of the pharmaceutical samples, the DPV technique was used. After performing the standard addition method, the following was observed: 4.978 mg/tablet, thus proving that the proposed electrode can be used for the quantitative assay of vitamin B_9. By comparing the results obtained for the pure vitamin B_9 and the pharmaceutical samples, the following conclusion can be reached: the synthesized nanoparticles are sensitive when it comes to the determination of the vitamin of interest.

Yuan et al. [53] modified a glassy carbon electrode (GCE) with platinum nanoparticles/graphene nanoplatelets/multi-walled carbon nanotubes/β-cyclodextrin

composite (PtNPs-GNPs-MWCNTs-β-CD). By using an ultra-sound assembly method, the nanocomposite was prepared. In order to obtain the modified electrode, different quantities of GNPs, MWCNTs and PtNPs were prepared in ultrapure water by using an ultrasound treatment. After this treatment, the polishing of the bare GCE took place. Then, a suspension of PtNPs-GNPs-MWCNTs-β-CD, which had different volumes, was dropped onto the surface of the electrode. Thus, the electrode of interest was obtained: PtNPs-GNPs-MWCNTs-β-CD/GCE. The practical applicability and the sensitivity of the proposed sensor was used for the determination of folic acid from pharmaceutical tablets. The concentration was in the following range: 0.02-0.50 mmol L^{-1}, the recoveries were between 97.55-102.96% and the LOD had a value of 0.48 μmol L^{-1}. These results prove the fact that the proposed electrode was able to determine folic acid from real samples.

Electrochemical Sensors Used for the Detection of Vitamin B_{12}

Dimitropoulou et al. [54] proposed the development of an electrochemical DNA biosensor for the determination of vitamin B_{12}, using a carbon paste electrode (CPE), which was modified by employing a manganese (II) complex. This electrode requires user-friendly and low-cost materials. In order to do so, they first began by studying the electrochemical behavior of Mn-CPE in an acetate buffer (pH 5.2), which had a concentration of 0.2 mol L^{-1} and containing 0.01 mol L^{-1} NaCl. Due to this, on the oxidation and the reduction peaks of the sensor, the effect of the scan rate was investigated. After this step, the physiosorbing of the dsDNa onto the Mn-CPE took place. By employing a CV in 0.2 mol L^{-1} acetate buffer (pH 5.2), which contained 0.01 mol L^{-1} NaCl, it was proved that the dsDNA was immobilized onto the Mn-

CPE successfully. Then, square wave voltammetry was used in order to prove that the dsDNA was physiosorbed onto the Mn-CPE. The following peaks were identified when the proposed electrode was used: the oxidation peak was found at + 1.021 V vs. Ag/AgCl and the reduction peak, which had a low intensity, was found at + 0.610 V vs. Ag/AgCl, thus proving that the vitamin of interest was immobilized with success onto the Mn-dsDNA-CPE. Furthermore, SWV was carried out, in order to analyze the electrochemical behavior of vitamin B_{12}. The following oxidation peaks were obtained: in the absence of vitamin B_{12}, the peak was at +0.770V vs. Ag/AgCl and in the presence of vitamin B_{12}, the peak was at +1040 V vs. Ag/AgCl, when the CPE was used. When Mn-CPE was used, the oxidation peak was identified at +1.038 V vs. Ag/AgCl in the presence of vitamin B_{12}.The oxidation of vitamin B_{12} on the Mn-dsDNA-CPE is very complex, thus, for the upcoming experiments, the group of researchers used the reduction peak of manganese in order to observe the behavior of the vitamin of interest. pH 5.2 was chosen as the dissolution pH for the rest of the experiment, due to the fact that the current of the peak increased up to this value, then it decreased until 6.2 value, and then it remained constant. It was observed that the interaction between the B_{12} vitamin and Mn-dsDNA-CPE was maximum, while the one with Mn-CPE was minimum. For the validation of the proposed electrode, Mn-dsDNA-CPE, human urine samples were assayed, in order to determine the B_{12} vitamin. The technique of choice was SWAsSV. The selectivity of the electrochemical sensor was tested by comparing the results for the slope of the calibration curve with those of the standard addition plot. For the assayed biological samples, the slope had a value of 0.0136 A L g^{-1}, which is close to the slope of the calibration curve, whose value was 0.0133 A L g^{-1}. These results prove that there was no interference created by the components of the sample matrix

when it came to the determination of the B_{12} vitamin. The values of the recoveries are between 99.2% and 101.6%, values which confirm the fact that the proposed electrochemical sensor is accurate when it comes to the bioanalysis of B_{12}. The proposed biosensor is selective, simple, sensitive, cost-effective, having a wide linear concentration range, with low limits of detection, when it comes to the determination of vitamin B_{12} from real samples.

Karastogianni S. and Girousi S. [55] proposed an electrochemical sensor for the detection of vitamin B_{12} known as cyanocobalamin, from pharmaceutical samples. After the modifier was added, in order to study the electrochemical properties of the obtained sensor, cyclic voltammetry (CV) was employed. Compared to the peaks obtained for the carbon paste electrode (CPE), where the potential for the anodic peak was at 122 mV and for the catodic peak at 7 mV, those of the Mn-CPE were reduced from 125 mV to 89 mV. This difference could be due to the electrochemical activity of the modified electrode. The proposed electrochemical sensor was used for the determination of vitamin B_{12} by square wave voltammetry (SWV). The correlation coefficient had a value equal to 0.9998 and the linear relationship between the peak current of the SWV and the B_{12} vitamin concentrations was from 13.86 to 1500 ng L^{-1}. Moreover, the following limit of detection was obtained: 4.34 ng L^{-1}. By using substances that are considered as interferences, the selectivity of the sensor was also studied. The recoveries of the B_{12} vitamin had a range of 95-105%. The obtained results proved that the studied substances did not interfere when it came to the determination of the vitamin of interest. Vitamin A and vitamin E, which are considered to be possible inhibitors, had no effect on the performed analysis, due to the fact that in aqueous solutions, their solubility is low. The proposed sensor showed good selectivity when it came to the determination of the B_{12} vitamins

from real samples.

Sharma et al. [56] proposed the development of an electrochemical sensor which was prepared by depositing gold doped tin oxide (Au-SnO_2) nanoparticles onto an indium tin oxide (ITO) substrate. In order to synthesize the nanoparticles of tin oxide (SnO_2) and Au-SnO_2, a sol gel method was employed. Due to the fact that the incorporation of Au with SnO_2 needs to be verified, characterization techniques such as EDX, FTIR, Raman and others were performed. Furthermore, a comparison of the performance of the Au-SnO_2/ITO electrode was made by using the following methods: electrochemical impedance spectroscopy (EIS), cyclic voltammetry (CV) and differential pulse voltammetry (DPV). In order to prove the electrocatalytic behavior of the modified sensor towards the B_{12} vitamin, the DPV method was used. For the electrochemical behavior of the three electrodes (ITO, SnO_2/ITO and Au-SnO_2), the following methods were used: CV, EIS and DPV; these experiments were carried out in a phosphate buffer solution (PBS) which contained 5 mmol L^{-1} $[Fe(CN)_6]^{3-/4-}$. In order to carry out all of the electrochemical studies, a system which contains three electrodes was employed. A platinum wire acted as the counter electrode and for the reference electrode, a Ag/AgCl wire was used. When the DPV method was used, the following potential range was applied: -0.6 V to 0.6 V. For the Au-SnO_2/ITO electrode, the value of the current increased (111.24 µA), due to the extraordinary conductivity of the Au dopants, which are able to accelerate the transfer of the electrons, thus leading to a faster electron diffusion between the proposed electrode and the redox species which are present in the electrolyte. Fresh cow's milk was used as the suitable type of sample for this research. The detection precision of the vitamin of interest was not affected by the possible interferences that can be found in the assayed samples. Using the DPV

method, the study of the current which corresponds to 20 µL of each concentration (0-1500 pmol L^{-1}) took place. Spiked samples were also prepared by mixing 10 µL of the standard sample and 10 µL of the milk sample. The following results were obtained: the value for the peak current which corresponds to 1 pmol L^{-1} for the spiked sample is slightly bigger than the one for the standard B_{12} vitamin sample (110.843 µA to 109.984 µA). The RSD obtained values are: 0.55% for the spiked sample and 4.23% for the real sample. These results prove that the proposed sensor is suitable for the detection of vitamin B_{12} from real samples.

Pereira et al. [57] suggested the use of a boron-doped diamond electrode for the redox pair monitoring of Co(I/II). This study proposes the development of a method which requires the involvement of a cathodic pretreated boron-doped diamond electrode (BDDE) for the assay of vitamin B_{12} in supplement products by monitoring the Co(I/II) redox pair. CV, EIS and SQWV were used for the evaluation of the proposed electrode. Vitamins B_{12}-fortified toothpaste and supplement tablets were used as samples in order to test the applicability of this electrode. Given the fact that the Co(I/II) redox pair of vitamin B_{12} has a higher current intensity and a faster electronic transfer, it was monitored. When tested under optimized conditions, the following linear concentration range was obtained: 0.25-5.0 µmol L^{-1}; the LOD had a value of 86.0 nmol L^{-1}.

Electrochemical Sensors Used for the Detection of Vitamin D

Chauhan et al. [58] proposed an electrochemical biosensor for the detection of Vitamin D_3, for which gadolinium oxide nanorods (Gd_2O_3NRs) were used. Aspartic acid (Asp) was used for the hydrothermal synthesis and functionalization of the electrode (Asp-Gd_2O_3NRs). Moreover, Asp had no influence over the structure, phase and shape of the proposed electrode. The zeta

potential for both electrodes had values of +29 mV for the bare electrode and +24 mV for the modified electrode. Between the two electrodes, the modified one showed more electrochemical property and an enhanced hydrophilicity than the bare electrode. Using the electrophoretic deposition, a thin film of Asp-Gd_2O_3NRs was deposited onto a glass substrate which was coated with indium-tin-oxide (ITO). In order to obtain the immunosensor and to determine the vitamin of interest, a Vitamin D_3 monoclonal antibody (Ab-D_3) was immobilized onto the surface of the modified electrode. Thus, a new immunoelectrode was obtained: BSA/Ab-VD/Asp-Gd_2O_3NRsThe limit of detection that was obtained for the immunosensor was 0.10 ng mL^{-1}, the sensitivity had a value of 0.38 µA ng^{-1} mL cm^{-2} and the linear concentration range was that of 10-100 ng mL^{-1}, range which covers the physiological one of the D_3 vitamin. The proposed immunosensor had an adequate response and there was no interference effect.

Another research article shows the work of Sarkar et al. [59], who modified carbon dots (CDs) with chitosan (CH) in order to obtain a sensor for the detection of D_2 vitamin. For the characterization of the CDs, the following were used: Raman spectroscopy, transmission electron microscopy, UV/VIS spectroscopy and Fourier transform infrared spectroscopy. In order to prepare the composite of carbon dots-chitosan (CD-CH), the chitosan solution (1%) was prepared using an acetic acid solution (1%); after the composite was prepared, it was deposited onto an indium-tin-oxide (ITO) glass substrate using the drop casting method. The following electrode was obtained: BSA/Ab-VD2/CD-CH/ITO. For this study, the DPV technique was used, in order to assay Ag-VD_2 within the following: the potential range was that of -0.2 to 0.5V, the pulse amplitude was that of 25 mV, the potential step was that of 5 mV

and the pulse period of 50 ms. For the proposed electrode, a response was recorded in the following range: 1-50 ng mL^{-1}, using the DPV technique. The LOD had the value of 1.35 ng mL^{-1}, the sensitivity was that of 0.2 µA ng^{-1} mL cm^{-2} and the linearity was between 10-50 ng mL^{-1}. The proposed biosensor had specificity towards the D_2 vitamin.

Men et al. [60] used a glassy carbon electrode, which was modified with AuPd bimetallic nanocrystals for the detection of vitamins D_2 and D_3. These two vitamins were determined from a mixed organic/water solution using the proposed modified electrode. The electrocatalytic response of the vitamins of interest was characterized by using the CV technique, at a scan rate of 50 mV/s and 0.0-1.5 V respectively. The linear concentration range for vitamin D_2 was between 1 and 10 µM and the detection limit was that of 0.05 µmol L^{-1}. For vitamin D_3, the linear range was between 5 and 50 µmol L^{-1} and the limit of detection was 0.18 µmol L^{-1}. These two vitamins were detected from tablets which were commercially available in their region. For vitamins D_2 and D_3, the recoveries were higher that 99% and 97%, respectively.

Another group of researchers, led by Anusha [61], proposed an electrochemical nanosensor for the assay of blood samples. For this study, bimetallic nanoparticles, represented by nickel and copper and fullerene-C60 were employed. In order to obtain the nanosensor, a glassy carbon electrode was modified with fullerene-C60 using the drop-casting method; after this modification took place, onto the surface of the newly modified electrode, CuNPs and NiNPs were deposited. For the proposed sensor, the following limit of detection was obtained: 0.0025 µmol L^{-1} and the concentration range was from 1.25 to 475 µmol L^{-1}. Due to the fact that vitamin D3 is not soluble in water, the influence of various solvents was investigated for the accurate analysis of the vitamin of interest. The following recoveries were obtained: in serum

and in urine samples, the recovery was higher than 98% and in tablets, the recovery was higher than 96%. Based on the obtained results, the proposed sensor was employed successfully for the determination of the vitamin of interest from pharmaceutical and biological samples.

Electrochemical Sensors Used for the Detection of Vitamin K

Jesadabundit et al. [62] proposed carbon and graphite screen printed electrodes for the determination of total vitamin K (vitamin K_1 and vitamin K_2) from natural samples. Compared to the screen-printed carbon electrode (SPCE), the screen-printed graphite electrode (SPGE) showed a higher sensitivity towards the determination of the vitamin of interest. The limit of determination was observed at 0.099 µg mL^{-1}. In order to study whether the proposed sensor is efficient or not, the electrochemical behavior of a mixture which contained both vitamin K_1 and vitamin K_2, a phosphate buffer solution pH 3.0 and ethanol (60:40) was individually assayed using both the SPCE and the SPGE by cyclic voltammetry (CV). The scan rate was 100 mV s^{-1} and the operated potential was in the following range: -1.0 V to +0.2 V. Based on these, the results of the background current was lower when the SPGE was used, compared to those of the SPCE. The CV of the two electrodes were also studied in the presence of vitamin K. While the SPGE clearly provided two cathodic and anodic peaks, with a much higher peak current, the SPCE showed a broad and anodic peak, at 0.123 V. The SPGE, which is the proposed electrode, provided the following: low costs, fast analysis, high sensitivity, simplicity and a low volume of the assayed samples was needed. Given the fact that the limit of detection was achieved at 0.099 µg mL^{-1} and the linearity was in a range of 1-15 µg mL^{-1}, the proposed sensor can be successfully used for the assay of total vitamin K, vitamin K_1 or vitamin K_2 from

real samples.

Conclusions

This minireview described some of the most recent electrochemical sensors which were used for the detection of water- and fat-soluble vitamins. The proposed sensors may be used for the detection of these vitamins from various types of samples, such as: biological samples, food samples and pharmaceutical samples. Due to their high sensitivity, and selectivity, good recoveries, and cost-effectiveness, these electrochemical sensors represent a good alternative for standard methods of analysis (e.g., HPLC) used for determination of vitamins in different samples.

References

1. H. Robert Horton, L. Moran, R. Ochs, J. Rawn, K. Scrimgeour, *Prentice-Hall* (1996).
2. K. Kodama, M. Suzuki, T. Toyosawa, S. Araki, *Life Sci.* 78, 134-139 (2005).
3. H.R. Scholte, H.F.M. Busch, H.D. Bakker, J.M. Bogaard, I.E.M. Luyt-Houwen, L.P. Kuyt, *Biochim. Biophys. Acta* 1271, 75-83 (1995).
4. T. Nie, K. Zhang, J. Xu, L. Lu, L. Bai, *J. Electroanal. Chem.* 717, 1–9 (2014).
5. D.M. Stanko ić, D. Kuzmano ićE, E. Mehmeti, K. Kalcher, *Monatsh. Chem.* 147, 995–1000 (2016).
6. T. Pe´rez-Ruiz, Martı´nez-Lozano, A. Sanz, V. Toma´s, Photokinetic determination of ribofla in and ribofla in 5′-phosphate using flow injection analysis and chemiluminescene detection, *Analyst* 119, 1825–1828 (1994).
7. E.J. Llorent-Martínez, P. Ortega-Barrales, A. Molina-Díaz, *Microchim. Acta* 162, 199–204

(2008).

8. M. Romeu-Nadal, S. Morera-Pons, A.I. Castellote, M.C. Lopez-Sabater, *J. Chromatogr. B* 830, 41–46 (2006).

9. D. Wirkus, A. Jakubus, R. Owczuk, P. Stepnowski, M. Paszkiewicz, *J. Chromatogr. B* 1043, 228–234 (2017).

10. P. Moreno, V. Salvadó, *J. Chromatogr. A* 870, 207–215 (2000).

11. H.Y. Gu, A.M. Yu, H.Y. Chen, *Anal. Lett*. 34, 2361–2374 (2001).

12. J. Ghasemi, M. Vosough, *Spectrosc. Lett.* 35, 153–169 (2002).

13. A.M.I. Mohamed, H.A. Mohamed, N.M. Abdel-Latif, M.R.A. Mohamed, *J. AOAC Int.* 94, 1758–1769 (2011).

14. J. Sun, C. Ren, L. Liu, X. Chen, *Chin. Chem. Lett.* 19, 855–859 (2008).

15. E.E. Snell and B.E. Haskell, *Comp Biochem*., 21, 47 (1970).

16. J. Ensiyeh and M.A.C. Sakineh, *Midwifery*, 25, 649 (2009).

17. R. Jennifer, MDT. Niebyl and M.D. MurphyGoodwin, *Am. J. Obstet. Gynecol*., 186, S253 (2002).

18. M. Jamigorn and V. Phupong, *Arch. Gynecol. Obstet.*, 276, 245 (2007).

19. M. Bijad, H. Karimi-Maleh, M. Farsi and S.A. Shahidi, *J. Food Meas. Charact*., 12, 634 (2018).

20. T. Eren, N. Atar, M.L. Yola and H. Karimi-Maleh, *Food Chem.*, 185, 430 (2015).

21. S. Cheraghi, M.A. Taher and H. Karimi-Maleh, *J. Food Compos. Anal*., 62, 254 (2017).

22. M. Bijad, H. Karimi-Maleh and M.A. Khalilzadeh, *Food Anal. Methods*, 6, 1639 (2013).

23. Z. Shamsadin-Azad, M.A. Taher, S. Cheraghi and H. Karimi-Maleh, *J. Food Meas. Charact*.,

13, 1781 (2019).

24. V. Herbert. *Annu Rev Med*. 16(1):359–70 (1965).

25. P. Nagaraja, R. A. Vasantha, H. S. Yathirajan, *Anal. Biochem.* 307, 316–321 (2002).

26. M. Dietrich, C. J. P.Brown, G. Block, *J. Am. Coll. Nutr.* 24, 266–274 (2005).

27. D. E. Breithaupt, *Food Chem.* 74, 521–525 (2001).

28. Y. Kou, J. Lu, X. Jiang, B. Tian, Y. Xue, M. Wang, L. Tan, *Electroanalysis* 31, 1155–1163 (2019).

29. Bandzuchova, L., R. Selesovska, T. Navratil, and J. Chylkova, *Electroanalysis* 25:213–22 (2013).

30. Y. Jia, Y. Hu, Y. Li, Q. Zeng, X. Jiang, Z. Cheng, *Microchim. Acta* 186, 84 (2019).

31. S.S. Kumar, R.S. Chouhan, M.S. Thakur, Trends in analysis of vitamin B12, *Anal. Biochem.* 398, 139–149 (2010).

32. A. Lichtenstein, M. Ferreira Júnior, M.M. Sales, F.B. de Aguiar, L.A.M. Fonseca, N.M. Sumita, A.J.S. Duarte, G.d.E. para o Uso and R.d.L.C. do Hospital, *Revista da Associação Médica Brasileira*, 59, 495 (2013).

33. A. Schmid and B. Walther, *Advances in Nutrition: An International Review Journal*, 4, 453 (2013).

34. Dawson-Hughes B, Heaney RP, Holick MF, Lips P, Meunier PJ, Vieth R., *Springer* (2005).

35. Ganji V, Milone C, Cody M M, McCarty F, Wang Y T. *Int Arch Med*; 3(1):29(2010).

36. Knekt P, Kilkkinen A, Rissanen H, Marniemi J, Sääksjärvi K, Heliövaara M. *Arch Neurol*, 67(7):808–11 (2010).

37. Hajiluian G, Nameni G, Shahabi P, Mesgari-Abbasi M, Sadigh-Eteghad S, Farhangi M. *Int*

J Obesity; 41(4):639–44 (2017).

38. Talaei A, Mohamadi M, Adgi Z. *Diabetol Metab Syndr*, 5(1):8.[7] (2013).

39. Mozos I, Marginean O. *Bio Med Res Int* (2015).

40. Lavie C J, Lee J H, Milani R V. *J Am Coll Cardiol*; 58(15):1547–56 (2011).

41. R. Maurizi, V. Greto, R. Buzzetti, N. Napoli, P. Pozzilli, S. Manfrini, *Metabolis*, 70, 57-71 (2017).

42. C. Vermeer, L. Braam, *J Bone Miner Metab*, 19, 201-206 (2001).

43. J. C. Swanson, J. W. Suttie, *Biochemistry*, 21, 6011-6018 (1982).

44. J. Stenflo, *J Biol Chem*, 249, 5527-5535 (1974).

45. M. R. Marchili, E. Santoro, A. Marchesi, S. Bianchi, L. R. Aufiero, A. Villani, *Ital J Pediatr*, 44, 1-5 (2018).

46. J. C. Phillippi, S. L. Holley, A. Morad, M. R. Collins, *J Midwifery Wom Heal*, 61, 632-636 (2016).

47. Li P., Liu Z., Yan Z., Wang X., Akinoglu E. M., Jin M., Zhou G. and Shui L. *J. Electrochem. Soc*, 166 B821 (2019).

48. Puangjan A., Chaiyasith S., Taweeporngitgul W., and Keawteo J. *MSC* 7548.

49. Vijayaprasath G, Habibulla I, Dharuman V, Balasubramanian S, and Ganesan R, *ACS Omega*, 5, 29 (2020).

50. Sangili, A., Veerakumar, P., Chen, SM. et al. *Microchim Acta* 186, 299 (2019).

51. Sadeghi H., Shahidi S.-A., Raeisis. N., Saraei A. G-H. and Karimi F. *Int. J.*

52. Sharma A and Arya S, *J. Electrochem. Soc*. 166 B1107 (2019).

53. Yuan, MM., Zou, J., Huang, ZN. et al. *Anal Bioanal Chem* 412, 2551–2564 (2020).

54. Dimitropoulou G., Karastogianni S., and Girousi S.. *J Appl Bioanal* **3**(4), 70-80 (2017).

55. Karastogianni S. and Girousi S. *Anal Lett*, 1-12 (2021).

56. Sharma A., Arya S., Chauhan D., Solanki P. R., Khajuria S. and Khosla A. *J. Mater. Res. Technol.* 9(6), 14321-14337 (2020).

57. Pereira D. F., Santana E. R., Piovesan J. V., Spinelli A., *Diamond and Related Materials*, 105, 107793 (2020).

58. Chauhan D., Kumar R., Panda A. K., Solanki P. R., *Journal of Materials Research and Technology*, 8, 6, 5490-5503 (2019).

59. Sarkar T., Bohidar H.B., Solanki P. R., *International Journal of Biological Macromolecules*, 109, 687-697 (2018).

60. Men, K., Chen, Y., Liu, J., & Wei, D., *Int. J. Electrochem. Sci*, 12(10), 9555-9564, (2017).

61. Anusha, T., Bhavani, K. S., Kumar, J. S., and Brahman, P. K., *Diamond and Related Materials*, 104, 107761 (2020).

62. Jesadabundit W., Chaiyo S., Siangproh W. and Chailapakul O. *Chem Electro Chem***,** 7(1), 155-162 (2020).

Progress in electroanalysis of p53, CEA and CA19-9. A minireview.

Abstract

Screening tests for panels of biomarkers such as the panel comprising p53, CEA and CA19-9 facilitated early diagnosis of cancers, and improvement of the quality of life. In this minireview, diverse electrochemical sensors used for the assay of p53, CEA, and CA 19-9 in biological samples will be shown.

Introduction

In the twentieth century, more than 18 million individuals from all around the globe had malignant growths and almost 10 million people passed away due to cancer. By the year 2040, the number of individuals will be practically multiplied, with the best expansion in lowland center nations.[1] During the last couple of years, an articulated improvement in malignant growth analysis and therapy has been accomplished: individuals experiencing probably the most well-known types of cancers are twice as prone to increase their life expectancy by nearly 10 years, in contrast with the patients analyzed in the mid 1970's.[2,3]

Enormous advancement in survival ratios has been accomplished for certain kinds of disease, which, among different components, was due to finding the beginning location of cancer cell and the more prominent accessibility of screening tests. A large number of cancer affected individuals enter the medical care framework via the gateway of a pathology determination: generally essential and repetitive conclusions of malignant growth are in the current situation, dependent on the affected tissue analyze[2]; that likewise implies that most tumors are analyzed past the point of no

return or are labeled with a wrong diagnosis, which limits a successful therapy. Therefore, the need of tools able to be used in fast screening tests.

Malignant tumor biomarkers are of greatest functional interest in disease screening, and assessment of the adequacy of treatments. With the help of the biomarkers, it can be identified the presence of malignancy or can give useful data of how the malignancy will behave (i.e., the likeliness of progression or a reaction to treatment). In patients that have no symptoms, growth analytes can be employed in evaluating analysis for the early recognition of threatening cancers. If patients presents symptoms, then the biomarkers cand make a difference in analyzing of harmless and threatening neoplastic lesions. After conclusion and careful evacuation of the neoplasm, investigation of tumor analytes can permit evaluating guess, postoperative perception, treatment forecast, and checking the reaction to foundational treatment.[4] Protein p53, carcinoembric antigen and carbohydrate antigen 19-9 are the most resorted biomarkers in screening research for a good confirmation of gastric, and colorectal cancers.

Electroanalytical methods proposed for the assay of p53, CEA and CA19-9

Electrochemical sensors proved to be excellent tools for the screening tests of biological samples.[5] Various electroanalytical methods (e.g., DPV, SWV, amperometry, stochastic methods) were proposed to date for the assay of p53, CEA, and CA19-9 (Table 1).

Table 1. Electrochemical sensors used for the analysis of gastric cancer biomarkers in different biological samples.

Tumor Marker	Sample	Electrochemical Method	Sensor	Detection Limit	Reference
p53	Saliva	DPV[a)]	SPCE[b)]/PEI[c)]/NPs[d)]-Ab[e)] B	5.00fg mL-1	[37]
p53	Plasma	SWV[f)], DPV	P-Cys[g)]-GQDs[h)]-GNP[i)]	0.065fmol L-1	[38]
p53	Cell lysates	Amperometry	AbC[j)]-p53-HRP[k)]-AbD/ MBs[l)]	1.29ng mL-1	[39]
p53	Serum	Immunochromatographic test strip	Pt[m)]-Pd[n)] NPs	50.00pg mL-1	[40]
p53	Whole blood	Stochastic method	L/DP[o)], L/GP[p)]	5.85×10^{-9} μg mL^{-1}	[41]
CEA	Serum	DPV	Ab2/PTh [r)]-Au [s)] /CEA/ BSA [t)] /Ab1/AuNPs [u)]/CS [v)] /rGO [w)]/GCE[x)]	147.10fg mL^{-1}	[52]
CEA	Blood	DPV	CEA/BSA/Ab1/Ag[y)]@C NFSs [z)]/GCE	5.12pg mL^{-1}	[53]
CEA	Blood	DPV	BSA/anti-CEA [aa)]/3D CS-Au NPs [ab)]/hPPy [ac)]	3.60pg mL^{-1}	[54]
CEA	Serum	EIS [ad)]	anti-CEA/rGO/GCE	50.00pg mL^{-1}	[55]
CEA	Serum	SWV	Ab2-AuNPs-Fc[ae)]	0.01ng mL^{-1}	[56]
CEA	Whole blood, urine, saliva, and fresh tissue	Stochastic method	CHIT [af)]/ E-NGr1[ag)] CHIT/ E-NGr2[ah)]	2.00g mL^{-1}	[57]
CA19-9	Cell lysate and serum samples	DPV	SPCE[ai)]/CB2[aj)]-Ab	70.00mU mL^{-1}	[78]
CA19-9	Serum	EIS	Au@Pd-Gra[ak)]/Thi-Ab2[al)]/HRP	6.00mU mL^{-1}	[79]
CA19-9	Serum	LSV[am)]	PDA-Ag-Ab[an)]/CA19-9/Au/GO-MA[ao)]/GCE	32.00mU mL^{-1}	[80]
CA19-9	-	Photoelectrochemical immunoassay	ITO[ap)]/TiO_2NWs[ar)]/Au/CdSe @ZnS[as)]	3.90mU mL^{-1}	[81]
CA19-9	Whole blood, saliva, urine, and tissue	Stochastic method	PIX[at)]/nanographene materials	985 mU mL^{-1}	[82]

[a)] differential pulse voltammetry; [b)] Screen-printed carbon electrode; [c)] Polyethyleneimine; [d)] Nanoparticles; [e)] Antibodies; [f)] Square wave voltammetry; [g)] Poly L-cysteine; [h)] Graphene quantum dots; [i)] Gold nanoparticles; [j)] Specific capture antibody; [k)] Horseradish peroxidase; [l)] Magnetic beads; [m)] Platinum; [n)] Palladium; [o)] 2,6-bis((E)-2-(furan-2-yl)vinyl)-4-(4,6,8-trimethylazulen1-yl)pyridine in diamond paste; [p)] 2,6-bis((E)-2-(furan-2-yl)vinyl)-4-(4,6,8-trimethylazulen1-

yl)pyridine in graphite paste; [r)] Anti-body/Polythionine; [s)] Gold; [t)] Bovine serum albumin; [u)] Antibody/Gold nanoparticles; [v)] Chitosan; [w)] Reduced graphene oxide; [x)] Glass carbon electrode; [y)] Silver; [z)] Nanocarbon nanosphere; [aa)] Bovine serum albumin/Carcinoembric antigen antibody; [ab)] Three dimensional chitosan gold nanoparticles; [ac)] Horn-like polypyrrole; [ad)] Electrochemical impedance spectroscopy; [ae)] Polyclonal anti-body ferrocene modified gold nanoparticles; [af)] Chitosan; [ag)] Graphene material obtained by electrochemical exfoliation of graphite rods in a mixture of 0.2 mol L^{-1} ammonia and 0.2 mol L^{-1} ammonium sulfate; [ah)] Graphene material obtained by electrochemical exfoliation of graphite rods in a mixture of 0.3 mol L-1 ammonia and 0.1 mol L-1 ammonium sulfate; [ai)] Screen-printed carbon electrodes; [aj)] Carbon black; [ak)] Gold palladium core/shell bimetallic functionalized graphene nanocomposites; [al)] Thionine secondary antibodies; [am)] Linear sweep voltammetry; [an)] Polydopamine-Ag antibody; [ao)] Graphene oxide-melamine; [ap)] Indium tin oxide; [ar)] Titanium oxide nanowires; [as)] Cadmium-selenium zinc-sulphur core shell; [at)] protoporphyrin IX.

Simultaneous assay of carbohydrate antigen 19-9, carcinoembric antigen, and tumor suppresor p53 was done using stochastic sensors based on graphene.[6-8] The stochastic sensors enjoyed the benefit of having the option to accomplish a qualitative and measurable investigation of different biomarkers in difficult samples. Stochastic sensors can recognize analytes in very low amounts which are not discernible by far most of the other existing sensors. Other extensive benefits of stochastic sensors contrasted with other accessible tools are high reliability, low cost of analysis, while no sample preparation is required. The response of stochastic sensors is based on channel conductivity; the qualitative analysis is based on the signatures detected for the biomarkers.[9] The selectivity of the stochastic sensors is based on the differences of the signatures obtained for the biomarkers and other substances found in biological samples; stochastic sensors proved to be highly selective. The quantitative assay happens inside the channel/pore.[9] The stochastic sensors are highly reliable, and can be used for the simultaneous assay of the three biomarkers.

Electroanalysis of tumor suppressor P53

The p53 protein was initially found in 1979 as a cell restricting accomplice of the Large T antigen of the Simian Virus 40.[10,11] It was demonstrated to be a phosphorylated protein[12,13] more exceptionally communicated in disease cells than in ordinary cells,[14] described by a low solidness that was constrained by posttranslational measures,[15] and ready to tie DNA.[16] At the cell level, the p53 protein was observed to be equipped for hindering cell development.[17] Later on, the TP53 gene that encodes the p53 protein was set up as a growth silencer suppressor and was observed to be the most mutated gene in diseases, with roughly 50% penetrance.[18,19]

The cancer suppressor p53 is a phosphoprotein scarcely perceivable inside the core of typical cells.[20] On cell stress, especially that was initiated by deoxyribonucleic acid distress, p53 has the ability to apprehend cell cycle movement, in this way, permitting the DNA to be fixed[21] or it can prompt apoptosis.[22] These capacities are accomplished, to a limited extent, by the transactivation feature of the protein, which actuate a progression of qualities associated with cell cycle guideline. Inside malignant cells that carries a mutant protein, p53 doesn't have the capability to control cell expansion, which brings about wasteful DNA fix and the development of hereditarily unstable cells.[23-26] The most widely recognized tumor suppressor alterations in human malignant growths are erroneous transformations inside the gene that suffers a successions of coding.[27,28] Inside major histogenetic groups can be found alike changes, including malignancies of the colon, stomach, lung, cerebrum, and throat.[29] It is assessed that these protein changes are the most continual hereditary events in human malignant growths, in the world being recorded over half of cases. Over 90% of the protein changes revealed thus far, are grouped amidst exons 4 and 10 and can be found in the DNA restricting area of the tumor supressor.[30] A striking feature of the protein p53 that attracted the attention of the researchers is represented by its expanded steadiness (half-life of

a few hours contrasted and 20 min for wild-type p53) and its gathering in the core of neoplastic cells.

The deficiency of useful movement of p53 is known to instigate quality transformations and cancer development as a result of structure dissimilarities in the constitution of the protein.[31,32] The levels of sera p53 of patients with gastrointestinal malignant growths changes from 0.52 ± 0.23 ng mL^{-1} to 1.03 ± 0.59 ng mL^{-1}.[33] The p53 protein suffers alterations due to overexpression, process that is caused by neoplastic cell arrangement, growth obtrusiveness and genotoxic-stresses. In this manner, examining the human blood/sera for the identification of adjusted level of the p53 protein level is a convincing procedure for diagnosis and prognosis of cancer in beginning phase. The early identification of disease upgrades chance of fruitful treatment. It not just diminishes the degree of infection yet additionally influences the expense of treatment. In the early stages of cancer, the costs of treatment are not equivalently with the progressed stage of cancer. As indicated by recently detailed information from high-income nations, the medication and the overall remedy of cancer patients in the latest phase of cancer are two to multiple times higher in contrast with patients that have an early phase of the disease.[34] On such a premise, improvement of methods for recognition of traces of malignant protein that can be found inside organic substances is worth of consideration. Numerous and recent strategies involved in the process of identification of the quantities of analyte/modified protein include customary techniques like enzyme-linked immunosorbent assay (ELISA), electrophoretic immunoassay, mass spectrometry-based proteomics and radioimmunoassay (RIA).[35] In any case, these techniques presents different inconveniences just us well-trained specialists to operate the equipment, expensive materials and instruments and also a tedious planning of tests.[36]

A research team[37] used differential pulse voltammetry as electrochemical method to investigate the cancer analyte p53 from saliva samples. They engineered an electrochemical immunosensor, by choosing SCPE (screen-printed carbon electrode) that was adapted with a matrix of carboxylated $NiFe_2O_4$ NPs by layer-by-layer deposition and included also polyethyleneimine as substrate to which p53 antibodies were deposited. The team refined the experimental conditions and updated them, by doing so they succeeded in obtaining high values of concentration range and also high values of antibodies. When processed in complex matrices including large amounts of proteins (i.e., fetal bovine serum and cell lysate), the immunosensors showed good selectivity with minimal interference. They reported to obtained a detection range of 1.0 to 10×10^{-3} pg mL^{-1}, a very low LOD (limit of detection) with a value of 5.0 fg mL^{-1}, all of this was successful achieved due to the established potential of 100 mV vs. Ag/AgCl.

A similar research analysis presented by Hasanzadeh et al.[38], fostered an ultrasensitive electrochemical immunosensor dependent signal amplification enhancement system, for the quantitation of the tumor suppressor p53. In this research, graphene quantum dots (GQDs) with a size diameter of ~5 nm, incorporated by pyrolisis of citric acid, were electrically deposited on the outer layer of poly-cysteine modified Au cathodes through the interaction of the NH^{3+} groups of cysteine with the oxygen-containing groups of GQDs. The resulting sono-electrodeposition with GQDs/AuNPs (GNPs) permitted the covalent immobilization of the biotinylated p53-immune response to the nanocomposite film comprised by poly L-cysteine (P-Cys) as conductive lattice and GNPs as synergetic component (P-Cys-GQDs-GNPs). The biosensor was then utilized for the identification of p53 protein by applying two electrochemical strategies, differential pulse voltammetry (DPV) and square wave voltammetry (SWV). A linear range of detection (0.0488-12.5 pM) and a low LOD of p53 in natural human plasma (23.4 fM) were reported. The biosensor

was assessed towards both ordinary and malignant cell line lysates (the typical cell line from mouse L929, the colon malignancy cells HCT, the prostate disease cell line PC-3, and the human prostate adenocarcinoma cell line MCF7).

Pedrero and her research team[39] described an amperometric immunosensor (Figure 1), constructed with magnetic beads, altered with carboxylic groups, on which specific antibody were covalently binded, followed by a time of incubation of the magnetic beads with a combination of HRP-anti-p53 (p53 antibody that was tagged with horseradish peroxidase). The fabrication of the sandwich configuration includes a screen-printed sensor under which a magnet was placed to retain the modified magnetic beads. The research team used amperometry as electrochemical technique, and the amperometric results were measured at -20V (vs. reference electrode (Ag/AgCl), succeed by two additional elements, HQ (hydroquinone) as a redox mediator and hydrogen peroxide (H_2O_2) being the enzyme substrate.

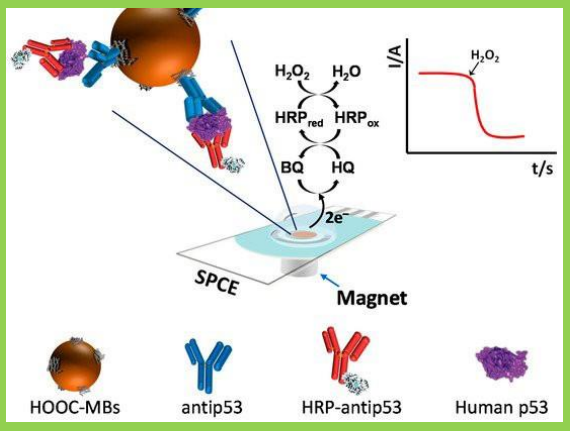

Figure 1. Schematic illustration of the fundamentals of the magneto-actuated amperometric sandwich immunosensor developed for human p53 determination. (Open access from the publisher " MDPI").[39]

Cell lysates served as biological samples for the assessment of p53 protein, samples that were simple diluted and the matrix posed no interference in the assembly. An ELISA commercial kit was employed as a comparative test for the initial analysis, the results obtained following the application of the two methods provides a good correlation between them, validating the hypothesis that electrochemical sensors can be a very appealing alternative for an effortless and quick determination of different biological analytes by utilizing transferable and budget friendly instrumentation.

Jiang et al.[40] detailed an immunochromatographic test strip for the identification of tumour protein p53 both quantitatively and qualitatively, test that is controlled by metallic nanoparticles of platinum-palladium that gives an enhanced catalysis likewise peroxidase. The peroxidase reaction with 3,3',5,5'- Tetramethylbenzidine (TMB) will show different colour intensities that will be visible with the naked eye that will be estimated by the researchers, marking it as the rule of this test. After the experiment was conducted, the result was colour visible after 30 seconds, in the biomarker's low area of the concentration range, due to the intense activity of the platinum-palladium nanoparticles. A detection limit of 0.05 ng mL^{-1} was obtained and also the concentration range had a value between 0.1-10 ng mL^{-1}, when he quantitative assessment of the protein was performed by employing a handheld test strip reader. The sensitivity of the test strip faced a 2000-fold enhanced sensitivity, when they compared it with a coloured gold-colloids based strip test.

Another research team conducted by van Staden et al.[41], presented a different sensor for the recognition of p53. The research analysis was accomplished by designing a sensors using 2,6-bis((E)-2-(furan-2-yl)vinyl)-4-(4,6,8-trimethylazulen-1-yl)pyridine as nanostructured material.

The designed sensor has successfully identified the protein suppressor 53 from no-treated blood samples and the values achieved by this sensor are in the range of fg mL^{-1}, meaning a very low concentration was accomplished. The values were detected in few millilitres of samples, the recoveries were larger than 98.00% and the values for the relative standard deviation was to a lesser degree, under 0.20%. Using the stochastic method, the validation of the mentioned method was done by analysis of 20 blood samples, and so the whole research analysis demonstrated that gastric proteins can be detected with electrochemical sensors by obtaining good interdependence between results.

For the analysis of tumor suppressor p53, using the electrochemical sensors presented, in various biological samples, the best detection limit was obtained when the SPCE/PEI/NPs-Ab[37] sensor was used, by applying the differential pulse voltammetry method (DPV).

Electroanalysis of carcinoembryonic antigen (CEA)

Gold et al.[42] successfully identifies in 1965 a new protein, called carcinoembryonic antigen (CEA), which is nowadays the most generally used tumor biomarker. At molecular level, it represents an onco-fetal protein that develops early in the fetal life, yet CEA can likewise be found in healthy grown-ups but in small quantities. Fundamentally, it was classified as glycoprotein weighing 200 kDa[43], being found in the epithelial interstitial cells on the endo-luminal side of the cell layer, and is also a component of the glycocalyx. CEA has a place with the super-group of immunoglobulins[44] called the group of CEA-related cell grip particles (CEACAMs). These incorporate CEACAM1, CEACAM3, CEACAM4, CEACAM5 (CEA), CEACAM6, CEACAM7 and CEACAM8. Inside the human body, the research showed that the protein is discharged into the bloodstream and can be found in the bile duct, the mucous secretions of the stomach, and inside the small digestive

tract. Patients affected by different malignancies, such as colorectal, stomach, pancreas, lungs and prostate presented different levels of CEA, depending on the malignancy. Despite the fact that its definite function has not been found, it was testified that CEA is a participant in the cell adhesion process thus it might hinder apoptosis.[44]

In adults, the normal serum CEA levels are beneath 2.5 ng mL^{-1}, an interval levels between 2.5–5.0 mg mL^{-1} are evaluated as being negligible, whereas a raised value is considered to be over 5 ng mL^{-1}. There are various harmless infections similar to inflammatory bowel disease, pancreatitis, endometriosis, chronic obstructive pulmonary disease and liver cirrhosis, where CEA values can be found around the upper limit. Smoking is a habit that can raise the normal levels of the protein, so in smokers the superior breaking point is viewed around 5 ng mL^{-1}. Notwithstanding, patients affected by a variety of malignancies were tested and had confirmed elevated CEA levels in a proportion domain between 5–40%.[44,45]

Carcinoembryonic antigen (CEA) was most successfully found in blood tests. It can likewise be analyzed in other body liquids and in biopsy tissues.[46] The best utilization of CEA was as a tumor growth marker, especially to gastrointestinal tract cancers.[47] When the CEA level was profoundly disordered before organ resection or other administration, it very well might be diminished to ordinary levels, after resecting all of the cancer.[48] Additionally, levels >20 ng mL^{-1} before treatment might be connected with malignancy, which had as of now spread (metastatic disease).[49] Patients with benign and malignant growths were able to increase the CEA levels. Rectum and colon cancer are two cancers that, when appeared in repetitive time, led to an increased CEA level.[50] Patients with benign growths that had other diseases or infections such as pancreatitis, inflammatory bowel diseases, liver cirrhosis, or continued smoking, presented high levels of

CEA.[51] The CEA levels, which changed thought the progression of cancer, generally should be related with other clinical outcomes.

Electrochemical methods had better results when analysing biological samples for determination of CEA. A research study presented by Lai and his team[52] exhibits a sandwich type sensor sketched out on gold nanoparticles on which were deposited reduced graphene oxide and chitosan, and further decorated with a blend of gold and polythionine serving as signal mark. For the electrochemical immunosensor design, glassy carbon electrode was adapted with a layer by layer mix of chitosan, gold nanoparticles and reduced graphene oxide, providing further with distinguished wide electrochemical active surface area and an impressively amplified electron transfer. The gold and polythionine blend were formulated with a chemical reduction method, by doing so the electrochemical signal was improved and resulted in high conductivity and great surface area. The immunosensor developed for the identification of carcinoembryonic antigen manifested a high stability over time, favourable sensitivity and selectivity towards CEA, by obtaining a large concentration range with values between 0.3 ng mL^{-1} to 30 ng mL^{-1} (R_2 = 0.9972), and 0.1471 pg mL^{-1} representing the detection limit.

For CEA recognition, in their study, Ding and his research personnel[53], managed to coat with nano-carbon outside silver nanospheres to make a frogspawn-like structure but in a three-dimensional way, structure that was used as a study to catch the anti-carcinoembryonic antigen. A schematic illustration of their developed structure is presented in Scheme 1. Moreover, they also synthesized silver carbon nanocables (Ag@C NCs) for comparison, and the results obtained showed that the globular 3D frogspawn-like structure had improved characteristics than the carbon silver nanospheres previously prepared, such as a better electrical conductivity, superior water solubility, a finer ability of the material being compatible with organic tissues, and an extensive external area

- being preferred for developing a greater capacity of antibody loading; the increased electrical conductivity of the structure had been associated with the synergistic outcome of mixing silver with graphite carbon and the displayed hydroxyl group of a different structure. The silver carbon nanospheres role was to be the platform from which the researchers were inspired to develop the immunosensor for the identification of CEA, and after the improvements it suffered, in the end, the sensor displayed a pg degree order as detection limit and a vast detection domain, ranging from 0.0001 ng mL^{-1} to 100 ng mL^{-1}. Also, the proposed immunosensor was employed in detecting CEA in serum samples, with great successes, mainly due to its improved design and characteristics, such as elevated specificity and stability, and also a proper reproducibility, making it overall a good choice in detecting both CEA and other biomarkers in different diseases.

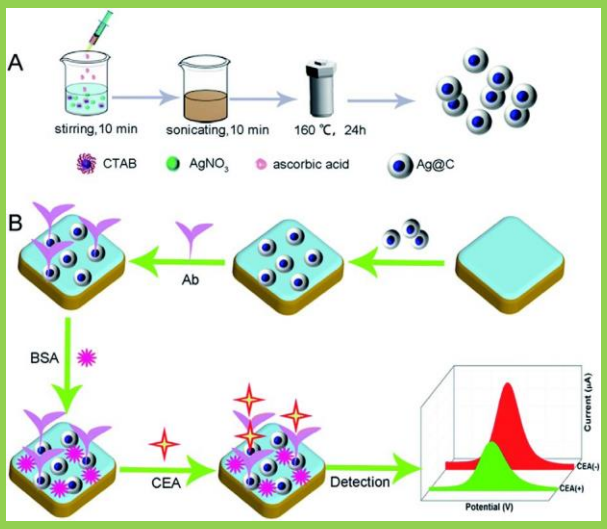

Scheme 2. Schematic illustration of (A) the preparation of Ag@C NFSs and (B) the fabrication of the Ag@C NFS-based electrochemical immunosensor for CEA detection. (Open access from the publisher "The Royal Society of Chemistry").[53]

As seen in Figure 2, a three-dimensional horn-like polypyrrole PPy(hPPy) and chitosan-gold nanoparticles micro/nanostructure was used as a sensing interface in the electrochemical detection platform in order to detect CEA in various concentrations. This platform can be used for clinical screening and early diagnosis, as studies conducted by Ma et al.[54] has shown. Because the sensing interface exhibits a vast specific surface area, astounding conductivity, stability and biocompatibility of three-dimensional structure comprised of CS-AU NPs/hPPy, it was observed that a low concentration of CEA could be detected precisely. The electrochemical immunosensor indicated a favourable linear relationship under optimal pH, incubation time, and temperature conditions, with a wide CEA detection range of 0.01 to 120 ng mL^{-1} and a low detection limit of 0.0036 ng mL^{-1} and a low detection limit of 0.0036 ng mL^{-1}. Furthermore, the constructed immunosensor demonstrated good specificity and stability for CEA detection.

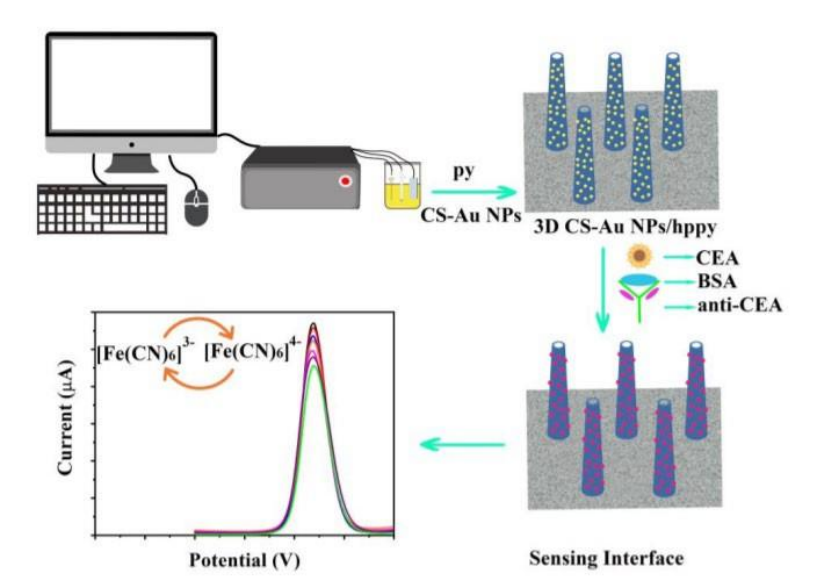

Figure 2. Schematic illustration of the preparation of the 3D CS-Au NPs/hPPy film and sensing for CEA. (Open access from the publisher "ESG").[54]

In another study, presented by Jozghorbani et al.[55], the starting point in designing the electrochemical immunosensor is represented by glassy carbon electrode. At first, the researchers used reduced graphene oxide as a coating agent for the carbon electrode, to further build a platform so that they are able to adhere the CEA antibody to the platform. The use of a linker, a carbodiimide hydrochloride (EDC), N-hydroxysuccinimide (NHS) linker is a good choice for carboxyl groups activation, the ones from the reduced graphene oxide, and after the activation, the researchers utilized the antibody to enclose the surface of the electrode. For proper interconnection between the antigen and the antibody, the parameters had to be improved, in order to do so, the team investigated those parameters with two electrochemical methods, such as cyclic voltammetry (CV) and electrochemical impedance spectroscopy (EIS). Also, these methods were enhanced in analyzing the electrochemical role of the sensor. A good detection limit was obtained, with a value result of 0.05 ng ml^{-1}, and also the presented immunosensor revealed a fine response in reach of a concentration domain between 0.1–5 ng mL^{-1}. Furthermore, the amperometric method was appraised by detecting carcinoembryonic antigen in real samples, such as human serum, the results obtained could be compared with the ones achieved from the standard enzyme-linked immunosorbent assay (ELISA).

A carcinoembryonic antigen identification immunosensor was proposed by Gu's team[56] in the form of an electrochemical sandwich-type with the improvement in the electrochemical signal as a feerocene derivative that was integrated into the design, by also adding an internal reporting system. The newly fabricated sensor made possible to detect CEA in buffers and biological samples. Gold nanoparticles that have been used to increase the conductivity of the sensor surface also contain attached secondary anti-CEA and ferrocene derivatives. The calibration of the sensor was done with solutions of different concentrations of the targeted protein by using square wave

voltammetry. The results of the calibration curve showed that the sensor has a concentration domain between 0.05–20 ng mL^{-1}, with a LOD for CEA of approximately 0.01 ng mL^{-1}. Human serum samples were used to verify the performance of the sensor, in order to identify CEA more accurately. The sensor also presents a good efficiency after being stored for 4 weeks.

van Staden et al.[57] proposed and developed two stochastic sensors for the validation of a screening test for the identification and quantification of three cancer biomarkers: carbohydrate antigen 19-9, carcinoembryonic antigen, and tumor suppressor p53. The biomarkers were identified from different biological samples: saliva, tissue, whole blood and urine. The results obtained when analyzing the biomarkers in organic samples utilizing the investigated sensors were compared with the results obtained from analyzing the same biomarkers with the standard methods, ELISA (for CEA and CA19-9) and chemiluminescence (for p53). The limit of determination reached $2x10^{-4}$ g mL^{-1} and the linear concentration range had values of $2.0x10^{-14}$ – $1.6x10^{-9}$ g mL^{-1}. Graphene materials that were dopped with nitrogen, representing the originality of this study, have been used as matrix enabling a tangible fixation of chitosan (n=371–744). The paste obtained from the process of physical mixing was introduced into a sensor having the shape of a needle – representing a new way for stochastic sensor field, due to the fact that they are used specially for analyzing organic samples. In this study, these materials were chosen for the sensor's design, owing to the fact that chitosan offers the pores available for stochastic sensing; in an early study, the existence of the pores and also the mechanical features of CS-GR compounds were established.[58] In general, graphene materials are preferred as active materials and support materials, for designing electrochemical sensors[59-61]; researchers continued to upgrade and make progress the properties of graphene, by electrochemical or chemical modification, where they included various organic or inorganic modifiers, thus improving the response characteristics of the sensors.[59-61]

As a comparison between the fabrication and design of the sensors presented in this part of the review, the sensor CHIT/E-NGr designed by van Staden et al.[57] reached the lowest limit of detection. The choice of matrices and active materials for the sensor's design made also possible a wide linear concentration rage and a multiple biomarker analysis from four different types of biological samples.

Electroanalysis of carbohydrate antigen 19-9 (CA19-9)

Carbohydrate antigen 19-9 (CA19-9) is the most regularly utilized and current best quality level analyte for pancreatic disease.[62, 63-65] This modified Lewis antigen was recognized initially by Koprowski and his colleagues in the year 1979, when a immune response was obtained from a mouse in which was introduced a human colorectal malignant growth cell line.[66] The Lewis antigen is required for the production of CA19-9, which is also known as the sialylated Lewis blood antigen.[67] Carbohydrate antigen correlates with cancer stage or weight in pancreatic patients with abnormal CA19-9 levels in their system, and hence can be used to estimate, conclude, and evaluates resectability.[68,69]

Observed in other typed of conditions and diverse cancers, CA19-9 has been adapted to prognosticate patients suffering from IPMNs - the malignancy of intraductal papillary mucinous neoplasms and pNENs - pancreatic neuroendocrine neoplasms, two non-cancerous pancreatic malignancy with a minimal risk of cancer.[70,71] For IPMNs, in individuals with life-threatening illness, the average level of serum CA19-9 was 78.72 U mL^{-1} contrasted with patients with benign malignancy, that showed a value of 27.03 U mL^{-1}.[70] CA19-9 has also been used as an analyte in a variety of malignant growths, notably those that originate in the intestine.[72] A study found that

patients suffering from colorectal malignancy and an increased level of carbohydrate antigen had a worse outcome than the patient suffering from the same disease but with a low level of carcinoembric antigen (P = 0.013).[73] For cholangiocarcinoma, a pooled investigation of 31 articles has exhibited that CA19-9 had an affectability of 0.72 (95% certainty stretch (95% CI): 0.70-0.75) and an explicitness of 0.84 (95% CI: 0.82-0.85), with an area under the Receiver Functioning characteristic (ROC) bend (AUC) of 0.83.[74]

The sensitivity of the carhobydrate antigen as a biomarker is around 80%,[75] and the significant difficulties include false negatives in Lewis-negative people but also false positives in inflammatory states and nonpancreatic tumors. When combined with indications or potentially hazard factors, CA19-9 has a screening potential. When using CA19-9 as a biomarker, it's important to check for Lewis antigen status. If used in the role of an indicator, CA19-9 presents numerous functions such as: evaluation of tumor stage, its prognosis, resectability, the times of reappearance, and also its therapeutic efficacy.[76] The survival time of a patient and a healthy human is in close contact with the standard levels of carbohydrate antigen. In the role of a promoter, the researchers can make use of CA19-9 to appraise the biology characteristics of pancreatic disease. Also, CA19-9 can increase the tumor evolution by intervening in the immunological reaction of the body, involves the proteins in the glycosylation preocess, regulating the value of E-selectin,[77] reinforcing angiogenesis, and in the same time CA19-9 is an appealing treatment target for disease, including systems that incorporate antibodies and immunizations of the people affected by various diseases and malignancies.

Numerous electrochemical immunosensors and research analyses have been created to assess the carbohydrate antigen 19-9 and are presented in the literature by different researchers. One of this research analyses presented by Ibáñez-Redín et al.[78] introduces new developed screen-printed

carbon electrodes (SPCEs) that were covered with sheets of carbon black (CB) and polyelectrolytes by using the layer-by-layer (LbL) deposition method. Using differential pulse voltammetry as an electrochemical method, the immunosensors developed in this research were efficient in recognizing the CA19-9 analyte within a dynamic range of 0.01 to 40 U mL^{-1} andalso obtaining an improved limit of detection with a value of 0.07 U mL^{-1}. Besides the advantage of detecting CA19-9 in standard solutions having the concentrations that are relevant to clinical investigations, the immunosensors were also able to detect CA19-9 in human serum samples and cell lysate. The development of this screen-printed electrodes with estimation of costs that are affordable to be reproduced, and also with budget friendly parts for engineering the sensors, shows that these types of electrodes may be able to identify malignant biomarkers; an advantage can be the recreation of this immunosensors that can be readjusted to create new and better electrodes.

Another study conducted by Yang et al.[79] defines an electrochemical immunosensor by using gold nanoparticles mixed with functionalized porous graphene (Au-PGO) to create a sandwich-type electrode that serves as the sensing platform. The research team also involved in the mixing and creating process of the sensor some graphene nanocomposites to which they added a bimetallic core consisting of palladium and gold particles (Au@Pd-Gra) working as signal enhancers for an ultrasensitive identification of carbohydrate antigen 19-9(CA19-9). The initial Au@Pd-Gra sensor was further prepared so that the researchers can immobilize horseradish peroxidase (HRP), a large amount of redox probe-thionine (Thi), and secondary antibodies (Ab2), resulting in the formation of the final bioconjugate sensor which they named Au@Pd-Gra/Thi-Ab2/HRP. The resulting sensor was presented as having numerous advantages such as a favoured biocompatibility towards organic components, an electrochemical redox activity with enhanced values and not least a superior electrocatalytic activity. In order for the detection limit to be improved on the proposed

immunosensor, a study regarding the synergistic effect between the bimetallic core and horseradish peroxidase was made, and the outcome was that in the presence of H_2O_2, a threefold magnification sensing signal was observed. The research team was able to obtain satisfactory performance of the electrochemical immunosensor for CA19-9 assessment with a wide linearity range of 0.015 to 150 U mL^{-1} and a comparatively low detection limit of 0.006 U mL^{-1}, with the circumstances being that ideal conditions are present. In conclusion the immunosensor exhibited proper specificity and vast sensitivity with clinical research in mind as a feasible implementation.

In order for ultrasensitive detection methods of malignant analytes to be developed, there is a need for convincing strategies of amplifying the sensitivity. In this process Zhang et al.,[80] shows that using a silver-silver/chloride process applied to an amperometric immunosensor having the structure of a sandwich-type sensor, results in precise recognition of carbohydrate antigen 19–9. While combining polydopamine-silver nanoparticles (PDA-Ag NPs) with antibodies that can be labelled, the mixture being employed as signal precursor, and graphene oxide-melamine (GO-MA) to be the substrate of the construction, they managed to develop a smart sensing interface. No current response was obtained following label incubation, most likely due to insufficient conductivity across labels and electrode. When H_2O_2 was introduced, however, the silver nanoparticles coming from the labels were engraved into silver ions, were further adsorbed by GO-MA to establish the electroactive substrate GO-MA-Ag. In the buffer which contains potassium chloride, the newly formed substrate showed a strong and stable electrochemistry peak of the silver-silver/chloride process. The developed immunosensor displayed very good characteristics such as a wide operating range of 0.0001 to 100 U mL^{-1} and an ultralow detection limit of 0.032 mU mL^{-1} when the optimal circumstances were put into practice. Using this method to build the

sandwich-type platform there is a great promise that electrodes can be successfully employed in clinical diagnostics for a better detection of malignant makers.

Zhu et al.[81] established a protocol for sensitive and specific recognition of carbohydrate antigen 19-9, in which they presented a novel, enhanced photoelectrochemical method. Using the layer-by-layer technique, the team described how they used gold nanoparticle and adorned them with titanium oxide nanowires (TiO_2NWs) to generate a hybrid configuration. Afterwards, a final structure was assembled, by covering the hybrid structure with a subtle layer of combined quantum dots with ions of cadmiu, seleniu, zinc and sulphur, resulting in a sensitive architecture of gold - titanium oxide nanowires with a CdSe@ZnS core (TiO2NWs/Au/CdSe@ZnS) to capture CA19-9 antibodies (Ab1). The components for the amplification signal were made of CA19-9 antibodies blended with molecules of bipyridinium (V^{2+}), to create new $Ab_2@V^{2+}$ conjugates. The immunosensor created displays a high intensity of the measure photocurrent, which can be explained by the fact that the newly developed structure has the capacity to absorb the energy light, in the same time it can interfere in the remerging process between the electrons-holes. The secondary CA19-9 antibodies provoke steric obstruction and this process connected with the removing of bipyridinium electrons induces a reduction of the photocurrent identification signal, the whole process being produced by the secondary carbohydrate antigen secondary antigens – bipyridinium conjugates. The researchers were able to achieve a vast concentration range of 0.01 to 200 U mL^{-1}, and a low LOD with a value of 0.0039 U mL^{-1} for target Ag identification, by employing this sort of photoelectrochemical immunoassay with a well-made immunosensor. This suggested photoelectrochemical procedure also shown a great stability in time of the sensor, a high repeatability of the tests, specificity for the analyte, and in the future, it might be used to detect additional relevant biomarkers.

A new study developed by van Staden et al.,[82] proposes to use as modificator, an immobilized protoporphyrin IX that will further be mixed within different graphene particles that contain a high amount of nitrogen, for designing a stochastic sensor able to simultaneous detect carbohydrate antigen 19-9, protein p53 and carcinoembryonic antigen in diverse organic samples such as saliva, urine, whole blood, and tissue samples. The sensors were crafted by mixing the graphene fine particles with paraffin oil and the solution of modificator, followed by forming the sensor where the newly formed paste was introduced in a plastic tube. Employing the stochastic method as the research electrochemical method, the sensor revealed high sensitivities and low LODs, while the concentration ranges obtained from the calibration curves displayed high values; all of these properties led to the recognition of the malignant analytes in distinct phases of gastric cancer. The LOD faced an increase in its values, from $2.1x10^{-13}$ to $2.6x10^{-4}$ g mL^{-1}, mostly because of the graphene powder that was thermically treated.

For the assay of CA19-9 using electrochemical techniques, the best sensor was the one based on glassy-carbon electrode decorated with graphene oxide-melamine (GO-MA) as substrate of the structure and polydopamine-silver nanoparticles (PDA-Ag NPs), in the role of signal precursor. The sandwich-type amperometric immunosensor PDA-Ag-Ab/CA19-9/Au/GO-MA/GCE[80] obtained the best limit of detection. The research team used linear sweep voltammetry as electrochemical technique for determining CA19-9 in real samples.

Conclusions

This review sums up the latest electrochemical techniques used for determination of p53, CEA and CA19-9 from biological samples. The electrochemical sensors utilized depended on different matrices adjusted with various electrocatalytic materials. The benefits like high sensitivity,

stability, selectivity and reproducibility make the electrochemical sensors that were presented in this review to be selected as possible instruments for screening tests of biological samples for p53, CEA and CA19-9 in order to be able to detect earlier gastric or colon cancers.

References

1. World Health Organization. WHO Report on Cancer. Setting Priorities, Investing Wisely and Providing Care for All. World Health Organization; Geneva, Switzerland, (2020).

2. S.S. Raab, and D.M. Grzybicki, *Cancer J. Clin.*, **60**, 139 (2010).

3. K. Malecka, E. Mikuła, and E.E. Ferapontova, *Sens.*, **2**, 736 (2021).

4. M.J. Duffy, *Med. Princ. Pract.*, **22**, 4 (2013).

5. A. Scozzari, In Algal Toxins: Nature, Occurrence, Effect and Detection; Evangelista, V., Ed.; Springer: Berlin/Heidelberg, Germany, 2008.

6. C. Cioates Negut , R.I. Stefan-van Staden, E.M. Ungureanu, and D. I. Udeanu, *J. Pharm. Biomed. Anal.*, **128**, 280 (2016).

7. R.I. Stefan-van Staden, I. R. Comnea-Stancu, C. A. Visan, and A. Streinu-Cercel, *J. Electrochem. Soc*., **162**, B351 (2015).

8. C. Cioates Negut, R.-I. Stefan-van Staden, I. Moldoveanu, E.M. Ungureanu, and C. Stanciu-Gavan, *Electrochem. commun.*, **51**, 98 (2015).

9. R.I. Stefan-van Staden, and I. Moldoveanu, *J. Electrochem. Soc.*, **161**, B3001 (2014).

10. D.P. Lane, and L.V. Crawford, *Nature*, **278**, 261 (1979).

11. D.I. Linzer, and A.J. Levine, *Cell*, **17**, 43 (1979).

12. V. Rotter, M.A. Boss, and D. Baltimore, *J. Virol.*, **38**, 336 (1981).

13. G. Jay, G. Khoury, A.B. DeLeo, W.G. Dippold, and L.J. Old, *Proc. Natl. Acad. Sci. USA.*, **78**, 2932 (1981).

14. S. Benchimol, D. Pim, and L. Crawford, *EMBO J.*, **1**, 1055 (1982).

15. M. Oren, W. Maltzman, and A.J. Levine, *Mol. Cell. Biol.*, **1**, 101(1981).

16. J. Bargonetti, P.N. Friedman, S.E. Kern, B. Vogelstein, and C. Prives, *Cell*, **65**, 1083 (1991).

17. S.J. Baker, S. Markowitz, E.R. Fearon, J.K. Willson, and B. Vogelstein, *Science*, **249**, 912 (1990).

18. T. Soussi and K.G. Wiman, *Cancer Cell*, **12**, 303 (2007).

19. D. Lane, and A. Levine, *Perspect. Biol*., **2**, a000893 (2010).

20. S. Benchimol, D. Pim and L. Crawford, *EMBO J.*, **1**, 1055 (1982).

21. M. B. Kastan, O. Onyekwere, D. Sidransky, B. Vogelstein, and R. W. Craig, *Cancer Res.*, **51**, 6304 (1991).

22. E. Yonish-Rouach, D. Resnitzky, J. Lotem, L. Sachs, A. Kimchi, and M. Oren, *Nature*, **352**, 345 (1991).

23. A. J. Levine, *Cell*, **88**, 323 (1997).

24. M. Oren, and V. Rotter, *Cell. Mol. Life Sci*., **55**, 9 (1999).

25. A.J. Giaccia, and M.B. Kastan, *Genes Dev*., **12**, 2973 (1998).

26. C. Prives, *Cell*, **95**, 5 (1998).

27. C. Caron de Fromentel, and T. Soussi, *Genes Chromosomes Cancer*, **4**, 1 (1992).

28. T. Soussi, Y. Legros, R. Lubin, K. Ory, and B. Schlichtholz, *Int. J. Cancer*, **57**, 1 (1994).

29. M.S. Greenblatt, W.P. Bennett, M. Hollstein, and C.C. Harris, *Cancer Res.*, **54**, 4855 (1994).

30. C. Béroud, and T. Soussi, *Nucleic Acids Res.*, **26**, 200 (1998).

31. N. Rivlin, B. Ran, O. Moshe, and R. Varda, *Genes & cancer*, **2**, 466 (2011).

32. A. Chen, B. Yuanwu, G. Xiaoxiao, S. Yongsoon, D. Dan, and L. Yuehe, *RSC Adv.*, **2**, 11029 (2012).

33. A.M. Attallah, M.M. Abdel-Aziz, A.M. El-Sayed, and A.A. Tabll, *Cancer Detect Prev*., **27**, 127 (2003).

34. World Health Organization Cancer Fact Sheet 2017. [(accessed on 22 September 2021)]; Available online: http://www.who.int/mediacentre/factsheets/fs297/en/

35. R. Aebersold, and M Matthias. *Nature*, **422**, 198 (2003).

36. B. Zhang, Z. Xue, Y. Hui-hui, X. Shi-jun, T. Dai-hua, and F. Wei-ling, *Biosens. Bioelectron*., **23**, 19 (2007).

37. G. Ibáñez-Redín, N. Joshi, G.F. do Nascimento, D. Wilson, M.E. Melendez, A,L. Carvalho, R.M. Reis, D. Gonçalves, and O.N. Jr. Oliveira, *Mikrochim Acta.*, **187,** 619 (2020).

38. M. Hasanzadeh, H.N. Baghban, N. Shadjou, and A. Mokhtarzadeh, *Int. J. Biol. Macromol*., **107**, 1348 (2018).

39. M. Pedrero, F.J.M. de Villena, C. Muñoz-San Martín, S. Campuzano, M. Garranzo-Asensio, R. Barderas, and J. M. Pingarrón, *Biosensors*, **6**, 56 (2016).

40. T. Jiang, Y. Song, D. Du, X. Liu, and Y. Lin, *ACS Sensors*, **1**, 717 (2016).

41. R.I. Stefan-van Staden, R.M. Ilie-Mihai, L. Dinu Gugoasa, and C. Stanciu-Gavan, *J. Electrochem. Soc.*, **166**, B183 (2019).

42. P. Gold, and S.O. Freedman, *J. Exp. Med*., **121**, 439 (1965).

43. P. Gold, and S.O. Freedman, *J. Exp. Med.*, **122**, 467 (1965).

44. S. Hammarström, *Semin. Cancer Biol*., **9**, 67 (1999).

45. J. Seth, C. Sturgeon, and I. Hanning, *Lancet*, **1**, 1399 (1988).

46. M.B. Garnick, and W.R. Fair, *Ann. Intern Med*., **123**, 205 (1996).

47. P.R. Carroll, M.A. Carducci, A.L. Zietman, and J.M. Rothaermel, Prostate Cancer Foundation, 1 (2005).

48. J.C. Routh, and B.C. Leibovich, *Mayo Clin. Proc.*, **80**, 899 (2005).

49. R.K. Tähtelä, *Int. J. Res*., 6 (2004).

50. A. Smith, F. Wisloff, and D. Samson. *Br. J. Haematol.*, **132**, 41 (2005).

51. H.M. Narjis, and H.J. Aziz, *Int. J.* Cell. Sci. Biol, 3 (2014).

52. L. Yuxuan, H. Hao, X. Zhihuan, L. Song, D. Yan, and L. Xueying, *Mater. Express.*, **9**, 444 (2019).

53. M. Ding, L. Zha, H. Wang, J. Liu, P. Chen, Y. Zhao, L. Jiang, Y. Li, R. Ouyang, and Y. Miaoa, *RSC Adv*., **11**, 16339 (2021).

54. S. Ma, Q. Zhang, M. Qin, H. Wang, Y. Zhu, Y. Zhang, and K. Zhang, *Int. J. Electrochem. Sci.*, **16**, 2021.

55. M. Jozghorbani, M. Fathi, S. Habib Kazemi, and N. Alinejadian, *Anal. Biochem.*, **613**, 114017 (2021).

56. X. Gu, Z. She, T. Ma, S. Tian, and H.B. Kraatz, *Biosens. Bioelectron.*, **102**, 610 (2018).

57. R.I. Stefan-van Staden, R.-M. Ilie-Mihai, F. Pogacean, and S. M. Pruneanu, *New J. Chem.*, **44**, 20203 (2020).

58. A.M. Pandele, M. Ionita, and H. Iovu, *UPB Sci. Bull*., **76**, 107 (2014).

59. S.A. Zaidi, F. Shahza, and S. Batool, *Talanta*, **210**, 120669 (2020).

60. M. Coros, S. Pruneanu, and R.I. Stefan-van Staden, *J. Electrochem. Soc*, **167**, 037528 (2020).

61. R.I. Stefan-van Staden, R.M. Ilie-Mihai, F. Pogacean, and S. Pruneanu, *J. Porphyrins Phthalocyanines*, **23**, 1 (2019).

62. D.P. Ryan, T.S. Hong, and N. Bardeesy, *N. Engl. J. Med.*, **371,** 2140 (2014).

63. G. Luo, M. Guo, K. Jin, Z. Liu, C. Liu, H. Cheng, Y. Lu, J. Long, L. Liu, J. Xu, Q. Ni, and X. Yu, *Pancreatology*, **16**, 1057 (2016).

64. G. Luo, C. Liu, M. Guo, H. Cheng, Y. Lu, K. Jin, L. Liu, J. Long, J. Xu, R. Lu, Q. Ni, and X. Yu, *Ann. Surg.*, **265**, 800 (2017).

65. R. Kannagi, *Chang Gung Med. J.*, **30**, 189 (2007).

66. H. Koprowski, Z. Steplewski, K. Mitchell, M. Herlyn, D. Herlyn, and P.Fuhrer, *Somatic Cell Genet.*, **5**, 957 (1979).

67. T.F. Orntoft, E.M. Vestergaard, E. Holmes, J.S. Jakobsen, N. Grunnet, M. Mortensen, P. Johnson, P. Bross, N. Gregersen, K. Skorstengaard, U.B. Jensen, L. Bolund, and H.Wolf, *J. Biol. Chem.*, **271**, 32260 (1996).

68. W. Hartwig, O. Strobel, U. Hinz, S. Fritz, T. Hackert, C. Roth, M.W. Buchler, and J. Werner, *Ann. Surg. Oncol.*, **20**, 2188 (2013).

69. U.K. Ballehaninna, and R.S. Chamberlain, *J. Gastrointest. Oncol.*, **3**, 105 (2012).

70. J.Y. Jang, T. Park, S. Lee, Y. Kim, S.Y. Lee, S.W. Kim, S.C. Kim, K.B. Song, M. Yamamoto, T. Hatori, S. Hirono, S. Satoi, T. Fujii, S. Hirano, Y. Hashimoto, Y. Shimizu, D.W. Choi, S.H. Choi, J.S. Heo, F. Motoi, I. Matsumoto, W.J. Lee, C.M. Kang, H.S. Han, Y.S. Yoon, M. Sho, H. Nagano, G. Honda, S.G. Kim, H.C. Yu, J.C. Chung, Y. Nagakawa, H.I. Seo, and H. Yamaue, *Ann. Surg.*, **266**, 1062 (2017).

71. G. Luo, K. Jin, H. Cheng, C. Liu, M. Guo, Y. Lu, C. Yang, J. Xu, W. Wang, H. Gao, S. Zhang, J. Long, Q. Ni, J. Chen, and X. Yu, *Oncol. Lett.*, **14**, 6795 (2017).

72. S. Scara, P. Bottoni, and R. Scatena, *Adv. Exp. Med. Biol.*, **867**, 247 (2015).

73. J. Stiksma, D.C. Grootendorst, and P.W. van der Linden, *Clin. Colorectal Cancer*, **13**, 239 (2014).

74. B. Liang, L. Zhong, Q. He, S. Wang, Z. Pan, T. Wang, and Y. Zhao, *Med. Sci. Monit*., **21**, 3555 (2015).

75. K.S. Goonetilleke, and A.K. Siriwardena, *Eur. J. Surg. Oncol.*, **33**, 266 (2007).

76. S.K. Goh, G. Gold, C. Christophi, and V. Muralidharan, *ANZ J. Surg*., **87**, 987 (2017).

77. A. Takada, K. Ohmori, T. Yoneda, K. Tsuyuoka, A. Hasegawa, M. Kiso, and R. Kannagi, *Cancer Res*., **53**, 354 (1993).

78. G. Ibáñez-Redín, E.M. Materon, R.H.M. Furuta, D. Wilson, G.F. do Nascimento, M.E. Melendez, A.L. Carvalho, R.M. Reis, O.N. Oliveira Jr., and D. Gonçalves, *Microchim. Acta*,**187**, 417 (2020).

79. F. Yang, Z. Yang, Y. Zhuo, Y. Chai, and R. Yuan, *Biosens. Bioelectron.,* **66**, 356 (2015).

80. N. Zhang, D. Zhang, C. Changshun, and Z. Ma, *Anal. Chim. Acta*, 1093 (2019).

81. H. Zhu, G.C. Fan, E.S. Abdel-Halim, J.R. Zhang, and J.J. Zhu, *Biosens Bioelectron.,* **77**, 339 (2016).

82. R.I. Stefan-van Staden, R.M. Ilie-Mihai, and S. Gurzu, *Anal. Lett.*, **53,** 2545 (2019).

2022:- Stage 2-Development, Evaluation of Screen-Printed Electrochemical/Optical Platform sensors/probes/devices on solutions of target analytes and reliable and suitable sensors/probes/devices to single type detection platforms on real samples.

Abstract

During this stage, the best materials for the screen-printed electrode design were identified and selected, cold plasma was used for carbon nanolayer deposits (e.g., graphite structures, graphene), nanographene, nanoparticles of rare metals were synthesized and used in the sensor design. These sensors have been integrated into 2D/3D platforms and used to determine substances of interest from food, pharmaceuticals, environment (water) and biological samples. All sensors were characterized using methods for surface analysis, impedance spectrometry, SEM. All the sensors designed were electrochemically evaluated and validated for biomarker determinations for the diagnosis of breast cancer, vitamins (thiamine), dyes, bisulphites, limonene, sorbic acid, pollutants (such as bisphenols) and some pharmaceutical compounds such as ibuprofen, ketoprofen, flurbiprofen, butoconazole nitrate. One paper was presented as a poster at an international conference, 4 papers are accepted for publication in ISI journals, 13 papers have been published in ISI journals and another 6 papers are under evaluation at ISI journals.

Minireview: current trends and future challenges for the determination of patulin in food products

ABSTRACT

This mini-review takes into account articles from the last five years and presents a summary of the conventional and current analytical methods for the determination of patulin (PAT) in food products.

Introduction

Patulin (PAT) is a mycotoxin produced by a variety of molds, in particular, *Aspergillus* and *Penicillium*, and *Byssochlamys*.PAT is commonly associated with apples and apple products; but it could also be found in other fruits such as pears, figs, and tomatoes (Funes and Resnik, 2009; Karaca and Nas, 2006; Cunha et al., 2014) as well as in vegetables like bell peppers, cereals such as wheat, rice, and corn, and in some cheeses (Van de Perre et al., 2014; Assuncao et al., 2016; Pattono et al., 2013).

Its presence is highly regulated.Four categories of food toxins are known, such as plant toxins, bacterial pathogens, phycotoxin, and mycotoxins(Malhotra et al., 2014).Plant toxin is a secondary metabolite produced by the plant(Mithofer and Maffei, 2016).There is another aggressive microorganism that causes harm to the body, a bacterial pathogen, *Mycobacterium tuberculosis*, which causes tuberculosis(Doss et al., 2017),typhoid fever, syphilis, and tetanus(Seale et al., 2014).Another toxin is found in the form of Phycotoxin and is produced by marine microalgae(Rasmussen et al., 2016).

The most common toxin existent in a vast variety of food and feedstuffs is Mycotoxin, a secondary metabolite produced by fungi belonging to the genera *Aspergillus*, *Alternaria*, *Fusarium*, and *Penicillium*, which is highly toxic to humans and animals' health. Crops are often contaminated by mycotoxins resulting in substantial economic loss worldwide(Moretti, Logrieco, and Susca, 2017).PAT can enter the body through the skin, respiratory, and digestive

tract; but the ingestion of food contaminated with mycotoxins remains the main route to enter the body (Agriopoulou, 2016).

A series of agricultural products like feed (Kebede et al., 2020),herbs and spices(Gambacorta et al., 2019),cereals (Varzakas, 2015),cocoa and coffee (Bessaire et al., 2019), grape juice, wines (Welke, 2019),beer (Pascari et al., 2018),dairy products, and milk (Viegas et al., 2019),fresh and dried fruits and vegetables (Sanzani, Reverberi, and Geisen, 2016),and nuts (Kluczkovski, 2019),can be contaminated with PAT.Due to the consumption of food or feed contaminated with PAT (Binder et al., 2007),the following adverse effects (acute and chronic effects) have been identified: carcinogenic, mutagenic, teratogenic, and immunosuppressive (Wild and Gong, 2010);thus, the International Agency for Research on Cancer (IARC) has included aflatoxin B1 (AFB1) in group 1 of compounds carcinogenic for humans (Ostry et al., 2017).

Concentrations of PAT found in juices and apple samples marketed in Brazil have exceeded the maximum permitted limit set in that country, being a real danger to consumers (Dias et al., 2019).

Although PAT has also shown teratogenicity and mutagenic effects in animal cell studies, it is not yet considered carcinogenic to humans (Mandappa et al., 2018). The analytical techniques used for PAT detection are chromatographic techniques, such as thin-layer chromatography (TLC), high-performance liquid chromatography (HPLC) coupled with ultraviolet (UV), fluorescence (FLD), diode array (DAD), or mass spectrometry (MS) detectors and ultra-high-performance liquid chromatography (UHPLC) or ultra-performance liquid chromatography (UPLC) with reduced column packing material (1–2 μm) (Pereira, Fernandes, and Cunha, 2014).PAT analyses are greatly advanced by coupling liquid chromatography (LC)

techniques with MS (e.q., LC-MS; liquid chromatography-tandem mass spectrometry (LC-MS/MS)) (Alshannaq and Yu, 2017).

For a rapid analysis of PAT, methods based on immunoassays such as enzyme-linked immunosorbent assay (ELISA)(Zhang et al., 2018)and lateral-flow (LFD) (Krska and Molinelli, 2008),dipsticks, and flow-through devices(Pereira, Fernandes, and Cunha, 2014)are used. Biosensors are rapid, reliable, and low-cost tools that make possible the identification of mycotoxins in food (Logrieco et al., 2005). The latest methods for the detection and analysis of PAT in foods can be achieved by proteomic and genomic methods, molecular techniques, electronic nose (Rodríguez et al., 2015), and hyperspectral imaging (HSI) (Liang et al., 2018). The latest study uses laser ablation electrospray ionization mass spectrometry imaging (LAESI imaging) to investigate the spread of patulin from the rotten to the healthy areas of the fruit (da Silva Lima et al., 2022).

Compared with the analytical methods which are currently used for the determination of PAT, the electrochemical sensors are remarkable due to the simplicity of the experiments, the low costs, and the selective detectability.

The purpose of this mini-review is to discuss the newest and most innovative analytical methods based on sensors, which can quantitatively and qualitatively determine PAT in food products.

General information on PAT

PAT($C_7H_6O_4$, 4-hydroxy-4H-furo[3,2-c] pyran-2(6H)-one) (Figure 1) belongs to the class of mycotoxins that is principally produced by the fungal species *Penicillium expansum* and was

first used due to the antibiotic properties (Sadok, Szmagara, and Staniszewska, 2018). Nowadays, PAT is a frequent contaminant in feed and food (Zbynovská et al., 2016).

Figure 1. Chemical structure of PAT.

The worst health effects of ingesting PAT in humans are edema, intestinal ulceration, agitation, seizures, vomiting, and inflammation (Nunes da Silva et al., 2007). Children are more at risk of food toxicities caused by PAT because they consume more contaminated food products. In recent decades, due to the toxicity of PAT, many countries have developed strict regulations on the maximum concentration of PAT in contaminated foodproducts. Table 1 shows the standards of contamination limit for PAT adopted by the European Union (EU) (Commission of the European Communities, 2006),China (National Health and Family Planning Commission of the People's Republic of China, State Food and Drug Administration, 2017), United States Food and Drug Administration (US Food and Drug Administration, 2004), Codex Alimentarius Commission (CAC)(Food and Agriculture Organization/ World Health Organization, 2019),South America, Uruguay, and Brazil (Ramos Girona et al., 2011).

Table 1. The standards of contamination limit for patulin in some foods according to the European Union, China,CAC, America, Uruguay, Brazil, and the US Food and Drug Administration.

Region of organization	Foodstuffs	Standard limit (μg/L)
	Fruit juices, concentrated fruit juices as reconstituted, and fruit nectars	50

European Union	Spirit drinks, cider, and other fermented drinks derived from apples or containing apple juice	50
	Solid apple products, including apple compote, and apple puree intended for direct consumption	25
	Apple juice and solid apple products, including apple compote and apple puree, for infants and young children	10
	Baby foods other than processed cereal-based foods for infants and young children	10
China	Fruit products	50
	Fruit and vegetable juice	50
	Liquor	50
Codex Alimentarius Commission	Apple juice	50
South America, Uruguay, and Brazil	Fruit juices	50
The US Food and Drug Administration	Apple juice, apple juice concentrates, and apple juice products	50

The emphasis on different standards is almost the same for fruits and fruit preparations. It has been observed that the standards set by the EU are more complete. The maximum level of PAT has been set by the EU at 50 µg/L for fruit juices and derived products, 25µg/L for solid apple products, and 10 µg/L for juices and foods destined for babies and young infants (Puel, Galtier, and Oswald, 2010). The World Health Organization (WHO) limits PAT to under 0.4 µg/L. The setting of maximum limits for some foods has led to a growing demand for efficient, selective, and sensitive analytical methods.

Since PAT is resistant to high temperatures and very stable in acidic conditions, thus is difficult to eliminate during the food manufacturing process (Zhong et al., 2018).

Conventional separation methods available for PAT detection

Related to food safety issues, there should be a sophisticated tool for quantifying the content of PAT in food (Table 2). Numerous conventional separation techniques are available for the

determination of PAT, such as TLC (Welke et al., 2009), HPLC (Wu et al., 2018), gas chromatography (GC) (Zhou and Tang, 2020),gas chromatography coupled mass spectroscopy (GC-MS) (Xiao and Fu, 2012), LC-MS (Schlegel and Elsinghorst, 2020), and capillary electrophoreses (CE) (Goud et al., 2018).ELISA (Leite et al., 2020)and polymerase chain reaction (PCR) (Tannous et al., 2015) are standard methods used in accredited laboratories.

Table 2. Reported methods for patulin determination.

Method	Linear concentration range	Limit of quantification	Limit of detection	References
MISPE-CZE-MS/MS[a]	1.0 - 100.0 µg/kg	1.0 µg/kg		Moreno-Gonzalez et al., 2021
HPLC-MS[b]	0.5 – 50.0 µg/L	0.3 µg/L	1.0 µg/L	Yang et al., 2017
HPLC-DAD[c]	5.0- 100.0 µg/kg	5.0 µg/kg	1.5 µg/kg	Sadok, Szmagara, and Staniszewska, 2018
MI-SPE-LC-MS/MS[d]	1.0-100.0 ng/mL	0.2-0.5 ng/g	0.05-0.2 ng/g	Zhao et al., 2019
UPLC-MS/MS[e]	-	42 µg/kg	50 µg/L; 12.5 µg/kg	Dias et al., 2019
MMISB[f]	-	50 ng/g	10 ng/g	Regal et al., 2017

[a]MISPE-CZE-MS/MS - molecularly imprinted polymer solid-phase extraction capillary zone electrophoresis coupled to mass spectrometry;
[b]HPLC-MS - high-performance liquid chromatography coupled with mass spectrometry;
[c]HPLC-DAD - high-performance liquid chromatography coupled with diode array;
[d]MI-SPE-LC-MS/MS - molecularly imprinted polymer acts as a sorbent in the solid-phase extraction column coupled with liquid chromatography-tandem mass spectrometry;
[e]UPLC-MS/MS – ultra-high-performance liquid chromatography coupled with tandem mass spectrometry;
[f] MMISB - magnetic molecularly imprinted stir-bar.

The in-line molecularly imprinted polymer solid-phase extraction capillary zone electrophoresis coupled to mass spectrometry (MISPE-CZE-MS/MS) is a new method for the detection of the PAT in the apple and its products samples developed by Moreno-Gonzalez et al. (2021). The analytical performance characteristics of the in-line method-MISPE-CZE-MS/MS for the determination of PAT in apple and its products samples were of 1.00-100.00 µg/kg linear concentration range with a coefficient of determination (R^2) equal to 0.997 and a limit of

quantification (LOQ) of 1.00 µg/kg below the maximum content of PAT according to the EU for this product; the migration time and peak zone accuracy were estimated at less than 1.60, and 14.90%, respectively. The PAT selectivity was examined in the presence of 5-hydroxymethylfurfural, which was the critical interference in this type of matrix. The PAT detection with this method showed an improvement in the degree of automation, in addition to accuracy, selectivity, and sensitivity.

By combining the HPLC technique with MS (Spadaro et al., 2020), a sensitive analytical tandem LC-MS was obtained, and used in important fields such as food processing (Stadler et al., 2020), agriculture (Hajrulai-Musliu et al., 2020), and pharmaceuticals (Wei et al., 2019).

An HPLC-MS approach for PAT detection in juice samples was successfully developed by Yang et al. (2017).The following analytical characteristics for PAT have been obtained: the linear concentration range was from 0.50 to 50 µg/L and R^2 was 0.9986, the calculated LOQ was 0.30 µg/L and the limit of detection (LOD) had a value of 1.0 µg/L from juice samples; the recoveries were between 91.6 and 95.7%, with a relative standard deviation (RSD) of 6.53–11.6% for the interday measurements, and an RSD of 6.87–11.0% for the intraday measurements. The applied method showed that it can be successfully applied in the analysis of various types of samples.

Sadok, Szmagara, and Staniszewska(2018)reported that the HPLC coupled with a diode array detectionwas suitable for PAT in strawberries.Optimized extraction of fruit samples by the modified Quick, Easy, Cheap, Effective, Rugged, and Safe (QuEChERS) method with acetonitrile acidified with acetic acid and citrate buffered salts, followed by a dispersive solid-phase extraction using an amine and graphitized carbon was described.The method presented a LOD with a value of 1.5, and a LOQ of 5.0 µg/kg and was validated in a real sample for three

concentration levels, respectively 5.0, 10.0, and 50.0 µg/kg. After validation, the recovery of PAT had a high percentage. The proposed method was successfully applied for the assay of both frozen and fresh strawberries.

Zhao et al. (2019)prepared a molecularly imprinted polymer (MIP) with specific adsorption for PAT. MIP was polymerized by precipitation polymerization from the 2-oxindole and 6-hydroxynicotinic acid as a pattern molecule, trimethylolpropane trimethacrylate as a crosslinker, methyl acrylic acid as a practical monomer, methanol as a porogen solvent, and 2,2-azobis-(2-methylpropionitrile) as an initiator.The MIP acts as a sorbent in the solid-phase extraction column (MI-SPE) which was used for the selective extraction of PAT from food samples. Using this method, a remarkable selectivity towards PAT in various types of samples, such as apple, apple juice, hawthorn, hawthorn juice, mixed juice, wines, and tomato for three spiked concentrations with a relative standard deviation lower than 4.5% and average recoveries between 81.3 and 106.3% were obtained. By combining the MI-SPE method with LC-MS/MS, wide linearity in the range of 1.0-100.0 ng/mL with R^2 higher than 0.998 was observed. The obtained values for the limit of quantification of ten determinations was 0.2-0.5 ng/g and the limit of detection of three determinations was 0.05-0.2 ng/g.Compared with the QuEChERSmethod, the proposed method had as results a better purification and higher recovery of PAT from food samples.

Dias etal. (2019)developed an innovative method for the determination of PAT in apple samples by liquid chromatography-tandem mass spectrometry (UPLC-MS/MS). Validation of the method by evaluating the linear domain, the limit of quantification and detection, accuracy (%, RSD), matrix effect, and accuracy, was performed. This method was suitable for the detection of PAT in apple samples and apple juices with recoveries between 102 and 108% in

apple juice and from 76 to 84% in apple samples, with an RSD value lower than 15% for both cases.

Regal et al. (2017)investigated a fast and selective method, easy to reproduce in other laboratories for isolating PAT from apple samples. The method is based on a magnetic molecularly imprinted stir-bar (MMISB) and which uses as a template, 2-oxindole. With this method, the extraction protocol was reduced and the imprinted stir bars were easy to use. The recoveries from the real apple samples were made in a percentage of 60.0-70.0%. In the future, the method could be improved by using more sensitive tools.

These techniques have some inconveniences that involve trained personnel needed to conduct the analysis, harmful chemicals used during experimental procedures, a large amount of analyte, tedious washing steps, and high costs.

Recent nanostructured sensors-based methods for PAT detection

The recent challenges of analytical chemistry are represented by the assay of the food samples. The sensors are remarkable due to the simplicity of the experiments, the low costs, and the selective detectability. These have important applications among the usual sensors, and are in the commercial stage for evaluations in agriculture, industry, environment, and clinical (Goud et al., 2019).In trace detection, extensive studies to improve the selectivity by modifying the electrode surface combined with the chemical selectivity were performed. This change can affect important parameters, such as stability, sensitivity, reproducibility, and repeatability.

Electrochemical methods used for the determination of PAT

The current electrochemical methods for PAT detection, such as amperometry, voltammetry, impedimetric, potentiometric, and electrochemiluminescence, in which

nanostructured materials were used as a transducer matrix for the design of the biosensing device, are compared in Table 3.

Table 3. Analytical methods used for patulin determination.

Modified electrode	Application	Concentration range (mol L^{-1})	Limit of detection (mol L^{-1})	References
MIP[a]/Au@PANI[b]/SeS_2@Co MOF[c]/SPE[d]	Potentiometric	1.0×10^{-12}-1.0×10^{-7}	6.6×10^{-13}	Selvam et al., 2021
Peroxidase-like MIP-capped AgNPs@ZnMOF[e]	Fluorescence	1.0×10^{-7}-1.0×10^{-5}	6.0×10^{-8}	Bagheri et al., 2018
DNA[f] aptamers	Colorimetric	3.0×10^{-10}-2.0×10^{-8}	3.0×10^{-10}	Wu et al., 2016
Apt[g]/PEG[h]/SPCE	Impedimetric	6.4×10^{-9}-1.6×10^{-7}	1.8×10^{-11}	Khan et al., 2019
MIP/Thionine-PtNP-NGE[i]/GCE[j]	Potentiometric	1.3×10^{-11}-1.3×10^{-8}	6.4×10^{-12}	Huang et al., 2019
MIP-Au[k]/CS-CDs[l]/GCE	Potentiometric	1.0×10^{-12}-1.0×10^{-9}	7.6×10^{-13}	Guo et al., 2017
rGO[m]/SnO_2[n]composite for receptor-free electrochemical technique	Voltammetric	5.0×10^{-9}-6.0×10^{-7}	6.6×10^{-10}	Shukla et al., 2020
Apt/DpAu[o]/ZnONRs[p]-CS/AuE[r]	Voltammetric	3.2×10^{-12}-3.2×10^{-7}	1.7×10^{-12}	He and Dong, 2018
AuNP-BP NSs[s]/GCE based aptasensing	Impedimetric	1.0×10^{-10}-1.0×10^{-5}	3.0×10^{-11}	Xu et al., 2019
MIP/Au@Cu-MOF[t]/N-GQDs[u]/GCE	Voltammetric	6.4×10^{-12}-4.5×10^{-7}	4.5×10^{-14}	Hatamluyi et al., 2020
anti-PAT-BSA[v]IgG[w] GCE	Voltammetric	3.2×10^{-8}-1.3×10^{-6}	3.2×10^{-8}	Song, Wang, and Kim, 2021
MIP-QCM[x]	Piezoelectric	4.8×10^{-8}-3.8×10^{-7}	1.9×10^{-8}	Fang et al., 2016
MIP capped Mn-doped ZnS QDs[y]	Phosphorescent	4.3×10^{-7}-6.5×10^{-6}	3.2×10^{-7}	Zhang et al., 2017
rGO-Fe_3O_4[z]	Fluorimetric traditional method	3.8×10^{-8}-5.1×10^{-7}	2.3×10^{-8}	Ma et al., 2018
	Fluorimetric amplification method	3.2×10^{-9}-1.9×10^{-7}	1.8×10^{-9}	

[a]Molecularly imprinted polymer;
[b]Gold-polyaniline nanocomposites;
[c]Selenium disulphide loaded metal-organic framework derived cobalt;
[d]Screen-printed electrode;
[e]Silver nanoparticle loaded metal-organic framework derived zinc;
[f]Deoxyribonucleic acid;
[g]Aptamer;
[h]Carboxy-amine polyethylene glycol chain;
[i]Platinum nanoparticles – Nitrogen-doped graphene;
[j]Glassy carbon electrode;
[k]Gold;
[l]Chitosan-carbon dots;

[m]Reduced graphene oxide;
[n]Tin oxide;
[o]Electrodeposition of gold nanoparticles;
[p]Zinc oxide nanorods composite;
[r]Gold electrode;
[s]Gold nanoparticle - black phosphorus nanosheets;
[t]Gold nanoparticles functionalized copper-metal organic framework;
[u]Nitrogen-doped graphene quantum dots;
[v]Bovine serum albumin;
[w]Immunoglobulin;
[x]Quartz crystal microbalance sensor;
[y]Manganese-doped zinc sulphide quantum dots;
[z]Magnetized reduced graphene oxide.

Selvam et al. (2021)developed a new molecularly imprinted polymer based on a gold-polyaniline nanocomposites (Au@PANI) platform and selenium disulfide loaded metal-organic framework derived cobalt (SeS_2-@CoMOF) for PAT detection. The Au@PANI nanocomposite was obtained by interfacial polymerization, while the SeS_2-loaded CoMOF by hydrothermal synthesis. The MIP/Au@PANI/SeS_2@CoMOF modified screen-printed analytical electrode performance characteristics were studied in 10 mmol L^{-1} acidic phosphate buffer solution (PBS), which presented a logarithmic linear concentration range between 1.0×10^{-12} - 1.0×10^{-7} mol L^{-1} and a LOD of 6.6×10^{-13}mol L^{-1} for PAT. The selectivity (the value of 15.4 was the imprinting factor for PAT), and the stability (only 6.7% was lost after 35 days) of the sensor were exceptional. The MIP-based on PAT sensor was involved to determine PAT in real-time apple juice samples with recovery values of 106.4%. The developed sensor showed advantages such as long-term storage stability, low costs, reversible cycle measurements, and real-time monitoring of PAT detection in samples. This strategy could be used in the future to develop other sensors.

The study of Khan et al. (2019)used a portable impedimetric aptasensor platformfor the label-free electrochemical detection of PAT.The determination of PAT was based on the diazonium salt interaction with the carboxy-amine polyethylene glycol chain (PEG) grafted on a screen-printed carbon electrode (SPCE). By electrochemical impedance spectroscopy, a good

linear concentration range between 6.4×10^{-9} and 1.6×10^{-7} mol L^{-1} was obtained. The limit of quantification was 2.6×10^{-11} mol L^{-1}, and the limit of detection was 1.8×10^{-11} mol L^{-1}. The selectivity of the aptasensor was tested opposite to other mycotoxins, which are commonly present in food. The accuracy of the proposed aptasensor was evaluated, and a toxin recovery of 99 % was obtained. These results showed that the proposed aptasensor has the potential for PAT detection in apple juice samples.

In the study of Huang et al. (2019), a new electrochemical sensor was proposed for the ultra-trace PAT detection by modification of a molecularly imprinted film by a thionine - platinum nanoparticles (PtNP) – nitrogen-doped graphene (NGE) (MIP/Thionine-PtNP-NGE). Thionine functioned as an indicator of the electrochemical signal for MIP, while PtNP is known as an amplifier of the electrical signal. NGE is frequently used in the domain of sensors because it shows good mechanical stability and electrical conductivity. The sensitivity of the modified sensor was improved by combining the advantages of these three components, thionine, PtNP, and NGE. The designed sensor showed a good determination of PAT in the concentration range of 1.3×10^{-11} - 1.3×10^{-8} mol L^{-1} and a limit of detection of 6.4×10^{-12} mol L^{-1}. This method, based on thionine-PtNP-NGE and MIP film, opens a new opportunity for sensitive and rapid recognition of PAT, with future applications to other mycotoxins. The developed electrochemical sensor was used for the determination of PAT in real apple and grape juice samples.

Guo et al. (2017)used the MIP for the PAT determination. For the first time, to improve the MIP, three modifiers such as carbon dots (CDs), chitosan (CS), and gold nanoparticles (AuNP) were added. MIPs are recognition materials obtained by a template-assisted synthesis. The printing process consists of the polymerization of the monomers and the crosslinking agent

in the presence of a target molecule that acts as a template (Piletsky et al., 2020).The electropolymerization process and its optimization were performed by cyclic voltammetry (CV) and differential pulse voltammetry (DPV) measurements.For the prepared MIP-Au/CS-CDs/ glassy carbon electrode (GCE) sensor the linear responses were from 1.0×10^{-12} to 1.0×10^{-9}mol L^{-1} and the LOD of 7.6×10^{-13}mol L^{-1}. Due to the good recoveries from fresh apple juice samples, selectivity, reproducibility, and stability, the MIP sensor was capable of being used for practical application for the determination of PAT.

Shukla et al. (2020)used a reduced graphene oxide (rGO)/tin oxide (SnO_2) (rGO/SnO_2) composite without receptor labeling for the electrochemical recognition of PAT. The composite showed promising electrochemical features and a good response to the direct measurement of PAT levels in contaminated apple juice samples. The DPV response of the proposed rGO/SnO_2/GCE sensor presented a detection range of 5.0×10^{-9} - 6.0×10^{-7}mol L^{-1} of the concentration of PAT and a low LOD of 6.6×10^{-10}mol L^{-1}, due to the high electrocatalytic activity of the SnO_2 and high surface area of the rGO.The modified electrode showed high sensitivity, good reproducibility, and selectivity, for the detection of PAT in apple juice.The electrochemical sensor was capable of quickly detecting PAT in the real samples and did not require extraction or clean-up phases. The levels of recovery with the modified sensor were comparable with those of the HPLC method, hence increasing the feasibility of the method used in industrial applications.

He and Dong (2018)developed an aptasensing with a gold electrode modified with chitosan and ZnO nanorods (ZnO-NRs). The composite was obtained by the interaction with ammonia followed by a hydrothermal growth process.The new sensor was designed for the quantitative assay of PAT with hexacyanoferrate as a redox probe and aptamer as a recognition

group. To improve the electrode performance, the ZnO nanorods, chitosan, and electrodeposited AuNP were modified on the electrode surface. Under the optimal conditions, the investigation of the aptamer sensor by the DPV method showed a linear relationship in the 3.2×10^{-12} to 3.2×10^{-7}mol L^{-1} domain of the PAT concentration and a low LOD of 1.7×10^{-12}mol L^{-1}. Moreover, the proposed sensor was employed in the determination of PAT from apple spiked juice samples with recoveries of 95.6-104.8 %. Therefore, the outcomes obtained led to the use of the aptamer sensor as a potential tool for the safe detection of PAT in the future.

Hatamluyi et al. (2020) introduced a new procedure for the development of a molecularly imprinted electrochemical sensor for ultra-sensitive and selective determination of PAT. In the first stage, the surface of a GCE was modified with nitrogen-doped graphene quantum dots (N-GQDs) and AuNPs-functionalized Cu-metal organic framework (Au@Cu-MOF), and in the second stage, a layer of MIP was filed on Au@Cu-MOF/N-GQDs/GCE through electropolymerization. The obtained MIP sensor showed a large linear concentration range between 6.4×10^{-12} to 4.5×10^{-7} mol L^{-1}, and 4.5×10^{-14} mol L^{-1}, as the detection limit, by DPV measurements under optimal conditions. This method based on the association between Au@Cu-MOF and N-GQDs combined with the MIP method has led to obtaining good sensitivity, selectivity, reproducibility, and stability. In terms of accuracy (recoveries %, 97.6–99.4) and precision (RSD%, 1.23–4.61), for this method, the results were remarkable when it came to the determination of PAT from apple juice samples, also confirmed by the chromatography method, leading to a good perspective by applying it to some other sensors and biosensors based on MIP.

Song, Wang, and Kim (2021)developed an immunosensor based on a GCE for the simple, sensitive, and rapid determination of PAT. To obtain the immobilized GCE sensor, a bare, polished GCE was covered with the graphene oxide (GO)/gold (Au) (GO/Au)

nanocomposite followed by the immobilization of anti-PAT- bovine serum albumin (BSA) Immunoglobulin G (IgG) from a rabbit. The preparation of the immobilized GCE sensor for the detection of PAT was shown in Figure 2. Following the DPV analysis, the peak current increased with the increased concentrations of PAT, up to 1.3×10^{-6} mol L^{-1} with a low detection limit of 3.2×10^{-8} mol L^{-1}. The GCE immunosensor indicated good specificity because does not react cross-linked with OTA but reacts cross-linked with BSA carrier protein, which may limit its application to BSA-containing samples.

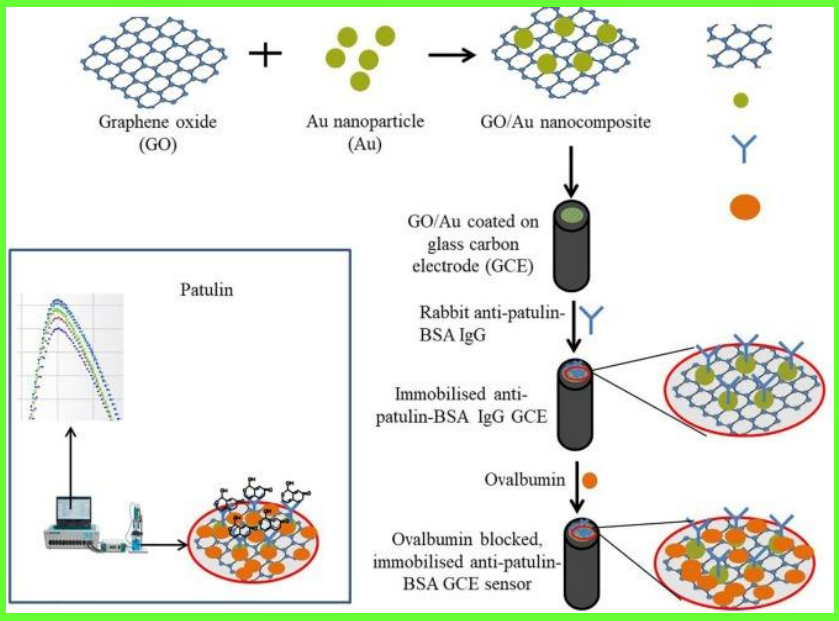

Figure 2. Schematic illustration of the preparation of an immobilized GCE sensor for the detection of PAT. BSA IgG is bovine serum albumin immunoglobulin.Reproduced with permission from (Song et al. 2021) by Elsevier.

Impedimetric methods used for the determination of PAT

Xu et al. (2019)used black phosphorus nanosheets (BP NSs) for the first time to obtain an impedimetric assay for the PAT determination. The GCE has been modified with AuNP-BP NSs,

obtained from BP NSs and AuNP by electrostatic attraction. The determination was been based on the differences between electron transfer resistance at the modified electrode surface. The modified electrode presents a wide linear concentration range of 1.0×10^{-10} to 1.0×10^{-5} mol L^{-1} and a limit of detection of 3.0×10^{-11}mol L^{-1}. For the proposed sensor, the recoveries were 96.2–104.0 % and RSD was < 5 % in real food samples. The method was used to assay the traces of PAT in contaminated foodstuffs samples. A long time for preparing the nanomaterials and modifying the electrodes are the disadvantages of this proposed sensing assay.

Fluorescence methods used for the determination of PAT

Aptamers are a class of single-stranded oligonucleotides that specifically bind to target molecules with a high affinity level, such as small molecules, proteins, and cells (Ellington and Szostak, 1990).They are easy to prepare and modify and are characterized by their high stability. Aptamers, in combination with fluorescent (Luo et al., 2017),colorimetric (Xia et al., 2017),and electrochemical (Tabrizi et al., 2017), transducers are usually used for analysis and determination. Recently, nanomaterials have attracted more attention in the design of the fluorescent biosensor.Currently, there is little research to determine the aptamer-based PAT. Wu et al. (Wu et al., 2016),previously reported a high-affinity DNA aptamer for the determination of PAT using fluorescence analysis.

Bagheri et al. (2018),used a MIP efficiently for the selective determination of PAT. Synthesized support of silver nanoparticle/ flake-like Zn-based on metal-organic frameworks (MOFs) nanocomposites (AgNPs@ZnMOF) successfully used. Until now, no detection studies have been reported using MIP-based MOF catalyzed fluorescence systems. The obtained MIP-capped AgNPs@ZnMOF can catalyze terephthalic acid - hydrogen peroxide reaction to generate

a strong fluorescence emission. The fluorescence emission intensity of generated product decreased linearly proportional to the PAT concentration in the domain of 1.0×10^{-7}-1.0×10^{-5}mol L^{-1}, and the LOD was 6.0×10^{-8}mol L^{-1}. The proposed method was practically applied for the measurement of PAT in a complex aquatic environment or apple juice, without any preparation steps.

Wu et al. (2016)reported a high-affinity ssDNA aptamer that was specifically bound to PAT by fluorescence analysis. An aptamer-based colorimetric method to confirm the application possibility of these as recognition receptors with high affinity and specificity in PAT detection was established. The analytical performance of the colorimetric aptasensor was realized in the linear domain of concentration from 3.0×10^{-10}up to 2.0×10^{-8} mol L^{-1} with the LOD of 3.0×10^{-10}mol L^{-1}. The developed method showed good reproducibility in terms of precision (6.87%). In analytical applications, the determination of PAT in the food samples was realized by the proposed method compared with the HPLC-MS method; there was a good correlation between both methods.

Zhang et al. (2017)presented an optical method based on MIPs capped manganese-doped zinc sulfide quantum dots (MIP-QDs) for the detection of PAT in apple juice. The nanosensor was synthesized using 6-hydroxynicotinic acid as the inactive template in the molecular printing sol-gel process. The binding of MIP onto QDs was confirmed by the Fourier transform infrared spectroscopy (FTIR) and X-ray diffraction (XRD) analyses. The binding tests showed that MIP-QDs have high selectivity and mass transfer rates and an adsorption capacity that is higher than those of unprinted polymers, which demonstrate a specific recognition for PAT among mycotoxin analogs. The Mn-doped ZnS QDs capped MIPs sensor was able to determine the concentration of PAT in the linear range of 4.3×10^{-7} - 6.5×10^{-6}mol L^{-1}, a detection limit of

3.2×10^{-7}, and a correlation coefficient of 0.9945.The recoveries of 102.9–127.2 % and RSD less than 4.95 % obtained in apple juice samples were in good agreement with the HPLC method (higher than 0.05), showing the feasibility of the method. The results obtained for this method provided a new strategy for the determination of PAT in complex matrices.

Ma et al. (2018)developed a selective and rapid fluorescent assay based on magnetized reduced graphene oxide (rGO-Fe_3O_4) and DNase I for PAT detection in apple juice and grape juice samples. In the first step, the magnetized reduced graphene oxide was introduced as a suitable extinguisher for separation, improving the sensitivity and accuracy of the method. In the second phase, DNase I was introduced to amplify the fluorescence signal, and the sensitivity was about 13 times higher than that of the traditional method without DNase I. In conclusion, the developed method opens a new way of monitoring the environment in terms of food safety.

A quartz crystal microbalance sensor used for the assay of PAT

Fang et al. (2016)reported a quartz crystal microbalance sensor (QCM) based on a MIP film to determine the PAT. The adsorption capacity of the MIP recognition element was demonstrated by analyzing the Scatchard equation. After the evaluation under optimal conditions the MIP-QCM sensor, it presented a linear concentration range for PAT in the region of 4.8×10^{-8} to 3.8×10^{-7} mol $L^{-1}$was presentedand the LOD was 1.9×10^{-8} mol L^{-1} (at a signal-to-noise ratio of 3). The sensor showed a selective affinity for PAT (selectivity coefficient was 3.82) and good long-term reproducibility and stability. Sensor testing for the determination of PAT in real samples was performed with recoveries ranging from 76.9 to 91.3%, according to the HPLC-MS method. With this type of sensor, the traces of PAT could be determined in the samples of cloudy apple juice, concentrated pear juice, and haw flakes (crushed into powder).

For the modified electrodes listed in Table 3, the limits of detection and the linear concentration ranges were mentioned. The double-recognition elements, such as the Au@Cu-MOF and N-GQDs combined with the MIP method have led to obtaining good sensitivity as 10^{-14} mol L^{-1} magnitude order, selectivity, reproducibility, and stability for the MIP/Au@Cu-MOF/N-GQDs/GCE modified electrode. This shows that the performance of the MIP/Au@Cu-MOF/N-GQDs/GCEsensor (Hatamluyi et al., 2020),is comparable to or even better than the others.

Conclusions

This mini-review outlined some recent trends in the development of electrochemical sensors for the detection and quantification of PAT.In addition to the conventional methods for determining PAT, the electrochemical sensors represent a fast, reliable and cheap alternative.

Most of the methods presented can determine only one component, which limits their practical application. It is urgent and very important to develop methods that can simultaneously detect multiple mycotoxins for better food safety.

Although much progress has been made so far, sustained efforts are needed from the scientific community to combat the limitations of current methods. The use of two-dimensional disposable and three-dimensional printed sensors may lead to a new generation of electrochemical sensors designed for on-site monitoring.

References

Agriopoulou, S. 2016. Enniatins: An Emerging Food Safety Issue. *EC Nutrition* 5 (3):1142-6.

Alshannaq, A. F., and J. -H. Yu. 2017. Occurrence, Toxicity, and Analysis of Major Mycotoxins in Food. *International Journal of Environmental Research and Public Health* 14 (6):632. DOI: 10.3390/ijerph14060632.

Assuncao, R., C. Martins, D. Dupont, and P. Alvito. 2016. Patulin and ochratoxin a co-occurrence and their bioaccessibility in processed cereal-based foods: A contribution for Portuguese children risk assessment. *Food and Chemical Toxicology* 96:205–14.

Bagheri, N., A. Khataee, B. Habibi, and J. Hassanzadeh. 2018. Mimetic Ag nanoparticle/Zn-based MOF nanocomposite (AgNPs@ZnMOF) capped with molecularly imprinted polymer for the selective detection of patulin. *Talanta* 179:710-8.

Bessaire, T., I. Perrin, A. Tarres, A. Bebius, F. Reding, and V. Theurillat. 2019. Mycotoxins in green coffee: occurrence and risk assessment. *Food Control* 96:59-67.

Binder, E. M., L. M. Tan, L. J. Chin, J. Handl, and J. Richard. 2007. Worldwide occurrence of mycotoxins in commodities feeds and feed ingredients. *Animal Feed Science and Technology* 137 (3-4):265-82.

Commission of the European Communities, EC No 1881/ 2006 Setting Maximum Levels for Certain Contaminants in Food Stuffs. Official Journal of the European Union. 2006.

Cunha, S. C., M. A. Faria, V. L. Pereira, T. M. Oliveira, A. C. Lima, and E. Pinto. 2014. Patulin assessment and fungi identification in organic and conventional fruits and derived products. *Food Control* 44:185–90.

da Silva Lima, G., G. Franco dos Santos, R. R. F. Ramalho, D. V. A. de Aguiar, J. V. Roque, L. I. L. Maciel, R. C. Simas, I. Pereira, and B. G. Vaz. 2022. Laser ablation electrospray ionization mass spectrometry imaging as a new tool for accessing patulin diffusion in mold-infected fruits. *Food Chemistry* 373:131490. https://doi.org/10.1016/j.foodchem.2021.131490

Dias, J.V., R. C. da Silva, I. R. Pizzutti, I. D. dos Santos, M. Dassi, and C. D. Cardoso. 2019. Patulin in apple and apple juice: Method development, validation by liquid chromatography-tandem mass spectrometry and survey in Brazilian south supermarkets. *Journal of Food Composition and Analysis* 82:103242. https://doi.org/10.1016/j.jfca.2019.103242.

Doss, J., K. Culbertson, D. Hahn, J. Camacho, and N. Barekzi. 2017. A review of phage therapy against bacterial pathogens of aquatic and terrestrial organisms. *Viruses* 9 (3):50. https://doi.org/10.3390/v9030050.

Ellington, A. D., and J. W. Szostak. 1990. *In vitro* selection of RNA molecules that bind specific ligands. *Nature* 346:818-22.

Fang, G., H. Wang, Y. Yang, G. Liu, and S. Wang. 2016. Development and application of a quartz crystal microbalance sensor based on molecularly imprinted sol-gel polymer for rapid detection of patulin in foods. *Sensors and Actuators, B: Chemical* 237:239-46.

Food and Agriculture Organization/ World Health Organization. 2019. General standard for contaminants and toxins in food and feed CXS 193-1995. Codex Alimentarius Commission. 2-66.

Funes, G. J., and S. L. Resnik. 2009. Determination of patulin in solid and semisolid apple and pear products marketed in Argentina. *Food Control* 20:277–80.

Gambacorta, L., N. El Darra, R. Fakhoury, A. Logrieco, and M. Solfrizzo. 2019. Incidence and levels of *Alternaria* mycotoxins in spices and herbs produced worldwide and commercialized in Lebanon. *Food Control* 106:106724. https://doi.org/10.1016/j.foodcont.2019.106724.

Goud, K. Y., K. K. Reddy, M. Satyanarayana, S. Kummari, and K.V. Gobi. 2019. A review on recent developments in optical and electrochemical aptamer-based assays for mycotoxins using advanced nanomaterials. *Mikrochimica Acta* 187 (1):29. DOI: 10.1007/s00604-019-4034-0.

Goud, K.Y., S. K. Kailasa, V. Kumar, Y. F. Tsang, S. E. Lee, K. V. Gobi, and K.-H. Kim. 2018. Progress on nanostructured electrochemical sensors and their recognition elements for detection of mycotoxins: A review. *Biosensors and Bioelectronics* 121:205-22.

Guo, W., F. Pi, H. Zhang, J. Sun, Y. Zhang, and X. Sun. 2017. A novel molecularly imprinted electrochemical sensor modified with carbon dots, chitosan, gold nanoparticles for the determination of patulin. *Biosensors and Bioelectronics* 98:299-304.

Hajrulai-Musliu, Z., R. Uzunov, S. Jovanov, D. Jankuloski, V. Stojkovski, L. Pendovski, and J. J. Sasanya. 2021. A new LC-MS/MS method for multiple residues/contaminants in bovine meat. *BMC Chemistry* 15(1):62. 10.1186/s13065-021-00788-5.

Hatamluyi, B., M. Rezayi, H. R. Beheshti, and M. T. Boroushaki. 2020. Ultra-sensitive molecularly imprinted electrochemical sensor for patulin detection based on a novel assembling strategy using Au@Cu-MOF/N-GQDs. *Sensors and Actuators, B: Chemical* 318:128219. https://doi.org/10.1016/j.snb.2020.128219.

He, B. and X. Dong. 2018. Aptamer-based voltammetric patulin assay based on the use of ZnO nanorods. *Microchimica Acta* 185 (10):462. https://doi.org/10.1007/s00604-018-3006-0.

Huang, Q., Z. Zhao, D. Nie, K. Jiang, W. Guo, K. Fan, Z. Zhang, J. Meng, Y. Wu, and Z. Han. 2019. Molecularly Imprinted Poly(thionine)-Based Electrochemical Sensing Platform for Fast and Selective Ultratrace Determination of Patulin. *Analytical Chemistry* 91:4116-23.

Karaca, H., and S. Nas. 2006. Aflatoxins, patulin, and ergosterol contents of dried figs in turkey. *Food Additives and Contaminants* 23:502–8.

Kebede, H., X. Liu, J. Jin, and F. Xing. 2020. Current status of major mycotoxins contamination in food and feed in Africa. *Food Control* 110:106975. https://doi.org/10.1016/j.foodcont.2019.106975.

Khan, R., S. Ben Aissa, T. A. Sherazi, G. Catanante, A. Hayat, and J. L. Marty. 2019. Development of an Impedimetric Aptasensor for Label-Free Detection of Patulin in Apple Juice. *Molecules* 24 (6):1017. https://doi.org/10.3390/molecules24061017.

Kluczkovski, A.M. 2019. Fungal and mycotoxin problems in the nut industry. *Current Opinion in Food Science* 29:56-63.

Krska, R. and A. Molinelli. 2008. Rapid test strips for analysis of mycotoxins in food and feed. *Analytical and Bioanalytical Chemistry* 393 (1):67-71.

Leite, M., A. Freitas, A. S. Silva, J. Barbosa, and F. Ramos. 2020. Maize (*Zea mays* L.) and mycotoxins: A review on optimization and validation of analytical methods by liquid chromatography coupled to mass spectrometry. *Trends in Food Science and Technology* 99:542-65.

Liang, K., Q. X. Liu, J. H. Xu, Y. Q. Wang, C. S. Okinda, M. X. Shena. 2018. Determination and Visualization of Different Levels of Deoxynivalenol in Bulk Wheat Kernels by Hyperspectral Imaging. *Journal of Applied Spectroscopy* 85:953-61.

Logrieco, A., D. W. M. Arrigan, K. Brengel-Pesce, P. Siciliano, and I. Tothill. 2005. DNA arrays, electronic noses, and tongues, biosensors and receptors for rapid detection of toxigenic fungi and mycotoxins: a review. *Food Additives and Contaminants* 22 (4):335-44.

Luo, Z., Y. Wang, X. Lu, J. Chen, F. Wei, Z. Huang, C. Zhou, and Y. Duan. 2017. Fluorescent aptasensor for antibiotic detection using magnetic bead composites coated with gold nanoparticles and a nicking enzyme. *Analytica Chimica Acta* 984:177-84.

Ma, L., T. Guo, S. Pan, and Y. Zhang. 2018. A fluorometric aptasensor for patulin based on the use of magnetized graphene oxide and DNase I-assisted target recycling amplification. *Microchimica Acta*185:487. doi: 10.1007/s00604-018-3023-z.

Malhotra, B., S. Srivastava, M. A. Ali, and C. Singh. 2014. Nanomaterial-Based Biosensors for Food Toxin Detection. *Biotechnology and Applied Biochemistry* 174:880-96.

Mandappa, I. M., K. Basavaraj, and H. K. Manonmani. 2018. Analysis of mycotoxins in fruit juices in fruit juices. In: Fruit juices: Extraction, Composition, Quality, and Analysis edited by: G. Rajauria, and B. K. Tiwari. Elsevier.

Mithofer, A. and M. E. Maffei. 2016. General mechanisms of plant defense and plant toxins. *Plant Toxins.* Toxinology:1-22. https://doi.org/10.1007/978-94-007-6728-7_21-1.

Moreno-Gonzalez, D., P. Jac, P. Riasova, and L. Novakova. 2021. In-line molecularly imprinted polymer solid-phase extraction-capillary electrophoresis coupled with tandem mass spectrometry for the determination of patulin in apple-based food. *Food Chemistry* 334:127607. DOI: 10.1016/j.foodchem.2020.127607.

Moretti, A., A. F. Logrieco, and A. Susca. 2017. Mycotoxins: An Underhand Food Problem. *Methods in Molecular Biology* 1542:3-12.

National Health and Family Planning Commission of the People's Republic of China, State Food and Drug Administration, GB 2761-2017 National food safety standard mycotoxin limit in foodstuff. Standards Press of China. 2017.

Nunes da Silva, S. J., P. Z. Schuch, C. R. Bernardi, M. H. Vainstein, A. Jablonski, and R. J. Bender. 2007. Patulin in food: state-of-the-art and analytical trends. *RevistaBrasileira de Fruticultura* 29 (2):406-13.

Ostry, V., F. Malir, J. Toman, Y. Grosse. 2017. Mycotoxins as human carcinogens-the IARC Monographs classification. *Mycotoxin Research* 33 (1):65-73.

Pascari, X., A. J. Ramos, S. Marín, and V. Sanchis. 2018. Mycotoxins and beer. Impact of the beer production process on mycotoxin contamination. A review. *Food Research International* 103:121-9.

Pattono, D., A. Grosso, P. P. Stocco, M. Pazzi, and G. Zeppa. 2013. Survey of the presence of patulin and ochratoxin in traditional semi-hard cheeses. *Food Control* 33:54–7.

Pereira, V. L., J. O. Fernandes, and S. C. Cunha. 2014. Mycotoxins in cereals and related foodstuffs: A review on occurrence and recent methods of analysis. *Trends in Food Science and Technology* 36 (2):96-136.

Piletsky, S., F. Canfarotta, A. Poma, A. M. Bossi, and S. Piletsky. 2020. Molecularly Imprinted Polymers for Cell Recognition. *Trends in Biotechnology* 38 (4):368-87.

Puel, O., P. Galtier, and I. P. Oswald. 2010. Biosynthesis and Toxicological Effects of Patulin. *Toxins (Basel)* 2 (4):613-31.

Ramos Girona, A.J., C. A. Da Rocha Rosa, L. R. Cavaglieri, and C. A. Guedes. 2011. In Legislation and economic impact of mycotoxins. Mycotoxins and mycotoxicosis, Editions 427-462. A. J. Ramos. Madrid. España.

Rasmussen, S., A. Andersen, N. Andersen, K. Nielsen, P. Hansen, T. O. Larsen. 2016. Chemical Diversity, Origin, and Analysis of Phycotoxins. *Journal of Natural Products* 79 (3):662-73.

Regal, P., M. Diaz-Bao, R. Barreiro, C. Fente, and A. Cepeda. 2017. Design of a molecularly imprinted stir-bar for isolation of patulin in apple and LC-MS/MS detection. *Separations* 4 (2):11. https://doi.org/10.3390/separations4020011.

Rodríguez, A., M. Rodríguez, M. J. Andrade, M. D. G. Cordoba. 2015. Detection of filamentous fungi in foods. *Current Opinion in Food Science*5:36-42.

Sadok, I., A. Szmagara, and M. M. Staniszewska. 2018. The validated and sensitive HPLC-DAD method for determination of patulin in strawberries. *Food Chemistry* 245:364-70.

Sanzani, S. M., M. Reverberi, and R. Geisen. 2016. Mycotoxins in harvested fruits and vegetables: Insights in producing fungi, biological role, conducive conditions, and tools to manage postharvest contamination. *Postharvest Biology and Technology* 122:95-105.

Schlegel, K. M., and P. W. Elsinghorst. 2020. Myco-DES: Enabling remote extraction of mycotoxins for robust and reliable quantification by stable isotope dilution LC-MS/MS. *Analytical Chemistry* 92 (7):5387-95.

Seale, A. C., H. Blencowe, A. A. Manu, H. Nair, R. Bahl, S. A. Qazi, A. K. Zaidi, J. A. Berkley, S. N. Cousens, and J. E. Lawn. 2014. Estimates of possible severe bacterial infection in neonates in sub-Saharan Africa, South Asia, and Latin America for 2012: a systematic review and meta-analysis. *The Lancet Infectious Diseases* 14 (8):731-41.

Selvam, S. P., A. N. Kadam, K. R. Maiyelvaganan, M. Prakash, and S. Cho. 2021. Novel SeS_2-loaded Co MOF with Au@PANI comprised electroanalytical molecularly imprinted polymer-based disposable sensor for patulin mycotoxin. *Biosensors and Bioelectronics* 187:113302. https://doi.org/10.1016/j.bios.2021.113302.

Shukla, S., Y. Haldorai, I. Khan, S.-M. Kang, C. H. Kwak, S. Gandhi, V. K. Bajpai, Y.S. Huh, and Y.-K. Han. 2020. Bioreceptor-free, sensitive, and rapid electrochemical detection of patulin fungal toxin, using a reduced graphene oxide@SnO_2 nanocomposite. *Materials Science and Engineering C* 113:110916. https://doi.org/10.1016/j.msec.2020.110916.

Song, X., D. Wang, and M. Kim. 2021. Development of an immuno-electrochemical glass carbon electrode sensor based on graphene oxide/gold nanocomposite and antibody for the detection of patulin. *Food Chemistry* 342:128257. https://doi.org/10.1016/j.foodchem.2020.128257.

Spadaro, D., G. R. Meloni, I. Siciliano, S. Prencipe, and M. L. Gullino. 2020. HPLC-MS/MS method for the detection of selected toxic metabolites produced by *Penicillium* spp. in nuts. *Toxins* 12 (5):307. https://doi.org/10.3390/toxins12050307.

Stadler, D., F. Berthiller, M. Suman, R. Schuhmacher, and R. Krska. 2020. Novel analytical methods to study the fate of mycotoxins during thermal food processing. *Analytical and Bioanalytical Chemistry* 412 (1):9-16.

Tabrizi, M. A., M. A. Shamsipur, R. Saber, S. Sarkar, and V. Ebrahimi. 2017. A high sensitive visible-light-driven photoelectrochemical aptasensor for shrimp allergen tropomyosin detection using graphitic carbon nitride-TiO_2 nanocomposite. *Biosensors and Bioelectronics* 98:113-8.

Tannous, J., A. Atoui, A. El Khoury, S. Kantar, N. Chdid, I. P. Oswald, O. Puel, R. Lteif. 2015. Development of a real-time PCR assayfor *Penicillium expansum* quantification and patulin estimation in apples. *Food Microbiology* 50:28-37.

US Food and Drug Administration; Silver Spring, MD, USA: 2004. Food and Drug Administration (FDA) Compliance Policy Guide. Compliance policy guidance for fda staff. Sec. 510.150 Apple juice, apple juice concentrates, and apple juice products—Adulteration with patulin.

Van de Perre, E., L. Jacxsens, W. Van Der Hauwaert, I. Haesaert, and B. De Meulenaer. 2014. Screening for the presence of patulin in molded fresh produce and evaluation of its stability in the production of tomato products. *Journal of Agricultural and Food Chemistry* 62:304–9.

Varzakas, T. 2015. Quality and safety aspects of cereals (wheat) and their products. *Critical Reviews in Food Science and Nutrition* 56 (15):2495-510.

Viegas, S., R. Assunção, M. Twaruzek, R. Kosicki, J. Grajewski, and C. Viegas. 2019. Mycotoxins feed contamination in a dairy farm – potential implications for milk contamination and workers' exposure in a One Health approach. *Journal of the Science of Food and Agriculture* 100:1118-23.

Wei, F., X. Liu, X. Liao, L. Shi, S. Zhang, J. Lu, L. Zhou, and W. J. Kong. 2019. Simultaneous determination of 19 mycotoxins in lotus seed using a multimycotoxin UFLC-MS/MS method. *Journal of Pharmacy and Pharmacology* 71 (7):1172-83.

Welke, J. E. 2019. Fungal and mycotoxin problems in grape juice and wine industries. *Current Opinion in Food Science* 29:7-13.

Welke, J. E., M. Hoeltz, H. A. Dottori, I. B. Noll. 2009. Effect of processing stages of apple juice concentrates on patulin levels. *Food Control* 20 (1):48-52.

Wild, C. P., and Y. Y., Gong. 2010. Mycotoxins and human disease: a largely ignored global health issue. *Carcinogenesis* 31 (1):71-82.

Wu, S., N. Duan, W. Zhang, S. Zhao, and Z. Wang. 2016. Screening and development of DNA aptamers as capture probes for colorimetric detection of patulin. *Analytical Biochemistry* 508:58-64.

Wu, Z., E. Xu, Z. Jin, and J. Irudayaraj. 2018. An ultrasensitive aptasensor based on fluorescent resonant energy transfer and exonuclease-assisted target recycling for patulin detection. *Food Chemistry* 249:136-42.

Xia, Y., M. Liu, L. Wang, A. Yan, W. He, M. Chen, J. Lan, J. Xu, L. Guan, and J. Chen. 2017. A visible and colorimetric aptasensor based on DNA-capped single-walled carbon nanotubes for detection of exosomes. *Biosensors and Bioelectronics* 92:8-15.

Xiao, H., and S. Fu. 2012. A Sensitive Gas Chromatography-Mass Spectrometry Method for the Determination of Patulin in Apple Juice. *Journal of AOAC International* 95 (6):1709-12.

Xu, J., X. Qiao, Y. Wang, Q. Sheng, T. Yue, J. Zheng, and M. Zhou. 2019. Electrostatic assembly of gold nanoparticles on black phosphorus nanosheets for electrochemical aptasensing of patulin. *Mikrochimica Acta* 186 (4):238. https://doi.org/10.1016/j.foodchem.2018.01.025.

Yang, Y., Y. Yang, B. Shao, and J. Zhang. 2017. A simple and rapid method for determination of patulin in juice by High-Performance Liquid Chromatography-tandem Mass Spectrometry. *Food Analytical Methods* 10 (9):2913-8.

Zbynovská, K., P. Petruška, A. Kalafová, and M. Capcarová. 2016. Patulin - a Contaminant of Food and Feed: a review. *Acta Fytotechnica et Zootechnica*19 (2):64-7.

Zhang, L., X.-W. Dou, C. Zhang, A. Logrieco, and M. Yang. 2018. A Review of Current Methods for Analysis of Mycotoxins in Herbal Medicines. *Toxins* 10 (2):65. https://doi.org/10.3390/toxins10020065.

Zhang, W., Y. Han, X. Chen, X. Luo, J. Wang, T. Yue, and Z. Li. 2017. Surface molecularly imprinted polymer capped Mn-doped ZnS quantum dots as a phosphorescent nanosensor for detecting patulin in apple juice. *Food Chemistry* 232:145-54.

Zhao, M., H. Shao, Y. He, H. Li, M. Yan, Z. Jiang, J. Wang, A. M. Abd El-Aty, A. Hacımüftüoğlu, F. Yan, Y. Wang, and Y. She. 2019. The determination of patulin from food samples using dual-dummy molecularly imprinted solid-phase extraction coupled with LC-MS/MS. *Journal of chromatography. B* 1125:121714.https://doi.org/10.1016/j.jchromb.2019.121714.

Zhong, L., J. Carere, Z. Lu, F. Lu, and T. Zhou. 2018. Patulin in Apples and Apple-Based Food Products: The Burdens and the Mitigation Strategies. *Toxins (Basel)* 10 (11):475. https://doi.org/10.3390/toxins10110475.

Zhou, Q., and D. Tang. 2020. Recent advances in photoelectrochemical biosensors for analysis of mycotoxins in food. *Trends in Analytical Chemistry* 124:115814. DOI: 10.1016/j.trac.2020.115814.

Disposable stochastic sensors for fast analysis of ibuprofen, ketoprofen, and flurbiprofen in their topical pharmaceutical formulations

Abstract

Three disposable stochastic sensors based on maltodextrin (dextrose equivalent = 4 - 7) and nanostructures (copper monolayer, carbon monolayer and carbon-copper composite layer)

deposited using cold plasma on copy paper were proposed for the fast analysis of ibuprofen, ketoprofen and flurbiprofen in pharmaceutical formulation samples. The widest linear concentration ranges recorded were: for ibuprofen 1 fmol/L – 1 mmol/L when the disposable stochastic sensor based on carbon monolayer was used, for ketoprofen 1 fmol/L – 1 mmol/L when the disposable stochastic sensors based on copper monolayer and carbon-copper composite layer were used, and for flurbiprofen 1 fmol/L – 10 mmol/L when the disposable stochastic sensor based on carbon-copper composite layer was used. The lowest limit of detection recorded for each non-steroidal anti-inflammatory drug was 1 fmol/L.

Introduction

Ibuprofen (IBP), denoted (RS)-2-(4-(2-methylpropyl)phenyl)propanoic acid, ketoprofen (KTP), denoted 2-(3-benzoylphenyl)propanoic acid and flurbiprofen (FBP), denoted 2-(3-fluoro-4-phenylphenyl)propanoic acid, are propionic acid derivatives (Figure 1) included in the non-steroidal anti-inflammatory drugs (NSAIDs) class. As a result of their exhibited anti-inflammatory, analgesic and antipyretic effects, they are indicated in mild to moderate pain, fever emerging from colds or the flu, rheumatoid disorders, osteoarthritis and dysmenorrhea. NSAIDs rank first place as most prescribed drugs in a study regarding polypharmacy in elder patients conducted in the United States [1].

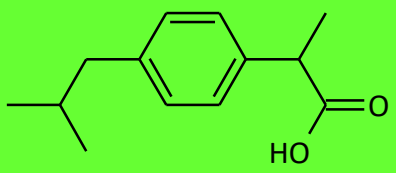

a)

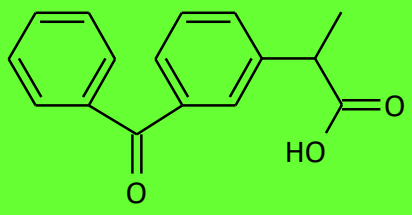

b)

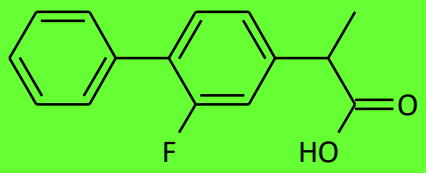

c)

Figure 1. Chemical structure of a) ibuprofen, b) ketoprofen, and c) flurbiprofen.

The European Pharmacopoeia recommends methods of analysis such as direct titration for IBP and potentiometric titration for KTP and FBP [2-4] whereas the United States Pharmacopeia proposes HPLC as a method of determination for IBP (in pure state and pharmaceutical formulations such as tablets and oral suspension) and FBP (tablets and ophthalmic solution) and direct titration for KTP and FBP in their pure state [5]. To date, the determination methods reported in the literature for the analysis of IBP, KTP and FBP in different matrices are: high-performance liquid chromatography (HPLC) [6-9], HPLC with fluorescence detection [10], ultraperformance liquid chromatography-tandem mass spectrometry (UPLC-MS/MS) [11] spectrofluorimetry [12,13], potentiometry [14-16], capillary electrophoresis (CE) [17,18] and gas chromatography-mass spectrometry (GC-MS) [19,20]. Despite being reproducible, sensitive and reliable, such methods require sample pretreatment which could be time-consuming, involve expensive and complex instrumentation and reagents and depend upon specialized personnel.

There is a need of fast quality control of these compounds (IBP, KTP, and FBP) especially during their synthesis processes. In order to assess the quality of the active compounds in the raw material obtained after synthesis, there is a need for fast and reliable methods of analysis. Finally, utilization of fast and cheap methods of analysis of the active compounds (IBP, KTP, and FBP) in their formulations are saving money and may decrease the cost of their topical dosage forms.

This paper proposed three disposable stochastic sensors based on deposition using cold plasma of nanostructures (copper, carbon and carbon-copper composite) on copy paper. The choice of these materials took into account also the production costs of the disposable sensors – which was very low, if these materials were chosen for the design of the sensors. Utilization of nanostructured materials proved to provide excellent results in electrochemical sensing [21-27]. The materials deposited on the copy paper: copper, carbon and carbon-copper composite do not interact directly with the profens; to get the stochastic sensing, a molecule able to provide the channels/pores is needed. Therefore, the sensors were modified with maltodextrin (MD) (dextrose equivalent = 4 – 7) for the determination of three compounds from the class of NSAIDs (IBP, KTP and FBP) from real samples (gels and oromucosal spray). MD promotes the response of stochastic sensors. Hence, the proposed sensors represent an advantageous low-cost alternative for the above-mentioned methods as these types of sensors are suitable for the simultaneous measurement of several analytes in a single run, are highly sensitive with a low detection limit and do not require sample pretreatment, regardless of the matrix type [28-30].

Experimental

Materials and reagents

Analytical grade ibuprofen, ketoprofen, flurbiprofen, and maltodextrin were purchased from Sigma Aldrich (Milwaukee, USA). Deionized water was used for the preparation of solutions. Phosphate buffer solution (PBS), pH = 5 was obtained using NaH_2PO_4 and Na_2HPO_4, bought from Sigma Aldrich.

Stock solutions of IBP, KTP and FBP (1.00×10^{-2} mol/L) were prepared in ethanol. The sets of solutions (concentrations up to 1.00×10^{-15} mol/L) necessary for the calibration of the disposable stochastic sensors were obtained from the stock solutions by using serial dilution method and

buffered with PBS (pH = 5). The value of pH was selected to match the pH of the samples to be directly analysed using the proposed stochastic sensors.

Apparatus and methods

Deionized water was obtained by using a Direct-Q3 Water Purification System (Millipore Corporation, France). Electrochemical measurements were conducted on a mini potentiostat EmStat Pico connected to a computer with PSTrace software version 5.8 (PalmSens BV, Houten, The Netherlands). A classical three-electrode electrochemical cell was assembled by employing a stochastic sensor as the working electrode, an Ag/AgCl wire (1 mol/L KCl) as the reference electrode and a Pt wire as the counter electrode.

Design of disposable stochastic sensors based on maltodextrin

The preparation of three nanostructures based on a monolayer of copper (Cu), carbon (C), and C-Cu nanocomposite layer onto paper were carried out using thermoionic vacuum arc plasma (TVA), a cold plasma deposition method. Further details on the TVA plasma can be found elsewhere [31]. This TVA plasma was previously used for film deposition of plastic, textile and copy paper substrates [32-35]. A4 printing paper was used as substrate. The paper was previously blow-dried with nitrogen gas followed by high vacuum treatment for at least 2 h, in order to remove residual contaminants and to optimize deposition conditions of the monolayers and composite layer. The monolayers of Cu and C and composite layer C-Cu were deposited at room temperature onto paper substrates, placed on the upper TVA plasma, to construct flexible sensors. This 2D configuration is shown in Figure 2

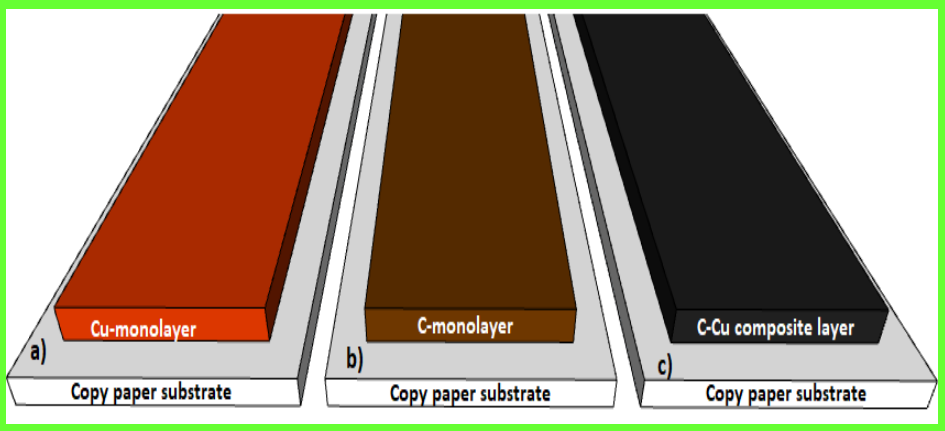

Figure 2. 2D configuration of the sensors based on a) copper monolayer, b) carbon monolayer, and c) copper-carbon composite layer.

The nanostructure coatings were synthesized based on two materials with high purity (Cu= 99.9 %, C=99.98%) used in design for 2D sensor applications. Three shapes of nanostructures were obtained on copy paper substrates: the first sensor was obtained by deposition of a nanolayer of Cu pellets placed in the graphite crucible; the second sensor was obtained by deposition of a nanolayer of C supplied by a pure graphite rod with a diameter of 10 mm; and the third sensor was obtained by deposition of C-Cu composite layer. For the deposition of C-Cu composite layer a special anode was designed and consists of C and Cu base. A one-step process deposition was used for synthesizing C-Cu composite layer. Briefly, the designed anode is a pure graphite crucible containing both materials to be evaporated. In the crucible, a carbon rod (with a diameter of 10 mm and high of 10 mm) was positioned and fully surrounded with 10 grams of Cu pellets. Single stable plasma plume from both materials was ignited and maintained by using electron bombardment from a single hot tungsten filament. The A4 copy paper substrate was placed face down at a 33 cm distance from the plasma plume and secured with clips to enable the direct deposition of the layer onto the surface. The film thickness was controlled by deposition time (which was 7 minutes), and it was of 215 nm. Vacuum pressure and electrical parameters of Cu, C and C-Cu plasma used during the deposition are presented in the Table 1.

Table 1. Parameters used for Cu, C and C-Cu plasma deposition on copy paper.

Plasma Plume	I_f (A)	I_a (A)	U_a (V)	Vacuum Pressure (mBar)
Cu	53	1.4	150	2×10^{-5}
C	53	2	350	3×10^{-5}
C-Cu	53	2.4	400	2×10^{-5}

I_f = tungsten filament current, I_d and U_d = discharge current and voltage.

To optimize the immersion time in the MD aqueous solution (1.00×10^{-3} mol/L), we did prepare 3 sensors of each type, and immerse them for 15, 30, 45, 60, 75, 90, 105, and 120min. The response of a bear senor of each type was compared with the response obtained after the 8 immersions; only after immersing the sensors for 120min in the MD solution, a stochastic signal was achieved. Therefore, all three sensors were immersed for two hours in a MD aqueous solution (1.00×10^{-3} mol/L) towards the modification of their surface. Afterwards, the sensors were dried for a period of 24 h before use.

When not in use, the sensors were stored in a dry container at room temperature.

Stochastic mode

Since the stochastic mode requires t_{off} and t_{on} values, a chronoamperometric technique was opted and the assays were performed at a constant potential of 115 mV vs. Ag/AgCl which was optimized in order to get the highest reliability for the reading of t_{off} and t_{on} values. The calibration of the sensor was performed by using NSAIDs standard solutions of various concentrations. The signature of the NSAID (t_{off}) identified in the diagrams was used for the qualitative analysis while the t_{on} value was used for determination of NSAID's concentration, based on the calibration equation of each sensor:

$$1/t_{on} = a + b \times C_{NSAID}$$

where a is the intercept, and b is the slope/sensitivity.

The unknown concentrations of the NSAIDs were calculated using the calibration equation.

Samples

Three topical pharmaceutical formulations (Ibutop Gel 50 mg/g gel, Ketonal 25 mg/g gel and Strepsils Intensiv 8.75 mg/dose oromucosal spray) containing ibuprofen, ketoprofen, and flurbiprofen, respectively, obtained from a local drug store were analyzed without any pretreatment. Ibutop Gel contains ibuprofen as active pharmaceutical ingredient (API) and excipients, such as isopropyl alcohol, 2,2-dimethyl-4-hydroxymethyl-1,3-dioxolan, poloxamer 407, medium chain triglycerides, lavender oil, neroli oil and purified water, whilst Ketonal comprises ketoprofen as API and excipients like carbomer, trolamine, lavender essential oil, ethanol 96% and purified water. Flurbiprofen is the API in Strepsils Intensiv and the product also contains betadex, disodium hydrogen phosphate dodecahydrate, citric acid monohydrate, methyl parahydroxybenzoate (E218), propyl parahydroxybenzoate (E216), sodium hydroxide, mint flavour, cherry flavour, N-2,3-trimethyl-2-isopropylbutanamide, saccharin, hydroxypropyl betadex and purified water as excipients.

Results and discussions

Characterization of the material used for the design o the disposable stochastic sensors

In Figure 3 digital photos of coated copy paper substrates with a) Cu, b) C, and c) C-Cu are shown:

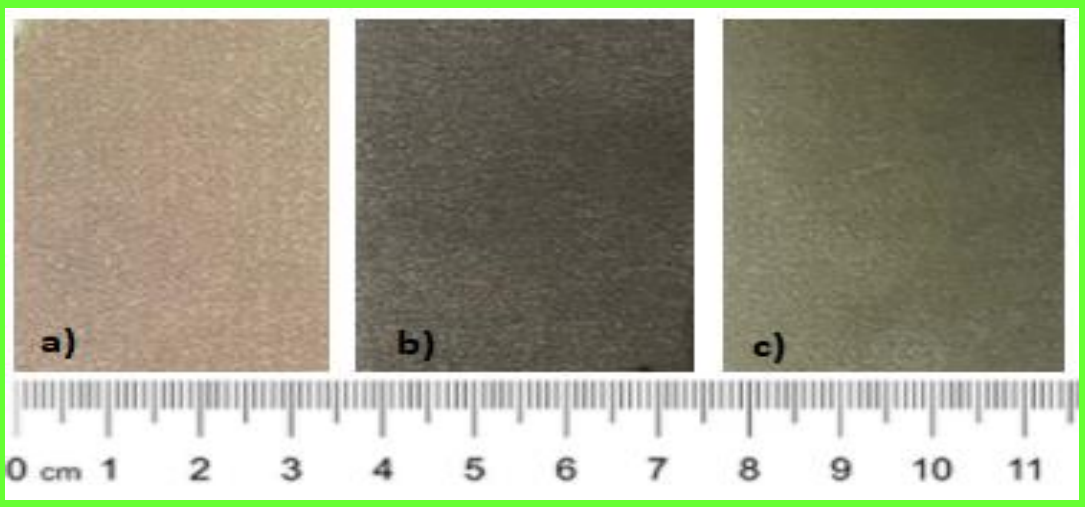

Figure 3. Digital photos of a) Cu monolayer, b) C monolayer, and c) C-Cu composite layer deposited on copy paper substrate.

Scanning electron microscope (Apreo S Thermo Fischer Scientific, Waltham, MA, USA) was used to characterize the surface morphologies evolution of uncoated and coated copy paper substrates. As shown in Figure 4, the images are done at the magnifications of 10000 × and 250 × SEM images for Cu layer, C layer, C-Cu composite layer coated on copy paper substrate, respectively, while a magnification of 10000 × and 250 × SEM images of uncoated copy paper was used. Based on the results presented in Figure 4, comparing the surface morphology differences between the coated and uncoated copy paper it can be observed that the porosity of copy paper was partially coated by Cu and C nanolayer, respectively, and totally coated by C-Cu composite layer. SEM images revealed a uniform and continuous coatings of layers (Cu, C, C-Cu) onto paper substrate. These results indicate that the nanostructures for all three types of coatings are facilitate to obtained sensors.

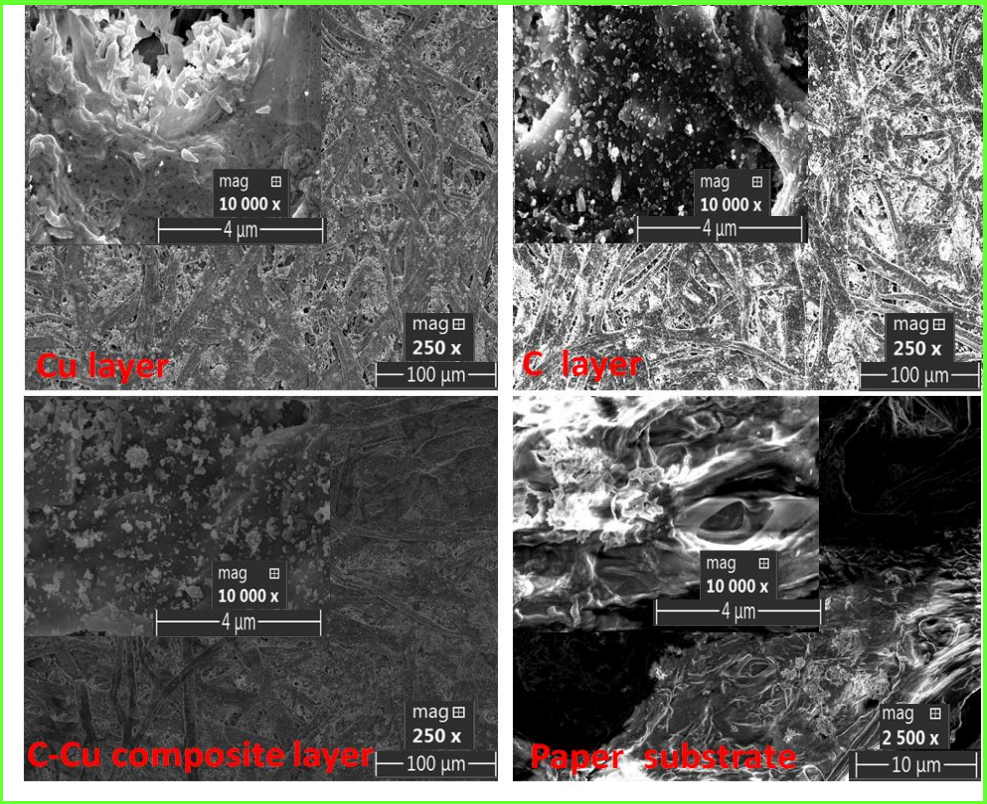

Figure 4. SEM morphology of Cu monolayer, C monolayer, C-Cu composite layer deposited on copy paper substrate and copy paper blank substrate: top view scanning electron microscope (SEM) image of the samples with different magnification (250 × - scale bar 100 µm respectively 10000 × - scale bar 4 µm and 2500 × - scale bar 10 µm respectively 10000 × - scale bar 4 µm).

Response characteristics of stochastic sensors

The stochastic method is centered on the channel conductivity and involves a response based on a two-step process. The first phase is represented by the blockade of the channel by the NSAID molecule, when the current drops to 0 whilst the second phase occurs when the NSAID enters the channel, binds to its wall and undergoes redox processes for a certain amount of time. During the second phase, the following equations of equilibrium take place:

$$Ch(i) + ibuprofen(i) \Leftrightarrow Ch \bullet ibuprofen\ (i)$$

$$Ch(i) + ketoprofen(i) \Leftrightarrow Ch \bullet ketoprofen\ (i)$$

$$Ch(i) + flurbiprofen(i) \Leftrightarrow Ch \bullet flurbiprofen\ (i)$$

where Ch is the channel and i is the interface.

t_{off} characterizes the first step and represents the signature of the NSAID (qualitative analysis), whereas t_{on} describes the second step, providing insight regarding the concentration of NSAID (quantitative analysis).

The response characteristics of the three stochastic sensors developed for the assay of IBP, KTP and FBP are listed in Table 2. For all three NSAIDs, distinctive t_{off} values were registered for each sensor, indicating a selective identification. This allowed the use of sensors for simultaneous determination of all three NSAIDs in the samples containing all of them.

The following linear concentration ranges and limits of determination were recorded: from 1.00×10^{-15} to 1.00×10^{-3} mol/L with a LOD of 1.00×10^{-15} mol/L for IBP when the stochastic sensor based on C-monolayer was employed, $1.00 \times 10^{-15} – 1.00 \times 10^{-3}$ mol/L with a LOD of 1.00×10^{-15} mol/L for KTP when the stochastic sensors based on Cu-monolayer and C-Cu-composite layer was employed, and $1.00 \times 10^{-15} – 1.00 \times 10^{-2}$ mol/L with a LOD of 1.00×10^{-15} mol/L for FBP when the stochastic sensor based on C-Cu-composite layer was employed. The wide linear concentration range values obtained for each disposable sensor indicate that the sensors for IBP, KTP, and FBP may be used for their quantification from pharmaceutical formulations without sample dilution, and from biological samples without any preconcentration step. The limits of quantification of fmol/L as well as the high sensitivity values obtained shown the high ability of the proposed sensors for the analysis of IBP, KTP, and FBP, while the different signatures recorded for them shown the ability of the sensors to be used for the purity tests of the active substance as well as for performing the uniformity content test of their pharmaceutical formulations.

Table 2. Response characteristics of the disposable stochastic sensors used for the assay of ibuprofen, ketoprofen, and flurbiprofen.

Disposable stochastic sensor based on MD and	Calibration equation and correlation coefficient (r)	Linear concentration range (mol/L)	t_{off} (s)	Sensitivity (s^{-1}/mol/L)	Limit of determination (mol/L)
Ibuprofen					
Cu-monolayer	$1/t_{on} = 0.13 + 9.35 \times 10^{8} \times C$ r = 0.9995	$1.00 \times 10^{-12} – 1.00 \times 10^{-2}$	1.9	9.35×10^{8}	1.00×10^{-12}
C-monolayer	$1/t_{on} = 0.15 + 1.85 \times 10^{11} \times C$ r = 0.9976	$1.00 \times 10^{-15} – 1.00 \times 10^{-3}$	1.1	1.85×10^{11}	1.00×10^{-15}
C-Cu composite layer	$1/t_{on} = 0.08 + 3.19 \times 10^{2} \times C$ r = 0.9966	$1.00 \times 10^{-6} – 1.00 \times 10^{-3}$	2.5	3.19×10^{2}	1.00×10^{-6}
Ketoprofen					
Cu-monolayer	$1/t_{on} = -0.03 + 5.01 \times 10^{11} \times C$ r = 0.9978	$1.00 \times 10^{-15} – 1.00 \times 10^{-3}$	1.4	5.01×10^{11}	1.00×10^{-15}
C-monolayer	$1/t_{on} = 0.10 + 1.15 \times 10^{2} \times C$ r = 0.9969	$1.00 \times 10^{-6} – 1.00 \times 10^{-2}$	0.7	1.15×10^{2}	1.00×10^{-6}
C-Cu composite layer	$1/t_{on} = 0.13 + 1.25 \times 10^{12} \times C$ r = 0.9998	$1.00 \times 10^{-15} – 1.00 \times 10^{-3}$	1.5	1.25×10^{12}	1.00×10^{-15}
Flurbiprofen					
Cu-monolayer	$1/t_{on} = 0.08 + 3.70 \times 10^{8} \times C$ r = 0.9982	$1.00 \times 10^{-13} – 1.00 \times 10^{-3}$	0.8	3.70×10^{8}	1.00×10^{-13}
C-monolayer	$1/t_{on} = 0.04 + 3.92 \times 10^{5} \times C$ r = 0.9994	$1.00 \times 10^{-8} – 1.00 \times 10^{-2}$	1.7	3.92×10^{5}	1.00×10^{-8}
C-Cu composite layer	$1/t_{on} = 0.03 + 7.97 \times 10^{10} \times C$ r = 0.9991	$1.00 \times 10^{-15} – 1.00 \times 10^{-2}$	1.0	7.97×10^{10}	1.00×10^{-15}

Taken into account the response characteristic of the proposed sensors for IBP, KTP, and FBP, the disposable stochastic sensor of choice is the one based on C-Cu composite layer.

Selectivity

The selectivity of the stochastic sensors is conferred by the values of the signature (t_{off} parameter) for possible interfering species. The response of the sensor to the analytes for which it was designed is not influenced by the quantity of interfering species. The selectivity of the designed sensors is confirmed by the different signatures obtained for IBP, KTP, and FBP, meaning that neither of them interferes in the assay of a selected NSAID. Paracetamol is usually

associated with IBP, KTP, and FBP, and therefore the selectivity of the proposed sensors was checked. The signatures obtained for paracetamol using the proposed sensors were: 2.5s when the sensor based on Cu-monolayer was used, 2.7s when the sensor based on C-monolayer was used, and 3.0s when the sensor based on C-Cu composite layer was used; these values proved no interference from paracetamol when the sensors are used for the assay of IBP, KTP, and FBP in pharmaceutical products. Further, none of the ingredients used for the formulation of the pharmaceutical compounds interfere, because their signatures' values are far different from the signatures recorded for IBP, KTP, and FBP.

Reproducibility of the design of the disposable stochastic sensors

Ten of each type of sensors were designed and used for the assay of ibuprofen, ketoprofen, and flurbiprofen. The sensitivities of the sensors were determined for all 10 sensors of each type. The RSD% values determined for the variation of the sensitivities recorded for the 10 microsensors of each type were as following: for the sensor based on Cu-monolayer 0.12% for ibuprofen, 0.10% for ketoprofen, and 0.11% for flurbiprofen; for the sensor based on C-monolayer 0.13% for ibuprofen, 0.13% for ketoprofen, and 0.11% for flurbiprofen; and, for the sensor based on C-Cu composite layer 0.10% for ibuprofen, 0.09% for ketoprofen, and 0.08% for flurbiprofen. The results have shown that the proposed design of the stochastic sensors is highly reproducible.

Stability

The disposable sensors were stored for a period of seven months and used for the determination of IBP, KTP and FBP. The results obtained were consistent throughout this period of time and there were not major differences regarding the sensitivity of the sensors, the variations of sensitivity being less than 1.00%.

Analysis of ibuprofen, ketoprofen, and flurbiprofen from their pharmaceutical formulations

Uniformity content tests are very important for pharmaceutical industry. The proposed sensors were suitable for the assay of IBP, KTP, and FBP directly from the pharmaceutical formulations because the concentration of the active substances is found on the linear concentration range of the disposable sensors. Therefore, the sensors were used in the qualitative and quantitative analysis of IBP, KTP, and FBP in three topical dosage forms. The results obtained are shown in Table 3 and the diagrams are depicted in Figures S1, S2 and S3.

Table 3. Analysis of ibuprofen, ketoprofen and flurbiprofen in topical dosage forms.

NSAID	Pharmaceutical dosage form	Stochastic sensor	Concentration of the NSAID in the pharmaceutical formulation
Ibuprofen	Gel (50 mg ibuprofen/g gel)	MD/Cu-monolayer	49.93 ± 0.03 mg/g gel
		MD/C-monolayer	49.98 ± 0.02 mg/g gel
		MD/C-Cu composite layer	49.46 ± 0.03 mg/g gel
Ketoprofen	Gel (25 mg ketoprofen/g gel)	MD/Cu-monolayer	24.94 ± 0.04 mg/g gel
		MD/C-monolayer	24.08 ± 0.03 mg/g gel
		MD/C-Cu composite layer	24.73 ± 0.03 mg/g gel
Flurbiprofen	Oromucosal spray (16.20 mg flurbiprofen/mL)	MD/Cu-monolayer	16.18 ± 0.02 mg/mL
		MD/C-monolayer	15.98 ± 0.03 mg/mL
		MD/C-Cu composite layer	16.13 ± 0.03 mg/mL

The values recorded for the recovery of NSAIDs (very closed to the declared values, recoveries values being higher than 98.00%) in their pharmaceutical formulations as well as the relative standard deviation values shown that the sensors can be used for the uniformity content test of the topical dosage forms.

The purity of the active substance is a major issue in pharmaceutical industry. Given the synthesis process of the NSAIDs from profen class, there is a need to have a method for the

discrimination between different profen active substances. To prove that there is possible to reliable analyses one profen in the presence of the others, a further validation of the sensors was done using various mixed solutions containing the three profens in different molar ratios (Table 4). The results shown in Table 4 represents an average recorded for various concentrations of profens drugs, mixed in different ratios in the mixed solutions prepared. The diagrams obtained are presented in Figure 5.

Table 4. Recovery (%) of ibuprofen, ketoprofen and flurbiprofen in mixed solutions.

IBP:KTP:FBP (mol : mol : mol)	Stochastic sensor	IBP	KTP	FBP
1 : 1 : 1	MD/Cu-monolayer	99.87 ± 0.02	99.93 ± 0.01	99.47 ± 0.03
	MD/C-monolayer	99.90 ± 0.03	99.98 ± 0.02	99.97 ± 0.02
	MD/C-Cu composite layer	99.95 ± 0.02	99.97 ± 0.03	99.98 ± 0.01
1 : 1 : 2	MD/Cu-monolayer	99.95 ± 0.01	99.18 ± 0.03	99.48 ± 0.02
	MD/C-monolayer	99.89 ± 0.03	99.87 ± 0.02	99.93 ± 0.03
	MD/C-Cu composite layer	99.90 ± 0.02	99.90 ± 0.02	99.85 ± 0.02
1 : 2 : 1	MD/Cu-monolayer	99.95 ± 0.02	99.90 ± 0.03	99.17 ± 0.02
	MD/C-monolayer	99.97 ± 0.03	99.85 ± 0.03	99.18 ± 0.03
	MD/C-Cu composite layer	99.90 ± 0.03	99.97 ± 0.03	99.98 ± 0.01
2 : 1 : 1	MD/Cu-monolayer	99.83 ± 0.02	99.90 ± 0.04	99.87 ± 0.03
	MD/C-monolayer	99.91 ± 0.02	99.87 ± 0.02	99.15 ± 0.02
	MD/C-Cu composite layer	99.94 ± 0.03	99.95 ± 0.01	99.80 ± 0.03
1 : 1 : 5	MD/Cu-monolayer	99.64 ± 0.02	99.58 ± 0.03	99.76 ± 0.02
	MD/C-monolayer	99.18 ± 0.03	99.96 ± 0.02	99.99 ± 0.01
	MD/C-Cu composite layer	99.48 ± 0.03	99.98 ± 0.03	99.95 ± 0.03
1 : 5 : 1	MD/Cu-monolayer	99.32 ± 0.02	99.37 ± 0.03	99.15 ± 0.02
	MD/C-monolayer	99.87 ± 0.02	99.37 ± 0.02	99.98 ± 0.03
	MD/C-Cu composite layer	99.80 ± 0.03	99.87 ± 0.03	99.98 ± 0.02
5 : 1 : 1	MD/Cu-monolayer	99.83 ± 0.02	99.90 ± 0.04	99.95 ± 0.03
	MD/C-monolayer	99.90 ± 0.03	99.15 ± 0.02	99.27 ± 0.04
	MD/C-Cu composite layer	99.80 ± 0.03	99.75 ± 0.03	99.93 ± 0.04
1 : 1 : 10	MD/Cu-monolayer	99.90 ± 0.03	99.80 ± 0.04	99.89 ± 0.03
	MD/C-monolayer	99.87 ± 0.02	99.15 ± 0.02	99.99 ± 0.03
	MD/C-Cu composite layer	99.90 ± 0.03	99.91 ± 0.04	99.90 ± 0.02
1 : 10 : 1	MD/Cu-monolayer	99.87 ± 0.03	99.98 ± 0.02	99.99 ± 0.03
	MD/C-monolayer	99.73 ± 0.02	99.96 ± 0.04	99.98 ± 0.03
	MD/C-Cu composite layer	99.80 ± 0.04	99.87 ± 0.03	99.85 ± 0.03
10 : 1 : 1	MD/Cu-monolayer	99.92 ± 0.03	99.93 ± 0.03	99.89 ± 0.02
	MD/C-monolayer	99.96 ± 0.03	99.87 ± 0.02	99.90 ± 0.03
	MD/C-Cu composite layer	99.87 ± 0.02	99.89 ± 0.03	99.27 ± 0.02

1 : 1 : 100	MD/Cu-monolayer	99.90 ± 0.03	99.98 ± 0.02	99.87 ± 0.03
	MD/C-monolayer	99.98 ± 0.02	99.95 ± 0.03	99.97 ± 0.02
	MD/C-Cu composite layer	99.93 ± 0.03	99.90 ± 0.04	99.92 ± 0.02
1 : 100 : 1	MD/Cu-monolayer	99.84 ± 0.02	99.87 ± 0.03	99.90 ± 0.03
	MD/C-monolayer	99.97 ± 0.02	99.95 ± 0.02	99.93 ± 0.02
	MD/C-Cu composite layer	99.89 ± 0.03	99.90 ± 0.02	99.91 ± 0.03
100 : 1 : 1	MD/Cu-monolayer	99.15 ± 0.02	99.85 ± 0.01	99.99 ± 0.03
	MD/C-monolayer	99.87 ± 0.03	98.57 ± 0.02	98.32 ± 0.03
	MD/C-Cu composite layer	99.90 ± 0.03	99.23 ± 0.02	99.47 ± 0.02

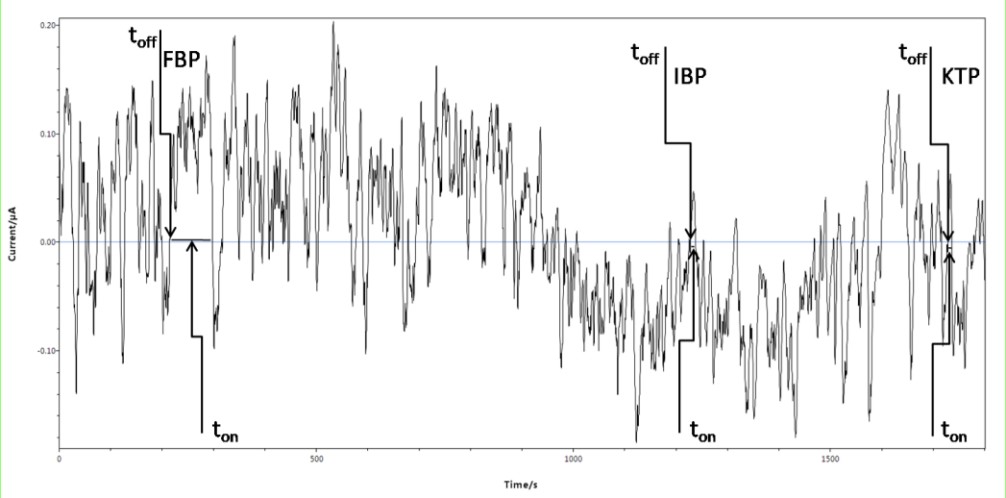

a)

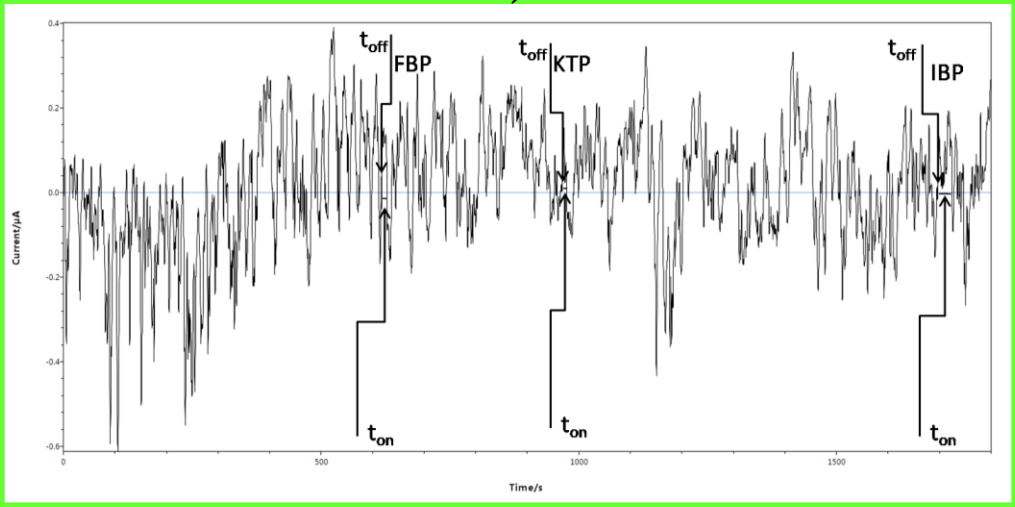

b)

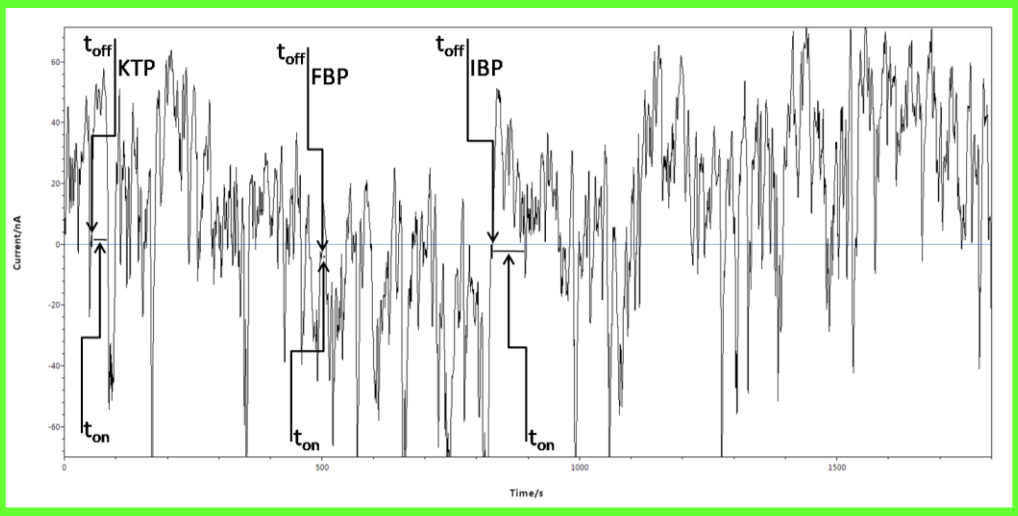

c)

Figure 5. Diagrams obtained after the measurement of mixed solution containing different proportions of ibuprofen, ketoprofen, and flurbiprofen having concentration magnitude order of 10^{-4} mol L^{-1} using the disposable stochastic sensors modified with maltodextrin and based on a) Cu-monolayer, b) C-monolayer, and c) C-Cu composite layer.

The results shown high recovery values with very low relative standard deviation, proving that there is possible the determination of one profen in the presence of the others with high reliability, and also that the disposable stochastic sensors can be reliable used for purity tests of the profen active compounds. Comparing with the chromatographic methods of analysis presented above [6-11, 17-20], the advantages of this method of analysis are: higher sensitivity was achieved, lower quantification limits was recorded; no sampling was applied for the assay of profens; the time of analysis was far lower, and the cost per analysis far smaller than the costs involved in the chromatographic methods of analysis.

Conclusions

Three disposable stochastic sensors based on deposition using cold plasma of copper monolayer, carbon monolayer and carbon-copper composite layer on copy paper and modified with maltodextrin (dextrose equivalent = 4 – 7) were used for the identification and determination of

ibuprofen, ketoprofen and flurbiprofen in topical dosage forms. The concentrations of ibuprofen, ketoprofen and flurbiprofen in their pharmaceutical formulations are within the linear concentration ranges of the three disposable stochastic sensors, favorizing their utilization for uniformity content tests. Furthermore, they can be used for the purity tests of ibuprofen, ketoprofen and flurbiprofen. The proposed sensors are excellent candidates for pharmaceutical industry, when purity tests and uniformity content tests are needed to be performed fast, for profen drugs.

References

[1] H. Young, S. Pan, A.G. Yap, K.R. Reveles, K. Bhakta, Polypharmacy prevalence in older adults seen in United States physician offices from 2009 to 2016, PLoS One, 16 (2021) e0255642.

[2] *European pharmacopoeia, Council of Europe*, 10th ed., Strasbourg (2017), p. 2921–2923.

[3] *European pharmacopoeia, Council of Europe*, 10th ed., Strasbourg (2017), p. 3035–3037.

[4] *European pharmacopoeia, Council of Europe*, 10th ed., Strasbourg (2017), p. 2680–2681.

[5] *The United States Pharmacopeia USP 34-NF 29*, (2011).

[6] A. Tartaglia, A. Kabir, F D'Ambrosio, P. Ramundo, S. Ulusoy, H.I. Ulusoy, G.M. Merone, F. Savini, C. D'Ovidio, U. Grazia, K.G. Furton, M. Locatelli, Fast off-line FPSE-HPLC-PDA determination of six NSAIDs in saliva samples, J. Chromatogr. B 1144 (2020) 122082.

[7] M. Locatelli, V. Ferrone, R. Cifelli, R.C. Barbacane, G. Carlucci, Microextraction by packed sorbent and high performance liquid chromatography determination of seven non-steroidal anti-inflammatory drugs in human plasma and urine. J Chromatogr A. 1367 (2014) 1-8.

[8] V. D'Angelo, F. Tessari, G. Bellagamba, E. De Luca, R. Cifelli, C. Celia, R. Primavera, M. Di Francesco, D. Paolino, L. Di Marzio, M. Locatelli, Microextraction by packed sorbent and HPLC–PDA quantification of multiple anti-inflammatory drugs and fluoroquinolones in human plasma and urine, Journal of Enzyme Inhibition and Medicinal Chemistry, 31 (2016) 110-116.

[9] M. Locatelli, A. Tartaglia, F. D'Ambrosio, P. Ramundo, H.I. Ulusoy, K.G. Furton, A. Kabir, Biofluid sampler: a new gateway for mail-in-analysis of whole blood samples, J Chromatogr B 1143 (2020) 122055.

[10] K.-M. Park, Z.-G. Gao, C.-K. Kim, Assay of flurbiprofen in rat plasma using HPLC with fluorescence detection, J. Liq. Chromatogr. Relat. Technol. 20 (1997) 1849–1855.

[11] M.E. Yaman, A. Atila, T.C. Akman, M. Albayrak, Y. Kadioglu, Z. Halici, A sensitive UPLC-MS/MS method for the determination of Flurbiprofen in rat plasma: Application to real sample, J. Chromatogr. Sci. 59 (2021) 502–509.

[12] P.C. Damiani, M. Bearzotti, M.A. Cabezón, Spectrofluorometric determination of ibuprofen in pharmaceutical formulations, J. Pharm. Biomed. Anal. 25 (2001) 679–683.

[13] R.N. Saha, S. Chandran, P.R. Jadhav, P.B. Kharwade, Rapid and sensitive spectrofluorimetric method for the estimation of celecoxib and Flurbiprofen, Indian J. Pharm. Sci. 68 (2006) 20–25.

[14] Z. Kormosh, I. Hunka, Y. Bazel, O. Matviychuk, Potentiometric determination of Ketoprofen and Piroxicam at a new PVC electrode based on Ion Associates of Rhodamine 6G, Mat. Sci. Eng. C. 30 (2010) 997–1002.

[15] A.A. Bunaciu, A. Grasu, H.Y. Aboul-Enein, Pharmaceutical applications of a flurbiprofen sensor, Anal. Chim. Acta. 311 (1995) 193–197.

[16] R.-I. Stefan-van Staden, R.G. Bokretsion, K.I. Ozoemena, J.F. van Staden, H.Y. Aboul-Enein, Enantioselective, potentiometric memberane electrodes based on different cyclodextrins as chiral selectors for the assay of S-flurbiprofen, Electroanalysis. 18 (2006) 1718–1721.

[17] J. Sádecká, M. Čakrt, A. Hercegová, J. Polonský, I. Skačáni, Determination of ibuprofen and naproxen in tablets, J. Pharm. Biomed. Anal. 25 (2001) 881–891.

[18] M. Friedberg, Z.K. Shihabi, Ketoprofen analysis in serum by capillary electrophoresis, J. Chromatogr. B: Biomed. Sci. Appl. 695 (1997) 193–198.

[19] E. Waraksa, M.K. Woźniak, E. Kłodzińska, R. Wrzesień, B. Bobrowska-Korczak, J. Namieśnik, A rapid and sensitive method for the quantitative analysis of ibuprofen and its metabolites in equine urine samples by gas chromatography with Tandem Mass Spectrometry, J. Sep. Sci. 41 (2018) 3881–3891.

[20] B. Yilmaz, E. Alkan, Determination of flurbiprofen in pharmaceutical preparations by GC–MS, Arabian J. Chem. 12 (2019) 2077–2083.

[21] H. Karimi-Maleh, A. Khataee, F. Karimi, M. Baghayeri, L. Fu, J. Rouhi, C. Karaman, O. Karaman, R. Boukherroub, A green and sensitive guanine-based DNA biosensor for idarubicin anticancer monitoring in biological samples: A simple and fast strategy for control of health quality in chemotherapy procedure confirmed by docking investigation, Chemosphere. 291 (2022) 132928.

[22] Y. Orooji, P.N. Asrami, H. Beitollahi, S. Tajik, M. Alizadeh, S. Salmanpour, M. Baghayeri, J. Rouhi, A.L. Sanati, F. Karimi, An electrochemical strategy for toxic ractopamine sensing in pork samples; twofold amplified nano-based structure analytical tool. Food Measure 15 (2021) 4098–4104.

[23] H. Karimi-Maleh, F. Karimi, L. Fu, A.L. Sanati, M. Alizadeh, C. Karaman, Y. Orooji, Cyanazine herbicide monitoring as a hazardous substance by a DNA nanostructure biosensor, J. Hazard. Mat. 423 (2022) 127058.

[24] H. Karimi-Maleh, O.A. Arotiba, Simultaneous determination of cholesterol, ascorbic acid and uric acid as three essential biological compounds at a carbon paste electrode modified with copper oxide decorated reduced graphene oxide nanocomposite and ionic liquid, J. Colloid Interf. Sci. 560 (2020) 208-212.

[25] H. Karimi-Maleh, M. Alizadeh, Y. Orooji, F. Karimi, M. Baghayeri, J. Rouhi, S. Tajik, H. Beitollahi, S. Agarwal, V.K. Gupta, S. Rajendran, S. Rostamnia, L. Fu, F. Saberi-Movahed, S. Malekmohammadi, Guanine-based DNA biosensor amplified with Pt/SWCNTs nanocomposite as analytical tool for nanomolar determination of daunorubicin as an anticancer drug: a docking/experimental investigation, Ind. Eng. Chem. Res. 60 (2021) 816–823.

[26] H. Karimi-Maleh, M.L. Yola, N. Atar, Y. Orooji, F. Karimi, P.S. Kumar, J. Rouhi, M. Baghayeri, A novel detection method for organophosphorus insecticide fenamiphos: molecularly imprinted electrochemical sensor based on core-shell Co3O4@MOF-74 nanocomposite, J. Colloid Interf. Sci., 592 (2021) 174-185.

[27] H. Karimi-Maleh, Y. Orooji, F. Karimi, M. Alizadeh, M. Baghayeri, J. Rouhi, S. Tajik, H. Beitollahi, S. Agarwal, V.K. Gupta, S. Rajendran, A. Ayati, L. Fu, A.L. Sanati, B. Tanhaei, F. Sen, M. Shabani-Nooshabadi, P.N. Asrami, A. Al-Othman, A critical review on the use of potentiometric based biosensors for biomarkers detection, Biosens. Bioelectron. 184 (2021) 113252.

[28] C. Cioates Negut, S.S. Gheorghe, R.-I. Stefan-van Staden, J.F. van Staden, Fast screening test for molecular recognition of levodopa and dopamine in biological samples using 3D printed stochastic microsensors, J. Pharm. Biomed. Anal. 205 (2021) 114292.

[29] R.-I. Stefan-van Staden, D.-C. Gheorghe, R.-M. Ilie-Mihai, L.-B. Tudoran, S.M. Pruneanu, Stochastic biosensors based on N- and S-doped graphene for the enantioanalysis of aspartic acid in biological samples, RSC Adv. 11 (2021) 23301–23309.

[30] R.-M. Ilie-Mihai, R.-I. Stefan-van Staden, L. Magerusan, M. Coros, S. Pruneanu, Enantioanalysis of tryptophan in whole blood samples using stochastic sensors—a screening test for Gastric Cancer, Chirality. 32 (2019) 215–222.

[31] C. Surdu-Bob, I. Mustata, C. Iacob, General characteristics of the Thermoionic Vacuum Arc plasma, J. Optoelectron. Adv. M., 9 (2007) 2932–2934.

[32] R.-I. Stefan-van Staden, S.S. Gheorghe, R.-M. Ilie-Mihai, M. Badulescu, Disposable stochastic sensor based on deposition of a nanolayer of silver on silk for molecular recognition of specific biomarkers, J. Electrochem. Soc. 168 (2021) 037515.

[33] R.-I. Stefan-van Staden, L.A. Gugoaşă, M. Badulescu, C.C. Surdu-Bob, Novel textile material based disposable sensors for Biomedical Analysis, RSC Adv. 5 (2015) 45545–45550.

[34] R.-I. Stefan-van Staden, I. Moldoveanu, C.C. Surdu-Bob, M. Badulescu, J.F. van Staden, Carbon modified paper based sensors, J. Electrochem. Soc. 162 (2015) B360–B362.

Nanographene-based electrochemical sensors for ultrasensitive determination of sorbic acid from food.

ABSTRACT

Two sensors based on nanographene decorated with gold nanoparticles paste modified with metal porphyrins (Zn protoporphyrin IX, and 2,3,7,8,12,13,17,18 octaethyl, 21H, 23H-porphirine Mn(III) chloride) were proposed for the determination of sorbic acid in bakery products and mayonnaise. The sensors were characterized using SEM and impedance. Response characteristics shown that the limits of detection for both sensors were of 0.33 µmol L^{-1} while the limits of quantification were 1 µmol L^{-1}. Both sensors can be used between 1 and 1000 µmol L^{-1}. The highest sensitivity (0.35nA/ µmol L^{-1}) was recorded when the sensor based on 2,3,7,8,12,13,17,18 octaethyl, 21H, 23H-porphirine Mn(III) chloride was used. High recoveries (values higher than 95.00%) and low RSD (%) values (lower than 5.00%) were recorded for both sensors when used for the determination of sorbic acid in bread and mayonnaise.

1. Introduction

Known as E200 in food industry, sorbic acid (2,4-hexadienoic acid) is a natural organic compound used as food preservative. Its role is to keep the organoleptic properties of foods in the global food chain, and to extend the shelf life of products. It has antimicrobial properties, and has positive properties on the human body, if used in reasonable quantities helping to detoxify and stimulate immunity. It is very effective in inhibiting the growth of molds, yeasts and fungi, which can spoil food and spread deadly diseases. Sorbic acid is widely used to inhibit yeast and mold in processed cheese, for various types of juices and wine and some bakery products. It is also used in processed meat as an alternative to nitrites. The main food groups that contribute to

the daily intake of nutrients have a sorbic acid content, which varies between 200–2000 mg / kg (liquid egg 5000 mg/kg, cooked seafood 6000 mg/kg) and soft drinks, wine 200 –300 mg/kg (grape juice 2000 mg/kg, liquid tea concentrates 600 mg/kg). The acceptable daily intake (ADI) for sorbic acid is 25 mg/kg body weight. Due to its importance in food industry correlated with the health state of population, there is a need to develop fast, cost-effective, reliable methods of analysis of sorbic acid in foods.

To date, the methods proposed for the assay of sorbic acid are: chromatographic methods of analysis [1-4], capillary electrophoresis [5-7], electrochemical methods of analysis [8], and proton nuclear magnetic resonance spectroscopic method of analysis [9].

Electrochemical methods of analysis are highly reliable and cost-effective, a minimum sampling being needed before the measurements. Therefore, this paper proposed new electrochemical sensors as tools for screening of bread and mayonnaise for sorbic acid. Two sensors based on nanographene decorated with gold nanoparticles paste modified with metal porphyrins (Zn protoporphyrin IX, and 2,3,7,8,12,13,17,18 octaethyl, 21H, 23H-porphirine Mn(III) chloride) were designed, characterized and validated for the determination of sorbic acid in bread and mayonnaise. Graphenes are the materials of choice for many researchers in the field of electrochemical sensors; utilization of nanographenes increased the sensitivity of the measurements by increasing the area of the active surface of the electrochemical sensors [10]. Modification of the nanographene material with gold nanoparticles improved the conductivity of nanographene, while porphyrins are well known for their electrocatalytic activity when used in amperometric/voltametric sensors' design [11].

2. Experimental

2.1. Materials and reagents

Sorbic acid, zinc protoporphyrin IX (ZnPIX), 2,3,7,8,12,13,17,18-Octaethyl-21H,23H-porphine manganese (III) chloride (Mn(TPP)Cl), nanographene powder (6-8 nm) (NPs-Gr), gold

nanoparticles (10 nm diameter, OD 1, stabilized suspension in 0.1 mmol L^{-1} PBS, reactant free), monosodium phosphate, disodium phosphate, sucrose, glucose, sodium benzoate, potassium sulphate, magnesium chloride, ascorbic acid, sodium acetate, fructose, ethyl propionate, potassium sorbate, were purchased from Sigma Aldrich, and paraffin oil (d_4^{20}, 0.86 g cm^{-1}) was purchased from Fluka (Buchs, Sweden).

The phosphate buffer solution (PBS, 0.1 mol L^{-1}) was prepared mixing monosodium phosphate and disodium phosphate solutions. The pH of the buffer solution was adjusted using different amounts of 0.1 mol L^{-1} NaOH or HCl solutions to obtain different pH values (2.0, 3.0, 4.0, 5.0, 6.0, 7.0 and 8.0). The stock solution of 10^{-2} mol L^{-1} sorbic acid was prepared fresh, before measurements, in deionized water.

2.2. Apparatus and methods

The cyclic voltammetry (CV), square wave voltammetry (SWV) and electrochemical impendence spectroscopy (EIS) measurements were carried out using a mini potentiostat EmSTAT Pico (software PsTrace 5.8 PalmSens) connected to a laptop for data acquisition. All electrochemical experiments were carried out at room temperature. The results were recorded using an electrochemical cell containing three electrodes: the modified nanographene paste electrode, Ag/AgCl (0.1 mol L^{-1} KCl) and Pt-wire as working, reference and auxiliary electrodes, respectively. The pH adjustment was done using a Mettler Toledo pH meter.

The surface morphology of the studied samples was investigated using scanning electron microscopy (SEM) (Inspect S), FEI Company Netherlands. All samples were analyzed in high vacuum mode using the ETD detector, high voltage (HV) of 30 kV, at 3000 magnification order.

2.3. Design of the electrochemical sensor

To prepare the electrochemical sensors for the assay of sorbic acid, the following steps were done: 40mg nanographene powder were mixed with 4 µL gold nanoparticles stabilized suspension (in 0.1 mmol L^{-1} PBS), and paraffine oil was added until a homogeneous paste was obtained. The paste was divide in two parts and to each part a solution of 20 µL 10^{-3} mol L^{-1}solution of porphyrin (zinc protoporphyrin IX,2,3,7,8,12,13,17,18-Octaethyl-21H,23H-porphine manganese (III) chloride, respectively) to obtain ZnPIX/AuNPs-Gr, and Mn(TPP)Cl/AuNPs-Gr electrodes. Two non-conducting plastic tubes designed using a 3D printer in our laboratory were filled with the modified pastes. A silver wire served as electrical contact between the modified paste and external circuit.

2.4. Samples preparation

The sample used for the sensors' validation were: white bread, black bread and light mayonnaise. 10 mL of PBS (pH=2) were added to 1g of black/white bread. The resulting mixture was vortexed for 4min and left in the ultrasonic bath for 30min.

1g of the mayonnaise sample was weighed to the analytical balance, it was dissolved in 10 mL of PBS (pH=2), and vortexed for 4min.

3. Results and Discussions

3.1. SEM characterization of the active surface of the electrochemical sensors

SEM images were used to characterize the surface morphology of the AuNPs-Gr ZnPIX/AuNPs-Gr, and Mn(TPP)Cl/AuNPs-Gr pastes.

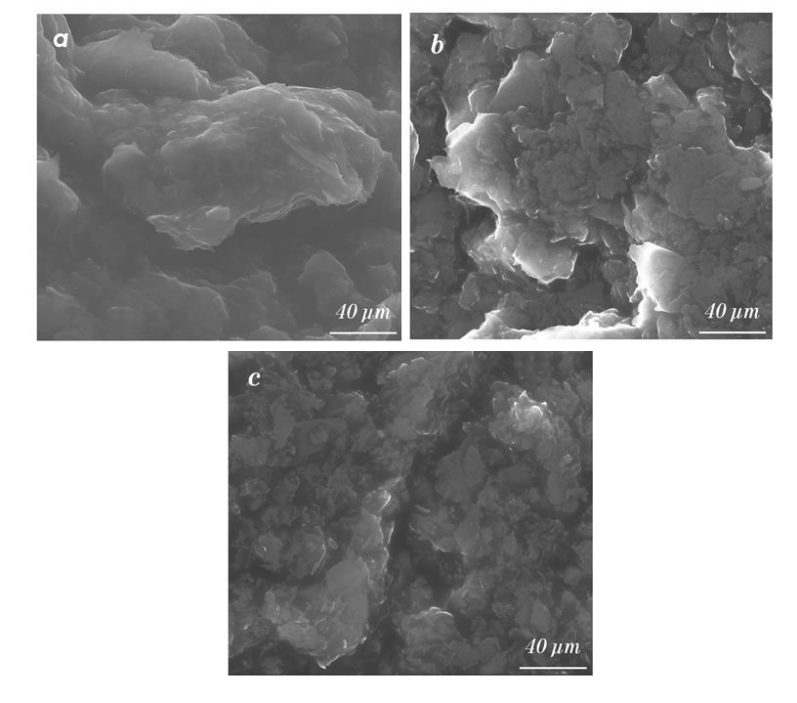

Figure 1. SEM images of (a) AuNPs-Gr, (b) ZnPIX/AuNPs-Gr, and (c) Mn(TPP)Cl/AuNPs-Gr pastes.

As shown in Figure 1 (a), the representative SEM image exhibit flat sheets presented in thin layers of nanosheets. In the case of ZnPIX/AuNPs-Gr paste (Fig. 1b) and Mn(TPP)Cl/AuNPs-Gr paste (Fig. 1c) the flat sheets are closely associated with each other, presented in aggregated forms.

3.2. Electrochemical characterization of the sensors

Electrochemical characterization of sensors ZnPIX/AuNPs-Gr and Mn(TPP)Cl/AuNPs-Gr versus the sensor based on AuNPs-Gr was performed using the following methods: cyclic voltammetry (CV) and electrochemical impedance spectroscopy (EIS) (Figure 4).

CV was used to study the electrochemical response of the modified sensors (Figure 4(a)). Cyclic voltammetry measurements were performed in a solution of 5.0×10^{-3}mol L^{-1} $K_3[Fe(CN)_6]$ (0.1 mol L^{-1} KCl) in a potential range between -0.6V and 1.0V, using as working electrodes, AuNPs-Gr, ZnPIX/AuNPs-Gr, Mn(TPP)Cl/AuNPs-Gr, (Figure 2(a)). It can be seen

that after modifying the AuNPs paste with solutions of ZnPIX and Mn(TPP)Cl the conductivity of the sensor increased. Accordingly, the modification of the sensors and the electrochemical response was improved.

The EIS study was performed to examine the sensor interface in a frequency range of 1.0 × 10^5 to 1.0 × 10^{-1}Hz. All EIS measurements were performed in a solution of 5.0 × 10^{-3} mol L^{-1} $K_3[Fe(CN)_6]$ (0.1 mol L^{-1} KCl). In Figure 4(b) are represented the Nyquist plots. In the Figure 2(b) it is observed that the largest semicircle belongs to the unmodified sensor, with Rct = 3.548 x 10^6Ω, the smallest semicircle belongs to the ZnPIX/AuNPs-Gr sensor (Rct = 399.5Ω), while for the Mn(TPP)Cl/AuNPs-Gr sensor, the diameter of the semicircle decreased to Rct = 1389 Ω. Therefore, the ZnPIX/AuNPs-Gr sensor showed a smaller semicircle and a lower Rct value than the Rct values obtained for the AuNPs-Gr sensor and Mn(TPP)Cl/AuNPs-Gr sensor. The EIS results showed that they are consistent with the results obtained by cyclic voltammetry (CV), which were obtained for a solution of 5.0 × 10^{-3} mol L^{-1} $K_3[Fe(CN)_6]$ (0.1 mol L^{-1} KCl).

The electrochemical behavior of the three sensors was examined using the square wave voltammetry (SWV) method, in a solution containing 400μmol L^{-1} sorbic acid buffered with PBS at pH=2.0. The voltammograms recorded for all sensors are illustrated in Figure 2(c). Comparing the three sensors (Figure 2(c)), using the SWV method, the ZnPIX/AuNPs-Gr sensor and the Mn(TPP)Cl/AuNPs-Gr sensor gave the best results for the oxidation of sorbic acid. The Mn(TPP)Cl/AuNPs-Gr sensor performed much better than the ZnPIX/AuNPs-Gr sensor. Therefore, the Mn(TPP)Cl/AuNPs-Gr sensor and the ZnPIX/AuNPs-Gr sensor were further characterized and tested for the electrochemical determination of sorbic acid in real food samples, such as white bread, black bread and mayonnaise.

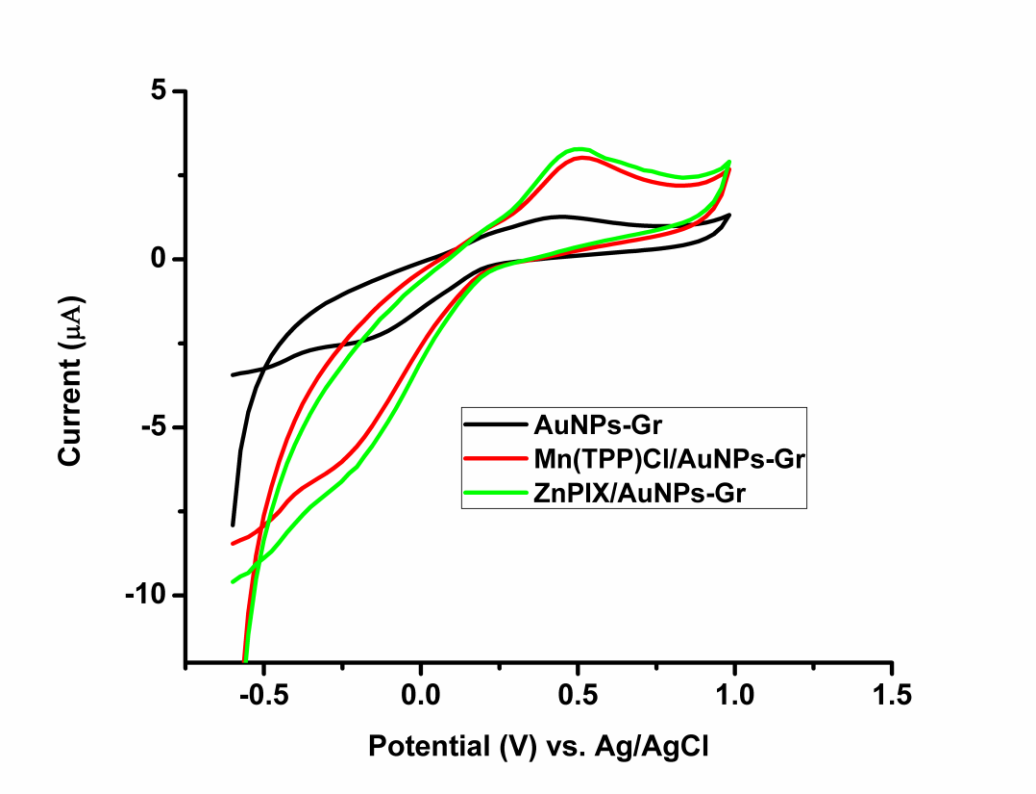
5
0
-5
-10
Current (μA)
-0.5
0.0
0.5
1.0
1.5
Potential (V) vs. Ag/AgCl
AuNPs-Gr
Mn(TPP)Cl/AuNPs-Gr
ZnPIX/AuNPs-Gr

Fig.2(a)

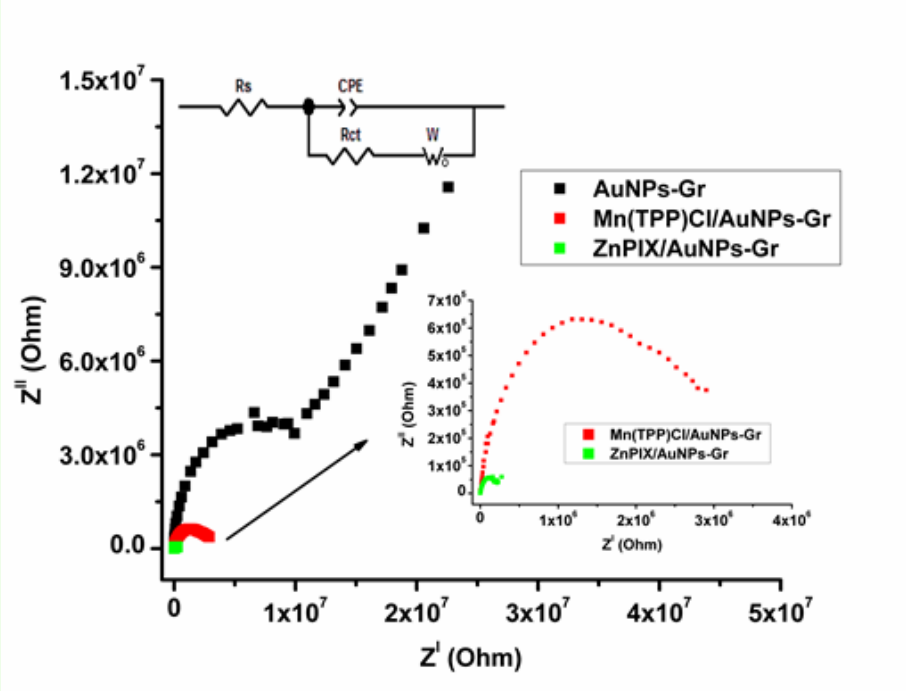
Rs
CPE
Rct
W
1.5x10^7
1.2x10^7
9.0x10^6
6.0x10^6
3.0x10^6
0.0
Z'' (Ohm)
0
1x10^7
2x10^7
3x10^7
4x10^7
5x10^7
Z' (Ohm)
AuNPs-Gr
Mn(TPP)Cl/AuNPs-Gr
ZnPIX/AuNPs-Gr
7x10^5
6x10^5
5x10^5
4x10^5
3x10^5
2x10^5
1x10^5
0
1x10^6
2x10^6
3x10^6
4x10^6

Fig. 2(b)

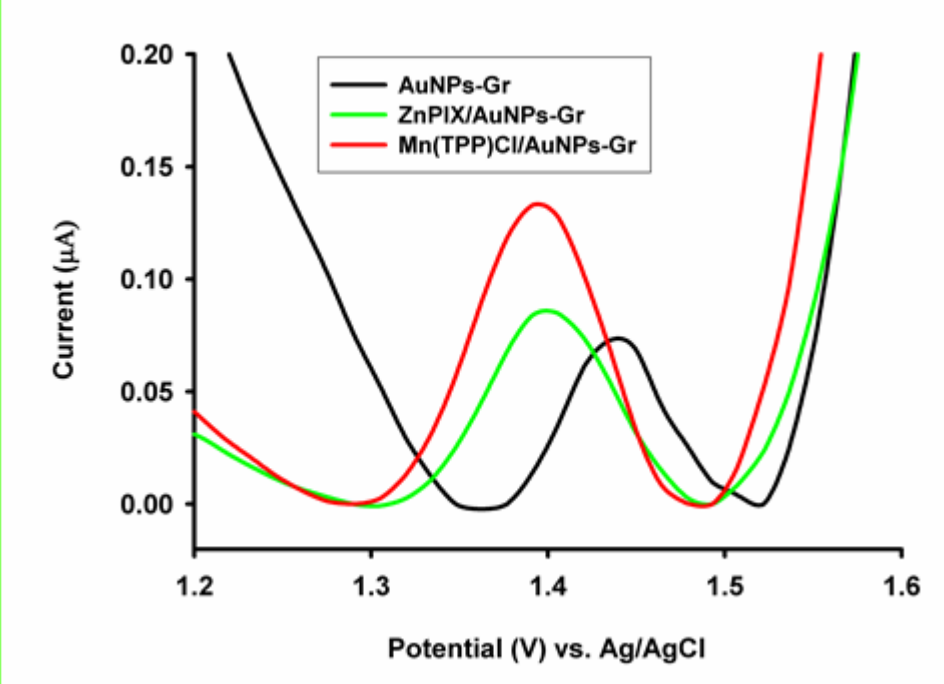

Fig. 2(c)

Figure 2. (a) Cyclic voltammograms of the current plotted against the potential (Working conditions: step potential 0.025 V; scan rate 0.1 V/s) in asolution of 5.0×10^{-3} mol L^{-1} $K_3[Fe(CN)_6]$ in 0.1 mol L^{-1} KCl using the AuNPs-Gr (black line), Mn(TPP)Cl/AuNPs-Gr (red line) and ZnPIX/AuNPs-Gr (green line); (b) Electrochemical impedance spectra recorded for AuNPs-Gr (black line), Mn(TPP)Cl/AuNPs-Gr (red line) and ZnPIX/AuNPs-Gr (green line) in a solution of 5.0×10^{-3} mol L^{-1} $K_3[Fe(CN)_6]$ in 0.1 mol L^{-1} KCl (Conditions: frequency range between 1.0×10^{5} to 1.0×10^{-1} Hz). Inset: equivalent circuit diagram of the electrochemical interface used to fit the impedance spectra where R_s is the solution resistance, CPE is the constant phase element, R_{ct} is the electron-transfer resistance, and Z_w is the Warburg diffusion resistance; (c) The recorded square-wave voltammograms in pH 2.0 PBS containing 400 μmol L^{-1} sorbic acid for the AuNPs-Gr (black line), ZnPIX/AuNPs-Gr (green line) and Mn(TPP)Cl/AuNPs-Gr (red line).

The electrocatalytic activity of the three sensors was investigated by calculating the electroactive surface area using the Randles-Sevcik equation.

By variation of the scan rate from 0.010 to 0.100 V/s, the anodic and cathodic peaks (Ip_a and Ip_c) showed a linear dependency on the square root of the scan rate, suggesting that the

redox process was controlled by diffusion. Figures 3 (a) and 4 (a) shows the trend between the increase of the scan rate and intensity of the current. The linear dependences for both peaks Ip_a *vs.* $\nu^{1/2}$ and Ip_c *vs.* $\nu^{1/2}$ are presented in Figures 3(b) and 4(b). The ZnPIX/AuNPs-Gr sensor had a bigger value for the area ($0.0041cm^2$) compared to the value ($0.0038cm^2$) obtained for the Mn(TPP)Cl/AuNPs-Gr sensor, and with the value ($0.0015cm^2$) obtained for the area of the AuNPs-Gr sensor (Figure S1).

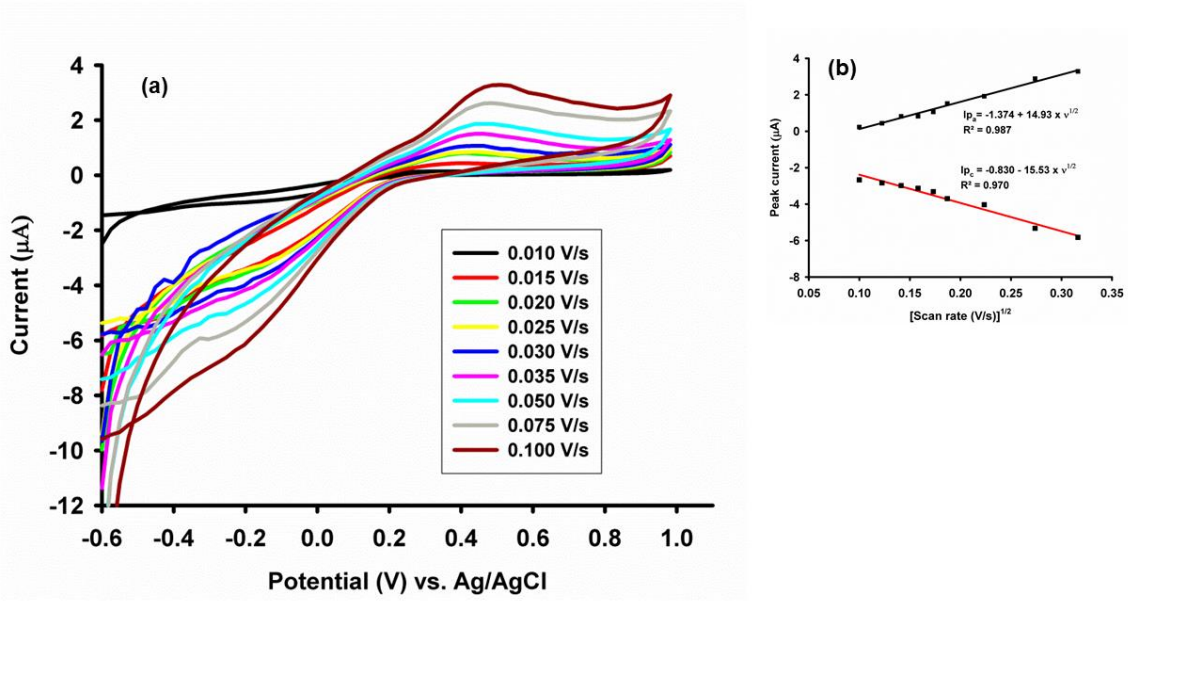

Figure 3. (a) Cyclic voltammograms in a solution of 5.0×10^{-3} mol L^{-1} $K_3[Fe(CN)_6]$ in 0.1 mol L^{-1} KCl at different scans rate from 0.010 to 0.100 V/s using the ZnPIX/AuNPs-Gr (Working conditions: potential range from -0.6 V to1.0 V; step potential 0.025 V);

(b) Dependence of the peak current on the square root of the scan rate, using the ZnPIX/AuNPs-G sensor.

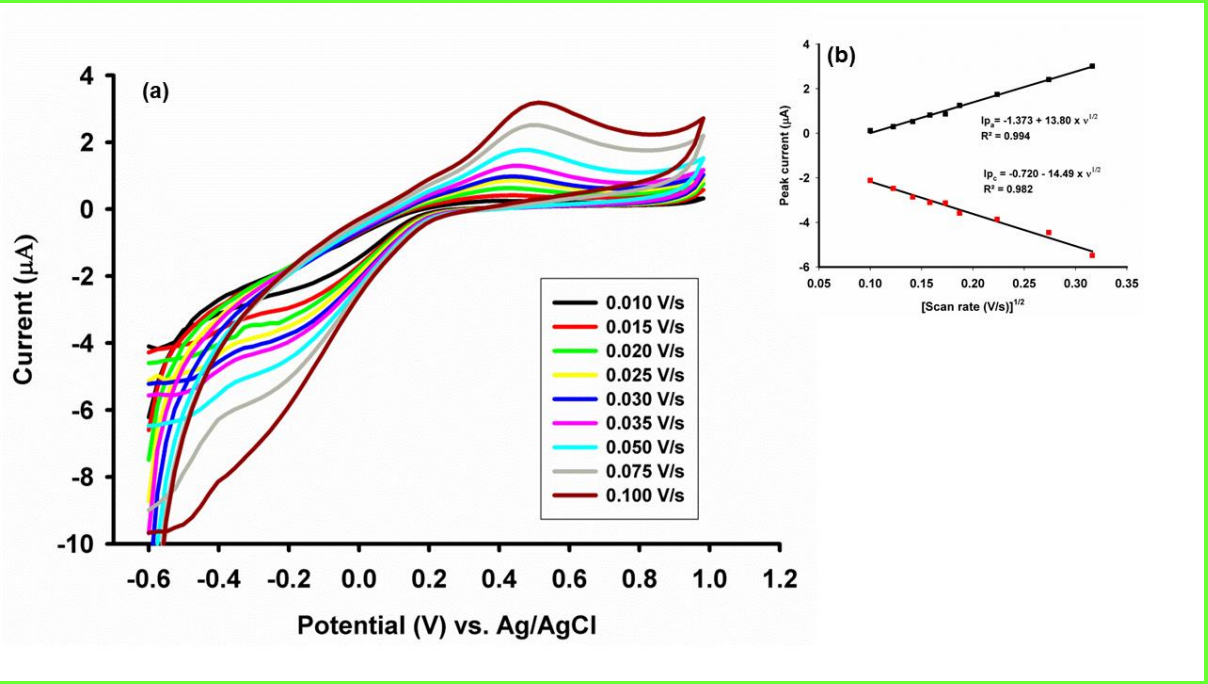

Figure 4. (a) Cyclic voltammograms in a solution of 5.0×10^{-3} mol L^{-1} $K_3[Fe(CN)_6]$ in 0.1 mol L^{-1} KCl at different scans rate from 0.010 to 0.100 V s^{-1} using the Mn(TPP)Cl/AuNPs-Gr sensor. (Working conditions: potential range from -0.6 V to1.0 V; step potential 0.025V);
(b) Dependence of the peak current on the square root of the scan rate, using the Mn(TPP)Cl/AuNPs-Gr sensor.

3.4. The influence of the pH value on the electrochemical behaviour of the sensors

The value of the pH of the solution is essential in electrochemical measurements. For determining the influence of the pH value on the assay of sorbic acid, a solution of sorbic acid with the concentration 100µmol L^{-1} was buffered with PBS at different pH values (2.0, 3.0, 4.0, 5.0, 6.0, 7.0, and 8.0). Figure 5 shows that for the ZnPIX/AuNPs-Gr sensor the intensity of the electric current decreased from pH = 2.0 to 5.0 with an obvious increase to pH = 6.0 and 7.0 then began to decrease until pH = 8.0 was reached (Figure 5). Figure 5 shows that at pH 2.0 the highest current intensity was achieved for the assay of sorbic acid. At a low pH value (acid medium) sorbic acid tends to oxidize more easily than at a high pH value (alkaline medium), which seems to be due to the fact that at alkaline pH it turns into its sorbent ion, which is less prone to oxidate. Therefore, the optimum pH value was 2.0.

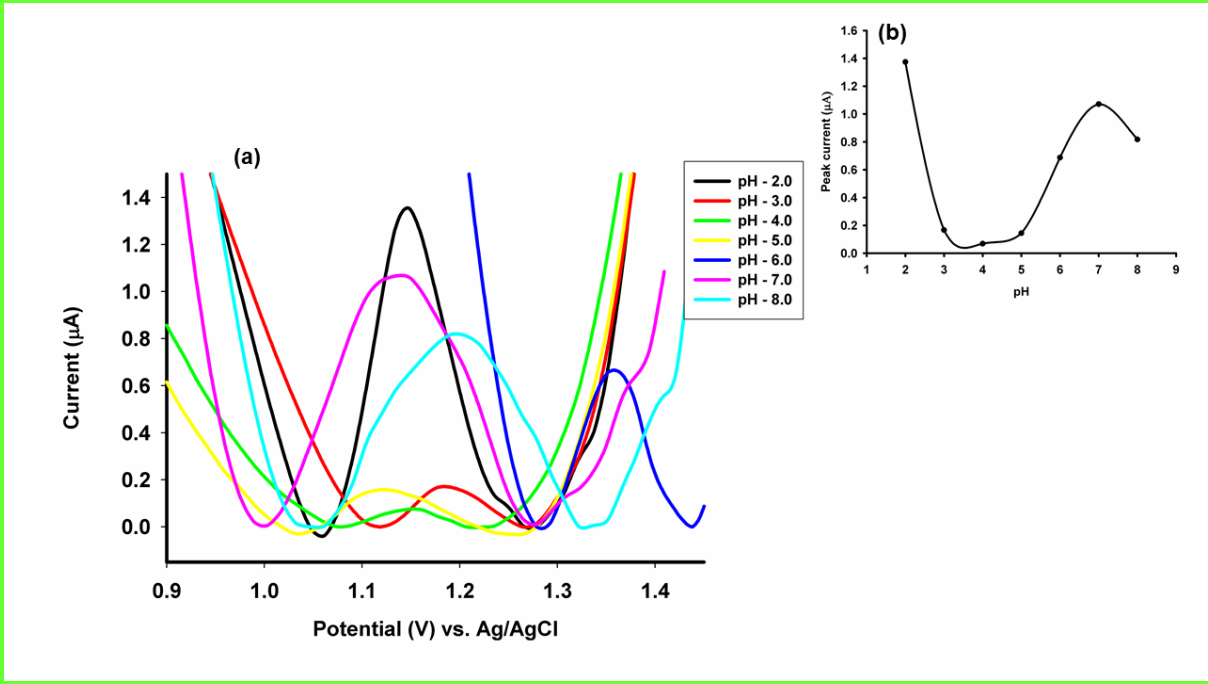

Figure 5. (a) Square-wave voltammograms of 100 μmol L^{-1} sorbic acid obtained using the ZnPIX/AuNPs-Gr sensor when the solution was buffered with PBS at the following pH values of 2.0, 3.0, 4.0, 5.0, 6.0, 7.0 and 8.0; (b) The effect of the pH on the peak current.

The same way was followed for the Mn(TPP)Cl/AuNPs-Gr sensor. Figure 6 shows that the intensity of the electric current decreased from pH = 2.0 to pH3.0, then increases to pH 4.0, decreases to pH 6.0, followed by an increase to pH 7.0, then a final decrease to pH 8.0. Figure 6 shows that at pH 2.0 is the highest current intensity for the assay of sorbic acid. Therefore, pH 2.0 was selected as optimum pH.

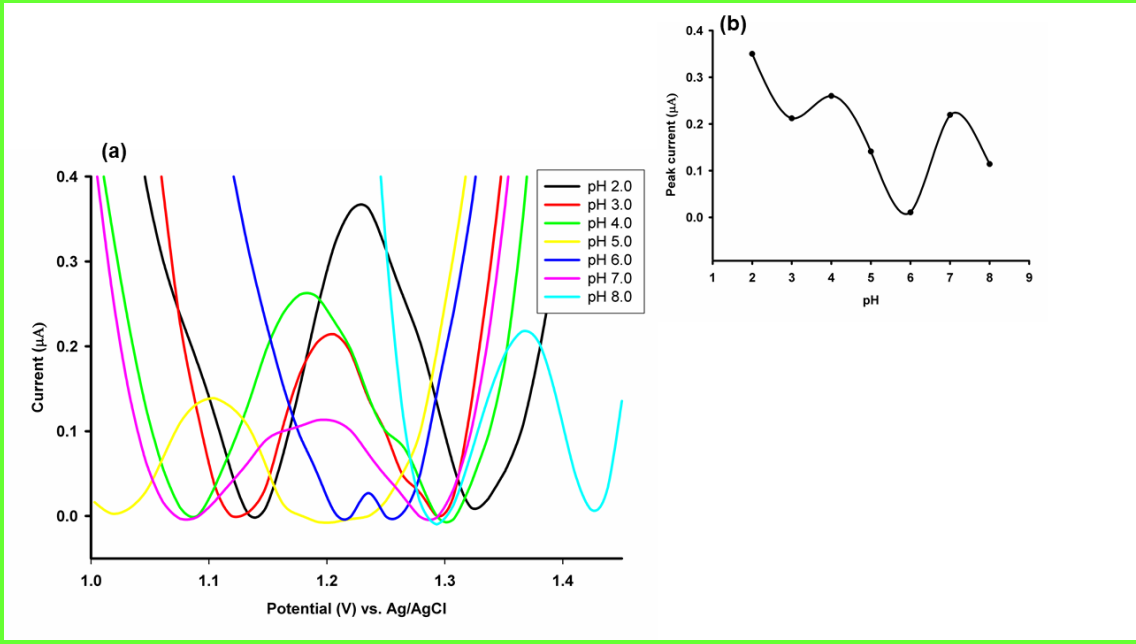

Figure 6. (a) (a) Square-wave voltammograms of 100 µmol L-1 sorbic acid obtained using the Mn(TPP)Cl/AuNPs-Gr sensor when the solution was buffered with PBS at the following pH values of 2.0, 3.0, 4.0, 5.0, 6.0, 7.0 and 8.0; (b) The effect of the pH on the peak current.

3.5. Response characteristics of the electrochemical sensors

The response characteristics of the proposed electrochemical sensors were determined using square-wave voltammetry, at the optimum pH value (2.0) and are summarized in Table 1.

Table 1. Response characteristics of the electrochemical sensors used for the determination of sorbic acid

Parameter	Electrochemical sensor	
	ZnPIX/AuNPs-Gr sensor	Mn(TPP)Cl/AuNPs-Gr sensor
Equation of calibration*	Ip_a=-5.29+0.22xC; r=0.9985	Ip_a=-5.01+0.35xC; r=0.9984
Linear concentration range (µmol L^{-1})	1-1000	1-1000
Sensitivity (nA/µmol L^{-1})	0.22±0.03	0.35±0.02
Limit of detection (µmol L^{-1})	0.33	0.33
Limit of determination (µmol L^{-1})	1	1
Repetability of peak current (%, RSD)	5.56	5.41

*<Ip_a>=nA; <C>=µmol L^{-1}

Figure 7 showed for the ZnPIX/AuNPs-Gr sensor the peaks obtained during the calibration as well as the calibration graph for sorbic acid. The linear concentration range was between 1 and 1000 µmol L^{-1} with a correlation coefficient of 0.9985. The limit of detection was 0.33 µmol/L, which was calculated as a third from the limit of quantification (the lowest concentration from the linear concentration range, 1 µmol L^{-1}).

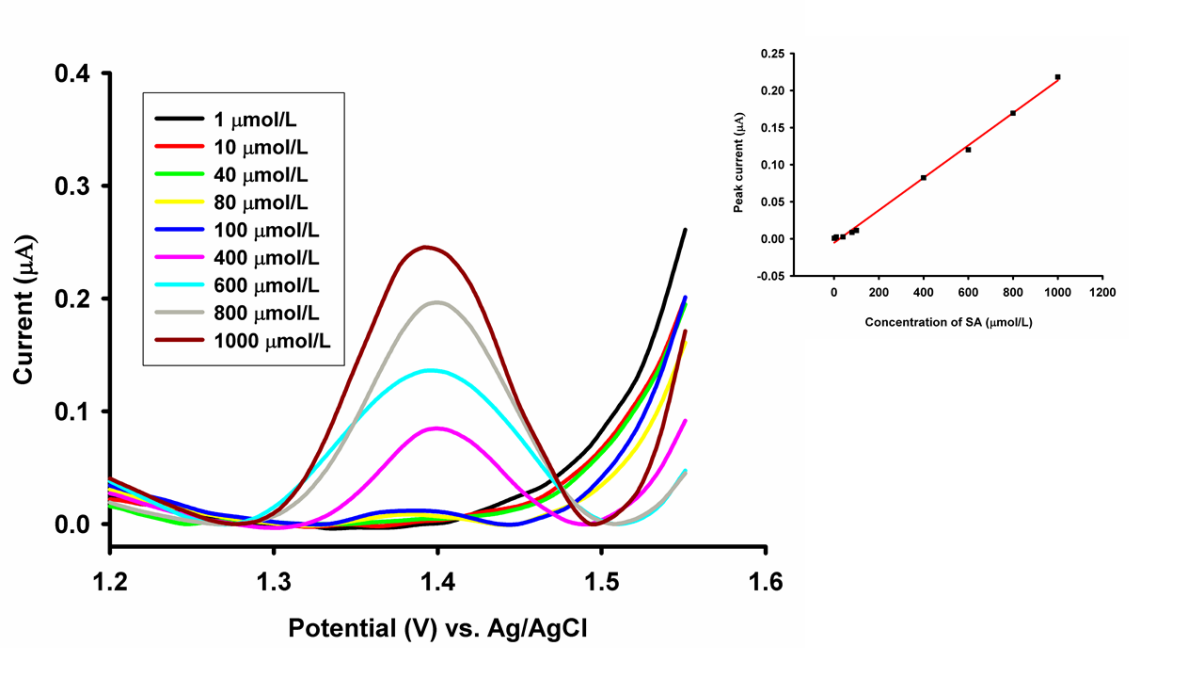

Figure 7 Square-wave voltammograms recorded with the ZnPIX/AuNPs-Gr sensor in PBS pH = 2.0 containing different concentrations of sorbic acid (1 to 1000 µmol L^{-1}), and the calibration graph obtained with the ZnPIX/AuNPs-Gr sensor from 1 to 1000 µmol L^{-1}. Working conditions: step potential of 0.025 V and frequency of 5.0 Hz.

The sensitivity of the ZnPIX/AuNPs-Gr sensor was 0.22 nA μmol^{-1} L.

Figure 8 showed the voltammograms obtained during the calibration of the Mn(TPP)Cl/AuNPs-Gr sensor, as well as the calibration graph for sorbic acid. The linear concentration range was between 1 and 1000 µmol L^{-1}. The limit of detection (calculated as a third from the limit of quantification) was 0.33 µmol L^{-1}. The sensitivity recorded for this sensor was 0.35 nA μmol^{-1} L.

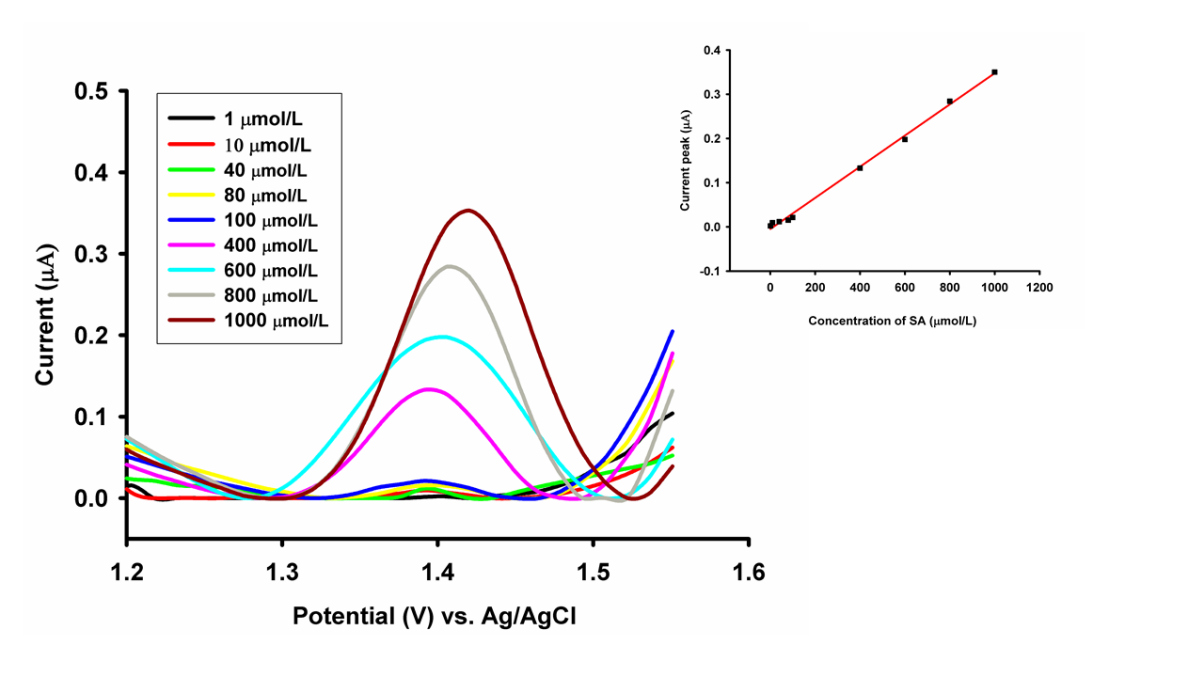

Figure 8. (a) Square-wave voltammograms recorded with the Mn(TPP)Cl/AuNPs-Gr sensor in PBS pH = 2.0 containing different concentrations of sorbic acid (1 to 1000 µmol L^{-1}); (b) Calibration curve obtained with the Mn(TPP)Cl/AuNPs-Gr sensor from 1 to 1000 µmol L^{-1}. Working conditions: step potential of 0.025 V and frequency of 5.0 Hz.

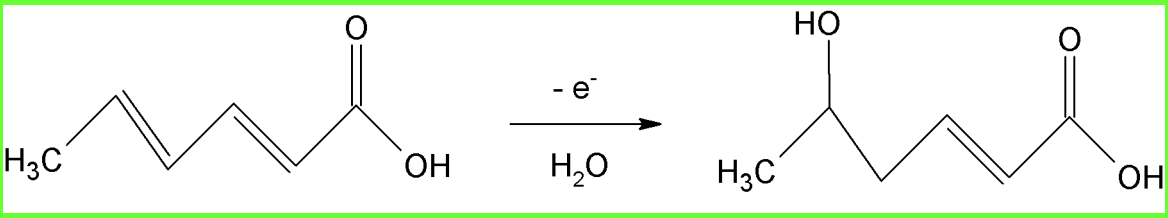

Scheme 1. The possible mechanism of the electrochemical oxidation of sorbic acid in acidic media (pH = 2)

The possible mechanism of reaction of sorbic acid is presented in **Scheme 1**, and involves the breaking of one double bond and the addition of OH^- followed by the chemical deprotonation of the oxidation product.

While the limits of quantification and detection as well as the linear concentration ranges are the same for both sensors, the sensitivity of the Mn(TPP)Cl/AuNPs-Gr sensor is higher. Therefore, this is the sensor of choice.

3.6. Interference studies

For the selectivity study, several ions, such as COO^{-}, $Mg2^{+}$, $SO4^{2-}$ and organic species such as sucrose, glucose, fructose, ascorbic acid, sodium benzoate, ethyl propionate, potassium sorbate, were tested as possible interferences in determination of sorbic acid. Possible interfering substances were chosen from substances commonly found with sorbic acid in white bread, black bread and mayonnaise. The tolerance limit was defined as the maximum interference concentration that caused a change in current intensity in terms of relative error (± 5% acceptance level) and bias (%) and signal changed (%). All evaluated solutions were obtained under optimal conditions, pH=2.0 PBS with a constant concentration of sorbic acid (400 µmol/L). The experimental results did not show any obvious influence on the detection of sorbic acid when a 10-fold excess of ascorbic acid for Ethyl propionate and Sucrose and a 1:1 ratio of CH3COO-, ascorbic acid, sodium benzoate, fructose, glucose, $SO4^{2-,}$ Mg^{2+}. (Table 2, Figure 9).

Table 2. Tolerance of interferences on the detection of 400 µmol/L sorbic acid using the ZnPIX/AuNPs-Gr sensor.

Interferent	**Tolerance level ratio (interferent: sorbic acid)**	**Signal changed (%)**	**Relative error (%)**	**Bias (%)**
Ethil propionate	10:1	-2.78	-2.71	-6.76
Sucrose	10:1	2.16	2.21	-5.37
CH_3COO^-	1:1	0.70	0.70	2.89
Ascorbic acid	1:1	-0.91	-0.90	0.61

Sodium benzoate	1:1	0.37	0.37	-1.18
Fructose	1:1	-2.18	-2.14	2.32
Glucose	1:1	0.62	0.62	2.32
SO_4^{2-}	1:1	0.20	0.20	3.34
Mg^{2+}	1:1	-3.14	-3.04	-6.03
Potassium sorbate	1:1	0.94	0.95	2.47

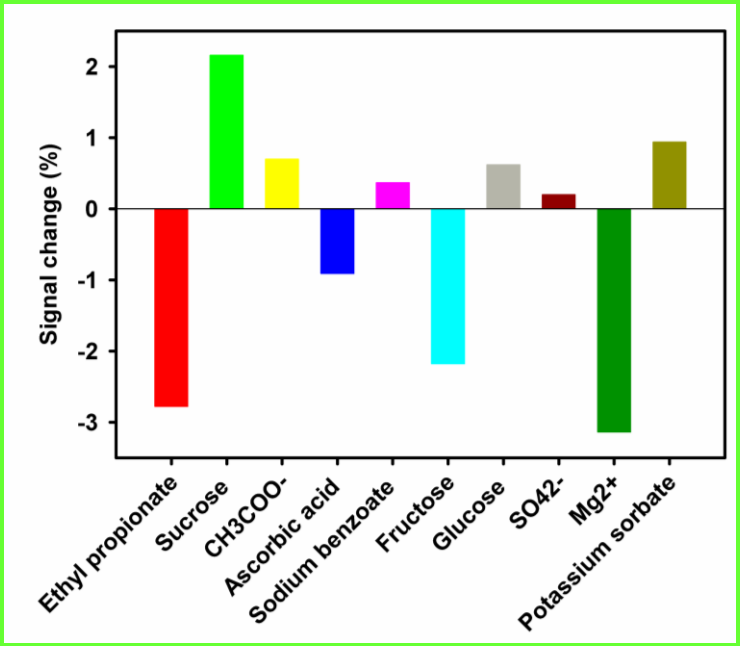

Figure 9. Selective responses of the ZnPIX/AuNPs-Gr sensor. $C_{sorbic\ acid}$= 400 µmol L^{-1}.

For the Mn(TPP)Cl/AuNPs-Gr sensor, the experimental results did not show any obvious influence on the detection of sorbic acid when a 10-fold excess of sucrose, $CH3COO^-$, sodium benzoate, fructose, Mg^{2+} and a 1:1 ratio of etil propionate, ascorbic acid, glucose, $SO4^{2-}$, potassium sorbate were used for the selectivity studies (Table 3, Figure 10).

Table 3. Tolerance of interferences on the detection of 400 µmol/L sorbic acid using Mn(TPP)Cl/AuNPs-Gr sensor.

Interferent	**Tolerance level ratio (interferent: sorbic acid)**	**Signal changed (%)**	**Relative error (%)**	**Bias (%)**

Sucrose	10:1	0.02	0.02	-0.39
CH_3COO^-	10:1	-3.26	-3.16	5.65
Sodium benzoate	10:1	-2.95	-2.86	0.41
Fructose	10:1	-0.38	-0.38	1.20
Mg^{2+}	10:1	4.38	4.58	-6.45
Etil propionat	1:1	-2.99	-2.91	-0.10
Ascorbic acid	1:1	-3.26	-4.50	-8.46
Glucose	1:1	-1.00	-0.99	0.41
SO_4^{2-}	1:1	2.47	2.53	-7.05
Potassium sorbate	1:1	-2.98	-2.89	-10.02

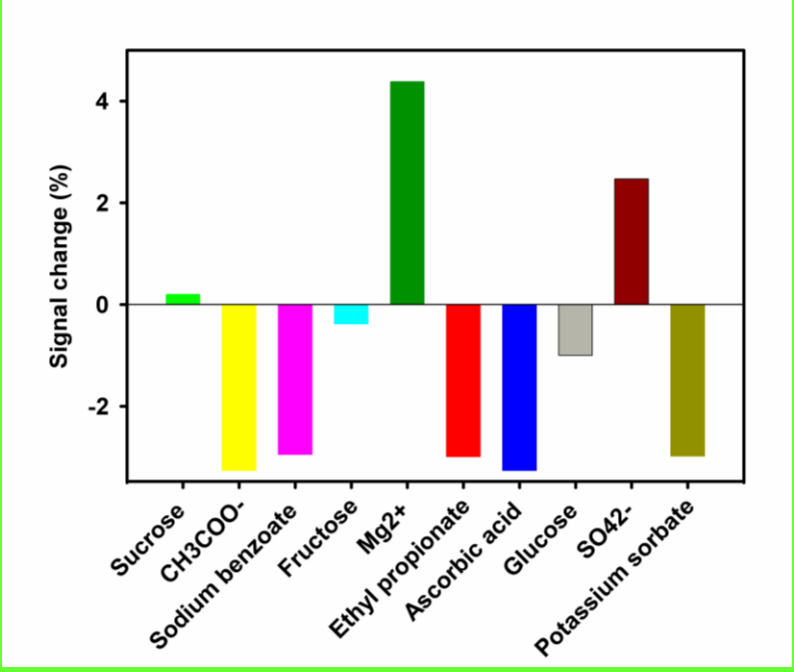

Figure 10. Selective responses of the Mn(TPP)Cl/AuNPs-Gr sensor. $C_{sorbic\ acid}$= 400 µmol L^{-1}.

3.7. Reproducibility, repeatability and stability

Reproducibility, repeatability and stability were tested under optimal working conditions using SWV for both sensors: ZnPIX/AuNPs-Gr sensor, and Mn(TPP)Cl/AuNPs-Gr sensor in a solution of sorbic acid of 400µmol L^{-1} prepared in PBS pH=2.0. To evaluate the reproducibility, 3 new sensors of each type. The relative standard deviation (RSD%) was 2.47% (n=4) for the ZnPIX/AuNPs-Gr sensor, and 0.76% (n=4) for the Mn(TPP)Cl/AuNPs-Gr sensor. The results

obtained were correlated with repeatability. For the same sensors, the repeatability between days was determined to be 4.31% for 4 repetitive measurements, for both sensors. Then, the stability of the sensors was examined by keeping the electrodes at room temperature for seven days. After 7 days, in the case of the ZnPIX/AuNPs-Gr sensor (Figure 11), the intensity of the current measured for the above concentration of sorbic acid was 87.32% (representing the ratio between the value of the intensity of current measured in the 7th day, and the intensity of current measured in the first day multiplied by 100) with a RSD (%) value of 5.41%; and in the case of the Mn(TPP)Cl/AuNPs-Gr sensor (Figure 12) the intensity of the current measured for the above concentration of sorbic acid was 86.37% (representing the ratio between the value of the intensity of current measured in the 7th day, and the intensity of current measured in the first day multiplied by 100) with a RSD (%) value of 5.56%. The above results demonstrated good stability and reproducibility of the proposed sensor in the detection of sorbic acid.

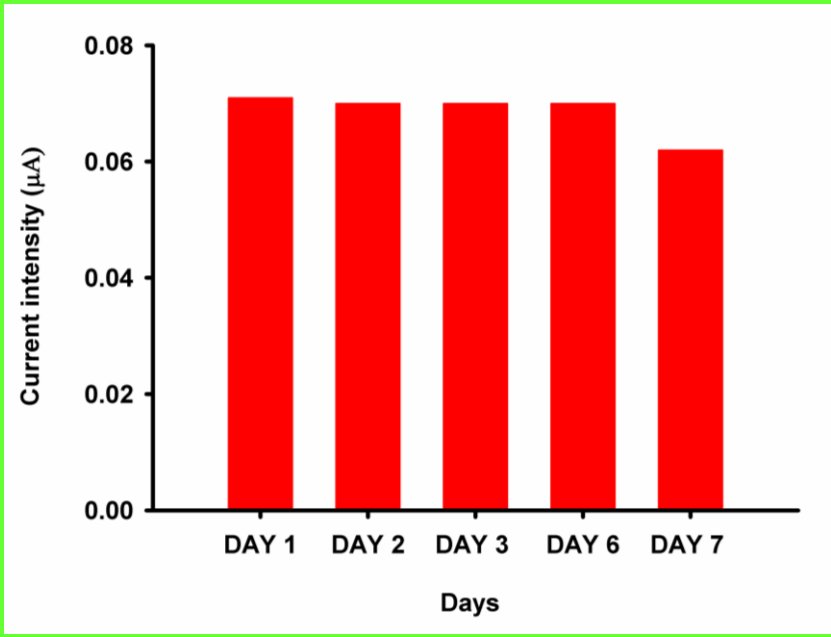

Figure 11. Stability of the ZnPIX/AuNPs-Gr sensor.

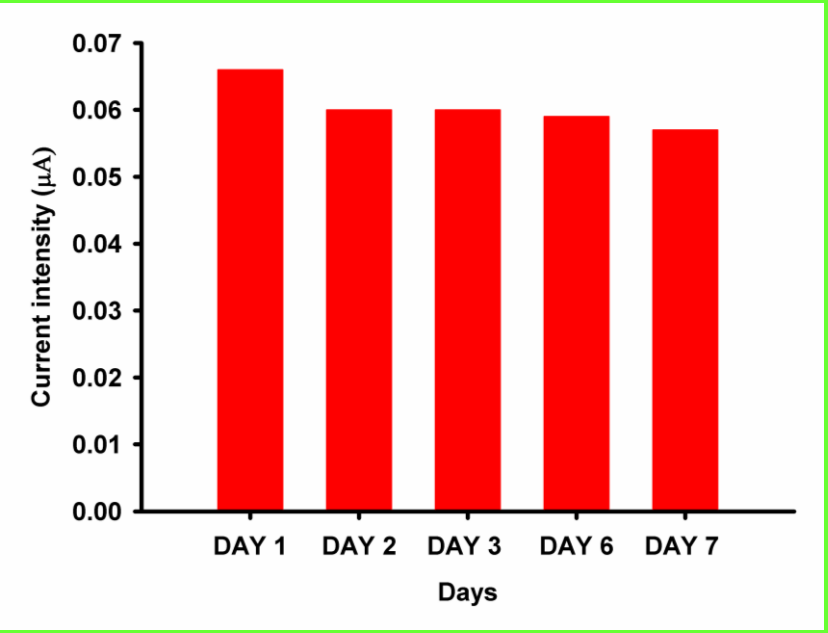

Figure 12. Stability of the Mn(TPP)Cl/AuNPs-Gr sensor.

3.8. Analytical application

Validation of the proposed sensors is essential for further utilization in the quality control of food, and food security. Therefore, for both sensors standard addition method was used for their validation in order to prove that they are highly reliable for the assay of sorbic acid in white and black bread as well as in mayonnaise.

Table 4. Determination of sorbic acid in white bread, black bread and mayonnaise samples using the ZnPIX/AuNPs-Gr sensor.

Sample	Amount added (μmol/L)	Amount found (μmol/L)	Recovery (%)	RSD %
White bread	400	386.41	96.60	0.71
sample	800	787.72	98.47	1.25
Black bread	400	393.12	98.28	3.93
sample	800	791.00	98.88	1.63
Mayonnaise	400	384.68	96.17	0.76
	800	798.21	99.78	3.62

Table 5. Detection of sorbic acid in white bread, black bread and mayonnaise samples using the Mn(TPP)Cl/AuNPs-Gr sensor.

Sample	Amount added (µmol/L)	Amount found (µmol/L)	Recovery (%)	RSD %
White bread sample	400	389.85	97.46	4.58
	800	773.53	96.69	0.24
Black bread sample	400	381.01	95.25	2.98
	800	791.56	98.94	2.84
Mayonnaise	400	397.19	99.30	0.81
	800	761.40	95.17	0.33

The samples were prepared as shown above, and for each of the samples the concentration of sorbic acid was determined. After this step, known amounts of sorbic acid were added, followed by measurements of its concentration.

The results shown in Tables 4 and 5 shown high reliability of the assay of sorbic acid in white and black bread as well as in the mayonnaise. When the ZnPIX/AuNPs-Gr sensor was used, the recoveries were higher than 96.00% for white bread with RSD, less than 1.50%; higher than 98.00% for black bread with RSD values less than 4.00%; while for the mayonnaise, the recovery was higher than 96.00% with RSD values less than 4.00% (Table 4). When the Mn(TPP)Cl/AuNPs-Gr sensor was used, the recoveries were higher than 96.50% for white bread with RSD, less than 5.00%; higher than 95.00% for black bread with RSD values less than 3.00%; while for the mayonnaise, the recovery was higher than 95.00% with RSD values less than 1.00% (Table 5). Accordingly the proposed sensors can be used for the assay of sorbic acid in white/black bread and mayonnaise.

4. Conclusions

This paper reported two electrochemical sensors used for the reliable determination of sorbic acid. The sensors were based on the modification of a nanographene paste decorated with gold with solutions of Zn protoporphyrin IX, and 2,3,7,8,12,13,17,18 octaethyl, 21H, 23H-porphirine Mn(III) chloride. High stability, selectivity, sensitivity, and reproducibility were recorded for both sensors. The feature of the proposed sensors is their utilization in food industry and supermarkets for the quality control of food, regarding the assay of the concetration of sorbic acid.

References

1. A. Özdemir, S. Şanlı, B. Sardoğan, S. Sardoğan, Determination of sorbic acid in cheese samples by rapid HPLC-DAD method, Int. J. Anal. Chem. |Article ID 6049028 (2020) 1-10.
2. C. De Luca, S. Passi, E. Quattrucci, Simultaneous determination of sorbic acid, benzoic acid and parabens in foods: A new gas chromatography-mass spectrometry technique adopted in a survey on Italian foods and beverages, Food Addit. Contam. 12 (1995) 1-7.
3. S. Yarramraju, V. Akurathi, K. Wolfs, A.V. Schepdael, J. Hoogmartens, E. Adams. Investigation of sorbic acid volatile degradation products in pharmaceutical formula-tions using static headspace gas chromatography. J. Pharm. Biomed. Anal. 44 (2007) 456–463.
4. T. D'Amore, A. Di Taranto, G. Berardi, V. Vita, M. Iammarino, Going green in food analysis: a rapid and accurate method for the determination of sorbic acid and benzoic acid in foods by capillary ion chromatography with conductivity detection, LWT 141 (2021) 110841.

5. X. Zhang, S. Xu, Y. Sun, Y. Wang, C. Wang, Simultaneous determination of benzoic acid and sorbic acid in food products by CE after on-line preconcentration by dynamic pH junction, Chromatographia 73 (2011) 1217–1221.
6. Y. Tang, M. Wu. A quick method for the simultaneous determination of ascorbicacid and sorbic acid in fruit juices by capillary zone electrophoresis. Talanta 65 (2005) 794–798.
7. F. Han, Y.Z. He, L. Li, G.N. Fu, H.Y. Xie, W.E. Gan, Determination of benzoic acid and sorbic acid in food products using electrokinetic flow analysis–ion pair solid phase extraction–capillary zone electrophoresis, Anal. Chim. Acta 618 (2008) 79-85.
8. I.C. Lopes, P.V.F. Santos, V.C. Diculescu, M. César, U. de Araújo, A.M. Oliveira-Brett, Sorbic acid and its degradation products: electrochemical characterization, Anal. Lett. 45 (2012) 408–417.
9. T. Ohtsuki, K. Sato, N. Sugimoto, H. Akiyama, Y. Kawamura, Absolute quantitative analysis for sorbic acid in processed foods using proton nuclear magnetic resonance spectroscopy, Anal. Chim. Acta 734 (2012) 54-61,
10. M Coros, S Pruneanu, RI Stefan-van Staden, Recent progress in the graphene-based electrochemical sensors and biosensors. A review. J. Electrochem. Soc. 167 (2020) 037528.
11. C Cioates-Negut, RI Stefan-van Staden, JF van Staden, Porphyrins – as active materials in the design of sensors. An overview. ECS J. Solid State Sci. Technol. 9 (2020) 051005.

Carbon Nanopowder Based Stochastic Sensor for Ultrasensitive assay of CA 15-3, CEA and HER2 in whole blood.

Abstract

Two microsensors obtained by physical immobilisation of 5,10,15,20-tetraphenyl-21H,23H-porphine (TPP) and 5,10,15,20-tetrakis (pentafluorophenyl chloride)-21H,23H-iron (III) porphyrin (Fe(TPFPP)Cl) in carbon nanopowder

decorated with gold nanoparticles (AuNp) were designed, characterized, validate, and used for molecular recognition and simultaneous ultrasensitive determination of CEA, CA15-3 and HER2 in whole blood. High sensitivities were recorded for both microsensors. Low limits of quantification were recorded for all biomarkers CEA (12.8 pg mL^{-1} by using Fe(TPFPP)Cl/AuNp, and 190fg mL^{-1} by using TPP/AuNp), CA 15-3 (100fU mL^{-1} for both microsensors), and HER2 (3.9 fg mL^{-1} by using Fe(TPFPP)Cl/AuNp, and 35fg mL^{-1} by using TPP/AuNp). A very good correlations between the results obtained using the proposed microsensors and ELISA certified by the student t-test proved that the screening test can be used for ultrasensitive assay of the three biomarkers in whole blood.

1. Introduction

CA 15-3, CEA and HER-2 have a role of prognostic biomarkers and can facilitate personalized treatment for breast cancer. Early diagnosed breast cancer as well as prescribing a personalized treatment for the confirmed breast cancer patient have a major impact on the patient's health as well as closely related to test results, rapid, reliable and accurate screening [1,2]. CA15-3 is useful for the early detection of tumor recurrence in patients previously treated for stage II and III breast cancer, with no clinical signs of disease activity. The combined determination of CA 15-3 and CEA may increase the sensitivity of recurrent tumor detection [3]. CA 15-3 and CEA levels in breast cancer proved to be sensitive biomarkers for the evaluation of patients with breat cancer [4]. HER2-positive breast cancers tend to be more aggressive than HER2-negative breast cancers. Along with tumor grade and cancer stage, HER2 status help determine the treatment options [5].

Regarding the assay of the three biomarkers, ELISA (based on assay kits available from many companies) remain the standard method of choice for the assay of CA15-3, CEA and HER2, although for HER2 immunohistochemistry method is preferred especially when determined from tumor tissue. Other methods of analysis are shown in Table 1.

Table 1. The latest method proposed for the assay of CA 15-3, CEA, and HER2.

Biomarker	Tool	Linear concentration range	Limit of determination	Ref.
CEA	Immunosensor	0.01pg mL^{-1} – 80.00ng mL^{-1}	10fg mL^{-1}	[6]
	Aptamer biosensor	1-30000 pg mL^{-1}	1pg mL^{-1}	[7]
	Graphene-based immunosensor	0.1 – 5.0ng mL^{-1}	0.1ng mL^{-1}	[8]
	Fe(TPFPP)Cl/AuNp	12.8pg mL^{-1}- 20.0µg mL^{-1}	12.8pg mL^{-1}	This work
	TPP/AuNp	100fg mL^{-1}- 1µg mL^{-1}	100fg mL^{-1}	This work

CA 15-3	Immunosensor	0.1fg mL^{-1} – 1.0μg mL^{-1}	0.1fg mL^{-1}	[9]
	Quantum dots/electrochemiluminescence	10μU mL^{-1}-500U mL^{-1}	10μU mL^{-1}	[10]
	Fluorescent biosensor	Up to 25.6μU mL^{-1}	-	[11]
	Fe(TPFPP)Cl/AuNp	100nU mL^{-1}- 1000U mL^{-1}	100nU mL^{-1}	This work
	TPP/AuNp	100nU mL^{-1}- 1000U mL^{-1}	100nU mL^{-1}	This work
HER2	Fiber-optic ball-tip resonator	3.7pg mL^{-1} – 128.0ng mL^{-1}	3.7pg mL^{-1}	[12]
	Bifunctional carbon nanorods	Up to 900pg mL^{-1}	7fg mL^{-1}	[13]
	Aptamer based colorimetric sensor	Up to 50.0pmol mL^{-1}	9.8pmol mL^{-1}	[14]
	Fe(TPFPP)Cl/AuNp	3.9fg mL^{-1}- 30.0pg mL^{-1}	3.9fg mL^{-1}	This work
	TPP/AuNp	35fg mL^{-1}- 39pg mL^{-1}	35fg mL^{-1}	This work

The importance of utilization of nanomaterials in the biomedical analysis of CA15-3 was shown in a review article [15].

Therefore, this paper proposed two new stochastic microsensors based on carbon nanopowder (nC) modified with gold nanoparticles (AuNp) and two porphyrins: 5,10,15,20-tetraphenyl-21H,23H-porphine (TPP) and 5,10,15,20-tetrakis (pentafluorophenyl chlo-ride)-21H,23H-iron (III) porphyrin (Fe(TPFPP)Cl) for the simultaneous assay of CEA, CA15-3, and HER2, because the screening test based on their simultaneous assay will provide more information about the diagnostic and personalized treatment of breast cancer. The novelty of the work is besides the new design used for the stochastic microsensors proposed for the assay of CEA, CA 15-3, and HER2, the utilization of only one tool for simultaneous assay of the three biomarkers.

The utilization of gold nanoparticles will increase the conductivity of the carbon nanopowder, while the porphyrin materials will provide the necessary channels (formed within the molecular aggregates) for stochastic sensing [16]. The selection of the stochastic sensor type for these molecules assay in whole blood was done because, the stochastic sensors are able to perform reliably qualitative and quantitative assay of biomarkers in whole blood [17-21]. The mechanism of current development for stochastic sensors is based on channel conductivity: the molecule is entering the channel and the current is dropping to zero until the whole molecule is inside the channel – the time needed to enter the channel depends on the size, volume, conformation, unfolding capacity (if it is proteine), and velocity driven by the applied potential, and it is known as the signature of the molecule assigned as t_{off} value on the diagrams. While in the channel, redox processes take place, in an equilibrium time named as t_{on} on the diagrams; the t_{on} value is read between two t_{off} values, and it depends on the concentration of the molecule in the biological fluid, from where the molecule is determined.

2. Materials and Methods

All chemicals were of analytical grade. Gold nanoparticles suspension, CA15-3, CEA, and HER2 were purchased from Sigma Aldrich; and the paraffin oil was purchased from Fluka. Deionized water was used for the preparation of the solutions used in the experiments. All CA15-3, CEA, and HER2 solutions were prepared in phosphate buffer solution (PBS, pH=7.40). When not in use, the solutions were kept at a temperature of -20˚C.

All electrochemical measurements were performed connecting a computer which had the GPES software to an AUTOLAB/PGSTAT 302 N (Metrohm). The electrochemical cell comprised three electrodes: the reference electrode (Ag/AgCl), the counter electrode (Pt) and the working electrode (the stochastic microsensor). All measurements were carried out at 25°C. A chronoamperometric method was used for the measurements of ton and toff values, at a constant potential (125 mV vs Ag/AgCl).

For microsensors' design: 100mg of carbon nanopowder were mixed with 10 μL gold nanoparticles suspension and paraffine oil was added until a paste was obtained. The paste was divided into two equal parts, and on each were added 50μL of one of the following porphyrins: 5,10,15,20-tetraphenyl-21H,23H-porphine (TPP/AuNp) and 5,10,15,20-tetrakis (pentafluorophenyl chloride)-21H,23H-iron (III) porphyrin (Fe(TPFPP)Cl/AuNp). Silver wire served as contact between the paste and the external circuit. Each modified paste was placed in a non-conducting (3D printed in the laboratory) plastic tube with internal diameter of 10μm and a length of 5mm. The stochastic microsensors were washed with deionized water, and dried between measurements. When not in use, they are kept in a dry place.

Stochastic method was carried out at 25°C. A chronoamperometric method was used for the measurements of t_{on} and t_{off} at a constant potential (125 mV vs Ag/AgCl). Based on the value of t_{off}, the analyte was identified in the diagrams recorded with the stochastic microsensors and further the value of t_{on} was read and used for the determination of concentration of each biomarker (Figure 1). The unknown concentrations of CA 15-3, CEA, and HER2 in whole blood samples were determined from the calibration equations ($1/t_{on} = a + bxC_{biomarker}$) recorded with each of the sensors for each of the biomarkers.

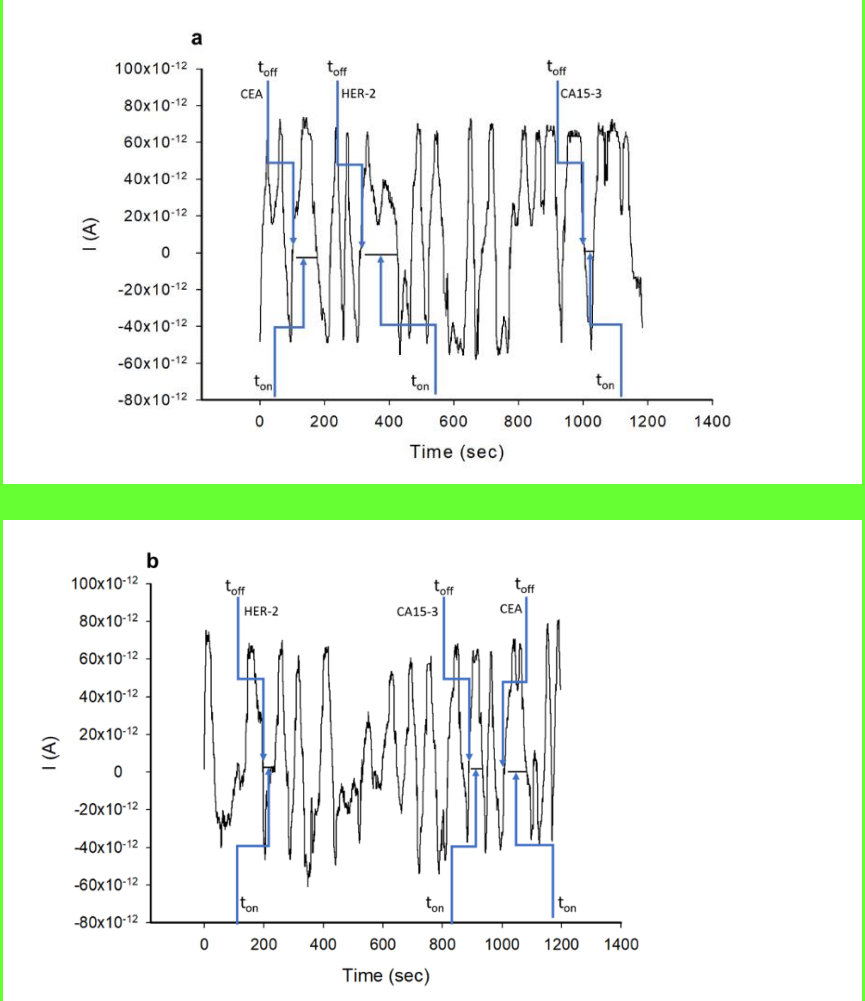

Figure 1. Pattern recognition of CA15-3, CEA and HER2 in whole blood samples, using stochastic microsensors based on: a) Fe(TPFPP)Cl/AuNp, and (b) TPP/AuNp.

The whole blood samples were obtained from the University Hospital Bucharest (approval of the ethics committee no 11/2013). These samples were obtained from confirmed patients with breast cancer. The biological samples did not require any pretreatment before the measurements. The electrochemical cell was loaded with biological sample, and after recording the diagram, and identifying the signatures of CA15-3, CEA and HER2, the unknown concentrations of the biomarkers in the whole blood samples were determined utilizing the stochastic method described above.

3. Results and Discussions

3.1. *Response characteristics of the stochastic microsensors*

The response characteristics of the proposed microsensors are shown in Table 2. All response characteristics were determined at 25°C, when a potential of 125mV versus Ag/AgCl was applied. First of all, different signatures (t_{off} values) were recorded for the CA15-3, CEA and HER2 for each of the stochastic microsenors proving that the three biomarkers can be determined simultaneously in whole blood samples.

Table 2. Response characteristics of the stochastic sensors used for the assay of CA15-3, CEA, and HER 2.

Stochastic microsensor based on nC	Signature t_{off} (s)	Linear concentration range	Calibration equations; correlation coefficient, r*	Sensitivity	LOQ
Fe(TPFPP)Cl/AuNp	CA15-3*				
	4.7	$1.00x10^{-7}$-$1.00x10^{3}$	$1/t_{on}= 0.03 +5.80\times10^{3}\times C$ r=0.9998	5.80×10^{3}	1.00×10^{-7}
	CEA**				
	0.6	$1.28x10^{-5}$- $2.00x10^{-1}$	$1/t_{on}= 0.04 + 6.16\times10\times C$ r=0.9993	6.16×10	$1.28x10^{-5}$
			HER 2**		
	2.6	$3.90x10^{-9}$- $3.90x10^{-5}$	$1/t_{on}= 0.02 + 1.43\times10^{5}\times C$ r=0.9999	1.43×10^{5}	$3.90x10^{-9}$
TPP/AuNp	CA15-3*				
	6.8	$1.00x10^{-7}$-$1.00x10^{3}$	$1/t_{on}= 0.04 +2.32\times10^{3}\times C$ r=0.9994	2.32×10^{3}	$1.00x10^{-7}$
	CEA**				
	1.9	$1.00x10^{-7}$- 1.00	$1/t_{on}= 0.03 + 1.90\times10^{4}\times C$ r=0.9997	1.90×10^{4}	$1.00x10^{-7}$
			HER 2**		
	1.3	$3.50x10^{-8}$- $3.90x10^{-5}$	$1/t_{on}= 0.03 + 3.53\times10^{4}\times C$ r=0.9986	3.53×10^{4}	$3.50x10^{-8}$

*<C>= U mL^{-1}; <t_{on}>=s; <Sensitivity> = s^{-1} U^{-1} mL; **<C>= µg mL^{-1}; <t_{on}>=s; <Sensitivity> = s^{-1} μg^{-1} mL; LOQ - limit of quantification.

All linear concentration ranges are wide, making possible determination of these biomarkers in any of the stages of breast cancer. The sensitivities are also very high; higher sensitivities were recorded for the assay of CEA and HER2 when the sensor based on TPP/AuNp was used. Comparing with the latest sensors used for the assay of CA15-3, CEA, and HER2 (Table 1), one can conclude that TPP/AuNp based sensor exhibited the lowest limit of determination (fg mL^{-1} magnitude order), and for the assay of HER2, the Fe(TPFPP)Cl/AuNp based sensor exhibited the lower limit of determination. For the assay of CA15-3, although the limits of determination are higher than those reported earlier [9-11], the proposed sensors can be used for the assay of CA15-3 without any processing of the sample, the linear concentration range covering patients with breast cancer in any of the stages of the illness. The advantages of the proposed sensors versus those shown in Table 1, are also the following: they can perform the simultaneous detection of the three biomarkers; no sampling is needed before the measurements; reliable qualitative analysis of each biomarker immediately followed by its quantitative analysis.

3.2. Stability and reproducibility measurements

10 stochastic sensors from each of the two types (TPP/AuNp, and Fe(TPFPP)Cl/AuNp) were designed, and measurements were performed daily for one month. The measurement for each type of sensor proved that there are no significative changes in the sensitivity, its variation being for each type lower than 0.12%; this proved the reproducibility of the design of each type of stochastic sensor. After 30 days of measurements, the variation of the sensitivities recorded for the TPP/AuNp based stochastic sensor was less than 0.11%, while for the Fe(TPFPP)Cl/AuNp based stochastic sensor was less than 0.08%; this proved that the sensors are stable for at least one month, when daily measurements are performed.

3.3. Selectivity of the stochastic microsensors

The selectivity of the stochastic microsensors is given by the difference between the signatures (t_{off} values) recorded for CA15-3, CEA and HER2 and those obtained for other biomarkers/substances from the biological samples. The possible interfering species selected were: p53, Ki67, maspin, and CA19-9.

Table 3. Selectivity of the stochastic microsensors.

Stochastic microsensor based on nC	CA15-3, Signature (s)	CEA, Signature (s)	HER2, Signature, (s)	Maspin, Signature (s)	Ki67, Signature (s)	CA19-9, Signature (s)	p53, Signature (s)
Fe(TPFPP)Cl/AuNp	4.7	0.6	2.6	2.0	1.3	3.0	3.5

TPP/AuNp	6.8	1.9	1.3	1.3	3.2	2.5	0.8

Results shown in Table 3, proved that none of the supposed interfering species are interfering the simultaneous assay of CA15-3, CEA, and HER2.

3.4. Ultrasensitive simutaneous determination of CA15-3, CEA and HER2 in whole blood

Ten whole blood samples from patients confirmed with breast cancer were screened using the two stochastic microsensors. Just after reading the t_{off} values, in between two t_{off} values, the corresponding t_{on} values were read. The t_{on} values were used to determine the concentrations of CA15-3, CEA and HER2 in the whole blood samples, accordingly with the stochastic method described above. The results obtained after the screening of whole blood samples are shown in Table 4.

Table 4. Determination of CA15-3, CEA, and HER2 in whole blood samples.

Sample no	U mL^{-1}, CA 15-3			ng mL^{-1}, CEA			pg mL^{-1}, HER 2		
	Stochastic microsensors based on								
	Fe(TPFPP)Cl/ AuNp	TPP/AuNp	ELISA	Fe(TPFPP)Cl/ AuNp	TPP/AuNp	ELISA	Fe(TPFPP)Cl/ AuNp	TPP/AuNp	ELISA
1	448.09±0.03	447.52±0.02	450.00±0.12	24.00±0.05	23.18±0.02	24.00±0.12	64.43±0.02	64.40±0.05	63.00±0.17
2	448.12±0.03	449.49±0.05	443.00±0.17	7.18±0.05	7.21±0.03	7.30±0.10	4.96±0.02	4.90±0.03	4.87±0.12
3	206.55±0.05	205.30±0.03	204.00±0.14	17.87±0.04	17.98±0.03	17.00±0.12	61.97±0.04	62.03±0.05	60.00±0.10
4	265.72±0.03	269.13±0.04	260.00±0.12	17.15±0.04	17.78±0.02	16.98±0.13	64.39±0.03	64.22±0.02	64.00±0.11
5	398.64±0.03	398.78±0.02	392.00±0.14	11.80±0.03	11.85±0.03	11.23±0.14	40.94±0.02	39.14±0.05	38.40±0.12
6	448.10±0.03	428.15±0.08	440.10±0.12	13.90±0.04	13.96±0.02	13.15±0.11	33.01±0.02	32.25±0.03	33.10±0.14
7	220.87±0.03	223.15±0.04	221.00±0.15	3.20±0.02	3.19±0.03	3.00±0.14	18.04±0.02	18.00±0.03	17.45±0.13
8	563.86±0.07	569.43±0.03	560.0±0.11	11.14±0.02	11.85±0.03	12.00±0.11	3.36±0.04	3.76±0.05	3.12±0.02
9	303.88±0.04	304.20±0.03	300.00±0.15	12.00±0.03	11.79±0.02	11.50±0.14	27.97±0.03	28.03±0.05	25.50±0.12
10	111.35±0.03	118.40±0.05	115.20±0.14	8.50±0.02	8.43±0.03	8.50±0.12	28.51±0.03	28.28±0.02	27.50±0.11
t-test	2.13	2.21	-	2.61	2.29		2.41	2.38	-

Very good correlations between the results obtained using the two stochastic microsensors were obtained. Paired t-test was also performed at 99.00% confidence level (tabulated theoretical t-value: 4.032) for each biomarker. All

calculated t-values were less than the tabulated value, proving that there is no statistically significant difference between the results obtained using the two stochastic microsensors and ELISA (the standard method used for the assay of these biomarkers in whole blood samples) (Table 4). Accordingly, the proposed stochastic microsensors can be reliably used for the ultrasensitive simulataneous determination of CA15-3, CEA and HER2 in whole blood samples.

5. Conclusions

The proposed stochastic microsensors were used for the simultaneous assay of CA15-3, CEA, and HER2 in whole blood samples. Their linear working concentration ranges covered patients with breast cancer in any stage of the illness, determinations being performed with high sensitivity. The screening test based on utilization of the two microsensors as screening tools may be used for early detection of breast cancer, for determining the need of a personalized treatment, as well as for the determination of the efficiency of the breast cancer treatment.

References

1. Lau, K.H.; Tan, A.M.; Shi, Y. New and emerging targeted therapies for advanced breast cancer. *Int.J.Mol.Sci.* 2022, *23*, 2288.
2. Maitra, D.; Srivastava, A. Tumor markers, prognostic and predictive factors in breast cancer. *Breast Cancer* 2022, *549*, 221-241.
3. Jo, Y.; Lee, J.H.; Cho, E.S.; Lee, H.S.; Shin, S.J.; Park, E.J.; Baik, S.H.; Lee, K.Y.; Kang, J. Clinical significance of early carcinoembryonic antigen change in patients with nonmetastatic colorectal cancer. *Front.Oncol.* 2022, *12*, 739614.
4. Hoyes, D.F.; Zurawski,Jr. V.R.; Kufe, D.W. Comparison of circulating CA15-3 and carcinoembryonic antigen levels in patients with breast cancer. *J.Clin.Oncol.*, 1986, *4*, 1542-1550.
5. Zhang, H.; Katerji, H.; Turner, B.M.; Hicks, D.G. HER2-low breast cancers. *Am.J.Clin.Pathol.* 2022, *157*, 328-336.
6. Liao, X.; Wang, X.; Zhang, M.; Mei, L.; Chen, S.; Qi, Y.; Hong, C. An immunosensor based on an electrochemical-chemical-chemical advanced redox cycle, amplification strategy for the ultrasensitive determination of CEA. *Anal.Chim.Acta* 2021, *1170*, 338647.
7. Zhang, K.; Pei, M.; Chen, Y.; Zhang, Z.; Niu, C.; Liu, X.; Liu, J.; Guo, F.; Huang, H., Lin, X. A novel electrochemical aptamer biosensor based on tetrahedral DNA nanostructures and catalytic hair pin assembly for CEA detection. *J.Electroanal.Chem.* 2021, *898*, 115635.
8. Jozghorbani, M.; Fathi, M.; Kazemi, S.H.; Alinejadian, N. Determination of carcinoembryonic antigen as a tumor marker using a novel graphene-based label-free electrochemical immunosensor. *Anal.Biochem.* 2021, *613*, 114017.

9. Martins, T.S.; Bott-Neto, J.L.; Oliveira, Jr. O.N.; Machado, S.A.S. A sandwich-type electrochemical immunosensor based on Au-rGO composite for CA15-3 tumor marker detection. *Microchim. Acta* 2022, *189*, 38.

10. Asbaghian-Namin, H.; Karami, P.; Naghshara, H.; Gholamin, D.; Johari-Ahar, M. Electrochemiluminescent immunoassay for the determination of CA15-3 and CA72-4 using graphene oxide nanocomposite modified with CdSe quantum dots and $Ru(bpy)_3$ complex. *Microchim. Acta* 2021, *188*, 238.

11. Wu, Y.; Chen, X.; Wang, X.; Yang, M.; Xu, F.; Hou, C.; Huo, D. A fluorescent biosensor based on prismatic hollow metal-polydopamine frameworks and 6-carboxyfluoresceine (FAM) – labeled protein aptamer for CA 15-3 detection. *Sens.Actuators B* 2021, 329, 129249.

12. Sypabekova, M.; Amantayeva, A.; Vangelista, L.; Gonzalez-Vila, A.; Caucheteur, C.; Tosi, D. Ultralow limit detection of soluble HER2 biomarker in serum with a fiber-optic ball-tip resonator. *ACS Mens.Sci.Au* 2022, https://doi.org/10.1021/acsmeasuresciau.2c00008

13. Guerrero-Esteban, T.; Gutierrez-Sanchez, C.; Garcia-Mendiola, T.; Revenga-Parra, M.; Pariente, F. Bifunctional carbon nanorods for highly sensitive HER2 determination based on electrochemiluminescence. *Sens.Actuators B* 2021, *343*, 130096.

14. Ranganathan, V.; Srinivasan, S.; Singh, A.; DeRosa, M.C. An aptamer-based colorimetric lateral flow assay for the detection of human epidermal growth factor receptor 2 (HER2). *Anal.Biochem.* 2020, *588*, 113471.

15. Oktaviyanti, I.K.; Ali, D.S.; Awadh, S.A.; Opulencia, M.J.C.; Yusupov, S.; Dias, R.; Alsaikhan, F.; Mohammed, M.M.; Sharma, H.; Mustafa, Y.F.; Saleh, M.M. Recent advances on applications of immunosensing systems based on nanomaterials for CA15-3 breast cancer biomarker detection. *Anal.Bioanal.Chem.* 2022, http://doi.org/10.1007/s00216-022-04150-z

16. Sabuzi, F.; Stefanelli, M.; Monti, D.; Conte, V.; Galloni, P. Amphiphilic porphyrin aggregates: a DFT investigation. *Molecules* 2019, *25*, 133.

17. Stefan-van Staden. R.I.; Comnea-Stancu, I.R.; Surdu-Bob, C.C.; Badulescu, M. Nanostructured materials detect epidermal growth factor receptor, neuron specific enolase and carcinoembryonic antigen. *Nanoscale* 2015, *7*, 15689-15694.

18. Stefan-van Staden, R.I.; Gheorghe, D.C.; Ilie-Mihai, R.M.; Barbu-Tudoran, L.; Pruneanu, S.M. Stochastic biosensors based on N and S-doped graphene for the enantioanalysis of aspartic acid in biological samples. *RSC Adv*., 2021,*11*, 23301-23309.

19. Ilie-Mihai, R.M.; Gheorghe, D.C.; Stefan-van Staden, R.I.; Lungu-Moscalu, A.; Pruneanu, S.M.; van Staden, J.F. Fast screening method of biological samples based on needle stochastic sensors for early detection of gastric cancer. *Rev de Chimie*, 2021, 72, 22-34.

20. Stefan-van Staden, R.I.; Gheorghe, S.S.; Ilie-Mihai, R.M.; Badulescu, M. Disposable Stochastic Sensor Based on Deposition of a Nanolayer of Silver on Silk for Molecular Recognition of Specific Biomarkers. *J. Electrochem. Soc.* 2021, *168*, 037515.

21. Stefan-van Staden, R.I.; Bogea, I.M.; Ilie-Mihai, R.M.; Gheorghe, D.C.; Coros, Pruneanu, S.M. Stochastic microsensors based on modified graphene for pattern recognition of maspin in biological samples. *Anal. Bioanal. Chem.* 2022, *414*, 3667-3673.

Sodium Metabisulfite in Food and Biological Samples: A Rapid and Ultra-Sensitive Electrochemical Detection Method

Abstract

The primary benefit of using sulfites as a food additive is their antimicrobial and antioxidant properties, which stop fungi and bacteria from growing in a variety of foods. Application of analytical methods are necessary to ensure food quality control related to the presence of sulfites in a variety of foods. For the detection of sodium metabisulfite in food and urine samples, two sensors based on reduced graphene oxide doped with Pd paste and modified with 5,10,15,20-tetraphenyl-21H,23H-porphine and 5,10,15,20-tetrakis (pentafluorophenyl chloride)-21H,23H-iron (III) porphyrin were proposed. The new sensors were evaluated and characterized using square-wave voltammetry. The response characteristics showed that the detection limits for the sensors were $3.0x10^{-12}$ mol L^{-1} for TPP/rGO@Pd0 and $3.0x10^{-11}$ mol L^{-1} for Fe(TPFPP)Cl/rGO@Pd0 based sensors, while the quantification limits were $1.0x10^{-11}$ mol $L^{-1}$for TPP/rGO@Pd0 and $1.0x10^{-10}$ mol $L^{-1}$for Fe(TPFPP)Cl/rGO@Pd0 based sensors. The sensors can be used to determine sodium metabisulfite in a concentration range between 1.0×10^{-11} to 1.0×10^{-7} mol L^{-1} for TPP/rGO@Pd0 based sensor and between 1.0×10^{-10} mol $L^{-1}$and 1.0×10^{-6} mol L^{-1} for Fe(TPFPP)Cl/rGO@Pd0 based sensor.

Keywords: sodium metabisulfite; square-wave voltammetry, food samples; electrochemical sensor

1. Introduction

Food additives have become increasingly important in the modern food industry as a result of changes in human lifestyle and subsequent nutritional demands [1,2]. It is common practice to

use food preservatives when storing food for extended periods of time to prevent spoilage due to microbial or fungal growth or unintended chemical changes [3]. It is unclear what toxic effects and mechanisms of action these chemicals have, despite their widespread use in the food industry. New research suggests a link between excessive consumption of certain food additives and an array of human diseases [4]. Concerns about food safety and the possible dangers of food additives have grown in response to this issue over the years. Sodium metabisulfite (SMB), a common preservative in the food industry, was found to have neurotoxic effects and increase tissue damage indicators in in vivo studies with animals [5].

In many food products, particularly fruits, vegetables, seafood, pastry and alcoholic beverages, SMB, also known as sodium pyrosulfite ($Na_2S_2O_5$), is a synthetic food additive that is used as an antioxidant and antibacterial preservative [6,7] Additionally, it is utilized as an excipient in the pharmaceutical sector to increase the stability of active principles [8]. High oral doses of SMB have been shown to increase cell damage indices and may have genotoxic effects on mouse tissues, according to previous reports [9]. Additionally, additional *in-vivo* studies showed that high levels of SMB can cause apoptosis and lipid peroxidation in rat stomach tissue [10].Numerous fields, including pharmacology, environmental analysis, food sciences, enzymatic kinetics, and medical diagnostics, have benefited from the use of electrochemistry-based analytical methods and sensors [11-13]. The creation of electrochemical sensors based on nanomaterials is an active research area that is anticipated to produce cutting-edge technologies for maintaining food integrity that will displace current methods.Reduced graphene oxide (rGO) is one unique material that can be utilized for the creation of electroanalytical sensors (rGO). Similar to graphene nanosheets, rGO is composed of a few layers of sp^2 carbon atoms and exhibits a singular two-dimensional structure. This pi-conjugated system results in high electron mobility and quick charge transfer, which makes an electro-catalytic effect visible [14].According to studies [15, 16] graphene-based electrodes are more electrocatalytically active and conductive than other carbon-based materials. Numerous studies [17] have shown that adding noble metal nanoparticles to graphene can improve the electrocatalytic activity of the material [18–20]. Because of its excellent electrocatalytic property, Palladium (Pd) nanoparticles in particular have been extensively investigated for the determination of various analytes [21].For chemical reactions, particularly those involving electron transfer, porphyrins [22, 23] and metalloporphyrins are well known for their electrocatalytic properties [24, 25].

As a result, the current study demonstrates the development and validation of a straightforward method for the quantification of sodium metabisulfite in foods and biological samples. This method was demonstrated in cookies, bean flakes, horseradish paste, and urine samples as a proof-of-concept.

2. Materials and Methods

Sodium metabisulfite, 5,10,15,20-tetraphenyl-21H,23Hporphine (TPP), 5,10,15,20-tetrakis(pentafluorophenyl)-21H,23H-porphyrin iron(III) chloride (Fe(TPFPP)Cl),monosodium phosphate, disodium phosphate, acesulfame K, sucrose, glucose, sodium benzoate, d-sorbitol, iron sulphate heptahydrate, maltodextrin, sodium nitrate and ammonium chloride were purchased from Sigma-Aldrich, and paraffin oil (d_4^{20}, 0.86 g cm^{-1}) was purchased from Fluka (Buchs, Sweden). Reduced graphene oxide dopped with Pd(0)(rGO@Pd0)was acquired from NanoInnova Technologies.The phosphate buffer solution (PBS, 0.1 mol L^{-1}) was prepared by mixing monosodium phosphate and disodium phosphate solutions. The pH of the buffer solution was adjusted using different amounts of 0.1 mol L^{-1} NaOH or HCl solutions to obtain different pH values (2.0, 2.5, 3.0, 3.5, 4.0, 4.5, 5.0, 5.5, 6.0, 7.0, and 8.0). The stock solution of $1.0x10^{-2}$ mol L^{-1}sodium metabisulfite was prepared fresh, before measurements, in deionized water.

Using a mini potentiostat EmSTAT Pico (software PsTrace 5.9 PalmSens) connected to a laptop for data acquisition, measurements for cyclic voltammetry (CV), square-wave voltammetry (SWV), and electrochemical impedance spectroscopy (EIS) were performed.

All electrochemical experiments were conducted at room temperature. The modified nanographene paste electrode, Ag/AgCl (0.1 mol L^{-1} KCl), and Pt-wire were used as the working, reference, and auxiliary electrodes, respectively, immersed in an electrochemical cell, for recording the results. A Mettler Toledo pH meter was used to adjust the pH. An amount of 100 mg palladium-doped reduced graphene oxide was mixed with paraffin oil until a homogeneous paste was obtained. The modified pastes (Scheme 1)were prepared by addition of 25 □L from a solution of 5,10,15,20-tetraphenyl-21H,23H-porphine ($1.0x10^{-3}$ mol L^{-1} in tetrahydrofuran) and 25 □L from a solution of 5,10,15,20-tetrakis(pentafluorophenyl)-21H,23H-porphyrin iron(III) chloride ($1.0x10^{-3}$ mol L^{-1} in tetrahydrofuran) to the bare paste. The TPP/rGO@Pd0and Fe(TPFPP)Cl/rGO@Pd0sensors were obtained, respectively, by placing the

pastes into non-conducting plastic tubes (internal diameter 25 mm) in which a silver wire inserted into the paste served as electrical contact between the paste and external circuit.

The new developed sensors were used to detect $Na_2S_2O_5$ in three types of food samples (cookie, bean flakes and horseradish paste)bought from a Romanian supermarket and also a biological sample, obtained from a healthy volunteer. The samples were diluted in PBS pH=4.5, in a 1:1 (v/v) ratio and afterward spiked with different concentrations of sodium metabisulfite.

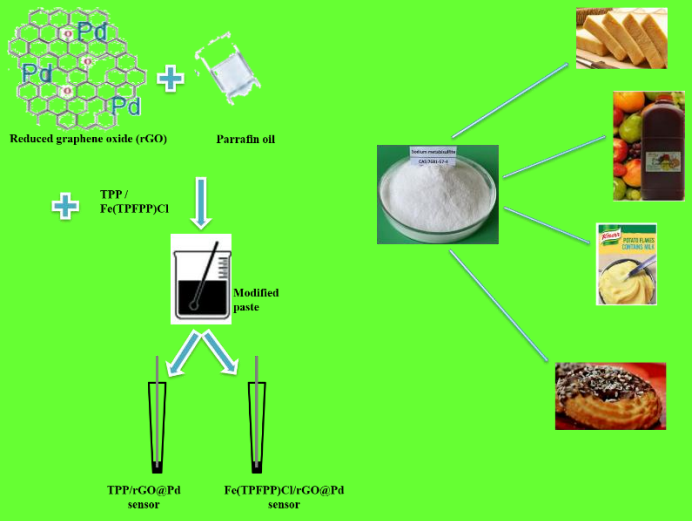

Scheme 1. Design of the modified electrochemical sensors

3. Results

3.1. Electrochemical Characterization of the sensors

CV, EIS and SWV were used as the characterization techinques for the bare sensor, simple reduced graphene oxide dopped with palladium (rGO@Pd), and the two modified sensors: reduced graphene oxide dopped with palladiumbased on 5,10,15,20-tetraphenyl-21H,23H-porphine (TPP/rGO@Pd0) and based on5,10,15,20-tetrakis(pentafluorophenyl)-21H,23H-porphyrin iron(III) chloride (Fe(TPFPP)Cl/ rGO@Pd0). To analyze the chemical response of the sensors, cylic voltammetry was used (Figure 1). The CVs (Fig. 1a)) were conducted using the rGO@Pd0, TPP/rGO@Pd0, and Fe(TPFPP)Cl/ rGO@Pd0, as working electrodes in a solution of $5.0x10^{-3}$ mol L^{-1} $K_3[Fe(CN)_6]$ (0.1 mol L^{-1} KCl) at potentials between -0.6 V and 1.0 V.It is evident that the conductivity of the sensor increased after the rGO electrode was modified with TPP and Fe(TPFPP)Cl.One of the reasons of the increased conductivity is the given by the

function of porphyrins as modifier.Due to their unique structure, the porphyrin canhave the ability to control redox reactions that the target analytes mediate.This has therefore shown that the modification was made and that the electrochemical response was enhancedThe EIS study was carried out in order to investigate the interface of the sensors over a frequency spectrum ranging from 1.0 x 10^5 to 1.0 x 10^{-1} Hz.Every single one of the EIS measurements was carried out in a solution that contained 5.0 x 10^{-3} mol L^{-1} K3[Fe(CN)$_6$] (0.1 mol L^{-1} KCl). Fig. 1b) depicts Nyquist diagrams. Fig. 1b) demonstrates that at low frequencies, where electrical resistance is high (Rct = 2.61x$10^5\Omega$), rGO@Pd0 exhibited a large, well-defined semicircle. The diameter of the semicircle shrank (Rct = 7.16x$10^4\Omega$) after rGO@Pd0 was modified with TPP. The bare sensor that had been modified with Fe(TPFPP)Cl exhibited even a smaller semi-circle (Rct = 1.71x10^4 Ω) afterward.In conclusion, compared to the unmodified graphene paste electrode, the sensors that had been treated with TPPand Fe(TPFPP)Cl exhibited a smaller semicircle and a higher Rct values. The EIS results for a 5.0 x 10^{-3} mol/L $K_3[Fe(CN)_6]$ (0.1 mol L^{-1} KCl) solution showed good agreement with the CV results. To compare the electrochemical behaviour between the three electrode, the bare sensor and the two modified sensors, a solution containing 1.0x10^{-7} mol L^{-1}sodium metabisulfite buffered with PBS at pH 4.5 was analyzed using a SWV method.From Fig. 1c)it can be seen that, amongts the three sensors, the Fe(TPFPP)Cl/ rGO@Pd0 and TPP/rGO@Pd0 sensorsgave the best results for sodium metabisulfit oxidation. After further characterization and testing, the two sensors were evaluated for their ability to electrochemically determine the presence of $Na_2S_2O_5$ in samples of cookie, potato flakes, horsereadish paste and urine.

Calculating the electroactive surface area of the four sensors was done with the help of the Randles-Sevcik equation [26] for quasi-reversible processes. This allowed for the investigation of the electrocatalytic activity of the sensors.The equation for the peak current intensity can be summarized as follows:

$$Ip_a = (2.69 \times 10^5) n^{3/2} A C_0 D_R^{1/2} \upsilon^{1/2}$$

where: Ipa – anodic peak current (A), n – number of transferred electrons (in this instance, n = 1), A – active surface area of the electrode (cm^2), C_0 –concentration of $K_3[Fe(CN)_6]$ (mol cm^{-3}), DR – diffusion coefficient (7.60 x 10^{-6} cm^2 s^{-1}), and υ– scan rate (V s^{-1}).The experiment was carried out in a solution that contained 5.0 x 10^{-3} mol L^{-1} of $K_3[Fe(CN)_6]$ and 0.1 mol L^{-1} of

KCl.The fact that the anodic and cathodic peaks, Ipa and Ipc, showed a linear dependency on the square root of the scan rate (Fig. 2 and 3) despite the fact that the scan rate was varied from 0.010 to 0.100 V s^{-1} provides evidence that the redox process was controlled by diffusion.Figure. 2a) and 3a) depicts the pattern that emerges as the scan rate and current intensity both continue to increase over time. Figure. 2b)and 3b) depicts the linear dependences of the two peaks, Ipa vs. $\upsilon^{1/2}$ and Ipc vs. $\upsilon^{1/2}$ respectively.As comparison, the sensor based on Fe(TPFPP)Cl/ rGO@Pd0 presents the highest active are (0.019 cm^2) beside the other modified sensor TPP/rGO@Pd0 (0.0095cm^2), and compared to the unmodified sensor rGO@Pd0 (0.0009cm^2).

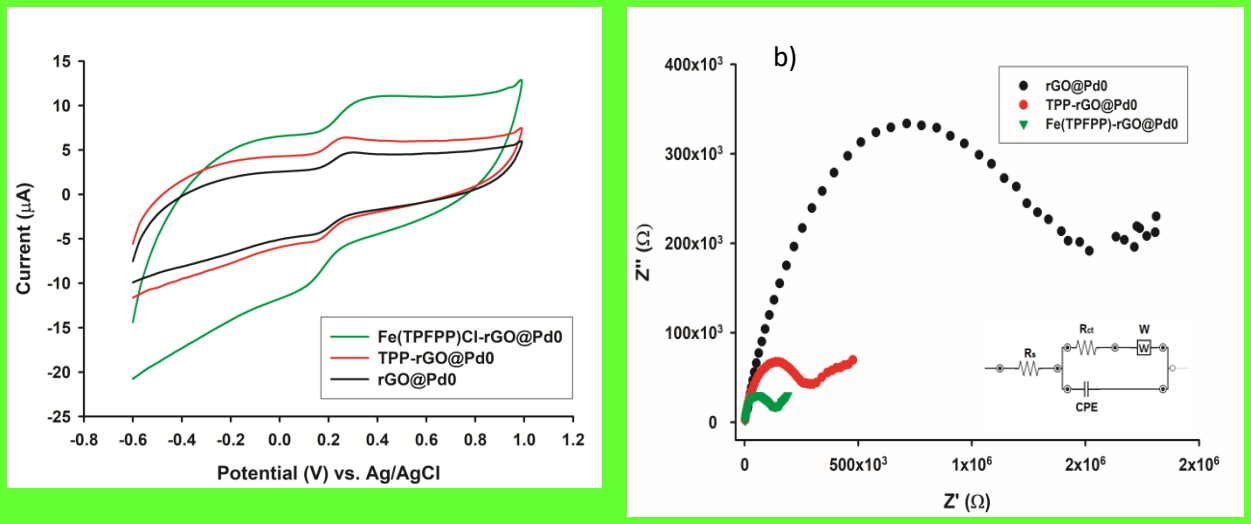

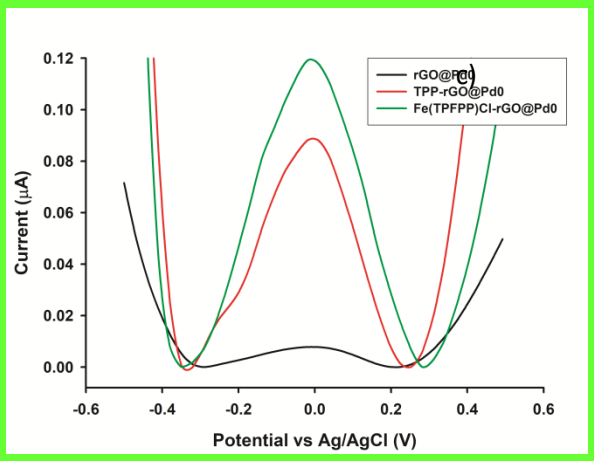

Figure 1. a) Cyclic voltammograms of the current plotted against the potential (working conditions: step potential 0.025V; scan rate 0.1 V s^{-1}) in a solution of 5.0 × 10^{-3} mol L^{-1}

$K_3[Fe(CN)_6]$ (0.1 mol L^{-1} KCl) using the rGO@Pd0 (black line), TPP/ rGO@Pd0 (red line) and Fe(TPFPP)Cl/ rGO@Pd0 (green line). (b) Electrochemical impedance spectra recorded for rGO@Pd0 (black line), TPP/ rGO@Pd0 (red line) and Fe(TPFPP)Cl/ rGO@Pd0 (green line) in a solution of 5.0×10^{-3} mol L^{-1} $K_3[Fe(CN)_6]$ (0.1 mol L^{-1} KCl (conditions: frequency range between 1.0×10^{5} to 1.0×10^{-1} Hz). Inset: equivalent circuit diagram of the electrochemical interface used to fit the impedance spectra where Rs is the solution resistance, CPE is the constant phase element, Rct is the electron-transfer resistance, and W is the Warburg diffusion resistance. (c) The recorded square wave voltammograms in PBS pH 4.5 containing 1.0×10^{-7} mol L^{-1} $Na_2S_2O_5$ for rGO@Pd0 (black line), TPP/ rGO@Pd0 (red line) and Fe(TPFPP)Cl/ rGO@Pd0 (green line); working conditions: step potential 0.03 V, amplitude: 0.1 V, frequency: 10 Hz.

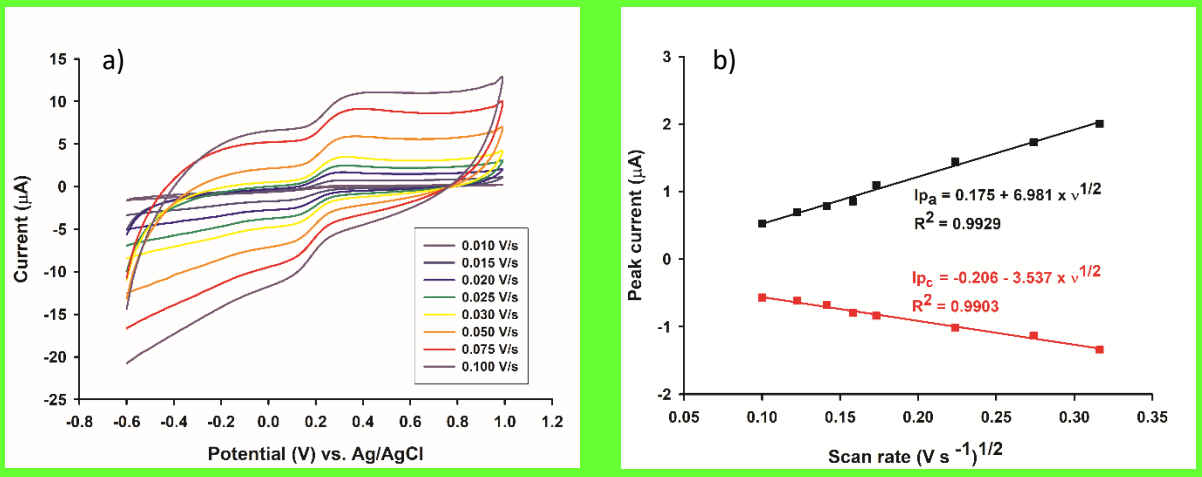

Figure 2. a) Cyclic voltammograms in a solution of 5.0×10^{-3} mol L^{-1} $K_3[Fe(CN)_6]$ (0.1 mol L^{-1} KCl) at different scan rates from 0.010 to 0.100 V s^{-1} using the Fe(TPFPP)Cl/rGO@Pd0 sensor (working conditions: potential range from −0.6 to 1.0 V; step potential 0.025 V). (b) Dependence of the peak current on the square root of the scan rate, using the Fe(TPFPP)Cl/rGO@Pd0 sensor

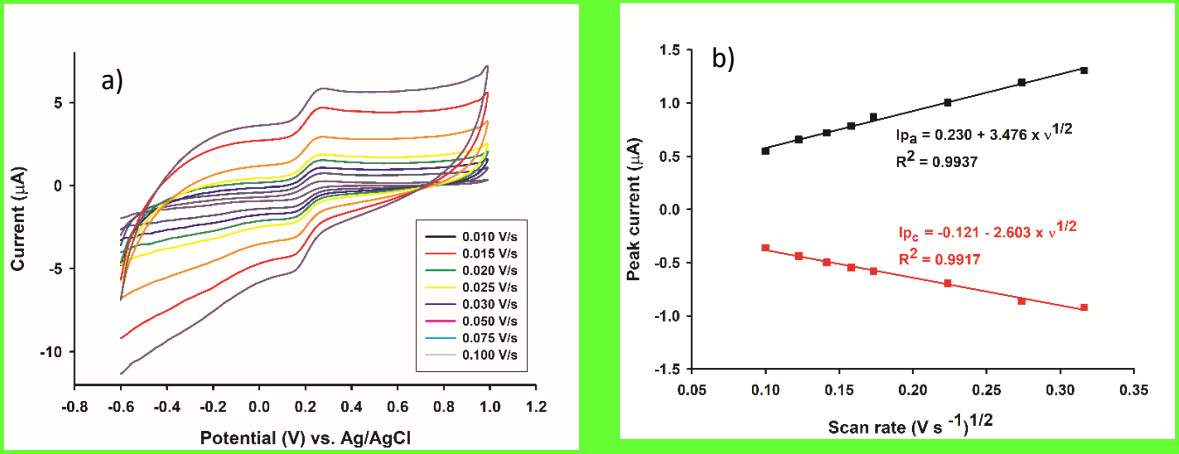

Figure 3. a) Cyclic voltammograms in a solution of 5.0×10^{-3} mol L^{-1} $K_3[Fe(CN)_6]$ (0.1 mol L^{-1} KCl) at different scan rates from 0.010 to 0.100 V s^{-1} using the TPP/rGO@Pd0 sensor (working conditions: potential range from −0.6 to 1.0 V; step potential 0.025 V). (b) Dependence of the peak current on the square root of the scan rate, using the TPP/rGO@Pd0 sensor

3.2. The Influence of the pH Value on the Electrochemical Behavior of the Sensors

When conducting electrochemical measurements (Fig. 4a) and 5a)), it is absolutely necessary to take note of the pH level of the solution, therefore a 100 □mol L^{-1}sodium metabisulfite solution was buffered with PBS with different pH values (2.0, 2.5, 3.0, 3.5, 4.0, 4.5, 5.0, 5.5, 6.0, 7.0, and 8.0). From Fig. 4b) it can be seen that, in the case of TPP/rGO@Pd0 sensor, there is a slight current increase at around pH 2.0, followed by a decrease to pH 3.5, reaching a maximum value of the current at pH 4.5, succeeded by a plateau from pH=5-8. When it comes toFe(TPFPP)Cl/ rGO@Pd0 sensor (Fig 5b)) one can see that at pH=2.5 a high increase in the current is obtained, followed by decline of current value. At pH=4.5 a maximum current values is achieved, continued by a final reduction in current value to pH=8. As demonstrated in both figures, the highest current intensity of sodium metabisulfitewas observed when the pH was 4.5 when both sensors were used. The correlation between the pH values and the peak potential (Epa) is shown in Fig. 4b) and 5b). A good observation can be made regarding the equation from Fig. 4b)when the sensor TPP/rGO@Pd0 sensor was used, where it can be seen that the obtained slope value is -0.078 V pH^{-1}which is close to the Nernstian theoretical valueof 0.059 V pH^{-1}, stating that the number of protons involved in the oxidation process is equal to the amount of electrons that are present in the process. On the other hand, Fig. 5b) provides an interesting result of the equation, Epa (V) = 0.230 - 0.059 pH, with a regression coefficient (R^2) of 0.9060 obtained for

Fe(TPFPP)Cl/rGO@Pd0, where theslope value of 0.059 V pH^{-1}, is the same to the Nernstian theoretical value of 0.059 V pH^{-1}, thusproving that the number of protons and electrons involved in the oxidation process are equal.

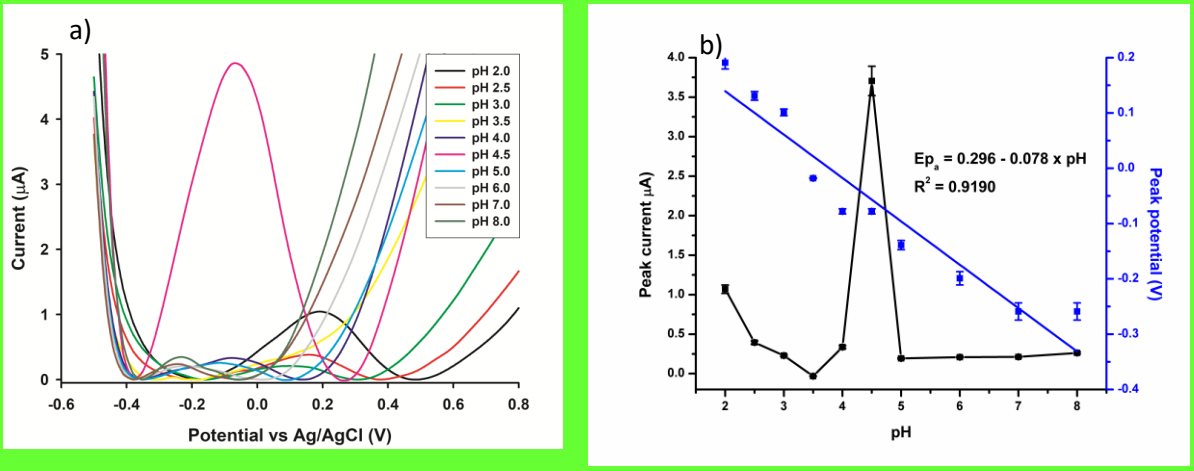

Figure 4. (a) Square wave voltammograms of 1.0 × 10^{-4} mol L^{-1} $Na_2S_2O_5$ using the TPP/rGO@Pd0 sensor in PBS at pH values 2.0 – 8.0. (b) The effect of the pH on the peak current (black dots) and the linear dependence of the peak potential with the pH (blue line)

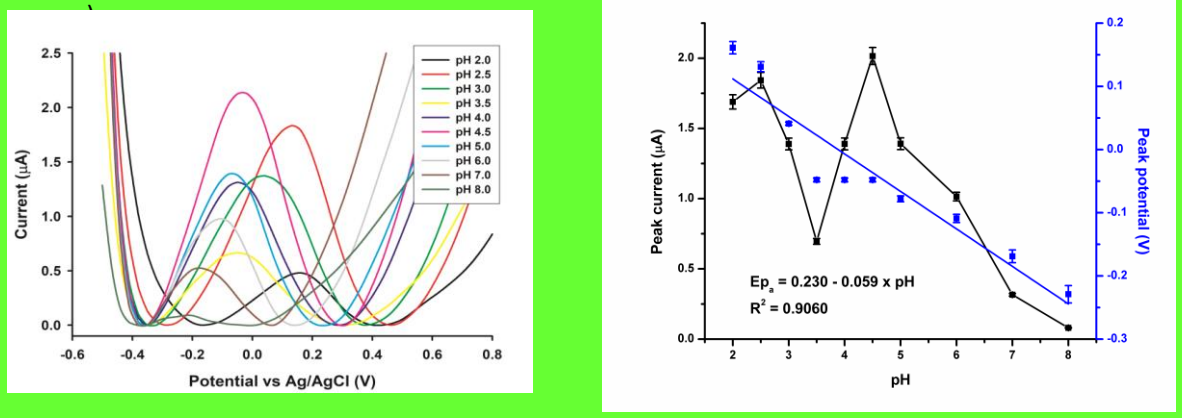

Figure 5. (a) Square wave voltammograms of 1.0 × 10^{-4} mol L^{-1} $Na_2S_2O_5$ using the Fe(TPFPP)Cl/rGO@Pd0 sensor in PBS at pH values 2.0 – 8.0. (b) The effect of the pH on the peak current (black dots) and the linear dependence of the peak potential with the pH (blue line)

3.3 Response Characteristics of the Electrochemical Sensors

At the ideal pH level (pH=4.5), the response characteristics of the proposed electrochemical sensors were identified using square-wave voltammetry and are listed in Table 1. A wide concentration range, high sensitivities and low limits of quantification and determination for the proposed sensors were obtained thanks to optimal working conditions and the electrocatalytic capacity of the porphyrins used in their design.The calibration graph for sodium metabisulfite is shown in Fig. 6b)along with the peaks that were obtained during the calibration of the TPP/rGO@Pd0 sensor.The linear concentrationrange was from 1.0× 10^{-11} mol L^{-1} to 1.0× 10^{-7} mol L^{-1} with a correlationcoefficient of 0.9970.The LOD and LOQ were calculated to be 3.0 × 10^{-12} and 1.0 × 10^{-11} mol L^{-1}, respectively. The values of LOD and LOQ as follows: LOD = 3 s / m and LOQ = 10 s/ m; where s is the standard deviation of the peak current of the blank (4 measurements) and m represents the slope of the calibration curve. The sensitivity of the TPP/rGO@Pd0 sensor was 9.015 x 10^{-7}mA/mol L^{-1}.

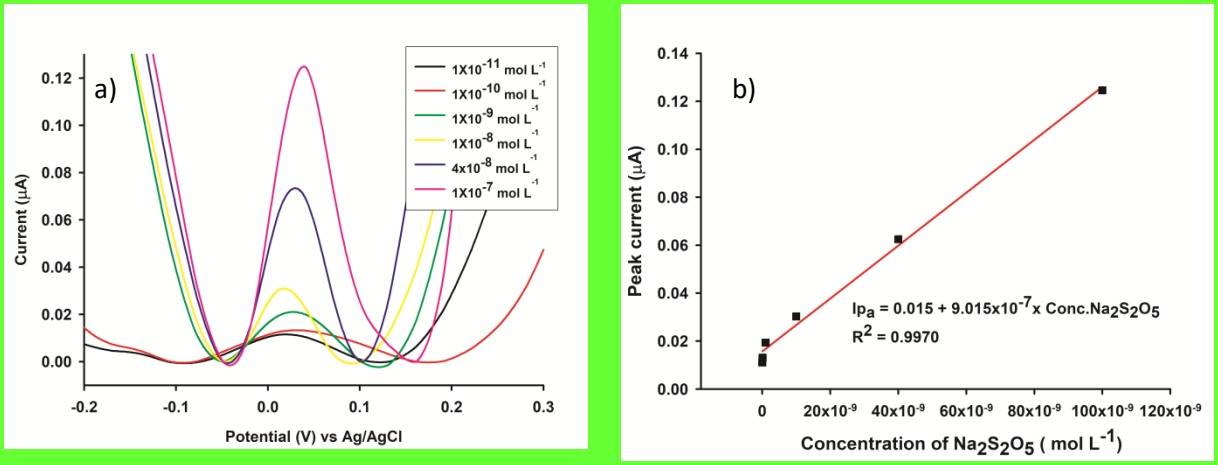

Figure 6. (a) Square wave voltammograms recorded with TPP/rGO@Pd0 sensor in PBS pH 4.5 containing different concentrations of $Na_2S_2O_5$ from 1.0× 10^{-11} mol L^{-1} to 1.0× 10_{-7} mol L^{-1}. (b) Calibration curve obtained with TPP/rGO@Pd0 sensor from 1.0× 10^{-11} mol L^{-1} to 1.0× 10^{-7} mol L^{-1}. Working conditions: step potential 0.03 V, amplitude: 0.1 V, frequency: 10 Hz.

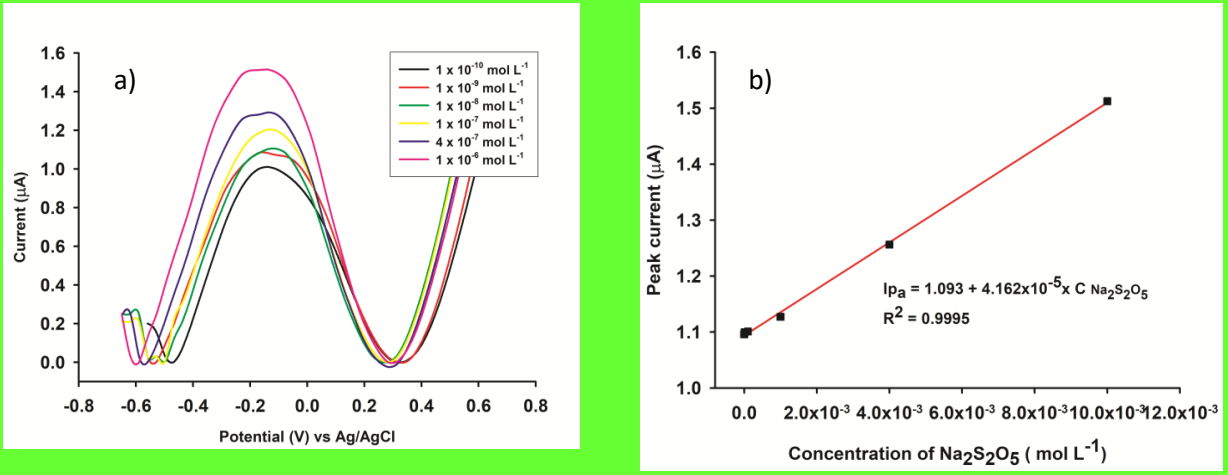

Figure 7. (a) Square wave voltammograms recorded with Fe(TPFPP)Cl /rGO@Pd0 sensor in PBS pH 4.5 containing different concentrations of $Na_2S_2O_5$ from 1.0× 10^{-10} mol L^{-1} to 1.0× 10^{-6} mol L^{-1}, (b) Calibration curve obtained with Fe(TPFPP)Cl /rGO@Pd0 sensor from 1.0× 10^{-10} mol L^{-1} to 1.0× 10^{-6} mol L^{-1}. Working conditions: step potential 0.03 V, amplitude: 0.1 V, frequency: 10 Hz.

Regarding the Fe(TPFPP)Cl/rGO@Pd0 sensor, Fig. 7b) presentsthe peaks acquired after calibration measurments, in addition to calibration graph of sodium metabisulfite. For LOD and LOQ calculation, the above-mentioned formulas were used. Therefore, very goodresults were obtained: linear concentration range from 1.0× 10^{-10} mol L^{-1} to 1.0× 10^{-6} mol L^{-1}, LOD and LOQ values calculated to be 3.0x10^{-11} mol L^{-1} and 1.0 × 10^{-10} mol L^{-1}, a far supperiorcorrelation coefficient of 0.9995, and a sensitivity of 4.162 x 10^{-5}mA/mol L^{-1}.

Table 1. Response characteristics of the electrochemical sensors used for detection of sodium metabisulfite.

Parameter	Electrochemical Sensors	
	TPP/rGO@Pd0	Fe(TPFPP)Cl/ rGO@Pd0
Equation of calibration*	Ipa=0.02+9.02x10^{-7} x$C_{Na2S2O5}$, R^2=0.9970	Ipa=1.09+4.16x10^{-5} x$C_{Na2S2O5}$, R^2=0.9995
Linear concentration range (mol L^{-1})	1.0× 10^{-11} - 1×10^{-7}	1.0× 10^{-10} - 1×10^{-6}
Sensitivity (mA mol L^{-1})	9.02 x 10^{-7}	4.16 x 10^{-5}
Limit of detection (mol L^{-1})	3.0x10^{-12}	3.0x10^{-11}
Limit of quantification (mol L^{-1})	1.0x10^{-11}	1.0x10^{-10}
Repetability of peak current (%, RSD)	2.78	2.75

The inorganic salt of sulfuric acid sodium metabisulfite ($Na_2S_2O_5$) dissolves in water to produce sodium, bisulfite, and sulfite ions[27]:$Na_2S_2O_5 + H_2O = 2Na^+ + 2HSO^{3-}$ and$HSO^{3-} = H^+ + SO_3^{2-}$ .Bisulfite anions are changed into sulfate anions when oxygen is present: $2HSO^{3-} + O_2 = 2H^+ + 2SO_4^{2-}$.

3.4. Interference studies of the electrochemical sensors

In order to test for potential interferences in the detection of sodium metabisulfite, a number of ions, including NH_4^+, Fe^{2+}, Na^+, and organic species, including acesulfame K, sucrose, glucose, sodium benzoate, d-sorbitol and maltodextrin, were tested.The substances frequently found with sodium metabisulfitein cookie, bean flakes and horseradish paste, and urine samples were chosen as potential interfering substances.The maximum interference concentration that resulted in a change in current intensity in terms of relative error (5% acceptance level), bias (%), and signal

changed (%) was referred to as the tolerance limit.All measurements were conducted using sodium metabisulfitesolutions (1.0 x 10^{-8} mol L^{-1}) buffered with PBS at a pH of 4.5.The experimental results when TPP/rGO@Pd0 sensor was used, exhibited no influence on the detection of sodium metabisulfite when an excess of 10-fold of NH^{4-}ion, 25-fold of sodium benzoate, 50-fold of glucose and sucrose, and 100-fold of Fe^{2+}, Na^{+} ions, acesulfame K, d-sorbitol and maltodextrin was added (Table2), which indicate that the proposed sensor presented a good selectivity on the determination of $Na_2S_2O_5$.

Table 2. The influence of possible interfering species on the detection of 1.0 × 10^{-8} Sodium metabisulfite (n=4) using the TPP/rGO@Pd0 sensor.

Possible interfering species	Concentration of possible interfering species (mol L^{-1})	Tolerance limit	Relative error (%)	Bias (%)
Fe^{2+}	1.0 × 10^{-7}	10	0.20	-1.83
Na^{+}	1.0 × 10^{-7}	10	1.33	-7.33
NH_4^{+}	1.0 × 10^{-7}	10	-0.35	0.15
Glucose	1.0 × 10^{-7}	10	0.74	0.45
Sucrose	2.5 × 10^{-7}	25	1.50	2.04
Sodium benzoate	5.0 × 10^{-7}	50	1.10	0.73
Acesulfam K	1.0 × 10^{-6}	100	-2.25	2.68
D-Sorbitol	1.0 × 10^{-6}	100	-0.62	1.29
MD	1.0 × 10^{-6}	100	-2.41	2.15

In the case of the second sensor, Fe(TPFPP)Cl/rGO@Pd0 sensor, the results indicated in Table 3 shows that an added excess of 10-fold of NH_4^+,Fe^{2+}, Na^+ ions and glucose, 25-fold of sucrose, 50-fold of sodium benzoate, and 100-fold of acesulfame K, d-sorbitol and maltodextrin manifests no influence on the detection of sodium metabisulfite, proving also that the sensor has a good selectivity on the determination of $Na_2S_2O_5$.Since porphyrins and metal complexes (including Fe(III)) with porphyrins mimic the enzymes' activity, it follows that they selectively promote the oxidation of sodium metabisulfite.The artificial enzymes TPP and Fe(TPFPP)Cl are acting as electrocatalysts in a process that is not a substrate-binding reaction.Since porphyrins are enzyme mimics, their use as artificial enzymes in electrochemistry has been thoroughly investigated [28–31].

Table 3. The influence of possible interfering species on the detection of 1.0×10^{-8} Sodium metabisulfite (n=4) using the Fe(TPFPP)Cl/rGO@Pd0 sensor.

Possible interfering species	Concentration of possible interfering species (mol L^{-1})	Tolerance limit	Relative error (%)	Bias (%)
NH_4^+	1.0×10^{-7}	10	-1.80	-3.76
Sodium benzoate	2.5×10^{-7}	25	0.35	-0.36
Glucose	5.0×10^{-7}	50	-2.30	2.65
Sucrose	5.0×10^{-7}	50	0.49	-1.74
Fe^{2+}	1.0×10^{-6}	100	-4.68	5.89
Na^+	1.0×10^{-6}	100	1.45	-2.35
Acesulfam K	1.0×10^{-6}	100	-1.94	2.37
D-Sorbitol	1.0×10^{-6}	100	-0.83	4.97
MD	1.0×10^{-6}	100	-0.05	2.03

3.5. Reproducibility, Repeatability and Stability

The repeatability, reproducibility and stability of the developed sensors (TPP/rGO@Pd0 and Fe(TPFPP)Cl/rGO@Pd0) were investigated using a solution of $Na_2S_2O_5$(1.0×10^{-8} mol L^{-1}) in PBS pH 4.5, under the optimal experimental conditions by SWV. The reproducibility was analyzed using three new sensors of each type, which were prepared in the same way. The relative standard deviation (RSD%) was calculated to be 2.55 % (n = 5) for the TPP/ rGO@Pd0 sensor and 0.94% (n = 5) for the Fe(TPFPP)Cl/rGO@Pd0 sensor.

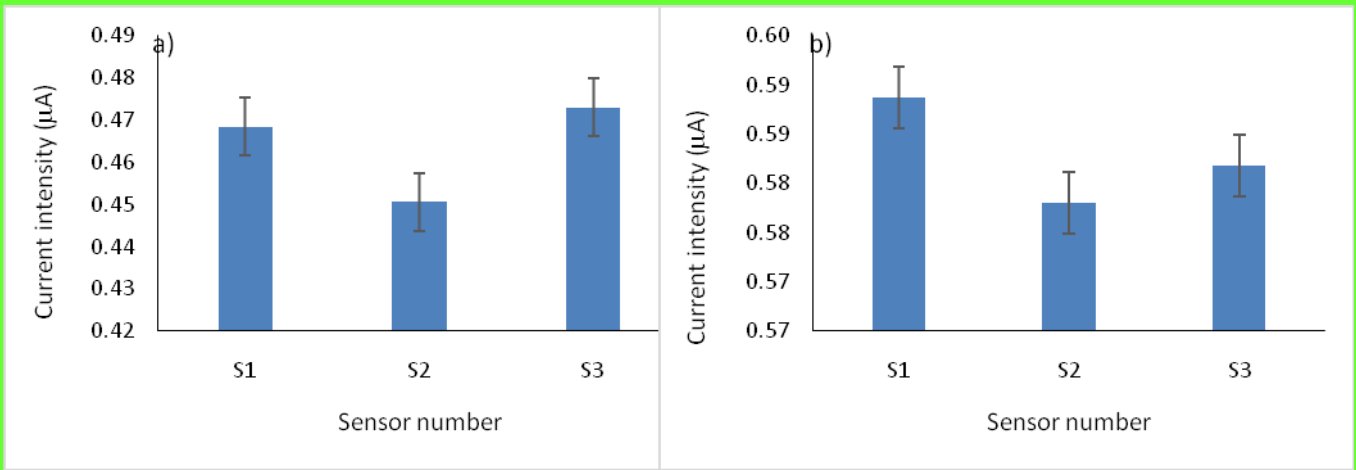

Figure 8. Reproducibility of the a) TPP/ rGO@Pd0 and b) Fe(TPFPP)Cl/rGO@Pd0

For the within-day repeatability, the repeatability was determined to be 1.54% (n = 5) for the TPP/ rGO@Pd0sensor and 0.97% (n = 5) for the Fe(TPFPP)Cl/rGO@Pd0sensor. The stability of the sensors was examined for 7 days.The modified electrodes were kept at room temperature throughout the stability examination. After 7 days, in the case of the TPP/ rGO@Pd0 sensor, the current intensity of the $Na_2S_2O_5$ (1.0×10^{-8} mol L^{-1}) decreased to a value of 80.70% of the initial value from the first day of assessment; and in the case of the Fe(TPFPP)Cl/rGO@Pd0, the peak current decreased up to a value of 71.59% from the initial value from the first day of assessment.

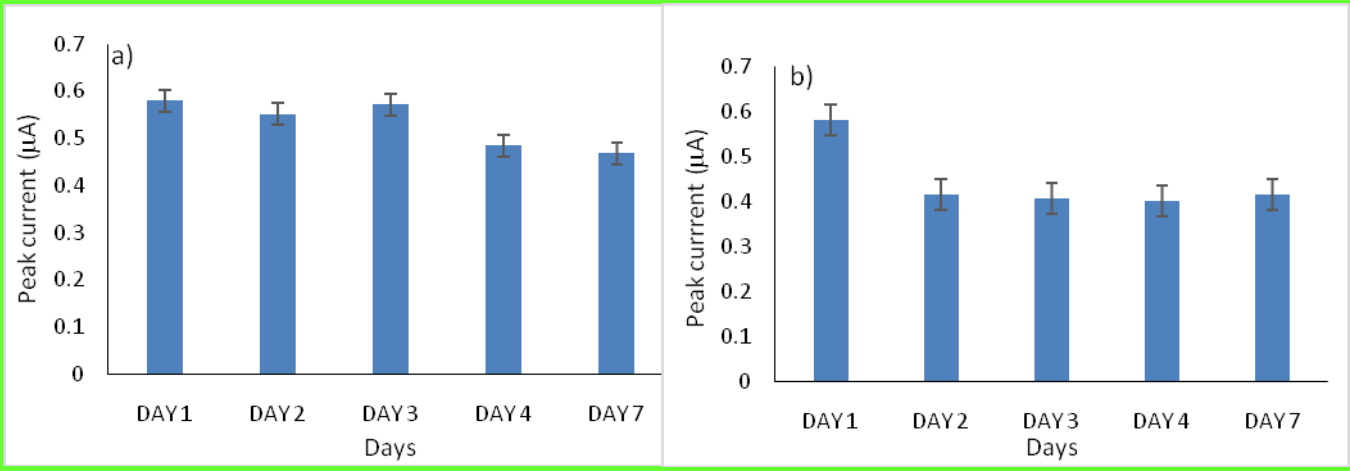

Figure 9. Stability of the a) TPP/ rGO@Pd0 and Fe(TPFPP)Cl/rGO@Pd0sensors for a period of 7 days.

3.6. Determination of sodium metabisulfite in food and biological samples

For the proposed sensors to be used more widely in the monitoring of food quality and the maintenance of food security, they must be validated.The sensors were validated using the standard addition method to show how accurate they are when measuring sodium metabisulfite in cookies, bean flakes, horseradish paste, and urine samples.As can be seen in Tables 4 and 5, the sodium metabisulfiteassay in cookies, bean flakes, horseradish paste, and urine samples has a very high degree of reliability.

For sample preparation, ten milliliters of PBS (pH = 4.5) was added to 1 g of cookie, bean flakes. The resulting mixture was vortexed for 4 minand left in the ultrasonic bath for 30 min.One gram of the horseradish paste sample was weighed usingan analytical balance, and it was dissolved in 10 mL of PBS (pH = 4.5) and vortexed for 4 min.The urine sample was diluted with PBS pH= 4.5 in a 1:1 (v/v) ratio and afterward spikedwith different concentrations of sodium metabisulfite.

After placing the samples into the electrochemical cell, the peak current was measured. $Na_2S_2O_5$ concentrations and the obtained values were input into the above calibration equation.Tables4 and 5 summarizes the recovery, RSD, and bias (%) values.

Table 4. Determination of sodium metabisulfite in food and biological samples using the TPP/rGO@Pd0 sensor.

Samples	Amount added (mol L^{-1})	Amount found (mol L^{-1})	Recovery (%)	RSD (%)	Bias (%)
Cookie	-	4.41×10^{-9}	-	1.30	-
	1.0×10^{-7}	9.98×10^{-8}	99.83	0.05	0.17
	1.0×10^{-8}	9.87×10^{-9}	98.68	0.24	1.34
Bean flakes	-	3.45×10^{-8}	-	0.47	-
	1.0×10^{-7}	9.97×10^{-8}	99.73	0.57	0.27
	1.0×10^{-8}	1.00×10^{-8}	99.96	1.21	0.04
Horseradish paste	-	6.92×10^{-8}	-	0.52	-
	1.0×10^{-7}	9.99×10^{-8}	99.87	0.80	0.13
	1.0×10^{-8}	1.00×10^{-8}	99.97	0.86	0.03
Urine	-	-	-	3.78	-
	1.0×10^{-7}	9.78×10^{-8}	97.82	4.50	2.23
	1.0×10^{-8}	9.97×10^{-9}	99.73	2.16	0.27

Table 5. Determination of sodium metabisulfite in food and biological samples using the Fe(TPFPP)Cl/rGO@Pd0 sensor.

Samples	Amount added (mol L^{-1})	Amount found (mol L^{-1})	Recovery (%)	RSD (%)	Bias (%)
	-	1.06×10^{-8}	-	1.31	-
Cookie	1.0×10^{-7}	9.93×10^{-8}	99.32	2.22	0.67
	1.0×10^{-8}	9.99×10^{-9}	99.98	4.48	0.01
	-	8.44×10^{-7}	-	4.03	-
Bean flakes	1.0×10^{-7}	9.99×10^{-8}	99.98	1.29	0.01
	1.0×10^{-8}	9.99×10^{-9}	99.98	3.45	0.01
	-	9.87×10^{-9}	-	2.92	-
Horseradish paste	1.0×10^{-7}	9.95×10^{-8}	99.54	1.86	0.46
	1.0×10^{-8}	9.71×10^{-9}	97.11	4.54	2.98
	-	-	-	5.94	-
Urine	1.0×10^{-7}	9.99×10^{-8}	99.95	0.21	0.05
	1.0×10^{-8}	9.99×10^{-9}	99.93	1.04	0.06

It can be seen from Table 4, that very good recovery values were obtained, when TPP/rGO@Pd0 sensor was used. For the food samples, the recoveries had high values, well above 99%, with one exception, for the spiked cookiesample (10^{-8} mol L^{-1}) sodium metabisulfite concentration), the recovery values were very close to 99%. Also, the urine sample presented recoveries value above 99.9%. The RSD values for the samples were between 0.05±4.50. In the case of Fe(TPFPP)Cl/rGO@Pd0 sensor, from Table 5 it can be observed that the recoveries in both food and urine samples are above 97%, with RSD values ranging from 0.21 to 5.94. Therefore, given

the fact that the results presented in Tables 4 and 5 have very good values, it can be claimed that both sensors, TPP/rGO@Pd0 and Fe(TPFPP)Cl/rGO@Pd0demonstrated that they are able to provide an increase in both the sensitivity and selectivity of the assay for sodium metabisulfite in food and biological samples.

5. Conclusions

Nanomaterials are a promising new tool for improving food safety and quality control monitoring, and their use in technology is sure to pave the way for the creation of even more sensitive electrochemical sensors. Therefore, the present study presents two electrochemical sensors, based on reduced graphene oxide doped with Pd paste and modified with 5,10,15,20-tetraphenyl-21H,23H-porphine and 5,10,15,20-tetrakis (pentafluorophenyl chloride)-21H,23H-iron (III) porphyrin were designed, characterized, tested and validated for determination of sodium metabisulfite in three different food samples and a biological sample.Both sensors showed very high levels of stability, selectivity, sensitivity, and reproducibility in their measurements. The proposed sensors have the benefit of being able to be utilized in the food industry for the purpose of quality control of food in relation to the determination of the amount of sodium metabisulfite present in the samples.

References

22. Martins, F.C.O.L.; Sentanin, M. A.; De Souza, D. Analytical methods in food additives determination: Compounds with functional applications. *Food Chem*. 2019, *272*, 732–750.

23. Zhong, Y.; Wu, L.; Chen, X.; Huang, Z.; Hu, W. Effects of food-additive- information on consumers' willingness to accept food with additives. *Int. J. Environ. Health Res*. 2018, *15*, 2394.

24. Leyva Salas, M.; Mounier, J.; Valence, F.; Coton, M.; Thierry, A.; Coton, E. Antifungal Microbial Agents for Food Biopreservation-A Review. *Microorganisms*2017, *5*, 37.

25. Mepham, B. Food additives: An ethical evaluation. *Br. Med. Bull*. 2011, *99*, 7–23.

26. Lai, M.C.; Hung, T.Y.; Lin, K.M.; Sung, P.S.; Wu, S.J.; Yang, C.S.; Wu, Y.J.; Tsai, J.J.; Wu, S.N.; Huang, C.W. Sodium Metabisulfite: Effects on Ionic Currents and Excitotoxicity. *Neurotox. Res*. 2018, *34*, 1–15.

27. Ahmadi, F.; Lee, Y. H.; Lee, W. H.; Oh, Y. K.; Park, K. K.; Kwak, W. S. Preservation of fruit and vegetable discards with sodium metabisulfite. *J. Environ. Manage*. 2018, *224*, 113–121.

28. Vieira, H. H.; Toledo, J. C. Jr.; Catelan, A.; Gouveia, T. H. N.; Aguiar, F. H. B.; Lovadino, J. R.; Lima, D. A. N. L. Effect of sodium metabisulfite gel on the bond strength of dentin of bleached teeth. *Eur. J. Dent.*2018, *12*, 163–170.

29. Trivedi, H. K. A Stability Indicating Method for the Determination of the Antioxidant Sodium Bisulfite in Pharmaceutical Formulation by RP-HPLC Technique. *Sci. Pharm*. 2011, *79*, 909–920.

30. Carvalho, I. M.; Melo Cavalcante, A. A.; Dantas, A. F.; Pereira, D. L.; Costa Rocha, F. C.; Andrade, T. J.; Da Silva, J. Genotoxicity of sodium metabisulfite in mouse tissues evaluated by the comet assay and the micronucleus test. Mutat. *Res. Genet. Toxicol. Environ. Mutagen*. 2011, *720*, 58–61.

31. Ercan, S.; Oztürk, N.; Celik-Ozenci, C.; Gungor, N. E.; Yargicoglu, P. Sodium metabisulfite induces lipid peroxidation and apoptosis in rat gastric tissue. *Toxicol. Ind. Health*2010, *26*, 425–431.

32. Toh, H. S.; Tschulik, K.; Batchelor-McAuley, C.; Compton, R. G. Electrochemical quantification of iodide ions in synthetic urine using silver nanoparticles: a proof-of-concept, *Analyst* 2014, *139*, 3986-3990.

33. Guan, P.; Li, Y.; Zhang, J.; Li, W. Non-Enzymatic Glucose Biosensor Based on CuO-Decorated CeO2 Nanoparticles. *Nanomaterials*2016, *6*, 159.

34. Favero, G.; Fusco, G.; Mazzei, F.; Tasca, F.; Antiochia, R. Electrochemical Characterization of Graphene and MWCNT Screen-Printed Electrodes Modified with AuNPs for Laccase Biosensor Development. *Nanomaterials*2015, *5*, 1995-2006.

35. Du, X.; Skachko, I.; Barker, A., Andrei, E.Y. Approaching ballistic transport in suspended graphene. *Nat. Nanotechnol*. 2008, *3*, 491–495.

36. Wang, Y.; Li, Y.; Tang, L., Lu, J.; Li, J. Application of graphene-modified electrode for selective detection of dopamine. *Electrochem. commun*. 2009, *11*, 889-892.

37. Alwarappan, S.; Erdem, A.; Liu, C.; Li, C.-Z. Probing the Electrochemical Properties of Graphene Nanosheets for Biosensing Applications. *J. Phys. Chem. C.*2009, *113*, 8853-8857.

38. Niculae, A.-R.; Stefan-van Staden, R.-I.; van Staden, J.F.; Georgescu State, R. Sulfur-Doped Graphene-Based Electrochemical Sensors for Fast and Sensitive Determination of (R)-(+)-Limonene from Beverages. *Sensors*2022, *22*, 5851.

39. Palanisamy, S.; Ku, S.; Chen, S.M. Dopamine sensor based on a glassy carbon electrode modified with a reduced graphene oxide and palladium nanoparticles composite. *Microchim. Acta*2013, *180*, 1037-1042.

40. Zhou, H.; Liu, Y.; Chi, W.; Yu, C.; Yu, Y. Preparation and antibacterial properties of Ag@ polydopamine/graphene oxide sheet nanocomposite. *Appl. Surf. Sci.*2013, *282*, 181-185.

41. Fu, L.; Yu, A. Electroanalysis of Dopamine Using Reduced Graphene Oxide-Palladium Nanocomposites, *Nanosci. Nanotechnol. Lett*. 2015, *7*, 147-151.

42. Chen, Z. H.; Jie, J. S.; Luo, L. B.; Wang, H.; Lee, C. S.; Lee, S. T. Applications of silicon nanowires functionalized with palladium nanoparticles in hydrogen sensors, *Nanotechnology*, 2007, *18*, 345502.

43. Comnea-Stancu, I.R.; van Staden, J.K.F.; Stefan-van Staden, R.-I. Facile Detection of Naphthalene with a 5,10,15,20-tetrakis(4-methoxyphenyl)-21H,23H-Porphine Nickel (II)/N-(1-Naphthyl) Ethylenediamine Dihydrochloride Renewable Graphene Oxide Paste Electrode. *J. Electrochem. Soc*. 2022, *169*, 037527.

44. Cioates Negut, C.; Stefan-van Staden, R.-I.; Sfirloaga, P. Simultaneous Molecular Recognition of Interleukins 2 and 4, and of Tumour Necrosis Factor-α in Biological Samples. *Electroanalysis*2022, https://doi.org/10.1002/elan.202200305.

45. Bedioui, F.; Griveau, S.; Nyokong, T.; Appleby, A.J.; Caro, C.A.; Gulppi, M.; Ochoae, G.; Zagal, J.H. Tuning the redox properties of metalloporphyrin- and metallophthalocyanine-based molecular electrodes for the highest electrocatalytic activity in the oxidation of thiols. *Phys. Chem. Chem. Phys*. 2007, 9, 3383–3396.

46. Georgescu State, R.; van Staden, J.K.F.; State, R.N.; Papa, F. Rapid and sensitive electrochemical determination of tartrazine in commercial food samples using IL/AuTiO2/GO composite modified carbon paste electrode. *Food Chem*. 2022, 385, 132616.

47. Zanello, P. Inorganic Electrochemistry: Theory, Practice and Application RSC Publishing, 2003.

48. Shabliy, T.; Gomelya, M.; Pohrebennyk, V.; Ivanenko, O.; Nosachova, Y. Development of New Water Deoxidization Systems for Heat and Power Plants. *J. Ecol. Eng.*2022, 23, 193–205.

49. Elemans, J.A.A.W.; Nolte, R.J.M. Porphyrin cage compounds based on glycouryl—From enzyme mimics to functional molecular machines. *Chem. Commun.*2019, 55, 9590–9605.

50. Zamborlini, G.; Jugovac, M.; Cossaro, A.; Verdini, A.; Floreano, L.; Lüftner, D.; Puschnig, P.; Feyer, V.; Schneider, C.M. On-surface nickel porphyrin mimics the reactive center of an enzyme cofactor. Chem. Commun. 2018, 95, 13423–13426.

51. Aghayan, M.; Mahmoudi, A.; Nazari, K.; Dehghanpour, S.; Sohrabi, S.; Sazegar, M.R.; Mohammadian-Tabrizi, N. Fe(III) porphyrin metal-organic framework as an artificial enzyme mimics and its application in biosensing of glucose and H2O2. J. Porous Mat. 2019, 26, 1507–1521.

52. Anderson, H.L.; Sanders, J.K.M. Enzyme mimics based on cyclic porphyrin oligomers: Strategy, design, and exploratory synthesis. J. Chem. Soc. Perkin Trans. 1995, 18, 2223–2229.